STABILITY OF LEVEES AND FLOODWALLS SUPPORTED BY DEEP-MIXED SHEAR WALLS: FIVE CASE STUDIES IN THE NEW ORLEANS AREA

Tiffany E. Adams

Dissertation submitted to the faculty of the Virginia Polytechnic Institute and State University in partial fulfillment of the requirements for the degree of

Doctor of Philosophy
In
Civil Engineering

George M. Filz (Chair)
James K. Mitchell
Thomas L. Brandon
Michael F. Hochella
Roseanne J. Foti

September 8, 2011
Blacksburg, VA

Keywords:
Levee stability
Deep-mixed shear walls
Column-supported embankment
Numerical finite difference analysis
Failure mode analysis

STABILITY OF LEVEES AND FLOODWALLS SUPPORTED BY DEEP-MIXED SHEAR WALLS: FIVE CASE STUDIES IN THE NEW ORLEANS AREA

Tiffany E. Adams

ABSTRACT

Increasing interest, from the U.S. Army Corps of Engineers (USACE) and other agencies, in using deep-mixing methods (DMM) to improve the stability of levees constructed on soft ground is driven by the need to reduce levee footprints and environmental impacts and to allow for more rapid construction. Suitable methods for analysis and design of these systems are needed to ensure that the DMM technology is properly applied.

DMM shear walls oriented perpendicular to the levee alignment are an effective arrangement for supporting unbalanced lateral loads. Shear walls constructed by overlapping individual DMM columns installed with single-axis or multiple axis equipment include vertical joints caused by the reduced width of the wall at the overlap between adjacent columns. These joints can be made weaker by misalignment during construction, which reduces the efficiency of the overlap. Depending on the prevalence and strength of these joints, complex failure mechanisms, such as racking due to slipping along vertical joints between adjacent installations in the shear walls, can occur. Ordinary limit equilibrium analyses only account for a composite shearing failure mode; whereas, numerical stress-strain analyses can account for other failure modes.

Five case studies provided by the USACE were analyzed to evaluate the behavior of levee and floodwall systems founded on soft ground stabilized with DMM shear walls. These projects identified and illustrated potential failure mechanisms of these types of systems. Two-dimensional numerical stability and settlement analyses were performed for the case studies using the FLAC computer program. Key findings and conclusions for the individual case studies were assessed and integrated into general conclusions about design of deep-mixing support for levees and floodwalls.

One of the significant findings from this research was to identify the potential for a partial depth racking failure, which can control design when the DMM shear walls are socketed into a relatively strong bearing layer. The potential for partial depth racking failure is not discussed in the literature and represents a new failure mode identified by this research. This discovery also highlights the importance of adapting suitable methods for analysis and design of these systems to address all potential failure modes.

ACKNOWLEDGEMENTS

First, I would like to thank my advisor, Professor George Filz, for the guidance and insight he provided through the course of this work. I am grateful for the opportunity to have worked with him on this research and have learned much from his approach to solving engineering problems.

I would also like to recognize the members of my committee, Professors James K Mitchell, Thomas L. Brandon, Michael F. Hochella and Roseanne J. Foti for their advice and suggestions during this research and for the skills gained from their classes that have contributed to my becoming a better engineer and researcher.

I would like to thank the U.S. Army Corps of Engineers for the opportunity to work with their engineers and subcontractors on the evaluation of real-world projects. The comments and inputs provided by Pete Cali, Mark Woodward, Neil Schwanz and Mike Navin of the U.S. Army Corps of Engineers, Robert Chamlee of Bioengineering Arcadis, Therese Koutnik of HNTB, and Eddie Templeton of Burns Cooley Dennis have contributed greatly to the quality and completeness of this dissertation.

I would also like to acknowledge the contributions of fellow students and Virginia Tech graduates Michelle Bolding, for her help with the data entry and statistical analysis, and Alfredo Arenas, Miriam Smith, and Jennifer Schaeffer for their ongoing support and advice towards debugging the numerical modeling and stability analysis. Mike McGuire's work in reviewing the verbiage for a large portion of this manuscript is also gratefully acknowledged.

Financial support for this work was provided by the U.S. Army Corps of Engineers, the U.S. National Science Foundation's grant No. DGE-0504196 to the Virginia Tech Exploring Interfaces through Graduate Education and Research (EIGER) program, and the Virginia Tech Via Foundation.

Finally, I would like my many families (back home, YMF, PanGEO, URS, EIGER, GSS, geotech grads, Cellar Dwellers, and Del) for their continuous advice, moral support and encouragement.

DISCLAIMER: Any opinions, findings, conclusions, and recommendations in this report are those of the author and do not necessarily reflect the views of the U.S. National Science Foundation.

TABLE OF CONTENTS

LIST OF FIGURES

LIST OF TABLES

LIST OF SYMBOLS

A_{dm}	area of the deep-mixed material in the shear walls
A_{soil}	area of the untreated soft soil between shear walls
a_e	overlap area ratio (ratio of area of overlap to area of individual column)
a_s	area replacement ratio (ratio of area of treated material to area of DMM zone)
b	effective width of the shear wall
c	chord length at the column overlap
c	total stress cohesion
c'	effective stress cohesion
C_c	compression index for virgin compression
C_r	compression index for recompression
c_v	coefficient of consolidation for virgin compression
c_{vr}	coefficient of consolidation for recompression
COV	coefficient of variation
d	column diameter
DMM	deep mixing method
E	Young's modulus
E_{50}	secant value of Young's modulus
E_{dm}	Young's modulus for the deep-mixed material
E_{dmz}	composite Young's modulus for the DMM zone
E_{soil}	Young's modulus for the untreated soil between the DMM shear walls
E_u	undrained Young's modulus
e	overlap distance between columns
e_0	initial void ratio
FS	factor of safety
F_c	factor of safety for crushing
F_e	factor of safety for extrusion
F_g	factor of safety for global stability
F_n	factor of safety for non-vertical shearing
F_o	factor of safety for overturning

F_s	factor of safety for sliding
F_v	factor of safety for vertical shearing
G	shear modulus
H_0	initial height
K	bulk modulus
k	permeability
k_h	horizontal permeability
k_v	vertical permeability
LL	liquid limit
M	constrained modulus
MOP	Method of Planes
p	means stress
p_0	initial pressure
PI	plasticity index
p_f	final pressure
PMT	pressuremeter test
p_p	preconsolidation pressure
QA	quality assurance
QC	quality control
q_u	unconfined compressive strength
S	center-to-center spacing between shear walls
S_{1yr}	total settlement after one year
S_{3yr}	total settlement after three years
S_{10yr}	total settlement after 10 years
S_{30yr}	total settlement after 30 years
S_{ult}	ultimate total settlement
s	shear strength
s_{dm}	shear strength of the deep-mixed material
s_{dmz}	composite shear strength of the deep mixed zone
$s_{dmz,v}$	composite shear strength of the deep mixed zone for vertical shearing along column overlaps

s_{soil}	shear strength of the untreated soft soil between shear walls
s_u	undrained shear strength
SRF	strength reduction factor
t_{50}	time to 50% consolidation settlement
t_{90}	time to 90% consolidation settlement
TXT	triaxial test
UCS	unconfined compressive strength
wc	water content

α	one-half the chord angle (radians)
Δp	change in vertical stress
ε	vertical strain
ϕ	total stress friction angle
ϕ'	effective stress friction angle
γ	unit weight
γ_{total}	total unit weight
γ_w	unit weight of water
ρ	settlement of a layer
ρ_c	consolidation settlement of a layer
ρ_{cc}	conventional, one-dimensional consolidation settlement of a layer
σ'_v	vertical effective stress
τ_{xy}	shear stress
ν	Poisson's ratio
ν_u	undrained Poisson's ratio

CHAPTER 1

INTRODUCTION

The performance of embankments constructed on soft ground can be improved by flattening the side slopes, using lightweight fill, or improving the foundations. Flood protection levees are particularly challenging, as these embankments must have sufficient weight to withstand the lateral forces of impounded water, and their proximity to existing roadways and structures in developed areas restricts the potential for flattening the slopes. In addition, they are often constructed on soft alluvial or coastal deposits which can extend relatively deep. Increasing interest, from the U.S, Army Corps of Engineers (USACE) and other agencies, in using deep-mixing methods (DMM) to improve the stability of levees constructed on soft ground is driven by the need to reduce levee footprints and environmental impacts and to allow for more rapid construction.

Previous research conducted at Virginia Tech on the stability of roadway embankments on DMM columns (Navin 2005) indicated that numerical analyses are preferable to limit equilibrium stability analyses because numerical analyses can capture column failure modes other than shearing, such as bending and tilting. Navin (2005) also recommended the use of continuous DMM shear walls, oriented perpendicular to the alignment of the embankment, instead of individual DMM columns, for improving embankment stability.

DMM shear walls (also called shear panels) can be constructed by overlapping individual DMM columns installed with single-axis or multiple axis equipment. A diagram of a levee embankment with shear walls oriented perpendicular to the levee alignment is shown in Figure 1-1. Shear walls constructed by overlapping single or multiple-axis DMM column installations include vertical joints caused by the reduced width of the wall at the overlap between adjacent columns. These joints can be made weaker by misalignment during construction, which reduces the efficiency of the overlap. Depending on the prevalence and strength of these joints, complex failure mechanisms, such as racking due to slipping along vertical joints between adjacent installations in the shear walls, can occur. Ordinary limit equilibrium analyses only account for a

composite shearing failure mode; whereas, numerical stress-strain analyses can account for other failure modes.

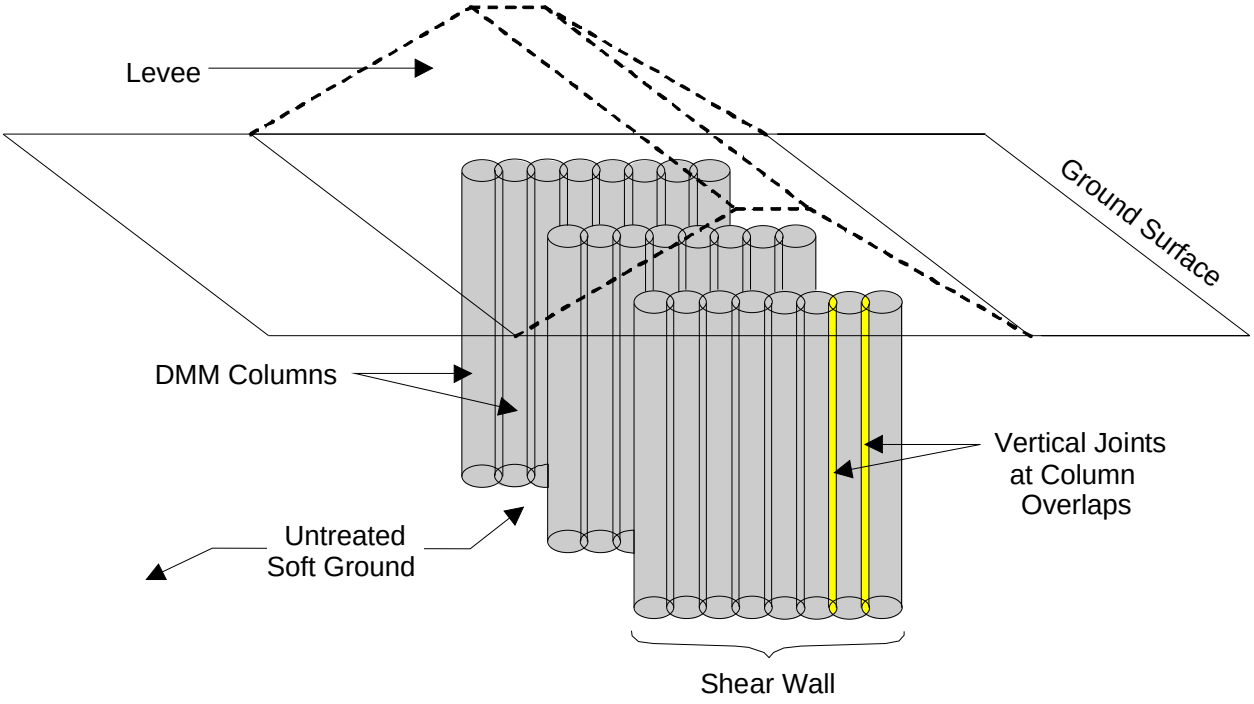

Figure 1-1. Diagram of a Levee supported on DMM Shear Walls Constructed with Overlapping Columns

1.1. Motivation for Research

The USACE has been investigating the potential for using DMM columns to stabilize levees and floodwalls that comprise flood protection systems in the vicinity of New Orleans since 2002 (Cali et al. 2005a, Cali et al. 2005b, Woodward 2009). After Hurricane Katrina, immediate and extensive repairs were needed to restore the flood and hurricane protection systems to the level of protection that existed before the hurricane. Six of these repair projects were subject to right-of-way and other restrictions, prompting the USACE to install deep-mixed soil-cement columns to strengthen soft foundation soils and reduce the levee footprint (Woodward 2009). The USACE took a conservative approach in the design of these projects and identified the need for advanced analyses to fully assess the stability of these systems and develop suitable design procedures.

The case study approach proposed by the USACE provided a unique opportunity to build on the previous research completed at Virginia Tech on the stability of earthen embankments supported by deep-mixed foundations by applying the framework developed for numerical analyses of these systems to real-world configurations of levees and floodwalls supported by continuous shear walls.

1.2. Objective and Scope of the Research

The primary objective of this research is to evaluate analysis and design approaches that geotechnical engineers can use for assessing the stability of levee and floodwall systems with deep mixed shear walls. The design cross-sections provided by the USACE for projects in the New Orleans area allow for evaluation of systems with complex, real world stratigraphy and material characterization. These projects provide an opportunity to evaluate the behavior of levee and floodwall systems founded on soft ground stabilized with DMM shear walls and to identify and illustrate potential failure mechanisms of these types of systems. Five case studies were identified by the USACE for this research:

1) Stability Analyses of the P24 Levee
2) Settlement Analyses of the P24 Levee
3) Stability Analyses of the Gainard Woods Pump Station T-wall
4) Stability Analyses of a T-wall on Level Ground
5) Stability Analyses of the Inner Harbor Navigation Canal Reach III B-1A I-wall

The goal of this research is to identify the failure modes for these systems, determine if numerical methods are necessary to accurately assess stability, and provide recommendations for modeling weak joints within the shear walls.

The scope of this research includes the following tasks:

(a) Perform a literature review

A literature review was performed for stability and settlement analyses of levees with deep mixed shear walls. This literature review summarizes the relevant aspects of the

Navin (2005) and Smith (2005) dissertations, as well as additional sources not included in the literature review sections of those documents.

(b) Perform numerical analyses for case studies

Two-dimensional numerical stability and settlement analyses were performed for five case studies of levees and floodwalls in the vicinity of New Orleans. The stability analyses were completed using the analysis sections and material properties that were used by the USACE and Burns Cooley Dennis (BCD) in their designs to allow for direct comparison among analysis methods. Parametric studies were performed for some of the stability case histories to evaluate the effect of specific design factors on the failure mode and/or factor of safety of the system. Design factors that were varied in the parametric studies included: 1) the efficiency of the vertical joints in the DMM shear walls; 2) the strength of the DMM zone; and 3) the geometry and location of the DMM zone. The settlement study was completed for as-built conditions to allow for direct comparison with settlement monitoring data for the site. Settlement calculations were performed for a range of consolidation properties and conditions to provide a range of predicted settlement values.

(c) Develop conclusions about the analysis and design of these systems

The key findings and conclusions for the individual case studies were assessed and integrated into general conclusions about design of deep-mixing support for levees and floodwalls.

1.3. Organization and Content of this Dissertation

This dissertation is divided into nine chapters and one appendix.

Chapter 2 presents a literature review, in which available information for the stability of levees and floodwalls supported on deep-mixed shear walls was collected and synthesized. The information is organized in a summary of key references, followed by a discussion of the main topics for column-supported embankments that require special consideration for adaptation to levees and floodwalls with DMM shear walls.

Chapter 3 provides a summary of the five case studies that were evaluated for this research. The purpose of the section is to provide an overview of the systems analyzed, the type of analysis completed, and the key findings for each case study.

The work completed for each of the case studies is documented in Chapters 4 through 8. A detailed description is provided of the analysis cross-section, material properties, analysis methods, and other aspects specific to each case study. Chapter 4 presents the case study on the stability analyses of the P24 levee. Chapter 5 presents the case study on the settlement analyses of the P24 levee. Chapter 6 presents the case study on the stability of the Gainard Woods Pump Station T-wall. Chapter 7 presents the case study on the stability analyses of a T-wall on level ground. Chapter 8 presents the case study on the stability of the Inner Harbor Navigation Canal Reach III B-1A I-wall.

Chapter 9 summarizes the work completed for this research and provides general conclusions about design of deep-mixing support for levees and floodwalls. Recommendations for further research are also provided.

The background documentation provided by the USACE and BCD for the five case studies is included in Appendix A.

CHAPTER 2

LITERATURE REVIEW

This chapter describes the results of a literature review on the stability of levees and floodwalls supported by deep-mixed shear walls. The results of the literature review are organized and presented in terms of the key references, followed by a discussion of the four main topics for column-supported embankments that require special consideration for adaptation to levees and floodwalls with DMM shear walls: 1) material properties of the DMM zone; 2) vertical joints in DMM shear walls; 3) failure modes for DMM shear walls; and 4) simplified methods for analysis of DMM shear walls.

2.1. Key References

This research is based in significant part on work completed by Michael Navin for his dissertation "Stability of Embankments Founded on Soft Soil Improved with Deep-Mixing Method Columns" (2005) and to a lesser extent, on the dissertation by Miriam Smith titled "Design of Bridging Layer in Geosynthetic-Reinforced Column-Supported Embankments" (2005). These documents include extensive literature reviews of over 500 references related to deep mixing installation methods, typical geometries, material properties, and methods for evaluating stability and settlement of embankments founded on deep-mixed columns. In addition to the background information provided in the literature reviews, these documents also provided comprehensive overviews of the mechanics and guidelines for numerical modeling of column supported embankments. Because they provide a basic foundation for the numerical analyses completed for this research, these documents are heavily represented in the literature review performed for this research. More recent sources not included in the literature reviews of these dissertations were reviewed as part of this research.

Since 2005, there have been two international conferences on the topic of deep mixing, Deep Mixing '05 in Stockholm and Deep Mixing '09 in Okinawa, and numerous other publications on deep-mixing. These publications provide an increased understanding of issues related to construction, testing, and design for deep-mixed materials. Publications on the stability of embankments on deep mixed foundations have focused primarily on group column-type

configurations of the DMM zone, similar to the majority of the work completed by Navin (2005), which are controlled by different failure mechanisms than the shear wall configuration used for this research. Some of the key references relative to the stability of levees on DMM shear walls are summarized below.

2.1.1. Navin (2005)

This dissertation focused on topics related to the edge stability of embankments founded on deep-mixed columns. Although this research was primarily focused on systems with group column-type DMM configurations, where isolated columns are installed within the zone of treated ground with no overlap between columns, analysis of DMM shear walls under the side slope of an example embankment was also performed. The literature review for this dissertation provided a summary of published information related to stability of these systems, including column installation methods, material property values and variability of DMM materials, analysis methods for stability, case histories and previous research, and a summary of information on related columnar technologies.

The important findings from the literature review presented by Navin (2005) for assessing the stability of levees and embankments with DMM shear walls are:

- The strength of deep-mixed materials cannot be reliably determined based on admixture content and site soil characteristics (CDIT 2002). It is recommended that strength be determined from mix design studies using soils from the project site.

- Reported values of unconfined compressive strength of deep-mixed materials range from 2 to 400 psi for soils treated using the dry method of deep-mixing, and from 20 to 4,000 psi for the soils treated using the wet method of deep-mixing (Japanese Geotechnical Society 2000, Baker 2000, Jacobson et al. 2003). Typically an undrained shear strength equal to one-half of the unconfined compressive strength has been used for the DMM material in the columns.

- Published correlations provide a ratio of the secant value of Young's modulus of elasticity, E_{50}, to the unconfined compressive strength, q_u. Reported values of the

stiffness ratio, E_{50}/q_u, range between 50 and 250 for the dry method of mixing (Baker 2000, Broms 2003, Jacobson et al.2005) and between 75 and 1000 for the wet method (Ou et al. 1996).

- Reported values for Poisson's ratio of the deep-mixed material range from 0.2 to 0.5 (CDIT 2002, McGinn and O'Rourke 2003, Terashi 2003, Porbaha et al. 2005).

- The unit weight of the deep-mixed material is reported to be similar to that of the untreated soil. Some slight increases and decreases have been reported, depending on the organic content of the untreated soil and the mixing procedure used (Broms 2003, CDIT 2002, CDM 1985).

- Much of what is known about embankments founded on DMM columns has been summarized in three references: EuroSoilStab (2002), CDIT (2002), and Broms (2003). These references describe slope stability analysis methods that are based on limit equilibrium approaches.

- The stability of systems with DMM columns is often analyzed using a representative strength for the DMM zone, s_{dmz}, based on the shear strength of the untreated soil within the zone, s_{soil}, the shear strength of deep-mixed material, s_{dm}, and the area replacement ratio, a_s. The area replacement ratio is the ratio of the area of deep-mixed material to the total area of the zone with DMM improvement.

$$s_{dmz} = s_{dm} a_s + s_{soil}\left(1 - a_s\right) \tag{2.1}$$

- Limit equilibrium methods only account for shear failure of the columns and do not capture other potential modes of failure of individual columns, which include bending, tilting, translation, crushing, and flow of the untreated soil around the DMM columns.

- Stability evaluations for shear walls should include vertical planes of weakness to account for joints at column overlaps. Slippage along these joints can cause a racking failure of the panels. Sources from the literature indicate that a shear strength

corresponding to 50% of the design shear strength for the DMM zone is appropriate for modeling these joints (Broms 2003, CDIT 2002).

- Few case histories have been published that document slope stability issues for embankments and slopes on deep mixed foundations. The results of three series of centrifuge tests have been published that evaluate the performance of DMM columns with embankment-type loading (Miyake et al. 1991, Kitazume et al. 1996, Inagaki et el. 2002).

The important findings from the research presented by Navin (2005) for assessing the stability of levees and embankments with DMM shear walls are:

- Guidelines are provided for using the FLAC finite difference software to analyze the stability of embankments on DMM columns. The guidelines recommend using short-term, "end-of-construction" analyses with Mohr-Coulomb undrained strengths, elastic moduli, and a Poisson's Ratio slightly lower than the theoretical value of 0.5 for undrained loading of saturated soil. Guidance is also provided for the determination of initial stresses for the model, discretization of the mesh, incremental loading, boundaries, and calculation of factor of safety using the strength reduction technique.

- Numerical stability analyses performed using FLAC with the approach described by Navin (2005) achieved relatively good agreement with the results of the series of centrifuge testing on a column-supported caisson (Kitazume et al.1996), and the series for a column-supported embankment (Inagaki et al. 2002). For both centrifuge testing series, the treatment configuration of the DMM zone consisted of a group of isolated columns.

- Numerical stability analyses performed using FLAC with the approach described by Navin (2005) achieved relatively good agreement with the observed displacements of the test embankment at the I-95/Route 1 Interchange in Virginia.

- Two-dimensional numerical deformation analyses performed using FLAC with the approach described by Navin (2005) achieved relatively good agreement with three-

dimensional numerical deformation analyses. Three dimensional numerical stability analyses were not performed due to excessive computation times for the factor of safety routine for the FLAC 3D model.

- Numerical stress-strain analyses are recommended for assessing the stability of embankments on group column-type configurations of isolated DMM columns to evaluate the potential failure modes not captured by limit equilibrium analyses.

- Reliability methods are recommended for their ability to reflect the high variability of the deep-mixed material as well as the potential for typical variations in the strength of the untreated clay soil in the DMM zone to induce tensile failure in the individual columns. This aspect is of particular importance for capturing the bending failure mode of isolated columns.

- At the same area replacement ratio, DMM shear walls are much more effective than isolated columns at improving embankment stability. This difference can be demonstrated with numerical analyses, but not with limit equilibrium slope stability.

2.1.2. Smith (2005)

This dissertation focused on topics related to the settlement of embankments founded on group column-type DMM configurations, where isolated columns are installed within the zone of treated ground with no overlap between columns. The literature review performed by Smith (2005) provides a more detailed discussion of the material properties of deep-mixed materials, citing many of the same references and presenting many of the same general findings as those discussed above.

Smith provides a definition of the area replacement ratio, a_s, which can be calculated based on the area of deep-mixed material within the DMM element, A_{dm}, and the area of the soil associated with the deep-mixed element, A_{soil}. In the context of the isolated column pattern considered by Smith (2005), A_{dm} is the cross-sectional area of the individual column, and $A_{dm} + A_{soil}$ is the tributary area associated with the individual column.

$$a_s = \frac{A_{dm}}{A_{dm} + A_{soil}} \tag{2.2}$$

The key finding of the research presented by Smith (2005) that is applicable to stability and settlement of levees and embankments with DMM shear walls is the approach she describes for performing numerical settlement analyses for the test embankment at the I-95/Route 1 Interchange in Virginia. Drained analyses using the FLAC two- and three- dimensional software achieved relatively good agreement with the observed settlements and pressure cell data from the test embankment. The treatment configuration of the DMM zone for the test embankment consisted of a group of isolated columns.

2.1.3. Deep Mixing '05

The proceedings for this conference includes numerous papers on issues related to construction, testing, and design for deep-mixed materials. Two papers in the Deep Mixing '05 proceedings on the stability of embankments and caissons on DMM foundations are of particular interest to research on levees with DMM shear walls, even though the research discussed in the papers was conducted on DMM configurations other than the shear walls considered in this dissertation. In addition, the proceedings include two papers on a full scale test section constructed for a USACE flood control levee in the New Orleans area using dry mixed soil columns.

Kitazume and Maruyama (2005) performed centrifuge testing for an embankment with the sideslope supported by a group column-type DMM configuration. The critical failure surface for the embankment without installation of the columns is a slip circle through the soft clay foundation underneath the embankment. Rather than the external failure mode of sliding that had been assumed for the system based on the standard design procedure in use at the time of the research (PWRC 1999), the columns exhibited what the authors called a collapse failure mode, where they tilted like dominoes and gave a similar failure pattern to the racking failure mode described for DMM shear walls. The factor of safety for this racking failure mode was lower than that calculated for the sliding failure mode and demonstrates the importance of considering the potential for tilting failure of the columns, and racking failure of the DMM zone, in evaluating stability of deep-mixed improved ground.

Ohishi et al. (2005) performed centrifuge testing on a caisson supported on a uniform block of DMM treated soil and compared the results from the tests with results from numerical modeling using FLAC and simplified design procedures (CDIT 2002). The authors achieved relatively good agreement between the results of the FLAC modeling and the centrifuge testing, but found that the design procedure predicted an internal failure in the DMM zone when the centrifuge and FLAC models showed stable conditions. While the results from the centrifuge testing and numerical modeling could be reproduced for this geometry using an upper bound solution, the results demonstrate the need for model testing and numerical analyses to aid in the development of a rational design method for these systems.

The full scale DMM test section for the levee in the New Orleans area described by Cali et al. (2005a, 2005b) was constructed using overlapping dry mixed soil cement DMM columns arranged in shear walls. Three configurations were tested: 1) continuous shear walls with an area replacement ratio of 20%; 2) discontinuous shear walls with an area replacement ratio of 12%; and 3) untreated ground, corresponding to an area replacement ratio of 0%. The shear walls were installed to a depth of 33 ft below the ground surface. The loading sequence for the test section included excavating a trench in front of the shear walls, and placing a dead load on top of the walls, just behind the trench. While the location of the shear surface within the DMM zone could be determined from inclinometer data, the failure mode for the DMM zone was not clear. No conclusion was reached from the results of the testing about the stability method appropriate for use in analysis, although the test section did provide information on the optimum binder design mixture, the design strength of the deep-mixed material, and the testing procedures for obtaining consistent quality assurance and control (QA/QC) data.

2.1.4. Deep Mixing '09

The proceedings for this conference also includes numerous papers on issues related to construction, testing, and design for deep-mixed materials. Two papers in the Deep Mixing '09 proceedings are of particular interest to research on levees and floodwalls with DMM shear walls.

Filz (2009) presents a simplified method for design of deep mixing support for embankments and levees. The paper discusses design considerations for developing engineering properties, configurations, and specifications for deep-mixed ground. Guidelines are provided for estimating the strength and stiffness of the deep-mixed ground for use in design. A simplified procedure for calculating factors of safety for the various failure modes associated with these systems is also presented.

Woodward (2009) discusses the quality control and verification techniques used to assess the shear strength and column continuity for deep mixed soil-cement columns constructed for USACE projects in the New Orleans area. The construction QA/QC methods evaluated by the USACE for these projects included reverse column penetration testing, pressuremeter testing, cone penetrometer testing, borehole cameras, exhumation (or excavation) of the columns, sonic drilling, coring and compressive strength testing, cross-hole seismology, and pocket penetrometer and field compression tests. While many of these methods have been used on the USACE projects constructed in the New Orleans area since 2002, coring and compressive strength testing has become the standard for deep mixing QA/QC of USACE projects in the New Orleans Area.

2.1.5. Levees and Floodwalls with DMM Shear Walls

Aside from publications on the research generated for this dissertation and on research being conducted at Virginia Tech in connection with this research (Adams et al. 2008a, Adams et al. 2008b, Adams et al. 2009, Filz 2009, Filz and Templeton 2009, Filz et al. 2010, Filz et al. 2011), very little information has been published that focuses on levees or floodwalls with DMM shear walls.

Several papers have been published on numerical analyses completed to assess the stability of a levee stabilized with a 3-m-wide, 20-m-high DMM wall oriented parallel to the levee alignment (Han et al. 2008a, 2008b, 2010). Because the orientation of the DMM wall in their numerical model results in a DMM zone with a height that is more than 6 times the width of the wall, the DMM zone would be expected to behave more like a column than like the shear walls evaluated in this research. The shear strain contours and plasticity indicators at failure indicate the wall

may have failed in a titling or bending failure mode, which are failure modes associated with isolated DMM columns.

2.2. Adaptation to Levees and Floodwalls with DMM Shear Walls

Many of the concepts presented by Navin (2005) and Smith (2005) are directly applicable to levee and floodwall systems with DMM shear walls, as summarized above. Four main topics for column-supported embankments required special consideration for adaptation to levees and floodwalls with DMM shear walls: 1) material properties of the DMM zone; 2) vertical joints in DMM shear walls; 3) failure modes for DMM shear walls; and 4) simplified methods for analysis of DMM shear walls.

2.2.1. Material Properties of the DMM Zone

For two-dimensional stability analyses of systems with DMM shear walls oriented perpendicular to the levee alignment (as shown in Figure 1-1), the DMM shear walls can be characterized as a zone of DMM improved ground (as shown in Figure 2-1) with representative material properties that consider the relative contributions of the DMM shear walls and the soft ground in between the walls.

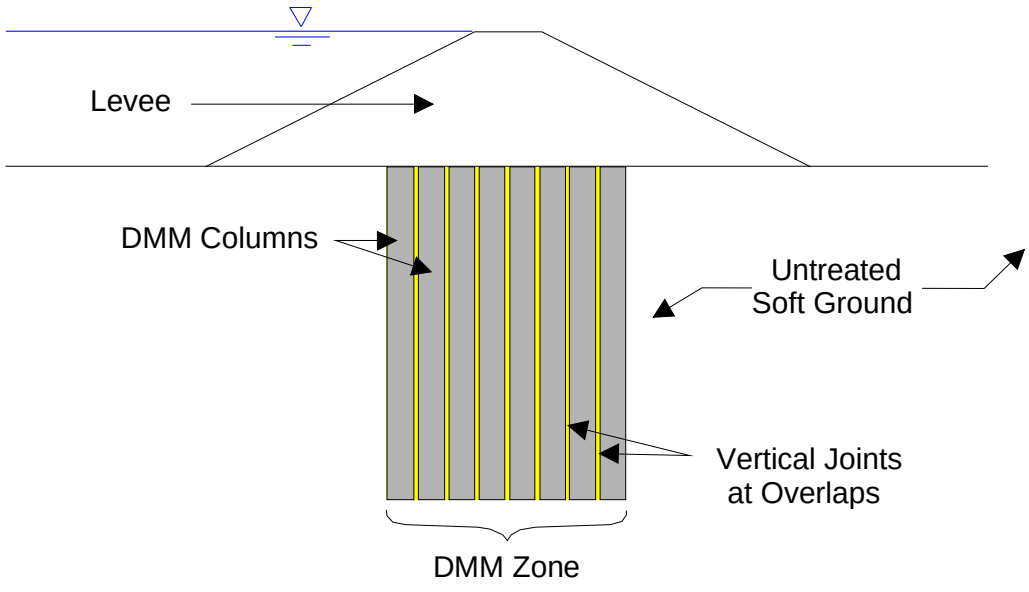

Figure 2-1. Profile of a Levee supported on DMM Shear Walls Constructed with Overlapping Columns

The material properties that are most important for levees supported on DMM shear walls are stiffness and strength. For two-dimensional analyses, the representative strength of the DMM zone is typically characterized based on an area weighted average of the shear strengths of the deep-mixed material and unimproved soil, in accordance with equation 2.1. Because the stiffness of the deep-mixed material is often several orders of magnitude higher than that of the untreated soil, and the strains required to mobilize the peak shear strength of the deep-mixed soil are typically much smaller than those required to mobilize the peak strength of the untreated ground between the walls, the strength of the untreated soil is often neglected.

For DMM shear walls constructed of overlapping columns, the geometry of the wall is often defined by the diameter of the column, the overlap distance between the columns, and the center-to center-spacing between the shear walls, as shown in Figure 2-2.

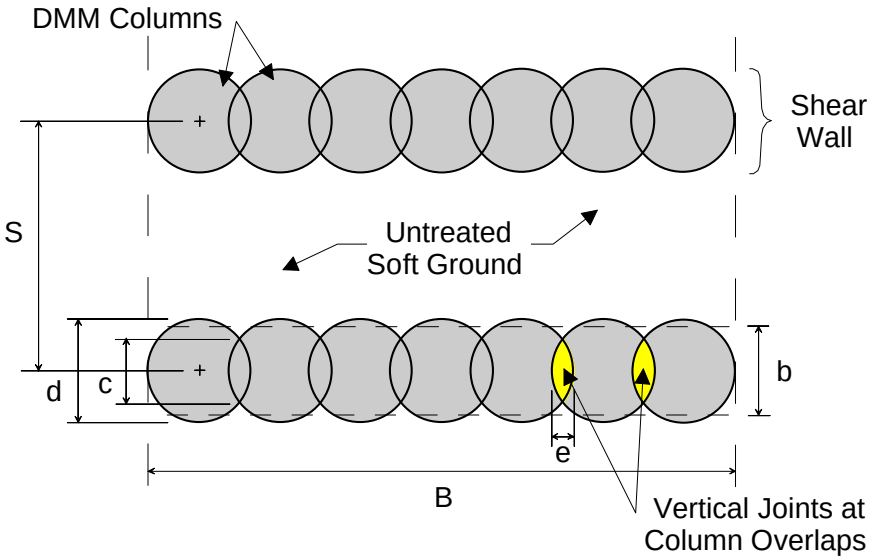

Figure 2-2. Plan of DMM Shear Wall Layout with Overlapping Columns

Filz (2009) provides the following equations for calculating the area replacement ratio within the deep-mixed zone, a_s, and the effective width of the shear wall, b:

$$\alpha = \arccos\left(1 - \frac{e}{d}\right) \tag{2.3}$$

$$a_e = \frac{2\alpha - \sin 2\alpha}{\pi} \tag{2.4}$$

$$a_s = \frac{\pi d(1 - a_e)}{4S\cos\alpha} \tag{2.5}$$

$$b = a_s S \tag{2.6}$$

where d = column diameter (ft)

e = overlap distance between columns (ft)

S = center-to-center spacing of shear walls (ft)

α = one-half the chord angle (radians)

a_e = overlap area ratio (ratio of area of overlap to area of individual column)

a_s = area replacement ratio (ratio of area of treated material to area of DMM zone)

b = effective width of the shear wall (ft)

A representative stiffness of the DMM zone, E_{dmz}, can also be calculated based on the area replacement ratio and the stiffnesses of the deep-mixed material in the shear walls, E_{dm}, and the untreated soil between the walls, E_{soil}.

$$E_{dmz} = E_{dm}a_s + E_{soil}(1 - a_s) \tag{2.7}$$

2.2.2. Vertical Joints in DMM Shear Walls

The possibility of weak vertical joints at column overlap locations is discussed in the Japanese and Scandanavian literature (CDIT 2002, Broms 2003) and is also recognized in U.S. practice (Sehn 2005). Sources in the literature suggest that vertical joint efficiencies on the order of 50% should be considered in design (CDIT 2002, Broms 2003).

A rational method for calculating the reduced strength to be applied to the vertical joints at the column overlaps is provided by Filz (2009). The shear strength at the column overlaps, $s_{dmz,v}$, can be derived based on the reduced width of the shear wall at these locations. The width of the shear wall at the location of the column overlap, c, is inherently less than the average width of

the wall, *b*, as shown in Figure 2-2. The chord length of the overlap area between adjacent columns can be calculated as:

$$c = \sqrt{2de - e^2} \tag{2.8}$$

The design strength of the DMM zone along vertical joints at the column overlap, $s_{dmz,v}$, can then be determined from the chord length, c, the strength of the deep-mixed ground, s_{dm}, the strength of the untreated soil between the panels, s_{soil}, and the spacing between the shear walls, *S*, as:

$$s_{dmz,v} = s_{dm}(c/S) + s_{soil}(1 - c/S) \tag{2.9}$$

This strength is applicable for vertical shearing along the column overlaps. Shearing through the DMM zone along any other orientation is best represented by the shear strength of the DMM zone, s_{dmz}, as calculated by equation 2.1. As with the calculation for the shear strength of the DMM zone, the strength of the untreated soil is often neglected in calculating the strength along the vertical joints.

2.2.3. Failure Modes for DMM Shear Walls

Failure modes identified in the literature that are applicable to levees and floodwalls supported by DMM shear walls are typically grouped in two categories: 1) external stability failure modes, where the DMM improved zone moves as an intact block; and 2) internal stability failure modes where failure occurs within the DMM improved zone (CDIT 2002, Filz 2009, Filz and Templeton 2009).

The external failure modes discussed in the literature include sliding and overturning or bearing capacity failures of the DMM zone, global shear surfaces that pass beneath the DMM zone, and excessive settlement either beneath the DMM zone or in the adjacent ground that can cause crest settlement and cracking of the levee The external failure modes identified in the literature are illustrated in Figure 2-3a.

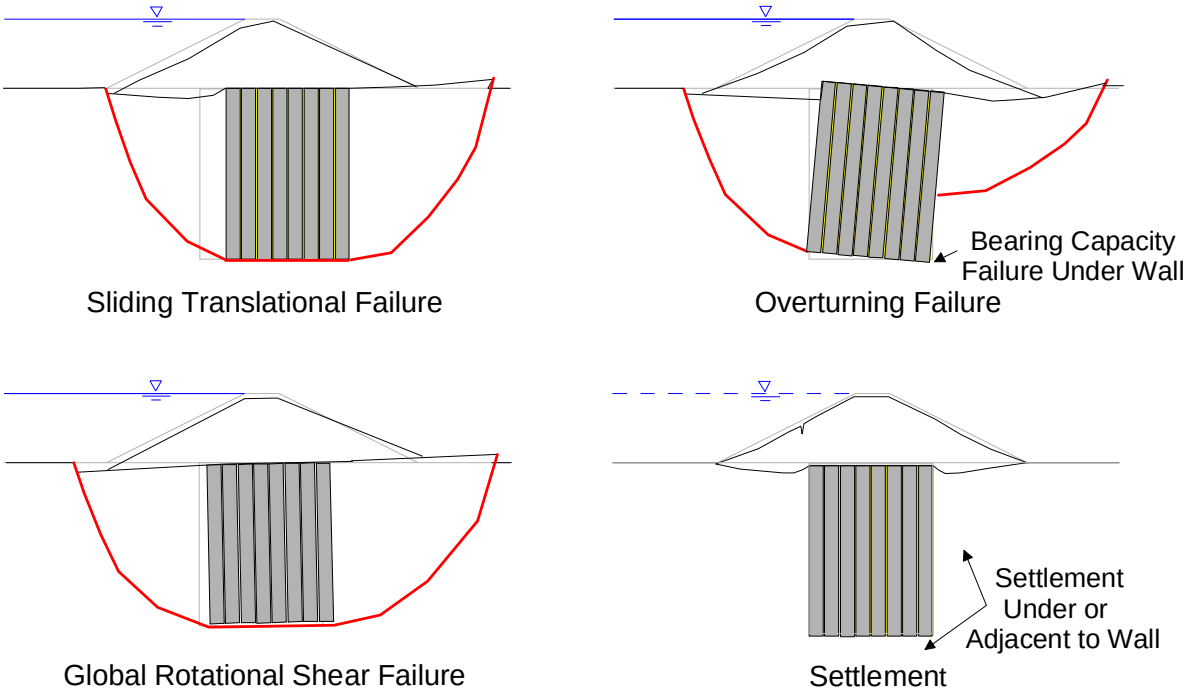

Figure 2-3a. External Stability Failure Modes

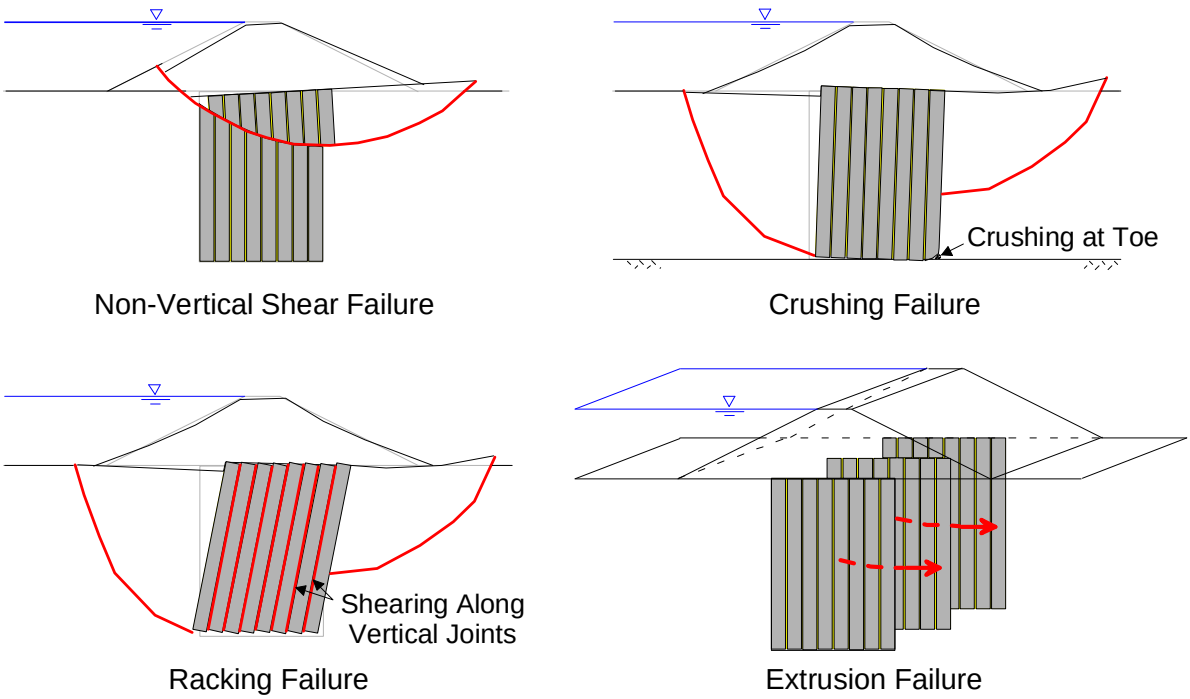

Figure 2-3b. Internal Stability Failure Modes

Figure 2-3. Failure Modes Identified in the Literature for Levees on DMM Shear Walls

The internal failure modes discussed in the literature include non-vertical shear failure through the DMM zone, crushing of the DMM material, racking failure of the DMM zone due to shearing along the vertical joints, and extrusion of the untreated ground from between the DMM shear walls. The internal failure modes identified in the literature are illustrated in Figure 2-3b.

The crushing failure mode can control when the shear walls are founded on or socketed into a relatively dense bearing layer, which forces failure of the DMM material before a bearing failure develops in the dense layer below the DMM shear walls. The extrusion failure mode is controlled by the spacing and length of the walls and is normally associated with soft clays.

2.2.4. Simplified Methods for Analysis of DMM Shear Walls

The Coastal Development Institute of Technology (CDIT 2002) describes the methodology developed by Japan's Ministry of Transport for improvement of port facilities with wall and block type deep-mixed configurations. This simplified method is cited regularly in the deep-mixing literature for the assessment of the stability of deep-mixed ground. The method provides guidance for calculating factors of safety for sliding, overturning, bearing capacity, crushing, extrusion, and limit equilibrium slip circle analysis. The method also recommends examining the potential for excessive settlement of the DMM zone.

Filz (2009), Filz and Templeton (2009), and Filz et al. (2011) present a simplified method for assessing external and internal stability of levees or embankments with shear walls that is an extension of the CDIT (2002) approach. Detailed procedures are provided for calculating factors of safety for each of the failure modes.

The three key differences between the procedure presented in Filz and Templeton (2009), relative to the procedure presented in CDIT (2002), are: 1) the factors of safety are defined in terms of the ratio of soil shear strength to shear stress, rather than the ratio of resisting to driving forces or moments; 2) the method incorporates a consistent factor of safety value for active and passive earth pressure forces as well as for bearing capacity analyses in an integrated methodology to evaluate overturning stability; and 3) the procedure includes methodology for assessing the factor of safety for a failure mode not addressed directly by the CDIT manual:

sliding on vertical planes through the DMM zone. Sliding along vertical planes through the DMM zone is the mechanism that creates the racking failure mode discussed in the previous section.

[Note: The final version of the "Design Guide for Levee and Floodwall Stability Using Deep-Mixed Shear Walls" by Filz and Templeton was published in April 2011 and incorporates findings from the research in this dissertation. References in this dissertation are to the draft version, published in February 2009, which was available at the time of this research.]

CHAPTER 3

OVERVIEW OF THE FIVE CASE STUDIES

This section provides a general description of the five case studies completed for this research. This summary is intended to provide an overview of the systems analyzed, the type of analysis completed, and the key findings for each case study. More detailed descriptions of the individual case studies are included in the following chapters of this dissertation:

- Chapter 4 - Stability Analyses of the P24 Levee
- Chapter 5 - Settlement Analyses of the P24 Levee
- Chapter 6 - Stability Analyses of the Gainard Woods Pump Station T-wall
- Chapter 7 - Stability Analyses of a T-wall on Level Ground
- Chapter 8 - Stability Analyses of the Inner Harbor Navigation Canal Reach III B-1A I-wall

3.1. Background

3.1.1. Selection of Case Studies

Five case studies were selected by the US Army Corps of Engineers (USACE) to provide a basis for analysis and design of other levees and floodwalls in Louisiana where deep mixing may be beneficial. The case studies addressed aspects of design for three projects in the New Orleans hurricane and flood protection system for which the deep mixing method was used to construct shear walls to stabilize soft foundation soils.

The original scope of work included evaluating the stability of the P24 Levee, settlement of the P24 Levee, and stability of the Gainard Woods Pump Station T-wall. Two additional case studies were added during the course of the work to address issues that could not be explored with the other three cases: (1) stability evaluation of a hypothetical T-wall similar to the Gainard Woods Pump Station but on level ground; and (2) stability evaluation of the Inner Harbor Navigation Canal (IHNC) Reach III B-1A I-wall.

3.1.2. General Approach

Numerical stability and settlement analyses were completed using the two-dimensional finite difference program FLAC (Itasca 2005) with a composite strength within the DMM zone. The composite strength was based on the strength of the deep mixed material in the shear walls and the strength of the unimproved ground between the walls.

For the stability analyses, vertical joints were included in the DMM zone to model potential weak joints between the DMM columns that comprise the shear walls. The possibility of weak vertical joints at column overlaps is discussed in the deep-mixing literature and recognized in U.S. practice. DMM shear walls constructed by overlapping columns are weaker along vertical planes at the column overlaps due to the reduced width of the shear wall at these locations. In addition, the strength at the column overlap could be further reduced by horizontal and/or vertical misalignment during construction. The influence of strength achieved at the column overlap on stability of the system was evaluated by varying the joint strength over a range extending from that corresponding to the full design mixture strength applied to the full design column overlap (100% efficiency) to that corresponding to the untreated soil for no overlap between the columns (0% efficiency). Depending on the prevalence and strength of these vertical joints, complex failure mechanisms can occur, such as racking due to slipping along vertical joints between adjacent column installations in the shear walls. Numerical, stress-strain analyses were used for the stability evaluations because they can capture these complex failure modes; whereas limit equilibrium methods typically used for evaluating slope stability only account for a composite shearing failure mode.

3.1.3. Validation

The methodology used in the numerical analyses was adopted based on previous research on the stability and settlement of embankments on DMM foundations (Navin 2005, and Smith 2005). The methodology for stability analyses was validated by Navin (2005), who compared the results from numerical analyses with the results from two series of centrifuge testing and with the observed displacements of the test embankment at the I-95/Route 1 Interchange in Virginia. The methodology for settlement analyses was validated by Smith (2005), who compared the results from numerical analyses with observed displacements of the test embankment at the I-95/Route

1 Interchange in Virginia. In addition, the studies found good agreement between the deformation (Navin 2005) and settlement (Smith 2005) predicted using two-dimensional and three-dimensional numerical analyses.

The results of the numerical slope stability analyses for this investigation of levees and floodwalls supported by deep-mixed shear walls were validated by comparing the results from numerical analyses with those obtained from limit-equilibrium analyses for the failure modes that could be captured by both methods. The limit equilibrium slope stability analyses that were completed during design by the USACE for the P24 levee and the Gainard Woods Pump Station T-wall, and by BCD for the Reach III B-1A I-wall, used the Method of Planes (USACE 2002) for wedge failure surfaces. The limit-equilibrium slope stability analyses that we completed for this investigation used Spencer's Method as implemented in the UTEXAS3 and UTEAXS4 computer programs (Wright 2001) for circular and non-circular failure surfaces.

Additional validation of the numerical analyses for this project was achieved using simplified models to validate components of the complex levee and floodwall systems. For the P24 levee project, the unbalanced lateral load corresponding to racking failure for a simplified numerical model of a DMM zone with a single vertical joint was compared with the calculated value from a closed form solution. For the T-wall deformation and stability analyses, the results of lateral and axial loading for a simplified numerical model of a single, vertical pile were compared with response curves from lateral and axial pile analyses to validate the methodology for assigning pile springs in the FLAC program. For the settlement analyses, the results of simplified, one-dimensional and two-dimensional numerical models of a footing on a uniform clay foundation were compared with those obtained from consolidation theory and chart solutions to validate the methodology for assigning soil moduli and boundary conditions. Some of these component validation studies will be documented in future publications.

In addition, the results of the numerical analyses were compared with the results of other analysis methods, such as simplified procedures for analyzing stability of DMM shear walls (Filz and Templeton 2009) and conventional settlement calculations, to assess the ability of these other methods to account for the complex response of DMM support systems, as disclosed by the numerical analyses. The comparison with conventional settlement calculations is described in

Chapter 5 and the comparison with simplified procedures for analyzing stability is described in Chapter 8.

3.2. Summary of Case Studies

3.2.1. Stability Analyses of the P24 Levee

This case study evaluated the stability of the P24 Levee using both limit equilibrium and numerical analyses, and it compared the results with those from the stability analyses performed by the USACE during their design process.

The new P24 levee structure was constructed on the protected side of an existing levee and floodwall system. Reconstruction included installation of DMM shear walls in the foundation of the levee segment between stations 408+00 and 427+00, where a narrow levee footprint was needed due to the close proximity of an existing roadway. For this segment of the levee, shear walls were constructed perpendicular to the levee alignment by overlapping dry-mixed, single-axis DMM soil-cement columns. The shear walls are 40 ft deep, 35 ft long, and positioned at a 7 ft center-to-center spacing in the direction of the levee alignment. The columns that comprise the walls are 31.5-in. diameter, and the specified overlap between adjacent columns is 6 in. The crest of the new levee has a design elevation of +17 ft. The ground surface elevation is +0 ft on the flood side of the levee and +1 ft on the protected side. The design cross-section for the P24 levee is shown in Figure 3-1.

The cross-section and material properties used by the USACE for their Method of Planes limit-equilibrium slope stability analyses were used in this investigation to provide for direct comparison between results of the numerical analyses and the USACE stability analyses. The scope of work included reviewing the Method of Planes limit equilibrium stability analysis work completed by the USACE, performing independent limit-equilibrium stability analyses for the design cross-section, and completing numerical stability analyses for the design cross-section.

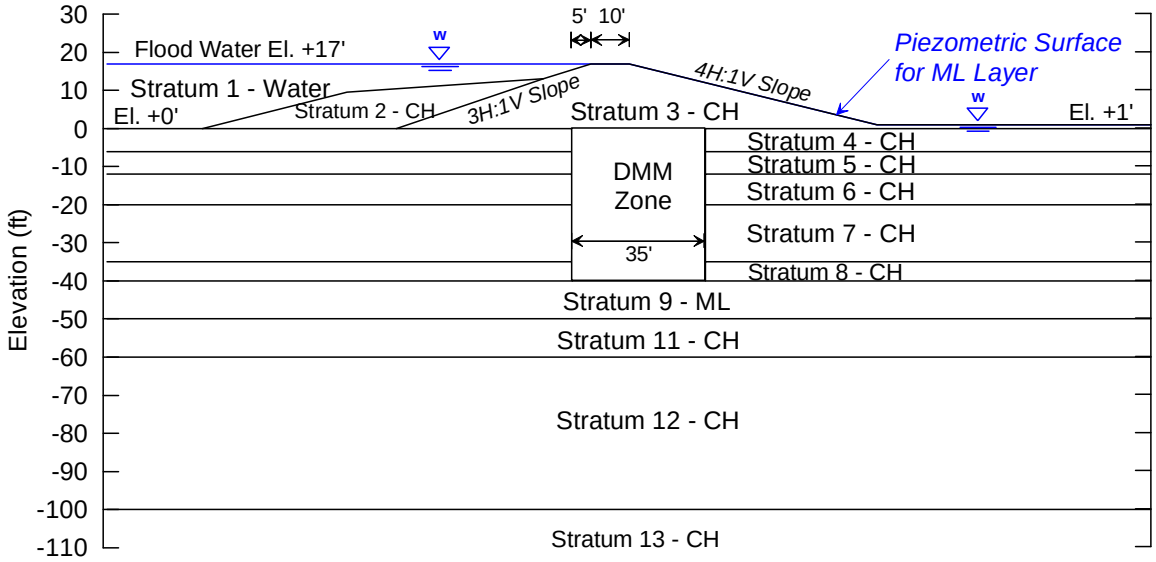

Figure 3-1. Design Cross-Section for Stability Analyses of the P24 Levee

The numerical analyses identified a deep failure mode and a shallow failure mode for the system, and they evaluated the effects of efficiency of the overlap between adjacent deep-mixed columns within the shear walls on the factor of safety for each of the failure modes. The failure surfaces for the deep failure mode pass beneath the DMM zone, and the failure surfaces for the shallow failure mode pass above the DMM zone on the protected side of the levee. Parametric analyses performed to evaluate the effect of vertical joint efficiency on the factor of safety considered vertical joint efficiencies ranging from 100%, corresponding to full strength of the deep-mixed material over the area of the full design overlap, to 0%, corresponding to no overlap between the adjacent columns and a joint strength equal to that of the in-situ soil. A detailed description of the analysis cross-section, material properties, analysis methods, and other aspects of this case study is included in Chapter 4 of this dissertation.

The key findings from this case study are summarized below:

- Comparison of the results from limit equilibrium slope stability analyses show that, for the shallow failure mode, the USACE minimum factor-of-safety value of 1.32 using the Method of Planes is in exact agreement with the minimum value found by the non-circular search routine in UTEXAS3 using Spencer's Method. For the deep failure mode, the USACE minimum factor-of-safety value of 1.31 using the Method of Planes is

substantially less than the minimum value of 1.51 from UTEAXS3 using Spencer's Method.

- The results from numerical stability analyses results show that the factor of safety values for shallow failure surfaces above the DMM zone are in good agreement with the results of the limit equilibrium analyses and only slightly dependent on the vertical joint efficiency. For the shallow failure mode, the factor of safety is 1.33 for 100% joint efficiency, and 1.29 for 0% joint efficiency.

- For the deep failure mode, the factor of safety depends on the efficiency of the vertical joints. The factor of safety from numerical analyses for deep failure surfaces is 1.51 when the vertical joint efficiency is 100%, which is in exact agreement with the results of the limit equilibrium analyses using Spencer's Method. The factor of safety when the vertical joint efficiency is 0% is 1.37, which is substantially lower than the minimum factor of safety for the deep failure mode from limit equilibrium analyses using Spencer's Method. Zero percent efficiency of vertical joints in the deep-mixed zone permits a tilting or racking type of failure mode, which is not captured by limit equilibrium analyses.

- Parametric analyses on the effect of vertical joint efficiency on the factor of safety for deep failure surfaces show that the factor of safety from numerical analyses is in exact agreement with the results of the limit equilibrium analyses using Spencer's Method when the efficiency of vertical joints between columns is at least 30%. For joint efficiencies smaller than 30%, the factor of safety decreases with decreasing joint efficiency due to increasing influence of the racking failure mode on the results. Only limited information is available in published literature about the efficiency of vertical joints at the overlaps between adjacent deep-mixed columns, but the available information indicates that a vertical joint efficiency of about 50% should be used for design. At this efficiency, the factor of safety from numerical analyses is unaffected by the racking failure mode for the conditions used for analyses of the P24 levee.

- The minimum factor-of-safety value of 1.31 from the Method of Planes limit equilibrium stability analyses for deep failure surfaces that pass beneath the DMM zone is less than the minimum factor-of-safety value of 1.37 obtained from numerical analyses for deep failure surfaces, which corresponds to a racking failure with a vertical joint efficiency of 0%.

3.2.2. Settlement Analyses of the P24 Levee

This case study evaluated the settlement behavior of the P24 levee using numerical analyses. The project is the same as that previously described for Stability Analyses of the P24 Levee, except that the cross-section for the settlement analyses was developed based on as-built information, and best-estimate material properties were selected to provide for direct comparison of the calculated settlement with field measurements. The as-built cross-section for the P24 levee is shown in Figure 3-2.

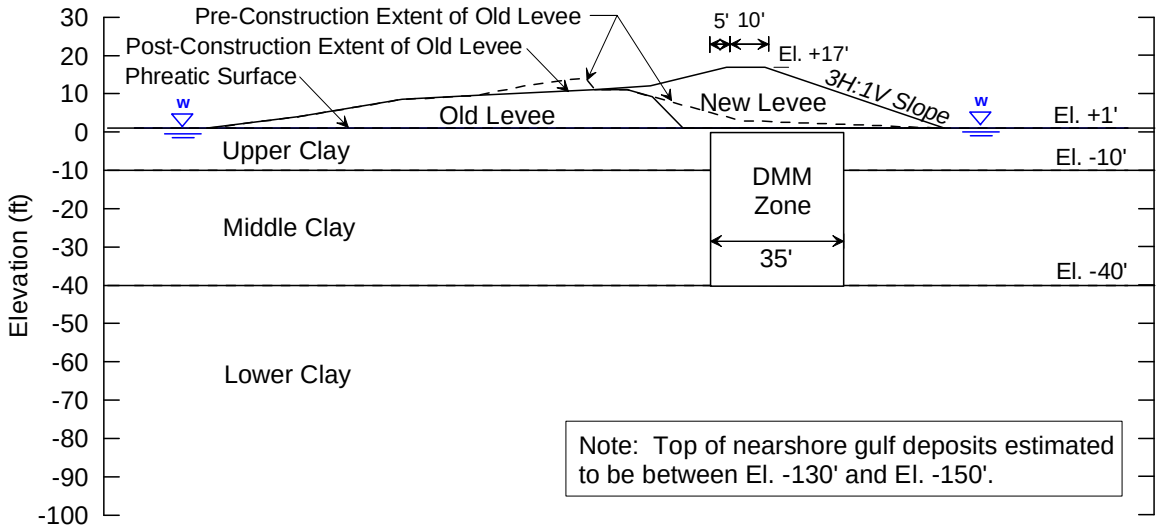

Figure 3-2. As-Built Cross-Section for Settlement Analyses of the P24 Levee

The scope of work included reviewing available information and performing settlement analyses for the as-built conditions of the P24 levee for an estimated range of consolidation properties and conditions to provide a range of predicted settlement values using numerical methods, comparing the results from the settlement analyses with settlement monitoring data provided by the USACE, comparing the results from the settlement analyses with settlement predictions from

simplified (hand calculation) methods, and making recommendations for settlement analyses of levees with DMM shear walls.

The analyses provided a range of predicted settlement values for the new levee and developed a simplified procedure for calculating settlement of the P24 levee. To determine the sensitivity of the settlement response to the model configuration, analyses were completed to assess the effect of the seepage boundary condition at the base of the new and old levees, the potential increased horizontal permeability in portions of the subsurface strata with sand and silt lenses, and the depth to the free-draining nearshore gulf deposits. A range of predicted settlement values for the levee was generated from numerical analyses using lower and upper estimates of compression index, coefficient of consolidation, and preconsolidation profile. The analyses also evaluated the potential for longitudinal tension cracks to form in the levee due to differential settlement on the protected side and the flood side of the DMM zone. Simplified hand calculations of settlement were generated considering 9 different combinations of stress concentration and stress distribution methods. The conventional one-dimensional consolidation settlement was adjusted in accordance with guidance from Skempton and Bjerrum (1957) for loads of limited lateral extent to account for pore pressures induced in the subsurface strata by shear distortion associated with immediate settlement during construction of the new levee.

A detailed description of the analysis cross-section, material properties, analysis methods, and other aspects of this case study is included in Chapter 5 of this dissertation.

The key findings from this case study are summarized below:

- For the site conditions and range of parameter values investigated for the P24 levee, predicted settlement magnitudes and rates for the levee crest are not highly sensitive to the depth of the free-draining nearshore gulf deposits, the boundary conditions specified at the base of the old and new levee fill, or the ratio of horizontal to vertical permeability in the portions of the subsurface clay strata with sand and silt lenses.

- Predicted settlement magnitudes and rates for the levee crest also remain relatively constant for the range of preconsolidation pressure profiles investigated in these analyses

because only the soil within the depth range of the DMM zone was affected by changes in preconsolidation pressure.

- The compression index values have a significant effect on the magnitude of the predicted ultimate settlement, as well as the predicted settlement for intermediate time intervals. The coefficient of consolidation values affect the calculated settlement rate, but they do not affect the ultimate settlement magnitude.

- The range of ultimate settlement of the P24 levee crest predicted from the settlement analyses is in the range from about 4 to 10 inches, with predicted settlement at 3 years in the range from near 0 to about 2 inches.

- Simplified hand calculations for settlement that evaluate the stress increase due to the new levee load using Load Case 2 and Load Distribution Case C and correcting the conventional consolidation settlement for the effect of shear distortion during load placement, as described in Chapter 5 of this dissertation, provide reasonable agreement with the numerical analyses for the conditions used to represent the P24 levee.

- None of the analyses produced tensile failure in the levee due to differential settlements.

- For the P24 levee, the existing levee reduced the amount of differential settlement of the new levee slopes beyond the flood and protected side boundaries of the DMM shear walls by decreasing the compressibility of the shallow soil layers due to pre-compression from existing levee loads. The potential for cracking due to differential settlement under the protected and flood side slopes of the levee beyond the limits of the DMM shear walls should be considered during design. A conservative estimate of differential settlement in this area could be made using simplified hand calculations to predict the settlement in the upper strata (adjacent to the DMM zone) due to the load from the portion of the levee slope that extends beyond the DMM zone.

3.2.3. Stability Analyses of the Gainard Woods Pump Station T-wall

This case study evaluated the stability of the Gainard Woods Pump Station T-wall using both limit equilibrium and numerical analyses and compared the results with those from the stability analyses performed by the USACE during their design process.

The Gainard Woods Pump Station project included a 90 ft long section of new T-wall construction west of the pump station, between stations 438+40.72 and 439+30.72. The T-wall consists of a reinforced-concrete flood wall supported on two rows of steel H-piles. The base of the T-wall is at elevation +1 ft, and the top of the T-wall is at elevation +17 ft. The flood-side piles were installed at a 1H:4V batter to a tip elevation of -71 ft, and the protected side piles were installed at a 1H:3V batter to a tip elevation of -93 ft. The design includes a sheet-pile cutoff underneath the T-wall to elevation -10.5 ft for seepage control. A zone of DMM shear walls was installed on the protected side of the T-wall, between the wall and an existing drainage canal, to improve the stability of the system. The shear walls, which are oriented perpendicular to the wall alignment, were constructed using overlapping wet-mixed, triple-axis DMM soil-cement columns. The shear walls are 30 ft long, and positioned at a 6 ft center-to-center spacing in the direction of the levee alignment. The columns that comprise the shear walls are 36-in. diameter, and the overlap between adjacent columns is 12 in. The DMM shear walls were located 30 ft from the protected side toe of the T-wall at the ground surface to provide a minimum of 10 ft of horizontal clearance between the bottom of the shear walls at elevation -55 ft and the battered piles on the protected side. This geometry leaves a gap between the DMM shear walls and the pile-supported T-wall, which created uncertainty about the effectiveness of the shear walls in improving stability of the T-wall. The design cross-section for the Gainard Woods Pump Station T-wall is shown in Figure 3-3.

The cross-section and material properties used by the USACE for their Method of Planes limit-equilibrium slope stability analyses were used in this investigation to provide for direct comparison between results of the numerical analyses and the USACE stability analyses. The scope of work included reviewing the Method of Planes limit-equilibrium slope stability analyses completed by the USACE as part of the T-wall design, completing numerical analyses to estimate the T-wall deflections and loads in the piles under design loads, completing numerical

analyses to estimate the factor of safety for the system, and completing numerical analyses to evaluate the effect of different DMM soil-cement column configurations. Two sets of subsurface strata stiffness correlations were provided by the USACE for use in the deformation analyses.

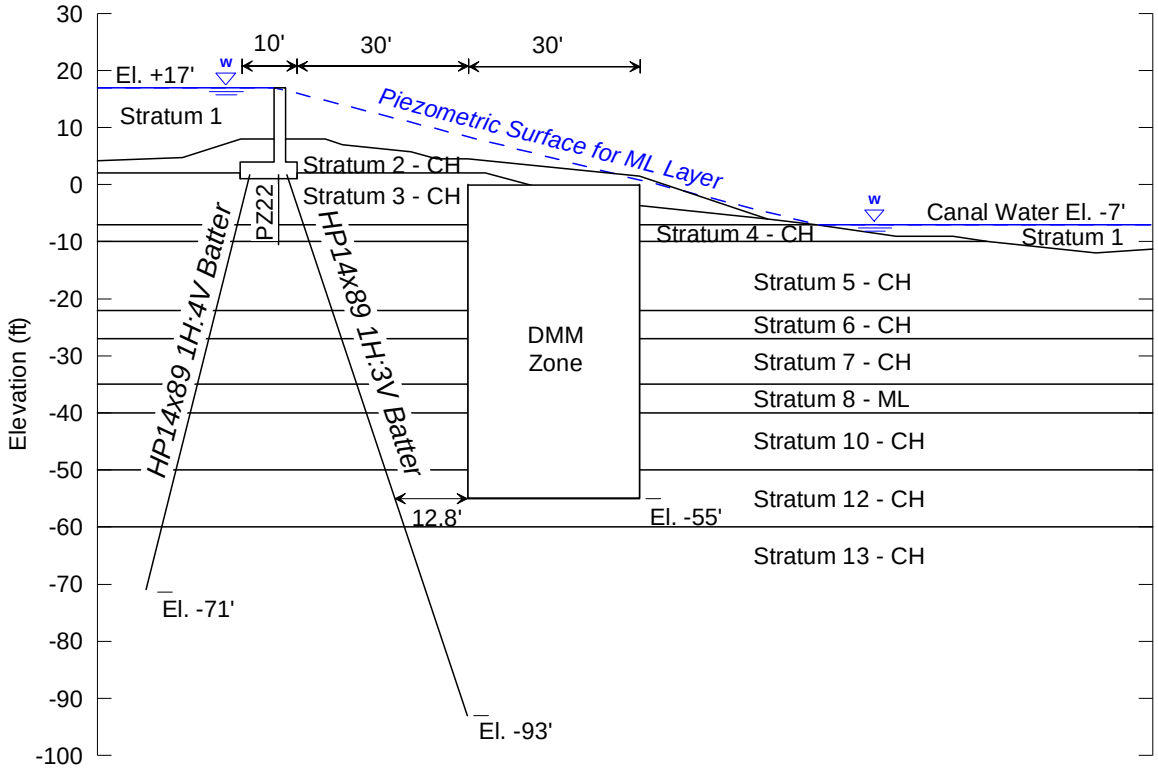

Figure 3-3. Design Cross-Section for Stability Analyses of the Gainard Woods Pump Station T-wall

The numerical analyses identified the potential failure modes for the system and assessed the effectiveness of the DMM shear wall configuration used for this project in stabilizing the T-wall. A detailed description of the analysis cross-section, material properties, analysis methods, and other aspects of this case study is included in Chapter 6 of this dissertation.

The key findings from this case study are summarized below:

- Calculated displacements of the T-wall are strongly dependent on soil stiffness. The difference in calculated displacements for the two soil stiffness profiles provided by the

USACE for use in the analyses underscores the importance of obtaining realistic soil modulus information to calculate accurate displacements of T-walls.

- Displacements of the Gainard Woods T-wall at design loads with a strength reduction factor (SRF) of 1.0, i.e., no reduction of soil shear strength from the design values, are independent of DMM vertical joint efficiency. Racking of the DMM zone did not occur in the numerical analyses under design loads at SRF =1.0, regardless of vertical joint efficiency.

- The factor-of-safety value for the Gainard Woods T-wall is only very slightly dependent on vertical joint efficiency. For 100% vertical joint efficiency, the factor of safety is 1.61. For 0% vertical joint efficiency, the factor of safety is 1.60. However, the failure mode is affected by the joint efficiency. For 100% efficiency of joints, the DMM zone rotates as a rigid block at failure. For 0% efficiency of joints, racking of the DMM shear walls occurs along the vertical joints at failure.

- The failure modes for this system are complex and cannot be captured by limit equilibrium slope stability analyses. For strength reduction factors corresponding to instability, the numerical analyses disclosed high shear strains along the flood side pile, rotation of the DMM zone as a rigid block for joint efficiencies of 100%, racking failure of the DMM zone for joint efficiencies of 0%, and a shallow rotational failure on the canal side of the DMM zone adjacent to the flood side pile.

- The factor of safety for the case with no DMM zone is 1.24, which corresponds to a shallow failure of the slope near the existing drainage canal located on the protected side. The addition of the DMM zone to the Gainard Woods analysis section shifts the critical failure mode from a shallow failure of the slope near the drainage canal to one that engages the T-wall, increasing the factor of safety of the analysis section from 1.24 to 1.61. Without the DMM zone, the slope near the canal fails before the full capacity of the pile-supported T-wall is engaged. Analyses were also performed without the designed DMM treatment zone, but with a limited zone of strengthened ground about 5 ft

deep at the location of the slope near the canal to prevent the shallow failure at that location, and the resulting factor of safety is 1.62. Thus, the increase in factor of safety due to the design DMM zone appears to be due primarily to stabilization of the shallow slope failure near the canal.

- The factor of safety for the pile-supported T-wall with the DMM zone is about 1.6, according to the numerical stability analyses. This value is substantially higher than the design factor of safety of 1.3 used by the USACE with Method-of-Planes analyses.

Because the results of the stability analyses of the T-wall at Gainard Woods Pump Station concluded that the increase in factor of safety due to the addition of DMM shear walls on the protected side of the T-wall was primarily due to stabilization of a shallow slope near the existing drainage canal, a recommendation was made to study the effects of different DMM zone configurations for a T-wall on level ground.

3.2.4. Stability Analyses of a T-wall on Level Ground

This case study evaluated the stability of a hypothetical T-wall on level ground for several different DMM zone configurations using numerical stability analyses to evaluate the effectiveness of these different configurations in stabilizing T-wall systems.

A level ground T-wall cross-section was developed based on the geometry of the Gainard Woods Pump Station T-wall design section. Numerical analyses were preformed for the T-wall and DMM system to identify DMM zone configurations that would be effective in improving the stability of the T-wall system. The scope of work included developing a level ground T-wall cross-section with a factor of safety of approximately 1.2 without a DMM zone, and completing numerical analyses to evaluate the effect of different DMM zone configurations on the factor of safety. The T-wall cross-section for the level ground study was similar to the Gainard Woods cross-section, except that the ground was level at elevation + 2 ft, the piles extended to elevation -70 ft, and the top of the T-wall and flood level was at elevation +27 ft. The cross-section developed for the T-wall on level ground stability analyses is shown in Figure 3-4.

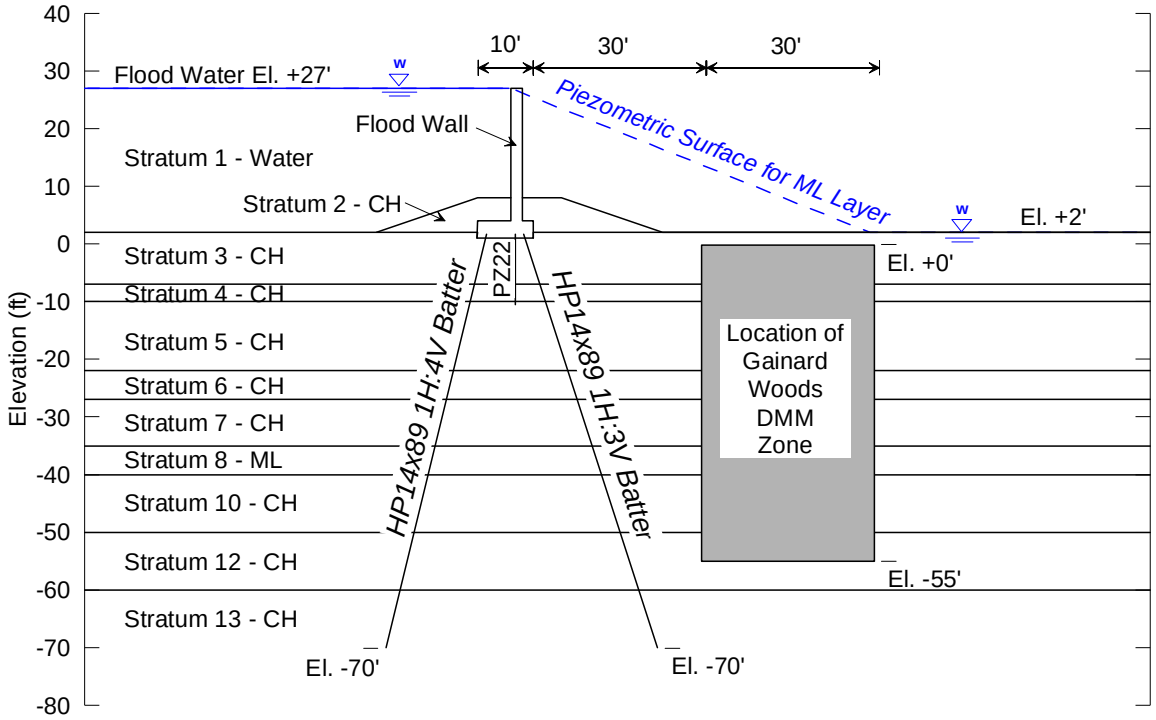

Figure 3-4. Cross-Section for Stability Analyses of a T-wall on Level Ground

Six different DMM zone configurations were evaluated for the study: 1) a single DMM zone on the protected side of the T-wall with a 10 ft horizontal gap between the DMM zone and the protected side pile; 2) a single DMM zone on the protected side of the T-wall with a 5 ft horizontal gap between the DMM zone and the protected side pile; 3) a single DMM zone on the flood side of the T-wall with a 10 ft horizontal gap between the DMM zone and the flood side pile; 4) a single DMM zone on the flood side of the T-wall with a 5 ft horizontal gap between the DMM zone and the flood side pile; 5) symmetric DMM zones on the protected and flood sides of the T-wall with a 10 ft horizontal gap between the DMM zones and the T-wall piles; and 6) a single continuous DMM zone centered underneath the T-wall. The 5 and 10 ft horizontal gaps were achieved by stair-stepping the DMM zones to maintain clearance between the walls and the battered piles.

The numerical analyses identified the relative effectiveness of the different configurations and provided guidance on how to optimize the shear wall geometry during design. A detailed description of the analysis cross-section, material properties, analysis methods, and other aspects of this case study is included in Chapter 7 of this dissertation.

The key findings from this case study are summarized below:

- The failure modes for these systems are complex and cannot be captured by limit equilibrium slope stability analyses. For strength reduction factors corresponding to instability, the numerical analyses disclosed high shear strains adjacent to the piles, around the DMM zones, and/or through the DMM zones.

- DMM zone configurations that minimize or eliminate the gap between the DMM and the T-wall result in higher factors of safety. The analyses show that the effect of a gap on the flood side is more pronounced than the effect of a gap on the protected side.

- Selecting an optimum DMM section for a given design requires considering both the desired factor of safety and the efficiency, where the efficiency of each DMM zone configuration was evaluated by dividing the increase in factor of safety by the volume of improved ground. Of the configurations included in this study, a continuous DMM zone centered underneath the T-wall is the most efficient configuration for stabilizing the wall.

- For the centered DMM zone configuration, peak efficiencies occurred for all DMM zone depths at a zone width of about 72 ft, and the efficiency decreases with increasing depth. Thus, the optimum solution for the conditions analyzed would be a 72 ft wide, centered DMM zone, with the minimum depth that satisfies a given factor-of-safety criterion.

- Alignment of the piles and DMM shear walls would have to be carefully considered before implementing a centered DMM zone in practice.

3.2.5. Stability Analyses of the IHNC Reach III B-1A I-wall

This case study evaluated the stability of the IHNC Reach III B-1A I-wall using numerical analyses, and the results were compared with those from the simplified design procedure used by Burns Cooley Dennis (BCD).

To improve the stability of the IHNC Reach III B-1A existing levee and I-wall, BCD was contracted by the USACE to design DMM shear walls for the protected side of the I-wall. The I-

wall consists of a concrete wall founded on a sheet-pile cutoff that extends to a tip elevation of -17 ft for stability and seepage control. The top of the I-wall is at elevation +13 ft, and the top of the berm on the protected side is at elevation +8.3 ft. The sheetpile cutoff consists of PZ-27 sections. The shear walls were constructed with overlapping DMM soil-cement columns. The original design of the shear walls for the Reach III B-1A section included 14-ft long shear walls that extended down to elevation -16 to -30 ft. Based on analyses performed by BCD after the construction contract was awarded, the length of the shear walls was increased to 18 ft, and the depth of the shear walls was extended to elevation -32 ft. Although the contract was not modified from the 14-ft long shear walls due to right-of-way constraints, the numerical analyses were performed using the 18-ft long shear walls to permit comparison with the results of BCD's post-award analyses. As designed, there is a 4-ft horizontal gap between the I-wall sheetpile and the DMM zone, and the top of the DMM zone is 3 ft below the existing grade of the earthen embankment on the protected side. The specifications included a minimum diameter of 31.5 in. for the individual soil-cement columns that comprise the shear walls, a minimum area replacement ratio of 30%, and a minimum horizontal overlap between any two adjacent columns such that the overlap area is at least 20% of the area of a single column. The design cross-section for the IHNC Reach III B-1A I-wall is shown in Figure 3-5.

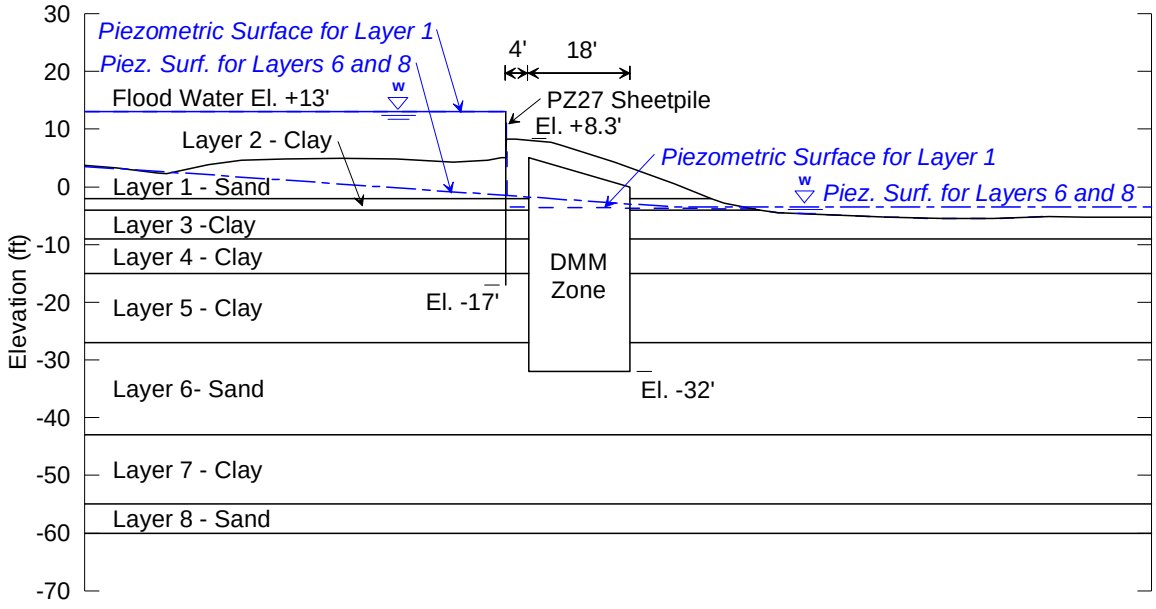

Figure 3-5. Design Cross-Section for Stability Analyses of the IHNC Reach III B-1A I-wall

The cross-section and material properties used by BCD for their Method of Planes limit-equilibrium slope stability analyses were used in this investigation to provide for direct comparison between results of the numerical analyses and BCD's stability analyses. The scope of work included completing numerical analyses to estimate the factor of safety for the I-wall system, completing a parametric study to evaluate the effects of the DMM zone strength and the efficiency of vertical joints, evaluating the potential for a water-filled gap to form behind the sheetpile during loading of the I-wall, and completing stability and deformation analyses for construction conditions to estimate I-wall deflection during installation of the DMM shear walls. In addition, the results of the numerical analyses were compared with factors of safety calculated by BCD for the Reach III B-1A I-wall using the simplified design procedure described in the "Design Guide for Levee and Floodwall Stability Using Deep-Mixed Shear Walls" prepared for the USACE by Filz and Templeton (2009).

A detailed description of the analysis cross-section, material properties, analysis methods, and other aspects of this case study is included in Chapter 8 of this dissertation.

The key findings from this case study are summarized below:

- Numerical analyses disclosed complex failure modes that could not be captured by limit equilibrium slope stability analyses. In addition to the DMM zone failure modes discussed below, the shear strain contours at failure also showed shearing on the flood side of the sheetpile and multiple zones of shearing on the protected side of the DMM zone.

- Because the DMM zone for the Reach III B-1A design cross-section was socketed into a relatively strong sand bearing layer, parametric numerical analyses identified five potential DMM zone failure modes for this system: 1) rotational failure of the DMM zone as an intact block; 2) crushing at the toe of the DMM zone; 3) near-horizontal shearing though the DMM zone at the top of the strong bearing layer; 4) full-depth racking failure along the vertical joints at the column overlaps in the DMM zone; and 5) partial-depth racking along the vertical joints in the portion of the DMM zone above the strong bearing layer.

- Two distinct racking failure modes were identified for the Reach III B-1A analysis section: partial-depth racking and full-depth racking. For the partial-depth racking failure, the vertical joints in the DMM zone do not exhibit racking deformations for the full depth of the joints, and the DMM zone exhibits a type of bending failure at the top of the relatively strong sand bearing layer. For the full-depth racking failure, the vertical joints in the DMM zone exhibit racking deformations for the full depth of the joints, and failure is induced in the sand bearing layer next to and below the DMM zone. The potential for a partial depth racking failure is not discussed in the literature and represents a new failure mode identified by this research.

- The controlling failure mode for the IHNC Reach III B-1A analysis section depends on the vertical joint efficiency and the strength of the DMM zone. For higher DMM zone strengths (3800 psf and above), rotational failure controls for vertical joint efficiencies greater than about 40%, and full-depth racking failure controls for lower vertical joint efficiencies. For lower DMM zone strengths (2300 psf and below), near-horizontal shear failure and crushing failure control for vertical joint efficiencies greater than about 70%, and partial-depth racking failure controls at lower vertical joint efficiencies. The DMM zone strength where the transition occurs between the "higher" DMM zone strength failure modes to "lower" DMM zone strength failure modes depends on the efficiency of the vertical joints.

- As described above for DMM zone strengths less than about 3800 psf, critical failure modes include near horizontal shearing through the DMM zone and partial-depth racking failure in the DMM zone. If the DMM shear walls were not socketed into the relatively strong sand bearing layer, rotation and full-depth racking failure modes would likely have controlled at all DMM zone strengths analyzed.

- The potential for increasing the factor of safety by extending the deep-mixed shear walls into a relatively strong bearing layer can be limited by internal failure modes, including near horizontal shearing and partial depth racking. These internal failure modes become less likely, and the benefit of extending the deep-mixed shear walls into the bearing layer

increases, as the strength of the deep-mixed zone and the efficiency of vertical joints increases.

- Based on a simple Rankine evaluation, the potential for a water-filled gap to form on the flood side of the I-wall sheetpile at IHNC Reach III B-1A is limited to a total vertical gap depth of less than 2 ft within the soft clay of Layer 2. Because a water-filled gap of this depth at this location would be entirely contained within the failure mass for any of the potential failure modes disclosed by these analyses, the net lateral destabilizing effect of hydrostatic water pressures in the open gap would be zero. In addition, tension cracks did not develop on the flood side of the I-wall sheetpile for any of the numerical analyses, which allowed for tensile failure of the soil elements.

- For all of the failure modes that were evaluated using both methods, the simplified design procedure (Filz and Templeton 2009) that was used by BCD resulted in lower factor-of-safety values than those from the numerical analyses. However, the factor of safety for vertical shearing calculated in the simplified design procedure is for a full-depth racking failure mode with 100% joint efficiency, and partial-depth racking is not explicitly included in the simplified procedure. According to the numerical analyses for the DMM zone design strength of 1928 psf that was established by BCD, and for joint efficiencies less than 70%, the partial-depth racking failure mode controls system behavior, and it produced factor-of-safety values that are less than the value from the full-depth racking analysis in the simplified procedure. The factor of safety for a partial depth racking failure could be determined in the simplified design procedure by calculating the factor of safety for vertical shearing in the portion of the DMM zone above the strong layer.

- When the DMM column diameter is not specified, specifying the minimum overlap between columns as a ratio of the column diameter or area is preferred to specifying a fixed overlap distance because specifying an overlap ratio allows the ratio of vertical joint strength to DMM zone strength to remain constant over a wide range of column diameters for a fixed area replacement ratio.

- The calculated factors of safety for all of the analyses completed for construction conditions are between 1.0 and 1.1, indicating that care was warranted during construction and that a restriction on the extent of mixing, as specified by BCD, was appropriate. The critical failure surface is a localized failure of the levee slope on the protected side of the sheetpile. The calculated reduction in factor of safety is about 5% for a 10% decrease in the shear strength of the DMM zone during the construction period. There is no reduction in the factor of safety for the critical surface associated with the addition of the 250 psf crane load because the crane load is outside of the critical failure surface for the construction condition. However, the addition of the crane load may reduce the factor of safety for other failure surfaces. Because the critical failure surface during construction is localized to a portion of the levee slope on the protected side, the results of the deformation analyses indicate that the displacements of the top of the I-wall should not have been greater than about ¼ in. during construction.

CHAPTER 4

STABILITY ANALYSES OF THE P24 LEVEE

This case study evaluated the stability of the segment of the U.S. Army Corps of Engineers (USACE)'s P24 levee project that included deep-mixed shear walls in the design. Limit equilibrium and numerical analyses were completed and the results were compared with those obtained from the limit equilibrium method used by the USACE in their design process. Details of the levee design section, material properties, analysis methods, and results are discussed in this chapter. Also provided in this chapter are the conclusions and recommendations specific to this case study.

4.1. Introduction

4.1.1. Purpose and Scope

The primary purposes of the stability analysis case study for the P24 Levee are to: 1) evaluate the stability of the section of the P24 levee supported on deep-mixed columns in Plaquemines Parish, Louisiana, using limit-equilibrium and numerical methods under the same conditions as used by the USACE in their stability analyses; 2) compare the results from numerical stability analysis completed for this study with USACE's Method of Planes (MOP) analyses of the P24 levee; and 3) make recommendations for future stability evaluations of levees supported on deep-mixed foundations.

The scope of work completed for this study includes:

- Reviewing the limit equilibrium stability analysis work completed by USACE.
- Performing independent limit-equilibrium stability analyses for the design cross-section.
- Completing numerical stability analyses for the design cross-section.

The levee cross-section, flood level, stratigraphy, unit weights, and strength property values for stability analyses provided by USACE are shown in Drawing 4a, "Typical Section 4 – Deep Mixing," and in a plate summarizing the MOP slope stability analyses performed by USACE.

These documents are included in Appendix A, along with Drawings 7 and 8, which provide the plan and profile of the project, including aerial photographs.

4.1.2. Project Description

USACE completed reconstruction of a section of flood protection levee known as the P24 project along the Mississippi River in Plaquemines Parish, Louisiana. The new levee structure is constructed on the protected side of an existing levee and floodwall system. Reconstruction included installation of deep-mixed columns in the foundation of the levee segment between stations 408+00 and 427+00, where a narrow levee footprint was needed due to the close proximity of an existing roadway. For this segment of the levee, shear walls were constructed perpendicular to the levee alignment by overlapping dry-mixed, single-axis columns installed by the deep mixing method. The shear walls are 40 ft deep, 35 ft long, and positioned at a 7 ft center-to-center spacing in the direction of the levee alignment. The columns are 31.5-in. diameter, and the specified overlap between adjacent columns is 6 in., which produces a center-to-center spacing of 25.5 in. and a chord length of 18.5 in. at the overlap.

The depth, length, and spacing of the shear walls, as well as the required strength of the improved ground, were established by USACE during their design process to achieve a factor of safety of 1.3 using limit-equilibrium stability analyses by means of the Method of Planes.

4.2. Analysis Section and Material Characterization

The design cross-section was provided by USACE was located in the segment of the levee alignment that included foundation improvement with deep mixing. The geometry of the section was established by USACE, and it includes the configuration of the soil-cement columns. Where differences were noted between the cross-section geometry shown in Drawing 4a (Figure A-1 of Appendix A) and the geometry shown in the plate summarizing the MOP analyses (Figure A-4 of Appendix A), such as the difference in the slope of the levee on the protected side, the geometry shown in Figure A-4 was used to allow for direct comparison between the results of this study and those from USACE's MOP analyses.

The design section used for the study is shown in Figure 4-1, and material property values are

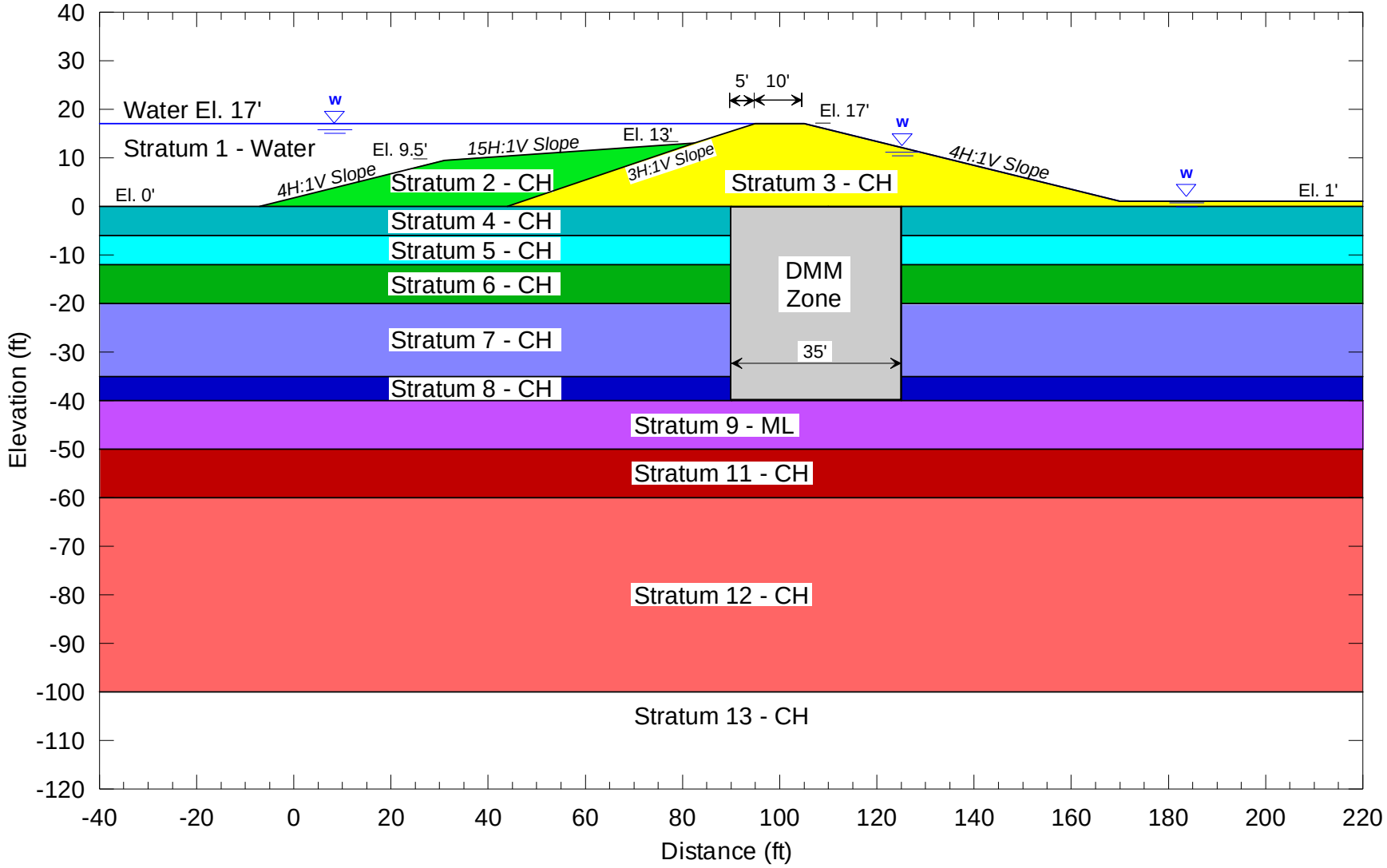

Figure 4-1. Analysis Cross-Section for Stability Analyses of the P24 Levee

Table 4-1. Summary of Material Property Values for Stability Analyses of the P24 Levee

Stratum	Elevations[1] (ft)	Unit Weight[2] (pcf)	c[2] (psf)	ϕ[2] (deg)	E[3] (psf)	ν[3]
Stratum 1 – Water	0 to 17	62.4	0	0	--	--
Stratum 2 – CH	0 to 13	100	200	0	60,000	0.45
Stratum 3 – CH	0 to 17	110	400	0	200000	0.45
Stratum 4 – CH	-6 to 0	110	400	0	200000	0.45
Stratum 5 – CH	-12 to -6	90	200	0	60000	0.45
Stratum 6 – CH	-20 to -12	100	200	0	60000	0.45
Stratum 7 – CH	-35 to -20	100	200 to 350[5]	0	60000 to 105000[7]	0.45
Stratum 8 – CH	-40 to -35	100	350 to 400[5]	0	105000 to 20000[7]	0.45
Stratum 9 – ML	-50 to -40	117	200	15	200,000	0.40
Stratum 11 – CH	-60 to -50	110	500 to 600[5]	0	150000 to 80000[7]	0.45
Stratum 12 – CH	-100 to -60	110	600 to 1000[5]	0	180000 to 300000[7]	0.45
Stratum 13 – CH	Below -100	110	1000+[5]	0	300000+[7]	0.45
DMM Zone	-40 to 0	Same as existing[4]	2300[6]	0	1150000	0.45

Notes:

1) Elevations are based on an existing ground level of 0 ft at the base of the new levee.
2) These parameter values were provided by USACE.
3) These parameter values were estimated for use in the numerical analyses.
4) The unit weight was unchanged from that assigned to the existing soil layers.
5) Cohesion increases with depth at a rate of 10 psf/ft.
6) Representative cohesion is a weighted average for the column/soil matrix within the DMM Zone, see discussion in text.
7) Young's Modulus, E, increases with depth at a rate of 3000 psf/ft

listed in Table 4-1. "Stratum 1" is the floodwater on the left-hand side, "Stratum 2" is a flood side stability berm, "Stratum 3" is the levee, and "Stratum 4" through "Stratum 13" are existing layers of soil at the site. Stratum 10 from the MOP analysis section is a thin layer located directly below Stratum 9 that allowed USACE to analyze failure surfaces that passed just below the ML layer in their MOP analyses. This stratum is not included in the analysis section for this study, as the continuous strength assignment options in the limit equilibrium and numerical analysis software used in these analyses allows surfaces to develop at the top of Stratum 11 without the need to insert a distinct layer. The location of the DMM columns that comprise the shear walls is also shown in Figure 4-1.

The location of the piezometric surface used by USACE in their MOP analyses coincides with the flood water elevation of 17 ft on the flood side of the levee and with the ground surface along the levee crest, the protected side slope, and the protected side ground surface beyond the levee, as shown in Figure 4-1. This same piezometric surface was used to calculate pore water pressures for the analyses reported here.

The material property values for the limit equilibrium analyses were provided by USACE on the plate summarizing their MOP analyses included as Figure A-4 in Appendix A. The soil strengths and unit weights did not vary horizontally across the soil strata, although the cohesion between Vert 2 and Vert 3 was raised for Strata 4 through 8 to model the increased strength in the DMM Zone. The cohesion assigned to soil Strata 7, 8, and 10 through 13 reflect a 10 psf/ft increase in cohesion with depth below elevation -20 ft. The MOP analyses modeled the impounded water on the flood side of the levee as a zero strength material. For the limit equilibrium and numerical analyses completed for this study, the impounded water is modeled as an applied pressure on the ground surface.

Additional material property values were required for the numerical analyses. Values for Young's Modulus, E, were estimated from published correlations for soil modulus based on soil plasticity and undrained shear strength (Barker et al. 1991). Poisson's ratio values for the subsurface soils and the material property values for the dry-mix columns were estimated based on guidelines provided by Navin (2005) and Filz and Navin (2006). These values are listed in Table 4-1.

4.2.1. DMM Zone Material Properties

The cohesion value of 2300 psf listed in Table 4-1 for the DMM Zone is a weighted average for the column/soil matrix. This value was provided by USACE, and it is based on a design shear strength for the DMM mixture of 50 psi, which corresponds to an unconfined compressive strength (UCS) of 100 psi. The representative cohesion for the DMM zone is a function of shear wall spacing, the average width of the wall, and the strengths of the DMM mixture and the native soils. Because peak strengths in the DMM treated ground would be expected to develop at much smaller strains than those corresponding to peak strength in the existing site soils between the shear walls, the strength of the existing site soils was neglected in establishing the representative DMM strength. Based on a shear wall spacing of 7 ft and an average width of the shear wall of 27.6 in., the composite strength can be determined as follows: (27.6 in.)(7200 psf)/(84 in.) = 2366 psf, which is approximately equal to USACE's value of 2300 psf listed in Table 4-1.

Statistical analyses were performed on strength test data provided by USACE for core samples taken from the DMM columns. A summary of the results is included in Table 4-2. A distinction is made in the table between the test results for the first set of tests run for each column and those for the testing of subsequent cores which were required when an initial test did not meet specifications. For all of the test data, the average unconfined compressive strength of the DMM mixture was much greater than the 100 psi strength used in design.

Table 4-2. Summary of Strength Test Results for P24 Levee Project DMM Cores

Test Group	No. of Tests	UCS (psi)			Sample Age (days)		
		Mean	Median	St. Dev.	Mean	Median	St. Dev.
Initial Tests	1695	305.5	270	179.1	21.6	18	10.8
Re-Tests	386	337.4	290	196.6	32.3	23	17.4
All Tests	2081	311.4	270	182.8	23.5	19	13.0

The analyses for this study were completed using the design composite DMM Zone strength of 2300 psf provided by USACE to allow for direct comparison with USACE's limit equilibrium analyses results. For the numerical analyses, the strength along vertical planes through the

DMM zone was reduced to account for the possibility of weak vertical joints in the wall at column overlaps, as described below in the Section 4.4, Numerical Analyses.

4.3. Limit Equilibrium Analyses

Limit equilibrium stability analyses were completed using UTEXAS3 (Wright 1991). The first set of limit-equilibrium analyses was conducted for comparison with the Method of Planes analyses completed by USACE, and this set was restricted to the specific non-circular failure wedge geometries evaluated by USACE. Subsequent limit-equilibrium analyses searched for critical slip surfaces using both circular and non-circular failure surfaces.

4.3.1 Review of Previous Limit-Equilibrium Analyses

The surfaces used for limit equilibrium stability analyses performed by USACE are shown in the summary of their MOP analyses in Figure A-4 of Appendix A. Based on conversations with USACE personnel, we understand that these analyses were completed using in-house software that computes factors of safety for wedge surfaces using the Method of Planes (USACE 2002). This method of slope stability analysis divides the failure mass into active, passive, and central blocks, and it assumes horizontal earth forces between blocks.

A comparison of the factors of safety calculated by USACE and those calculated using the computer program UTEAXS3 for the same failure surfaces is shown in Table 4-3. Factors of safety calculated by UTEXAS3 were obtained using the Corps of Engineers' Modified Swedish Method and Spencer's Method. Corps of Engineers' Modified Swedish Method is a force-equilibrium method where all of the interslice forces are assumed to be inclined at the same angle. A horizontal inclination was specified for these analyses to be consistent with the horizontal forces between blocks in the Method of Planes. Spencer's Method satisfies both force and moment equilibrium and it allows for non-horizontal inclination of the interslice forces.

The critical shallow failure surface located by USACE's Method of Planes analyses is surface J2, for which the factor of safety is 1.32. The critical deep failure surface located by USACE's

Method of Planes analyses is surface S1, for which the factor of safety is 1.31. The critical shallow and deep failure surfaces from USACE's MOP analyses are shown in Figure 4-2a.

Table 4-3. Comparison of Computed Factors of Safety for USACE Failure Surfaces

Surface	Computed Factor of Safety		
	Previous Analyses by USACE	UTEXAS3 Analyses	
	Method of Planes	Corps of Engineers' Modified Swedish Method [(1)]	Spencer's Method
A1	2.35	2.35	2.61
B1	4.67	4.86	5.86
C1	2.70	2.65	3.00
D1	1.73	1.94	2.09
E1	3.61	3.59	4.44
F1	2.75	2.72	3.14
G1	1.41	1.72	1.80
H1	2.75	2.73	3.45
I1	2.76	2.74	3.19
J2	1.32	1.32	1.35
K1	1.94	2.23	3.00
L1	2.97	2.96	3.54
M2	1.58	1.58	2.28
N1	1.33	1.33	1.68
O1	2.74	2.78	3.50
P2	2.18	2.17	2.67
Q1	1.34	1.34	1.72
R1	2.39	2.36	3.04
S1	1.31	1.31	1.77
T2	1.88	1.67	2.24
U1	1.83	1.83	2.80

Note: 1) This method satisfies force equilibrium only. Horizontal interslice forces were specified.

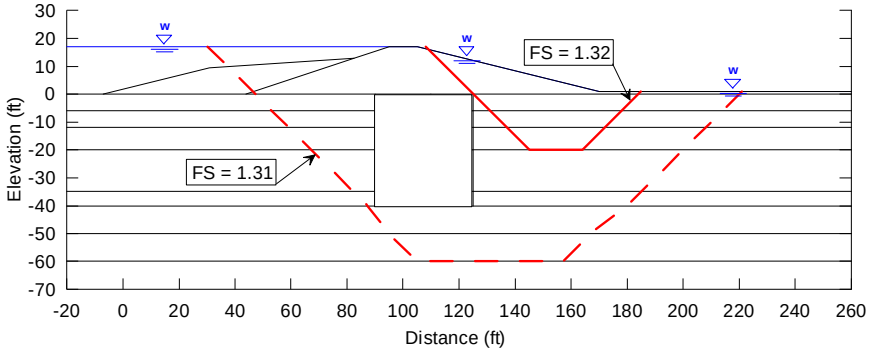

Figure 4-2a. MOP Wedge Results, Method of Planes

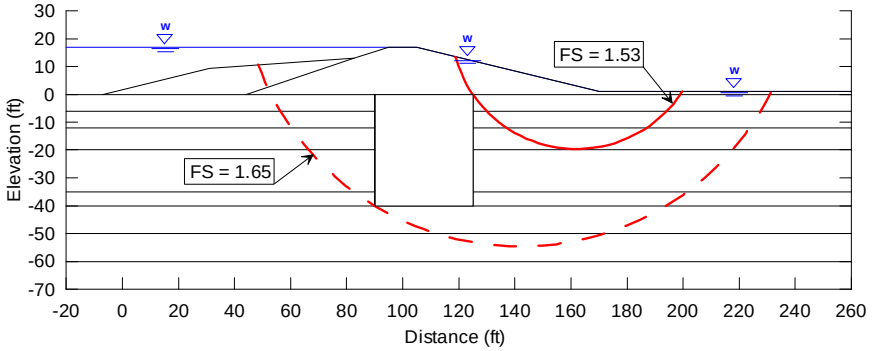

Figure 4-2b. UTEXAS3 Circular Search Results, Spencer's Method

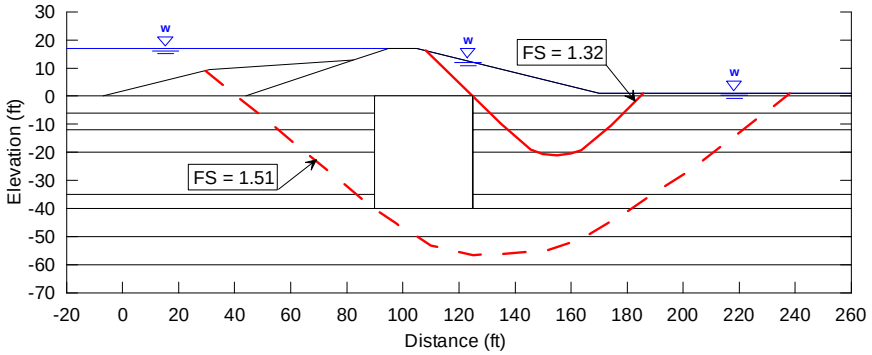

Figure 4-2c. UTEXAS3 Non-Circular Search Results, Spencer's Method

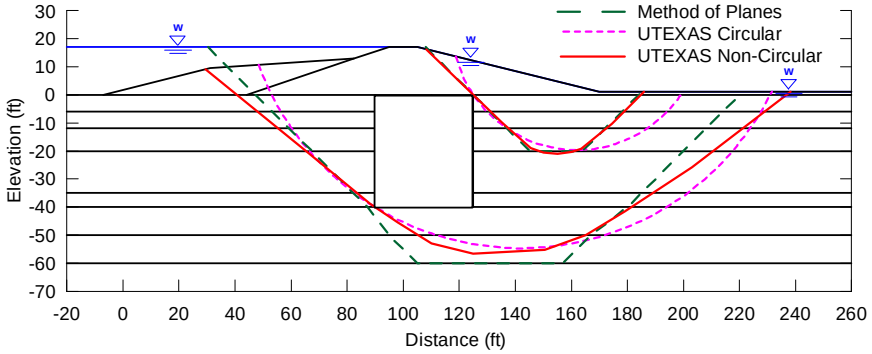

Figure 4-2d. Comparison of Critical Shallow and Deep Surfaces

Figure 4-2. Limit Equilibrium Analysis Failure Surfaces

The factors of safety obtained from the Corps of Engineers' Modified Swedish Method in UTEXAS3 are generally in good agreement with the factors of safety calculated using the Method of Planes (within a few percent), with the exception of surfaces D1, G1, K1, and T2. These surfaces cross a vertical boundary of the DMM Zone within an existing soil stratum rather than at the horizontal boundary between adjacent soil strata, and it appears that the Method of Planes program may not subdivide the failure surface where it crosses such a vertical boundary. For example, in the active wedge of failure surface K1, if a shear strength of 275 psf is used for the entire length of the shear surface from El -35 to El -20 (Stratum 7), a factor of safety of 1.94 is computed using the Corps of Engineers' Modified Swedish Method in UTEAXS3, which is in exact agreement with the result from USACE's Method of Planes for that surface.

The factors of safety obtained from Spencer's Method in UTEXAS3 are larger than the computed factors of safety from the Method of Planes or the Corps of Engineers' Modified Swedish Method for all the failure surfaces listed in Table 4-3. This is to be expected because Spencer's Method allows for friction between slices, which can increase the degree of constraint within the sliding mass and thereby increase stability.

4.3.2. Limit-Equilibrium Results from Searches using Circular and Non-Circular Surfaces

The computer program UTEAXS3 was used to search for critical circular and non-circular surfaces. The analyses were performed using Spencer's procedure. The critical surfaces are shown in Figure 4-2.

For circular surfaces, the minimum calculated factor of safety is 1.53 for a shallow failure surface located downstream of the DMM columns. For a deeper mode involving the DMM columns, the minimum computed factor of safety is 1.65. The critical shallow and deep circular failure surfaces from the UTEAXS3 analyses are shown in Figure 4-2b.

For non-circular surfaces, the minimum calculated factor of safety values are lower than for circular surfaces: 1.32 for a shallow failure downstream of the DMM columns and 1.51 for a deeper failure surface below the DMM treated zone. The critical shallow and deep non-circular failure surfaces from the UTEAXS3 analyses are shown in Figure 4-2c.

The minimum factor of safety computed for the shallow non-circular surface using Spencer's Method, 1.32, is in exact agreement with that obtained from USACE's analyses using the Method of Planes, 1.32. Although Spencer's Method would generally be expected to produce a larger computed factor of safety than the Method of Planes for a specific surface because of the additional constraint produced by inclusion of friction between slices in Spencer's Method, this trend can be offset by the ability of the automated search routine in UTEXAS3 to analyze differently shaped, and potentially more critical, surfaces than analyzed by USACE using the Method of Planes. In addition, if the inclination of the interslice forces from the Spencer's Method solution is near horizontal, then the Spencer's Method factor of safety would be approximately equal to the factor of safety from Method of Planes for the same surface.

The minimum factor of safety computed for the deep non-circular surface using Spencer's Method, 1.51, is substantially greater than the minimum value obtained from USACE's analyses using the Method of Planes deep failure surfaces, 1.31.

The critical shallow and deep surfaces from the Method Planes, UTEXAS3 circular, and UTEXAS3 noncircular analyses are shown together in Figure 4-2d.

4.4. Numerical Analyses

Numerical stability analyses of the P24 levee were completed using the finite difference computer code FLAC (ITASCA 2005). This section describes the analysis methods and the results for different assumptions of vertical joint efficiencies at overlaps of the DMM columns.

4.4.1. Analysis Methods

The mesh used for the numerical analyses extended approximately 95 ft beyond the toe of the levee on the flood side, 130 ft beyond the toe of the levee on the protected side, and 60 ft below the base of the DMM zone. The extent of the model is shown schematically in Figure 4-3 and the discretized mesh in the vicinity of the levee is shown in Figure 4-4. No lateral displacements were allowed on the left- and right-hand sides of the mesh, and no lateral or vertical displacements were allowed on the bottom of the mesh.

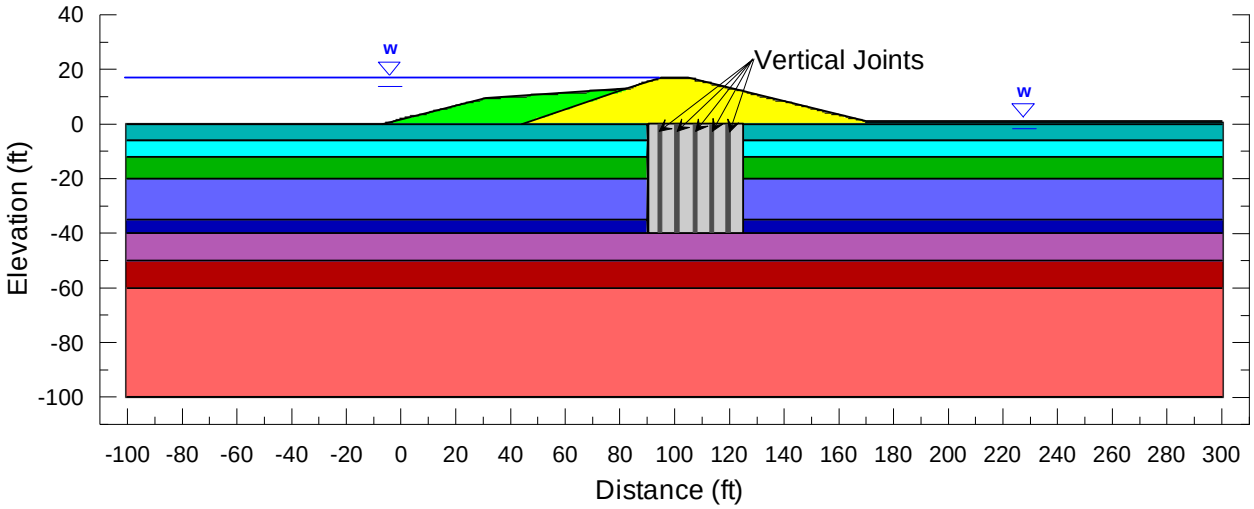

Figure 4-3. Extent of FLAC Model

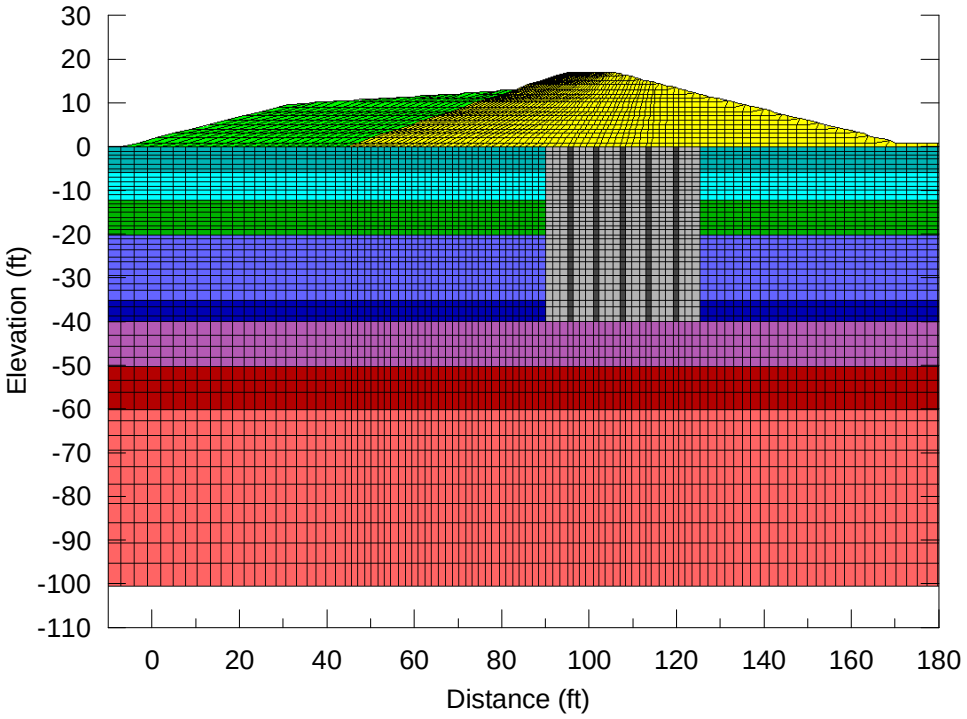

Figure 4-4. FLAC Mesh Discretization near Levee and DMM Zone

Vertical joints were included in the DMM improved zone to model potential weak joints between columns. The possibility of weak vertical joints at column overlaps is discussed in the Japanese and Scandinavian literature (CDIT 2002, Broms 2003) and is also recognized in U.S. practice

(Sehn 2005). DMM shear walls constructed by overlapping columns are weaker along vertical planes at the column overlaps due to the reduced width of the shear wall at these locations. In addition to this reduction of the composite strength inherent to the design layout, the strength at the column overlap could be further reduced by misalignment during construction. The influence of strength achieved at the column overlap on stability of the system was evaluated by varying the joint strength over a range extending from that corresponding to the full design mixture strength applied to the full design column overlap (100% efficiency) and that corresponding to no overlap between the columns (0% efficiency).

The vertical joint strength corresponding to 100% efficiency was determined based on the width of the shear wall at the location of the design column overlap (18.5 in.). Because peak strengths in the DMM treated ground would be expected to develop at much smaller strains than those corresponding to peak strength in the existing site soils between the DMM walls, the strength of the existing site soils was neglected in establishing composite vertical joint strength for 100% efficiency. Based on the design shear strength for the DMM mixture provided by USACE of 7200 psf (50 psi), neglecting the shear strength of the existing site soils, and considering that the shear walls are at a 7-ft center-to-center spacing, the composite strength on vertical planes at the column overlaps for 100% efficiency is 1586 psf, determined as follows: (18.5 in.)(7200 psf)/(84 in.) = 1586 psf.

The joint strength corresponding to 0% efficiency was set equal to the representative soil strength of 280 psf in the DMM treated zone, based on a weighted average of soil strengths along the vertical joint. This condition corresponds to no overlap between columns. The vertical joint strength for intermediate efficiencies is obtained by interpolation between the values for 0% and 100% efficiencies.

The joints were modeled by assigning FLAC's "Ubiquitous Joint" model to selected columns of elements within the DMM improved zone and assigning a vertical orientation for the reduced strength. On any other plane within the Ubiquitous Joint elements, the full composite shear strength of 2300 psf applies. The DMM improved material between vertical joints was modeled using the full composite strength of 2300 psf in all directions. The modulus of the joint material was not reduced for shearing on the vertical plane from the representative characterization for the

DMM Zone listed in Table 4-1. While the Ubiquitous Joint model does allow for a different strength assignment along a specified plane, it does not allow for the assignment of a different modulus for shearing on that plane. According to the FLAC manual, modulus values have an insignificant effect on factor of safety calculations.

Analyses were performed using 5 and 8 equally spaced vertical joints to investigate the influence of the number of such weak joints on values of factor of safety. The locations of the vertical joints shown in Figure 4-3 are for the analyses with 5 joints.

Factors of safety were calculated using an automated procedure in the FLAC program, which reduces the shear strength of all of the materials in the model by a uniform reduction factor until the program is not able to satisfy convergence criteria in a limited number of iterations. The factor of safety is the smallest reduction factor at which convergence is not achieved.

Both shallow and deep failure modes were investigated in the numerical analyses. When the factor of safety for shallow failure surfaces was less than the factor of safety for deep failure surfaces, it was necessary to slightly increase the shear strength of a block of soil crossing the shallow failure surface to investigate deeper failure modes. In these cases, a minimum shear strength of 300 psf was applied to the foundation soils underneath the downstream slope of the levee to permit investigation of deeper failure surfaces. This approach is analogous to the technique often employed in limit equilibrium analyses to avoid shallow failure surfaces when using automated search routines.

4.4.2. 100% Efficiency of Vertical Joints at all Locations

For 100% efficiency of vertical joints, the computed factors of safety are summarized in Table 4-4, and shear strain contours that illustrate the failure modes are shown in Figure 4-5. As indicated in the entries in Table 4-4 for this case, the numerical analyses resulted in computed factors of safety similar or equal to those calculated using limit equilibrium analyses by Spencer's Method with non-circular surfaces. For the shallow failure surface that passes downstream of the DMM columns, the shape of the failure surface in Figure 4-5a is similar to that determined by limit-equilibrium analyses, as shown in Figure 4-2. For a deep failure mode, the numerical analyses indicate a more complex failure mode in Figure 4-5b than that determined

using limit-equilibrium analyses, as shown in Figure 4-2, with rotation and translation of the DMM treated zone occurring in the numerical analyses. Nevertheless, the values of factor of safety for the deep failure mode from limit equilibrium and numerical analyses are the same for this case.

Table 4-4. Comparison of FS from Limit-Equilibrium and Numerical Analyses

Analysis Case	Minimum Factor of Safety	
	Limit Equilibrium	Numerical Analyses
100% Efficiency of Vertical Joints:		
Shallow Failure Surface	1.32[(2)]	1.33
Deep Failure Surface[(1)]	1.51[(2)]	1.51
0% Efficiency of Vertical Joints:		
Shallow Failure Surface	1.32[(2)]	1.29
Deep Failure Surface[(1)]	1.51[(2)]	1.37

Notes: 1) "Deep Failure Surface" refers to failure surfaces that involve significant translation, rotation, and/or racking of the DMM treated zone.
2) Value from Spencer's Method using automated non-circular search routine.

4.4.3. 0% Efficiency of Vertical Joints at Five Locations

For 0% efficiency of vertical joints, i.e., only the native soil strength due to no overlap between columns, at five locations, the computed factors of safety are summarized in Table 4-4, and shear strain contours that illustrate the failure modes are shown in Figure 4-6. For the shallow failure mode, the results of the numerical analyses show a slightly reduced value of factor safety, and a relatively minor influence of racking of the columns. For the deep failure mode, the numerical analyses show significant racking of the columns, and a more significant decrease in the value of the factor of safety, compared to the case with 100% efficient vertical joints between columns.

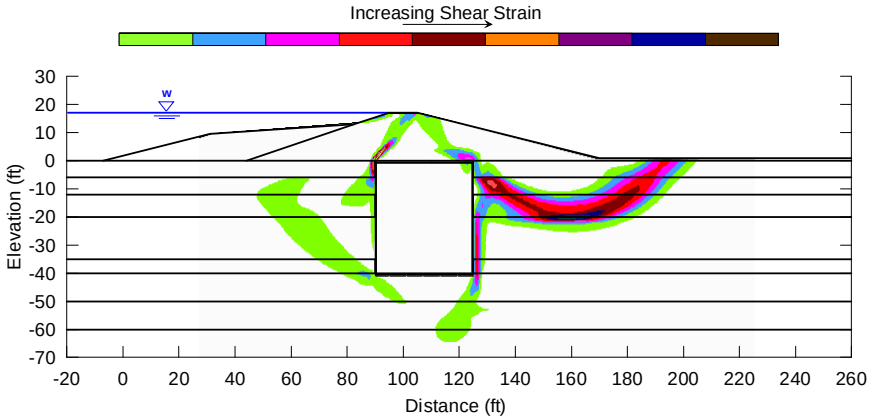

Figure 4-5a. Shear Strain Contours at Failure for Predominately Shallow Surface (FS=1.33)

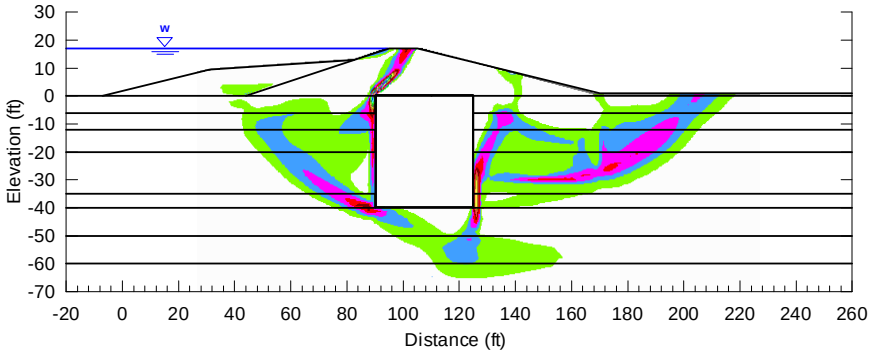

Figure 4-5b. Shear Strain Contours at Failure for Deep Surface (FS=1.51)

Figure 4-5. Numerical Analysis Failure Modes, 100% Efficiency of Vertical Joints

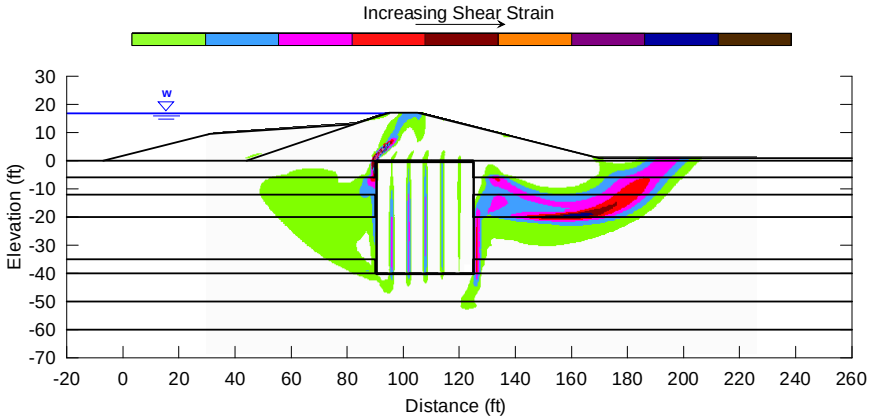

Figure 4-6a. Shear Strain Contours at Failure for Predominantly Shallow Surface (FS=1.29)

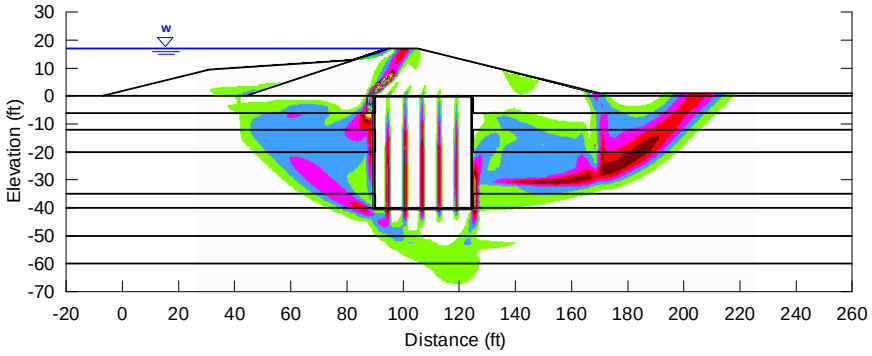

Figure 4-6b. Shear Strain Contours at Failure for Deep Surface (FS=1.37)

Figure 4-6. Numerical Analyses Failure Modes, 0% Efficiency of Vertical Joints at 5 Locations

4.4.4. Sensitivity Analysis for Efficiency of Vertical Joints

Sensitivity analyses of the factor of safety for deep failure modes were completed for vertical joint strengths corresponding to different efficiencies ranging from 0% to 100%. The sensitivity analyses were performed with 5 and 8 equally spaced vertical joint locations in the DMM treated zone. The results are summarized in Figure 4-7, which shows a decrease in the calculated value of factor of safety as the efficiency of the vertical joints decreases and racking failure becomes more likely. There is very little difference between the results for 5 and 8 vertical joints, and the racking failure mechanism ceases to control performance at vertical joint efficiencies equal to or greater than 30%, which corresponds to a vertical joint strength of about 670 psf.

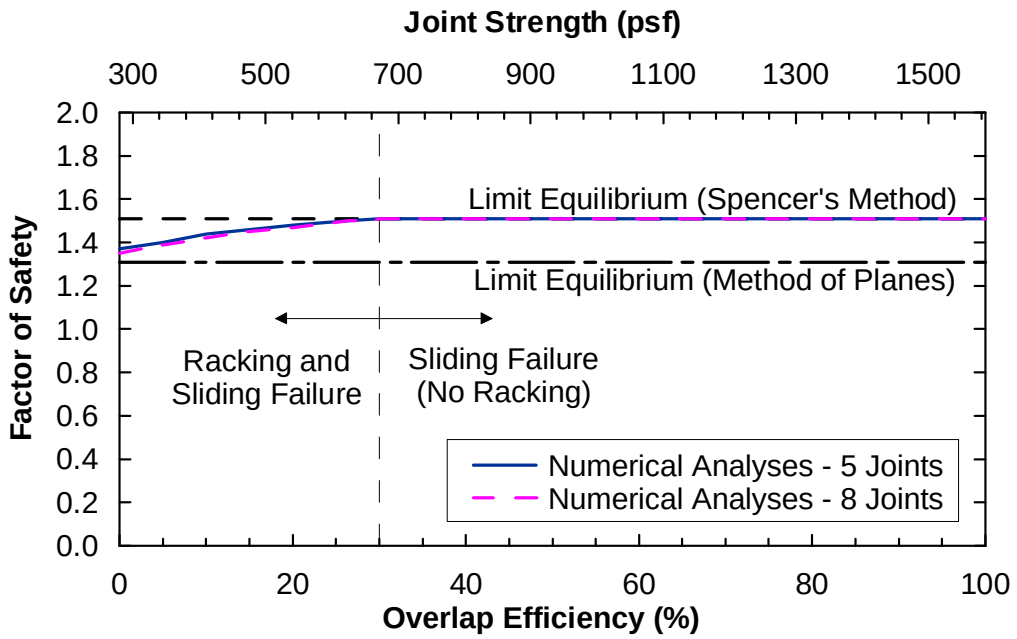

Figure 4-7. Factor of Safety Versus Joint Overlap Efficiency

Sources in the literature suggest that vertical joint efficiencies on the order of 50% should be considered in design (CDIT 2002, Broms 2003). The results in Figure 4-7 indicate that, for the conditions used to represent the P24 levee, there is no reduction in the value of factor of safety due to a reduction in the joint efficiency from 100% to 50%.

Figure 4-7 also shows the minimum values of factor of safety from limit equilibrium analyses using Spencer's Method and the Method of Planes. Spencer's Method is in agreement with the numerical analyses for vertical joint efficiencies equal to or greater than 30%. The Method of Planes produced a lower value of factor of safety than the numerical analyses, even for a vertical joint efficiency of 0%.

4.5. Conclusions and Recommendations

The following conclusions can be drawn from this study, for the conditions used to represent the P24 levee project:

- For shallow failure surfaces, the minimum factor of safety of 1.32 calculated by USACE using their in-house software and the Method of Planes compares with the limit equilibrium analyses completed for this study as follows:

    - It is in exact agreement with the minimum value of 1.32 from UTEXAS3 using the Corps of Engineers' Modified Swedish method, which satisfies only force equilibrium, with horizontal inclination of interslice forces for the same set of failure surfaces as used by USACE.

    - It is slightly lower than the minimum value of 1.35 from UTEXAS3 using Spencer's Method, which satisfies both force and moment equilibrium and allows inclination of interslice side forces, for the same set of failure surfaces as used by USACE.

    - It is less than the minimum value of 1.53 found by the circular automated search routine in UTEXAS3 using Spencer's Method, and it is in exact agreement with the minimum value of 1.32 found by the non-circular automated search routine in UTEXAS3 using Spencer's Method.

- For deep failure surfaces, the minimum factor of safety of 1.31 calculated by USACE using their in-house software and the Method of Planes compares with the limit equilibrium analyses completed for this study as follows:

    - It is in exact agreement with the minimum value of 1.31 from UTEXAS3 using the Corps of Engineers' Modified Swedish method with horizontal inclination of interslice side forces for the same set of failure surfaces as used by USACE.

    - It is substantially lower than the minimum value of 1.68 from UTEXAS3 using Spencer's Method for the same set of failure surfaces as used by USACE.

- It is substantially less than the minimum values of 1.65 and 1.51 found by the circular and non-circular automated search routines, respectively, in the program UTEAXS3 using Spencer's Method.

- Numerical stability analyses using FLAC show that the factor of safety values for predominantly shallow failure surfaces are only slightly dependent on the efficiencies of vertical joints between columns. The factor of safety values for this case decrease from 1.33 for 100% vertical joint efficiency to 1.29 for 5 vertical joints at 0% vertical joint efficiency. These values are in good agreement with the results of the limit equilibrium analyses for shallow failure surfaces, which produced minimum values of factor of safety equal to 1.32 for both the Method of Planes and the Corps of Engineers' Modified Swedish method considering the same set of failure surfaces as used by USACE, and for the critical surface from non-circular searches using Spencer's Method.

- Numerical stability analyses using FLAC show that the factor of safety values for deep failure modes involving the DMM treated zone depend on the efficiency of vertical joints between columns:

  - For 100% vertical joint efficiency, the value of factor of safety from numerical analyses is 1.51, which agrees exactly with the minimum value of 1.51 from Spencer's Method for limit equilibrium analyses of deep failure surfaces.

  - As the vertical joint efficiency decreases, the factor of safety from the numerical analyses for deep failure surfaces is constant at a value of 1.51 from 100% to 30% vertical joint efficiency, but it decreases from 1.51 at 30% vertical joint efficiency to 1.37 and 1.35 for 5 and 8 vertical joints, respectively, at 0% vertical joint efficiency due to increasing influence of racking failure mode on the results.

  - The deep mixing literature indicates that a vertical joint efficiency of about 50% should be used for design. At this efficiency, the factor of safety from numerical analyses is unaffected by the racking failure mode.

- The minimum factor of safety value of 1.31 from the Method of Planes analyses for deep failure surfaces is less than the minimum value of factor of safety from the numerical analyses for deep failure surfaces, even for a vertical joint efficiency of 0%.

Overall, it can be concluded that the Method of Planes analysis used by the USACE for design of the shear walls produced conservative results for the conditions used to represent the P24 levee project in the limit equilibrium analyses and numerical analyses discussed in this report.

The following recommendations are made:

- Until more experience with stability analyses of levees supported on DMM treated ground is obtained, it is recommended that numerical analyses be performed to investigate the potential for failure modes not addressed by limit equilibrium analyses. The numerical analysis results should be compared with the results of limit equilibrium analyses using a method satisfying force and moment equilibrium, such as Spencer's Method, and they can also be compared with USACE's Method of Planes if that approach is applied.

- The numerical results indicate that there is an influence of vertical joint efficiency on system performance. Although the effect did not appear in the P24 numerical analyses until vertical joint efficiency dropped below 30%, it is recommended that column overlap dimensions be given special attention during design and in quality assurance and quality control (QC/QA) operations during construction.

- It is recommended that reliability analyses be performed to evaluate the probability of failure. This is especially important because of the relatively high variability of deep mixed materials. It is also recommended that statistically based specifications be applied, and that high quality QC/QA operations be implemented to control and verify DMM strength during construction. Potentially useful information in this regard in presented in Filz and Navin (2006).

- The potential influence of water-filled tension cracks on stability of the P24 levee was not evaluated in this study. It would be worthwhile to investigate whether current state-of-practice methods for assessing the impact of tension cracks on stability of levees without DMM support are also appropriate and sufficient for levees with DMM support.

CHAPTER 5

SETTLEMENT ANALYSES OF THE P24 LEVEE

This case study evaluated the settlement of the segment of the U.S. Army Corps of Engineers (USACE)'s P24 levee project that included deep-mixed shear walls in the design. Numerical analyses were completed and the results were compared with settlement predictions from simplified (hand calculation) methods. Details of the as-built levee section, material properties, analysis methods, and results are discussed in this chapter. Also provided in this chapter are the conclusions specific to this case study.

5.1. Introduction

5.1.1. Purpose and Scope

The primary purpose of this study is to evaluate the settlement behavior of the P24 Levee, which is supported on deep-mixed columns in Plaquemines Parish, Louisiana.

The scope of work for this study includes:

- Reviewing available information about the as-built levee geometry, soil compressibility, and ground water conditions.
- Performing settlement analyses for the as-built conditions of the P24 levee for an estimated range of consolidation properties and conditions to provide a range of predicted settlement values using numerical methods.
- Comparing the results from the settlement analyses with settlement monitoring data provided by USACE.
- Comparing the results from the settlement analyses with settlement predictions from simplified (hand calculation) methods.
- Make recommendations, if possible, for settlement analyses of levees with DMM shear walls.

The analyses were completed using a representative as-built section for the DMM reinforced section, soil boring logs and lab testing data, and construction staging information provided by USACE.

5.1.2. Project Description

In 2006, USACE completed reconstruction of a section of flood protection levee known as the P24 project along the Mississippi River in Plaquemines Parish, Louisiana. The new levee structure was constructed on the protected side of an existing levee and floodwall system. Reconstruction included installation of deep-mixed columns in the foundation of the levee segment between stations 408+00 and 427+00, where a narrow levee footprint was needed due to the close proximity of an existing roadway. For this segment of the levee, shear walls were constructed perpendicular to the levee alignment by overlapping dry-mixed, single-axis columns installed by the deep mixing method. The shear walls were 40 ft deep, 35 ft long, and positioned at a 7 ft center-to-center spacing in the direction of the levee alignment. The soil-cement columns were 31.5-in. diameter, and the specified overlap between adjacent columns was 6 in.

5.2. Analysis Section and Material Characterization

Because the objective of these analyses is to provide settlement estimates for comparison with observed behavior, an as-built cross-section was developed for use in the analyses, as shown in Figure 5-1. The best estimate material property values for use in the analyses are listed in Table 5-1. The basis for the material properties is discussed in the following sections. The levee geometry and the subsurface stratigraphy for the settlement section were modified from the design section used for the P24 stability case study, as discussed in Chapter 4, because the goal of this study is to calculate expected settlements for the as-built conditions rather than allow for direct comparison with analyses completed by USACE during design.

5.2.1. Levee Geometry

Survey cross-sections of the pre-construction and post-construction ground surface at station 414+00 were provided by USACE. These cross-sections, as well as design drawing 4a for the segment of the P24 reconstruction that included DMM shear walls, are included in Appendix A.

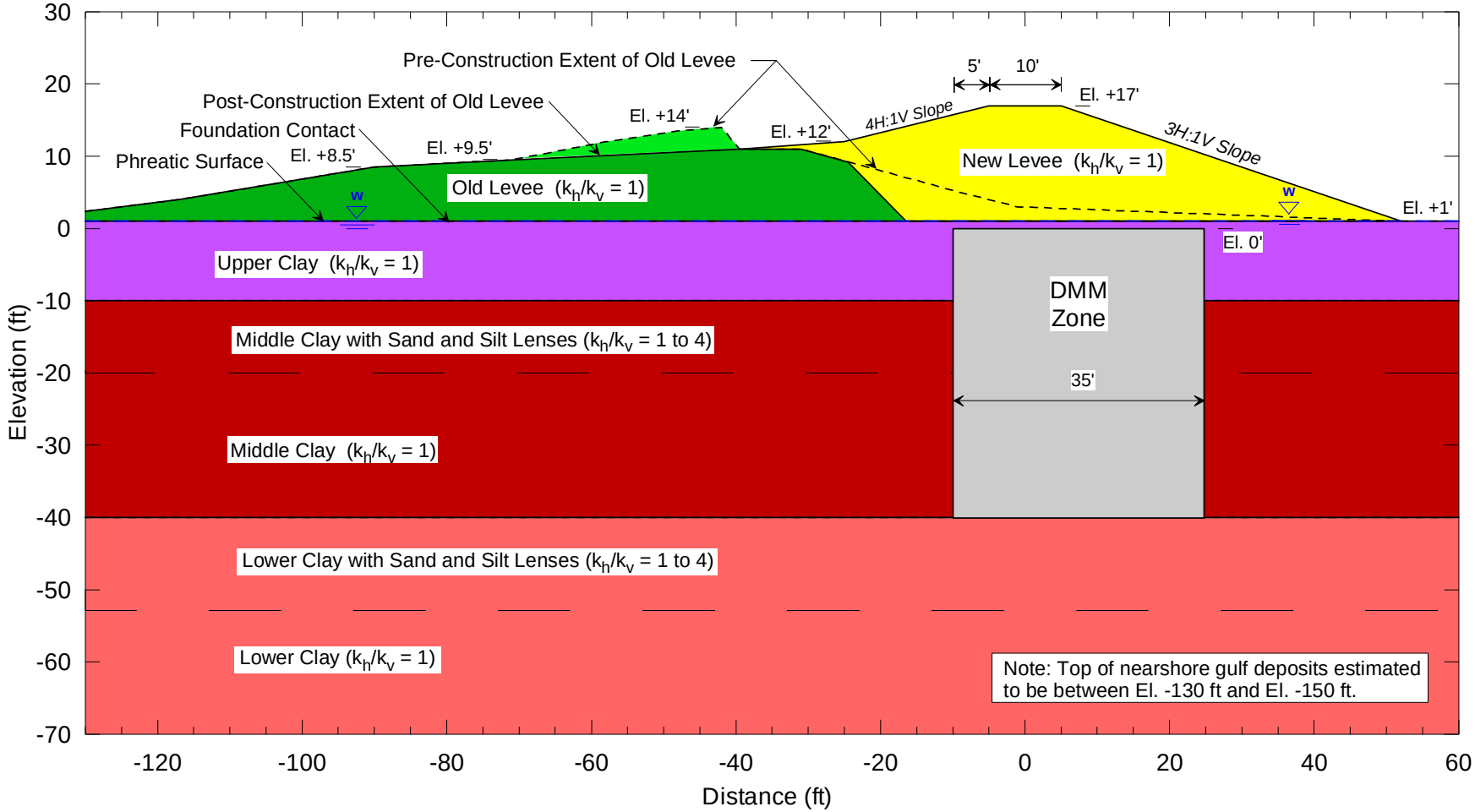

Figure 5-1. Analysis Cross-Section for Settlement Analyses of the P24 Levee

Table 5-1. Summary of Material Property Values for Settlement Analyses of the P24 Levee

Stratum	Elevations (ft)	γ_{total} (pcf)	wc (%)	ϕ' (deg)	c' (psf)	s_u (psf)	ν	C_c	C_r	G (psf)	c_v (ft^2/ day)
Old Levee	+1 to +14	125	21	-	-	2000	0.35[3]	-	-	40000[5]	-
New Levee	+1 to+17	125	21	-	-	2000	0.35[3]	-	-	40000[5]	-
Upper Clay	-10 to +1	115	35	27	0	-	0.35[3]	0.43	0.051	Varies[6]	0.4[7]
Middle Clay	-40 to -10	102	60	25	0	-	0.37[3]	0.70	0.12	Varies[6]	0.04[8]
Lower Clay	Below -40	110	43	27	0	-	0.35[3]	0.35	-	Varies[6]	0.1[9]
DMM Zone	-40 to 0	Same as existing[1]		27[2]	4260[2]	-	0.33[4]	-	-	745000[2]	Varies[10]

Notes:

1) The unit weight and water content are unchanged from the values assigned to the existing soil layers.
2) Representative DMM zone drained strength and modulus is a weighted average for the column/soil matrix within the DMM zone. See discussion in text.
3) Drained Poisson's ratios calculated based on the drained friction angle: $\nu = (1-\sin\phi')/(2-\sin\phi')$.
4) Poisson's ratio for the DMM zone estimated based on Smith (2005).
5) Shear moduli, G, for levee strata calculated based on an undrained Young's modulus of $E_u = 60s_u$ (corresponding to an OCR value of 10 in the levee) and a poisons ratio for undrained loading of $\nu_u = 0.5$: $G = E_u/(2(1+\nu_u))$.
6) Modulus values for subsurface soils were assigned to each zone, based on the effective vertical stress in the zone before construction, the change in vertical stress due to construction, the preconsolidation pressure, and the compression index for the zone. See discussion in text. Profiles of shear modulus are shown in Figure 5-8.
7) Coefficient of consolidation for upper clay corresponds to c_{vr} value from Table 5-3.
8) Coefficient of consolidation for middle clay is an average of the c_v and c_{vr} values from Table 5-3.
9) Coefficient of consolidation for lower clay corresponds to c_v value from Table 5-3.
10) Coefficient of consolidation for DMM zone not calculated. Instead, the permeability values for the DMM zone were not changed from the values assigned to the existing soil layers at the same elevation.

The geometry of the new and old levees, the DMM zone, and the foundation contact were determined based on these drawings.

5.2.2. Groundwater

The elevation of the groundwater table was established based on data provided by Mark Woodward of the New Orleans District. The average water level of the Mississippi River at Empire Lock, which is located approximately 7 miles downstream of the P24 rehabilitation project, is about El + 2 ft, based on readings between July 2007 and Aug 2008. At the P24 project, the average of water level readings in borings PSV-10UT, PSV-11UT and PSV-12UT, which are located near the centerline of the new levee crest, is about El -0.7 ft. The settlement analyses described in this report incorporate a simplified phreatic surface at elevation +1 ft, as shown in Figure 5-1.

5.2.3. Subsurface Stratigraphy and Material Properties

The subsurface soils were divided into strata, and material properties were assigned based on boring logs and laboratory test results provided by USACE for borings B-1 through B-9 and PSV-10UT through PSV-12UT. The laboratory test results for water content, liquid limit, plasticity index, and undrained shear strength are plotted versus elevation in Figures 5-2 through 5-5. Based on the trends for CH and CL materials, the subsurface soils were divided into an upper clay between El +1 ft and El -10 ft, a middle clay layer between elevations – 10 ft and -40 ft, and a lower clay layer that extends below El -40 ft. According to Mark Woodward of the New Orleans District, the lower clay layer is underlain by a relatively free draining layer of sand and silty sand, called the nearshore gulf deposits. Based on boring logs R-37, R36-2, and R36.6 in the vicinity of the P24 levee, the top of the nearshore gulf deposits is estimated to be between El -130 ft and El -150 ft.

The dry unit weights and porosities used in the numerical analyses were determined by averaging the values from test results for each soil stratum. The drained Mohr-Coulomb friction angles for the strata were obtained from correlations with the average plasticity index (PI) for each layer using correlations published by Duncan and Wright (2005). The drained Poisson's ratio was estimated based on the friction angle using the relationship $\nu = (1-\sin\phi')/(2-\sin\phi')$.

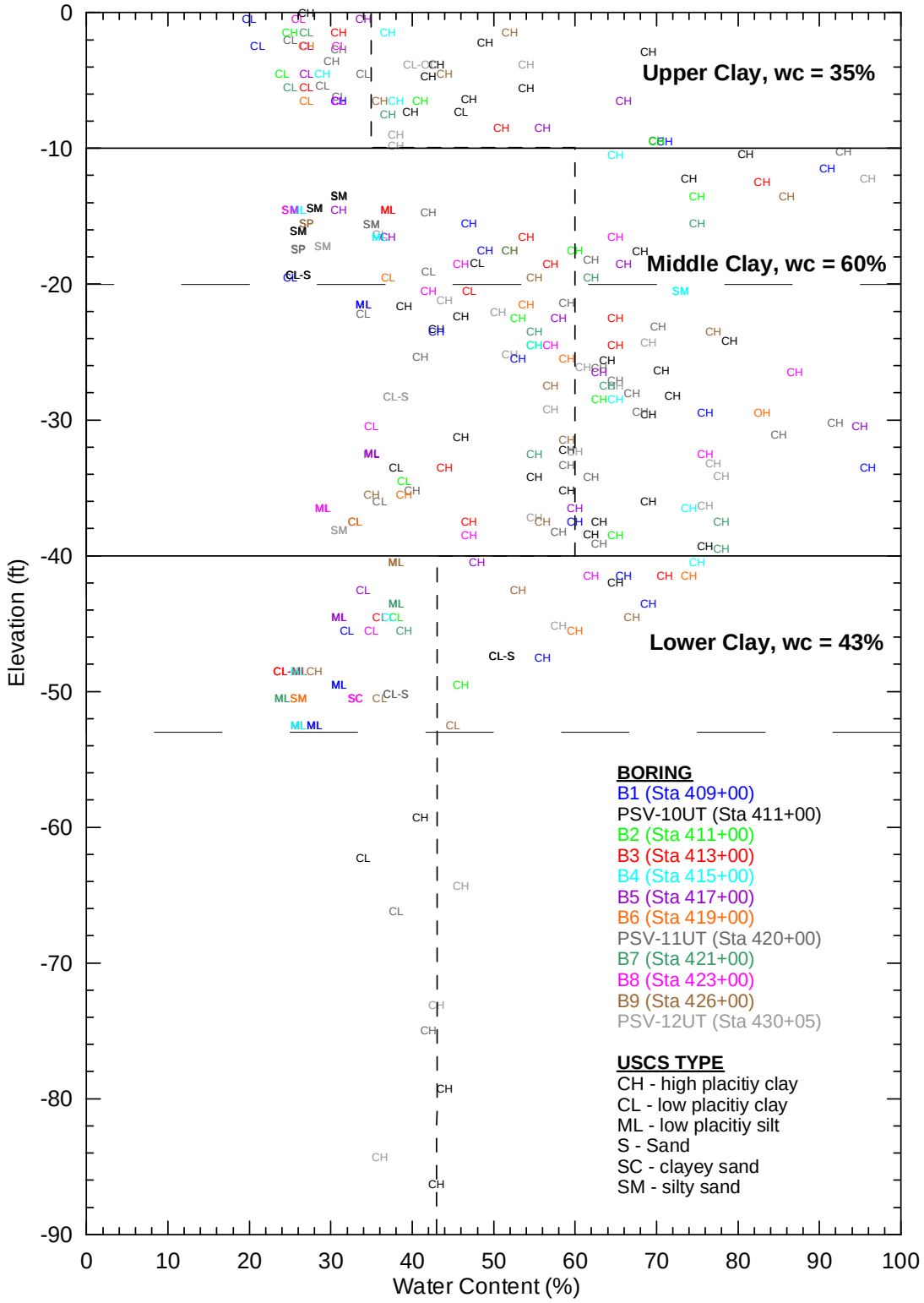

Figure 5-2. Water Content Versus Depth for Subsurface Strata

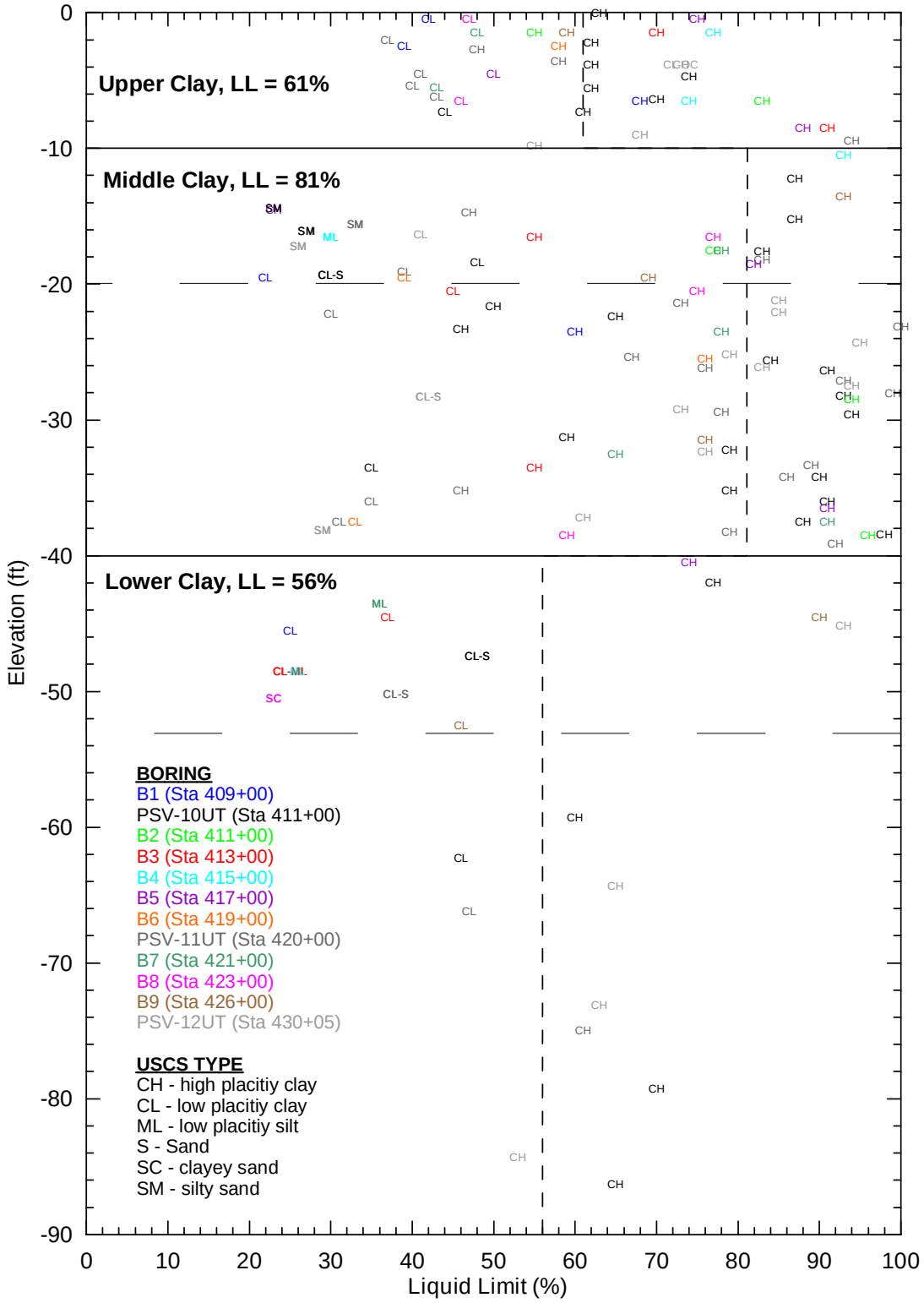

Figure 5-3. Liquid Limit Versus Depth for Subsurface Strata

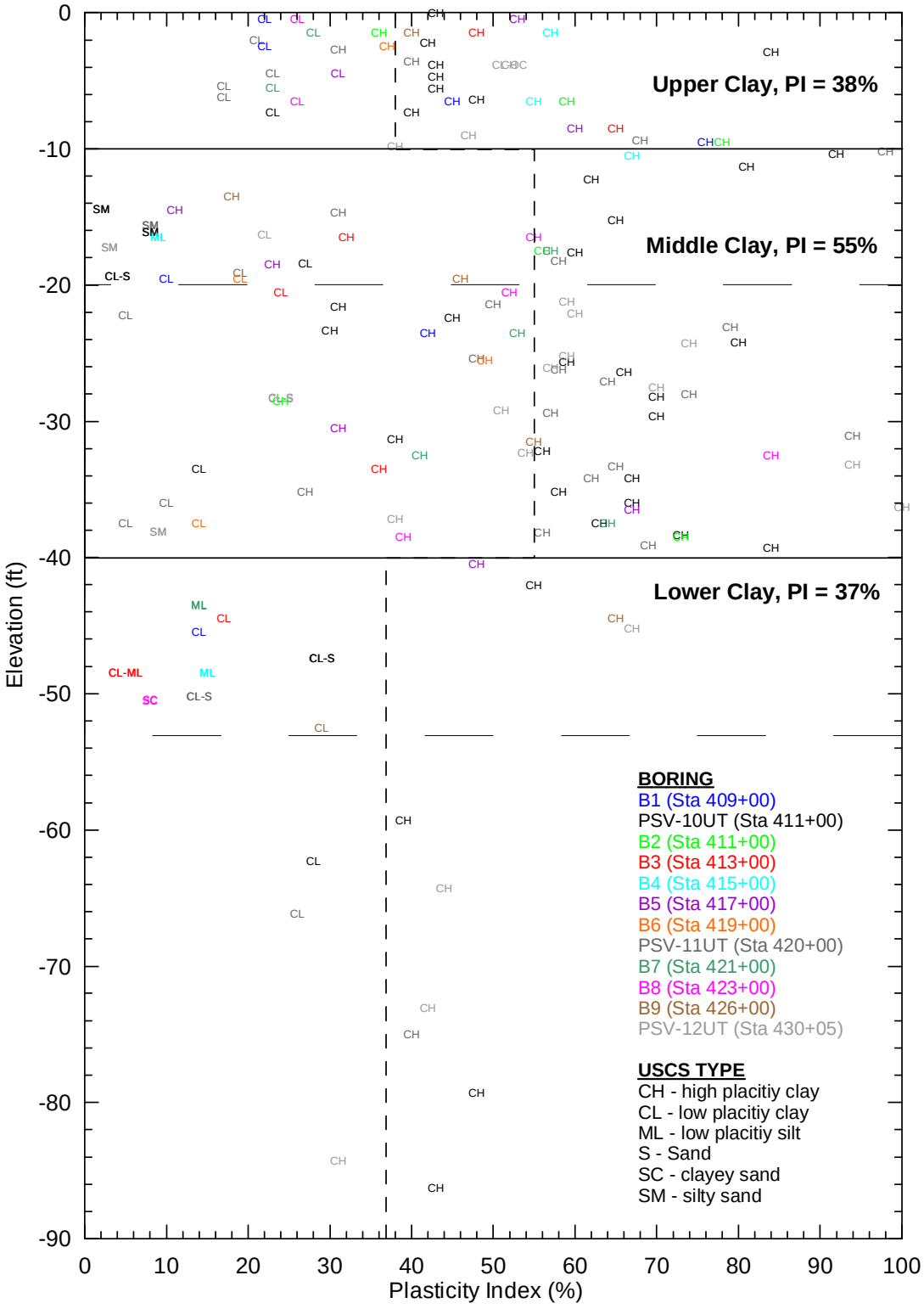

Figure 5-4. Plasticity Index Versus Depth for Subsurface Strata

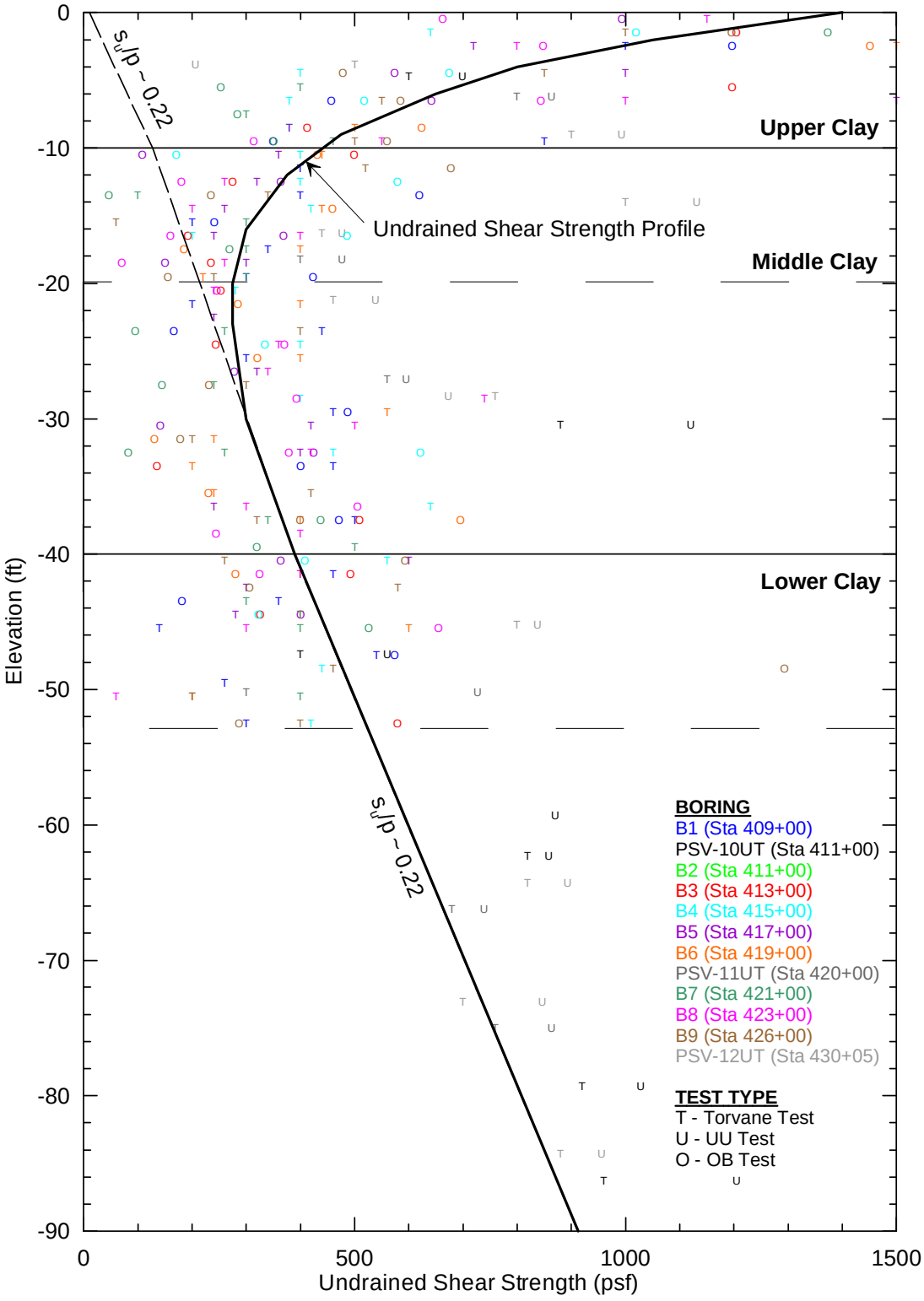

Figure 5-5. Undrained Shear Strength Versus Depth for Subsurface Strata

The compressibility of the subsurface strata was determined based on compression index values for virgin compression (C_c) and recompression (C_r) taken from consolidation tests and published correlations with liquid limit (Terzaghi and Peck 1968). Representative compression index values for the upper and middle clay layers, based on average values from interpretation of the consolidation test results and correlations, are listed in Tables 5-1 and 5-2.

Table 5-2. Summary of Compression Index Values for Clay Layers

Data Source	Elev. (ft)	e_0	Oedometer Test			Correlations				Representative Values	
			p_p (tsf)	C_c	C_r	LL	C_c[(1)]	wc	C_c[(2)]	C_c	C_r
PSV-10UT	-7.3	1.12	3.0 – 4.3	0.66	0.072	61	0.46	41	0.26	0.43	0.051
PSV-11UT	-3.6	0.89	2.7 – 3.4	0.27	0.035	58	0.43	33	0.15		
PSV-12UT	-3.8	1.58	0.5 – 0.6	0.48	0.045	73	0.57	58	0.44		
PSV-10UT	-26.4	1.89	0.9 – 1.3	0.84	0.13	91	0.73	69	0.61	0.70	0.12
PSV-11UT	-23.1	1.98	1.0 – 1.1	0.99	0.16	100	0.81	72	0.63		
PSV-12UT	-22.1	1.46	1.0 - 1.2	0.46	0.059	85	0.68	53	0.39		
Figures 5-2 & 5-3[(3)]	Below -40					56	0.41	43	0.29	0.35	

Notes:

1) Compression index obtained from correlation with liquid limit (Terzaghi and Peck 1968): $C_c = 0.009(LL-10\%)$.
2) Compression index obtained from correlation with water content (Lambe and Whitman 1969).
3) Consolidation test data was not available for the lower clay layer. Compression index for this layer is based on correlations with the average water content from Figure 5-2 and average liquid limit from the Atterberg limits test results shown in Figure 5-3.

The pre-consolidation pressure profiles for the subsurface strata are shown in Figure 5-6. The best and upper estimate profiles were determined based on the range of pre-consolidation pressures (p_p) from consolidation tests, as listed in Table 5-2. The lower estimate profile was determined from calculated preconsolidation pressures using the normally consolidated

undrained shear strength to effective stress (s_u/p) ratio of 0.22 and the undrained shear strength profile in Figure 5-5. Also shown in Figure 5-6 are initial stress and final stress profiles at four locations in the profile that demonstrate the range of stresses that occur in the subsurface strata for the model. Free field conditions are represented by the profiles for X = -250 and X = 250. The stresses beneath the old levee crest are represented by the profile for X = -45, and the stresses underneath the portion of the new levee on the protected side beyond the DMM shear walls is represented by the profile for X = 43. For the range of stresses in the FLAC model, the upper clay layer is overconsolidated, the lower clay layer is normally consolidated, and the middle clay layer transitions from overconsolidated to normally consolidated in the elevation

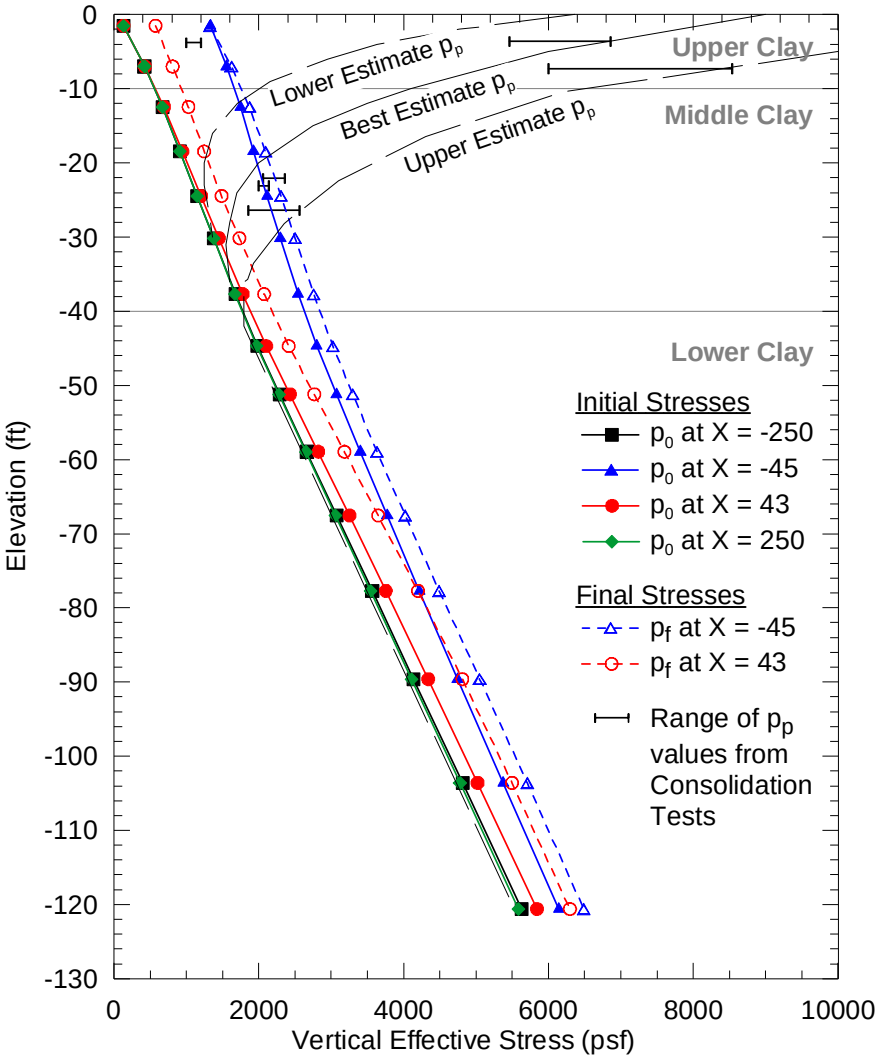

Figure 5-6. Preconsolidation and Effective Stress Pressure Profiles for Subsurface Strata

range from about El -25 to -38 ft for the best estimate p_p curve. The upper and lower estimate preconsolidation pressure curves indicate the range in preconsolidation pressures supported by the available data. The actual range in values for the subsurface conditions along the P24 levee alignment may be larger than the range shown in Figure 5-6.

Two sets of modulus values were developed for use in the numerical analyses. For the consolidation portion of the analyses, when the settlement of the levee is due primarily to vertical compression of the subsurface layers as the excess pore pressures dissipate, moduli were developed based on the compression index values listed in Table 5-1. For the construction portion of the analyses, when the immediate settlement experienced by the levee is due to distortion without volume change, moduli were based on guidance provided by Duncan and Buchignani (1987) from field observations of immediate settlement.

The moduli used to model the consolidation portion of the analyses were obtained by converting the compression index values listed in Table 5-1 to shear modulus (G) and bulk modulus (K) values through relationships with the constrained modulus (M). For each subsurface strata zone in the FLAC model, a constrained modulus was calculated based on the vertical effective stresses before and after construction of the levee, the preconsolidation profile, and the compression index. The following equations were used to calculate the constrained modulus for each individual zone:

$$M = \frac{p_f - p_0}{\varepsilon} \quad \text{where} \quad \varepsilon = \left(\frac{C_c}{1+e_0}\right)\log\frac{p_f}{p_0} \qquad \text{for } p_0 = p_p \qquad (5.1)$$

$$\varepsilon = \left(\frac{C_r}{1+e_0}\right)\log\frac{p_p}{p_0} + \left(\frac{C_c}{1+e_0}\right)\log\frac{p_f}{p_p} \qquad \text{for } p_0 < p_p < p_f \qquad (5.2)$$

$$\varepsilon = \left(\frac{C_r}{1+e_0}\right)\log\frac{p_f}{p_0} \qquad \text{for } p_f < p_p \qquad (5.3)$$

M = Constrained Modulus

p_0 = Vertical effective stress before construction of new levee

p_f = Vertical effective stress after construction of new levee

ε = Vertical strain from consolidation under the change in effective stress

p_p = Preconsolidation pressure

C_c = Compression index for virgin compression

C_r = Compression index for recompression

e_0 = Void ratio before construction of new levee

The vertical effective stresses before new levee construction were obtained from the gravity turn-on stage of the settlement analysis, using the preconstruction geometry shown in Figure 5-1. For the purpose of calculating constrained modulus values, the final stresses were determined by adding the calculated change in vertical effective stress due to construction, obtained in a separate elastic analysis, to the initial stresses from the gravity turn-on stage of the settlement analysis. For zones where the change in vertical effective stress due to construction was negligible, a constrained modulus was assigned based on the following equations:

$$M = \frac{2.3 p_0 (1 + e_0)}{C_c} \qquad \text{for normally consolidated conditions} \qquad (5.4)$$

$$M = \frac{2.3 p_0 (1 + e_0)}{C_r} \qquad \text{for overconsolidated conditions} \qquad (5.5)$$

Because the initial and final stresses vary spatially across the subsurface strata, the modulus values calculated for the individual zones also vary spatially. Profiles of the constrained modulus values calculated for the individual zones are shown in Figure 5-7 for several locations along the cross-section. Free field conditions are represented by the profiles for X = -250 and X = 250, and the estimated moduli beneath the old levee crest and underneath the protected side portion of the new levee beyond the DMM shear walls are represented by the profiles for X = -45 and X = 43, respectively. As can be seen in the profile for X = -45, the pre-loading provided by the old levee results in a significant increase in the stiffness of the upper 25 feet of the subsurface strata on the flood side of the DMM zone. The profiles shown in Figure 5-7 also reflect a

transition from overconsolidated crust in the upper 25 ft of the subsurface strata to normally consolidated conditions below El -40 ft.

The shear and bulk moduli were calculated for each zone based on the constrained modulus and the drained Poisson's ratio values listed in Table 5-1. The shear moduli were calculated using the relationship G = (M(1-2ν))/(2(1-ν)) and the bulk moduli were calculated using the relationship K = (M(1+ν))/(3(1-ν)). Profiles of the shear modulus values are also shown in Figure 5-7 for several locations along the cross-section.

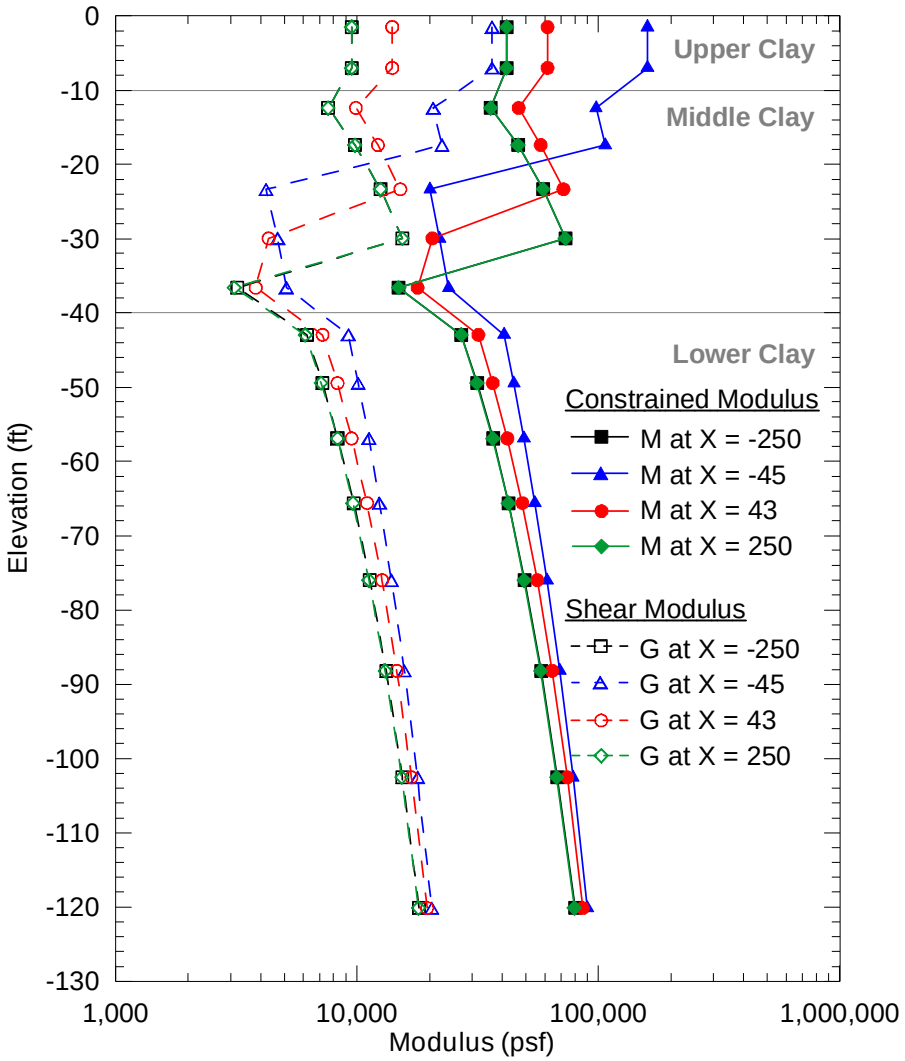

Figure 5-7. Subsurface Strata Constrained and Shear Modulus Profiles for Consolidation Settlement

The moduli used during the construction portion of the analyses, were obtained using published correlations in Duncan and Buchignani (1987) for calculating an undrained Youngs Modulus (E_u) based on undrained shear strength, overconsolidation ratio, and plasticity index. These moduli values were determined from field measurements, and they may be preferable to the moduli derived from the consolidation tests for computing immediate settlement because they are based on field measurements, not affected by disturbance, and incorporate the effect of load path associated with the lateral deformations that occur during immediate settlement. The undrained shear strength profile and overconsolidation ratio obtained from Figure 5-5 were used with the average plasticity index values shown in Figure 5-4 to generate the E_u profile shown in Figure 5-8. Shear moduli were calculated from the undrained Young's moduli using the relationship $G = (E)/(2(1+\nu))$ with a poisson's ratio of 0.5, the theoretical value upper limit value for undrained behavior. The resulting shear moduli profile used in the numerical analyses for the immediate settlements during the construction portion of the analyses is shown in Figure 5-8. For the lower clay layer, the shear moduli for immediate settlement are about an order of magnitude higher than for consolidation settlement.

The permeability values for the subsurface strata were determined based on coefficients of consolidation for virgin compression (c_v) and recompression (c_{vr}) taken from consolidation tests in the upper and middle clay layer and from published correlations with liquid limit (NAVFAC 1982). Representative coefficient of consolidation values for the upper and middle clay layers, based on average values from interpretation of the consolidation test results and correlations, are listed in Tables 5-1 and 5-3. For each row of zones in the FLAC model, an average vertical permeability (k_v) was calculated based on the coefficient of consolidation, the unit weight of water (γ_w), and the average constrained modulus (M) for each row based on the equation $k_v = c_v\gamma_w/M$. The vertical permeability profile used for the subsurface soils is shown in Figure 5-9. The range of values is generally consistent with typical values for clays.

The ratio of horizontal to vertical permeability was assumed to be 1 for all subsurface strata in the base case analyses. However, the upper 10 ft of the middle clay layer and the upper 13 ft of the lower clay layer were identified as having lenses or thin layers of sand and silt that would increase the horizontal permeability in these sub-layers. The extent of these sub-strata is shown

in Figure 5-1. The sensitivity of the results to the horizontal permeability in these sub-strata was determined by varying the ratio of horizontal to vertical permeability between 1 and 4, based on published values in Holtz et al. (2001).

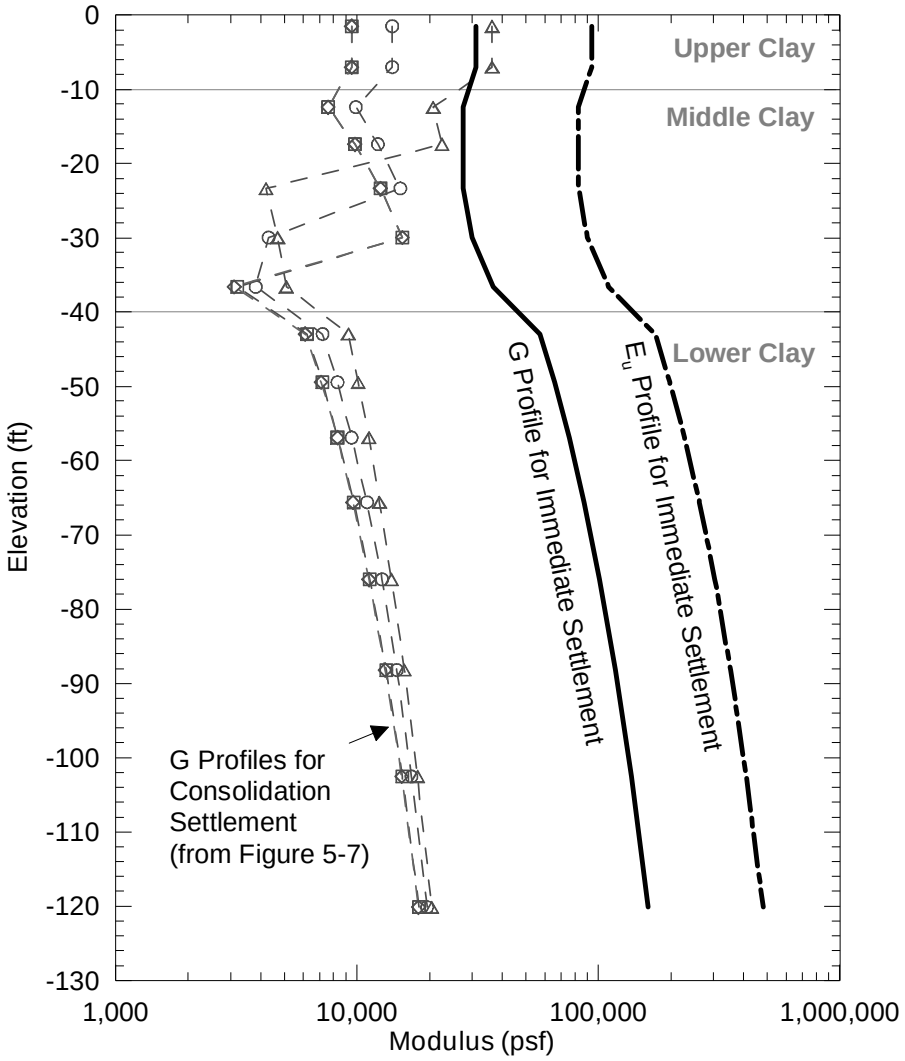

Figure 5-8. Subsurface Strata Young's and Shear Modulus Profiles for Immediate Settlement

Table 5-3. Summary of Coefficient of Consolidation Values for Upper and Middle Clay Layers

Data Source	Elev. (ft)	Oedometer Test		Correlations[1]			Representative Values	
		c_v (ft^2/day)	c_{vr} (ft^2/day)	LL	c_v (ft^2/day)	c_{vr} (ft^2/day)	c_v (ft^2/day)	c_{vr} (ft^2/day)
PSV-10UT	-7.3	0.05	0.4	61	0.09	0.3	0.09	0.4
PSV-11UT	-3.6	0.25	0.9	58	0.2	0.4		
PSV-12UT	-3.8	0.04	0.1	73	0.05	0.1		
PSV-10UT	-26.4	0.01	0.05	91	0.03	0.05	0.02	0.05
PSV-11UT	-23.1	0.01	0.06	100	0.02	0.04		
PSV-12UT	-22.1	0.04	0.4	85	0.03	0.07		
Figure 5-3[2]	Below -40			56	0.1	0.4	0.1	0.4

Notes:
1) Coefficient of consolidation obtained from correlation with liquid limit (NAVFAC 1982).
2) Consolidation test data was not available for the lower clay layer. Coefficient of consolidation for this layer is based on the average liquid limit from the Atterberg limits test results shown in Figure 5-3.

The values listed in Table 5-1 for the consolidation material properties of compression index (C_c, C_r) and coefficient of consolidation (c_v) represent best estimate values for the available data. These values were used in the base case analyses. Lower and upper estimates were developed to evaluate the sensitivity of the settlement analysis results to these parameters based on guidance provided by Duncan (2000). A 90% confidence interval was selected to illustrate the probable range in properties, and the lower and upper estimates of each property were determined by subtracting and adding 1.65 standard deviations to the best estimate values. For the compression index values, the published range for coefficient of variation (COV) values is 10-37% (Duncan 2000). For an average COV value of 24%, the resulting lower estimate and upper estimate values for each of the subsurface strata were calculated as 60% and 140% of the best estimate values listed in Table 5-1. For the coefficient of consolidation values, the published range for COV is 33-68% (Duncan 2000). For an average COV value of 50%, the resulting lower estimate and upper estimate values were calculated as 17% and 183% of the best estimate values listed in Table 5-1. These upper and lower estimates provide a range in consolidation material property

values for use in analyses. The actual range in values for the subsurface conditions along the P24 levee alignment may be different from the range used for these analyses.

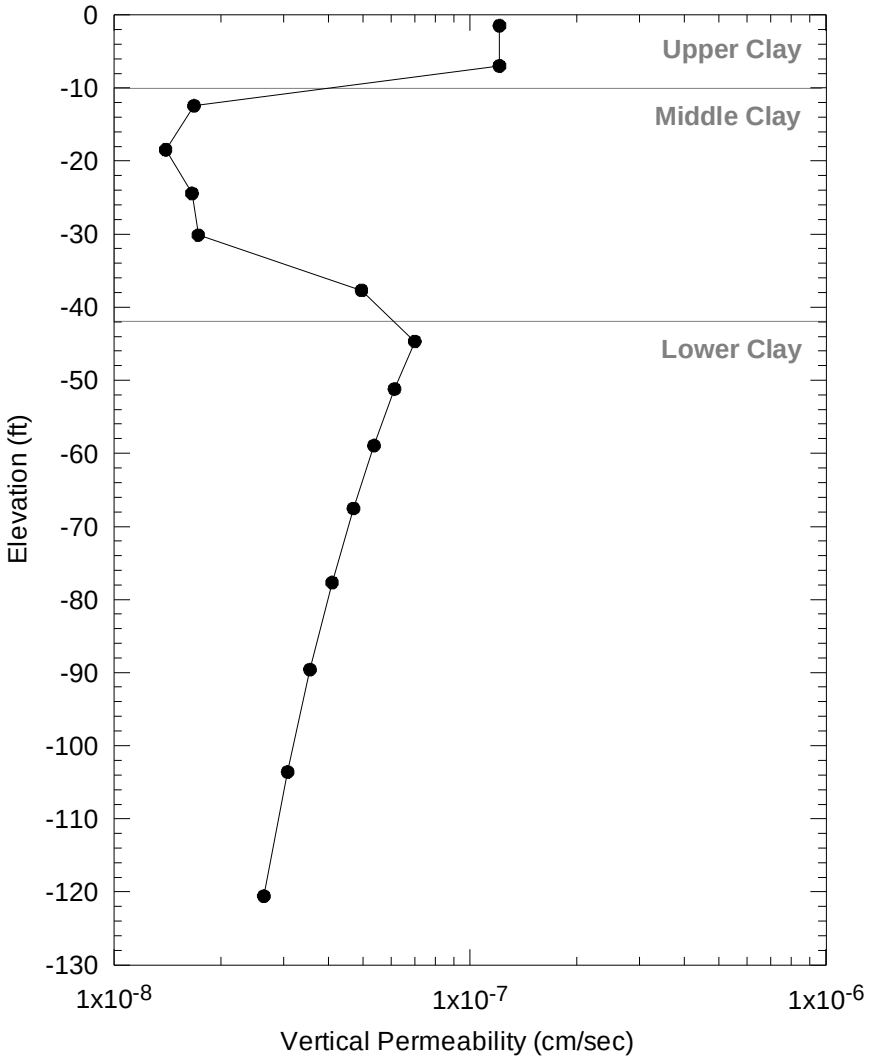

Figure 5-9. Vertical Permeability Profile for Subsurface Strata

5.2.4. Levee Material Properties

Material properties for the new levee soils were developed based on boring logs and laboratory test results provided by USACE for borings B-14F through B-37F, which were advanced from the new levee crest after construction was complete. The unit weight, water content, porosity and shear strength of the levee were determined by averaging the test results. These values are listed in Table 5-1.

The undrained Young's modulus, E_u, was estimated from the published correlations in Duncan and Buchignani (1987) based on soil plasticity, overconsolidation ratio, and undrained shear strength of the levee soils. An E_u/s_u ratio of 60 was used for the levee based on a representative overconsolidation ratio of 10. This value is representative of the conditions in the portion of the new levee on the protected side toe beyond the DMM shear walls. This stiffness ratio is lower than may be expected for the entire levee, considering that increased overburden and potential negative pore pressures due to capillarity in other portions of the levee would result in lower estimated overconsolidation ratios and higher correlated stiffness ratios. Sensitivity analyses showed that the levee stiffness has an insignificant effect on predicted settlements of the levee crest, but has a large effect on the settlement of the protected levee toe. Higher stiffness contrasts between the levee and the foundation strata caused the unsupported portion of the levee to rotate as a rigid block, rather than developing the characteristic 'dished' shape that would be expected in this portion of the levee foundation contact. Because the potential for cracking from the top of the levee on the protected and flood sides of the DMM zone depends on its ability to experience settlement in these areas, the levee was assigned a conservative stiffness based on the lower E_u/s_u ratio.

The shear modulus, G, of the levee was calculated from the undrained Young's modulus E_u using an undrained Poisson's ratio of 0.5. The bulk modulus, K, value for the FLAC model was then calculated from G using a drained Poisson's ratio to allow for compression of the potentially unsaturated levee materials. The drained Poisson's ratio listed in Table 5-1 for the new levee is based on an effective stress friction angle of 27^o, from a correlation with the soil plasticity (Duncan and Wright 2005).

The material properties for the old levee were assumed to be the same as those for the new levee.

5.2.5. DMM Zone Material Properties

Material property values for the DMM zone were estimated based on guidelines provided by Smith (2005). For the dry-mix columns, an equivalent drained strength of the DMM material can be determined from the unconfined compressive strength test results using a drained friction angle of 30 degrees and a cohesion of 0.289 times the unconfined compressive strength. Based

on the mean value of the unconfined compressive strength test results for the DMM material at the P24 project of 311.4 psi (as presented in Table 4-2 of Chapter 4), the effective stress cohesion intercept of the soil-cement material was calculated as (0.289)(311.4 psi) = 90 psi (12960 psf). The representative strength for the DMM zone is a function of shear wall spacing, the average width of the wall, and the strengths of the DMM mixture and the native soils. Based on a shear wall spacing of 7 ft, an average width of the shear wall of 27.6 in., and an average friction angle for the native soils between the DMM shear walls of 26^o, the composite drained friction angle was determined as $\phi' = \tan^{-1}((27.6 \text{ in.})(\tan 30^o) + (84 \text{ in.} - 27.6 \text{ in.})(\tan 26^o)) / (84 \text{ in.})) = 27^o$. Similarly, the composite drained cohesion was determined as c' = ((27.6 in.)(12960 psf) + (84 in. – 27.6 in.)(0 psf)) / (84 in.)) = 4260 psf.

The representative modulus for the DMM zone is also a function of shear wall spacing, the average width of the wall, and the stiffnesses of the DMM mixture and the native soils. For the dry-mix columns, published values for the ratio of the undrained Young's modulus, E_u, to unconfined compressive strength range from 65 to 300, and the Poisson's ratio ranges from 0.25 to 0.5 (Smith 2005). A stiffness ratio of 150 and a drained Poisson's ratio of 0.33 were selected for use in the P24 settlement analyses. From the stiffness ratio, the undrained Young's modulus of the DMM material was calculated as (150)(311.4 psi) = 46710 psi (6.73×10^6 psf), and the shear modulus of the DMM mixture was calculated using an undrained Poisson's ratio of 0.5 as (6.73×10^6 psf)/(2(1 + 0.5)) = 2.24×10^6 psf. Based on an average shear modulus for the native soils between the DMM shear walls of about 1.3×10^4 psf, the composite shear modulus for the DMM zone was determined as follows: G = ((27.6 in.)(2.24×10^6 psf) + (84 in. – 27.6 in.)(1.3×10^4 psf)/(84 in.)) = 7.45×10^5 psf. The bulk modulus, K, value for the FLAC model was then calculated from G using the drained Poisson's ratio.

The unit weight and permeability of the DMM zone was considered unchanged from that assigned to the existing soil layers.

5.3. Numerical Analyses

Settlement analyses for the P24 levee were completed using the finite difference computer code FLAC (ITASCA 2005). This section describes the analysis methods and results.

5.3.1. Analysis Methods

The mesh used for the numerical analyses extended 400 ft on either side of the centerline of the new levee crest. The bottom of the mesh extended to elevation -150 ft. The extent of the model is shown schematically in Figure 5-10. No lateral displacements were allowed on the left- and right-hand sides of the mesh, and no lateral or vertical displacements were allowed on the bottom of the mesh. The mesh was adjusted for analysis cases with the top of the nearshore gulf deposits at El -130 ft by turning off rows of zones at the bottom of the mesh.

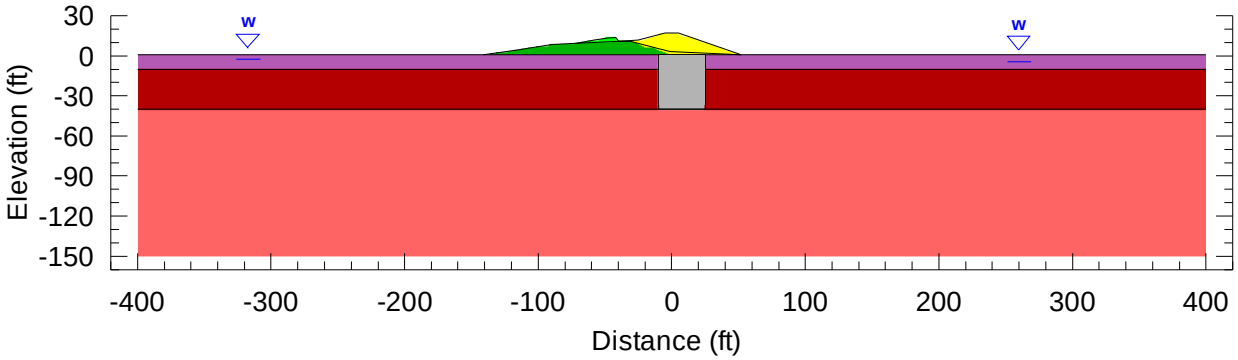

Figure 5-10. Extent of FLAC Model

The pore pressures for nodes along the left- and right-hand sides of the model, and along the base of the model, were fixed at values consistent with a hydrostatic pore pressure distribution under the phreatic surface shown in Figure 5-1. For the left- and right-hand boundaries this simulates free-field hydraulic conditions. At the base of the model, this creates a free-draining boundary directly below the lower clay layer, at the top of the nearshore gulf deposits. Because the pore water pressures inside the levees were not of interest for this study, and because consolidation analyses with unspecified phreatic surfaces take considerably longer to run in FLAC, the semi-permeable boundary along the base of the old and new levees was simplified by analyzing it as either fully permeable or impermeable. For the analyses with a fully permeable levee, the nodes along the base of the new and old levees were set to zero pressure to allow for water to flow freely out of the subsurface clays. For the analyses with an impermeable levee, the nodes along the base of the new and old levee fill were assigned zero-flow conditions, to prevent water from exiting the subsurface clays along this contact. The saturation at the nodes in the levees was fixed at zero, to prevent flow from developing in this part of the model.

Two meshes were developed for the P24 settlement analyses. The standard mesh has zone widths in the vicinity of the levee and DMM zone in the range of 5 to 9 ft. The discretized standard mesh in the vicinity of the levee and DMM zone is shown in Figure 5-11a. A second mesh was developed with finer spacing to verify that the results computed using the standard mesh were independent of mesh size. The fine mesh has zone widths in the vicinity of the levee and DMM zone in the range of 2 to 5 ft. The discretized fine mesh in the vicinity of the levee and DMM zone is shown in Figure 5-11b. Analyses completed for several cases using the fine mesh resulted in similar deformations and time-rate of consolidation behavior as that determined using the standard mesh. Because the differences between the settlements calculated using the standard and fine mesh analyses were small, and because settlement analyses completed using the fine mesh took about 15 times as long as settlement analyses using the standard mesh, the quicker standard mesh was used for the settlement analyses presented in this report.

The settlement analyses were completed in three distinct stages: 1) pre-construction; 2) construction; and 3) post-construction. In the first stage, initial stresses for the model were generated with the pre-construction ground profile shown in Figure 5-1. For this stage of the model, the DMM zone was assigned properties consistent with the native soil layers, and the stresses were developed using a gravity turn-on approach. For the construction stage of the model, the DMM zone properties listed in Table 5-1 were assigned in the DMM zone, and the crest of the old levee was re-graded to the post-construction ground profile shown in Figure 5-1. The new levee was added to the model in five, 3.2 ft high lifts for the standard mesh FLAC model and ten, 1.6 ft high lifts for the fine mesh FLAC model. The geometry of the model remained constant for the post-construction stage of the model, and the excess pore pressures generated during the construction stage of the model were allowed to dissipate.

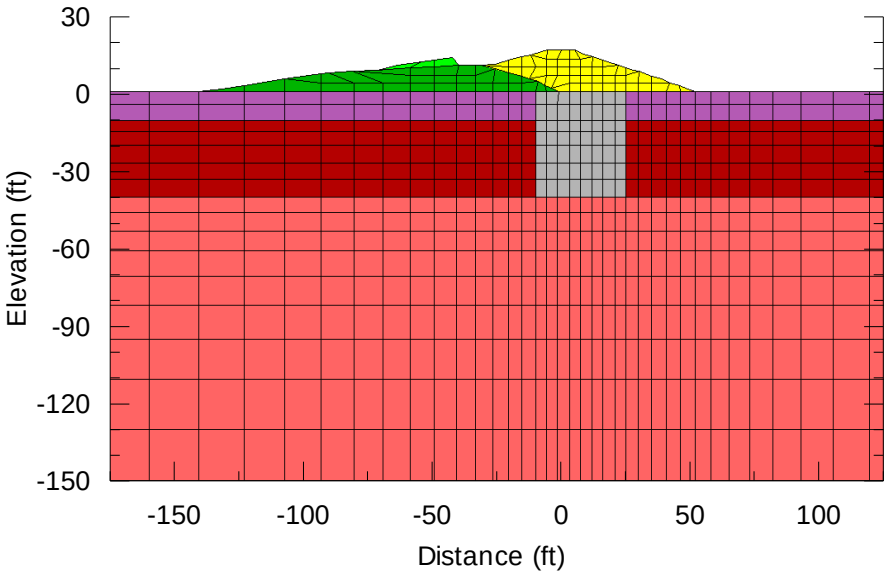

Figure 5-11a. Standard Mesh

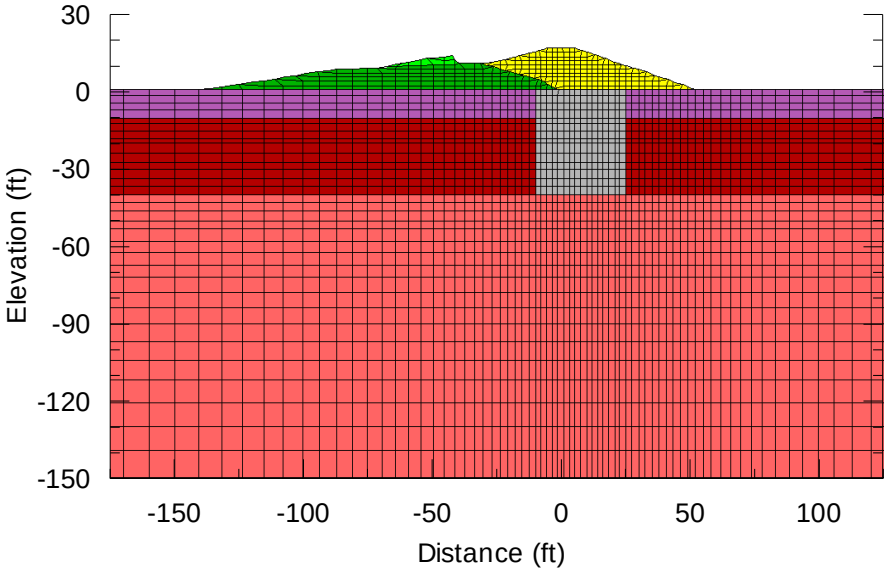

Figure 5-11b. Fine Mesh

Figure 5-11. FLAC Mesh Discretization Near Levee and DMM Zone

The settlement analyses were performed using FLAC's coupled analyses option for mechanical loading and fluid flow. In these analyses, the program alternates between "flow" steps to bring unbalanced pore pressures to a steady-state regime and "load" steps to bring unbalanced forces in the model due to changing stress conditions into equilibrium. When there are large changes in

applied stresses that occur instantaneously relative to the consolidation time, the FLAC manual recommends that the flow be turned off and the unbalanced forces from the applied load be brought to equilibrium before continuing the consolidation analyses. For the model, the flow was turned off during the construction stage. This simplification in the model is consistent with rapid construction of the new levee, before significant consolidation of the subsurface clays can take place. According to Mark Woodward from the New Orleans district, levee construction was completed in 4 months or less, which is a relatively short time compared to the 60+ years required to reach 90% consolidation for the numerical model, as discussed below.

Turning the flow off in the FLAC model during the construction stage also allows the results of the settlement analyses to be separated into immediate settlement and consolidation settlement components. In the analyses, the displacements in the model were set to zero at the end of the construction stage, before the flow was turned on for the post-construction stage. In this way, the immediate settlement, caused by distortion of the clay layers without volume change, was separated from the settlement due to consolidation of the clay layers. This distinction is important because immediate settlement occurs as the levee is being constructed and does not contribute to settlement of the levee crest because the final lift is graded to the design elevation. Settlement monitoring based on changes in the elevation of the levee crest after construction do not include the magnitude of immediate settlements. The settlement analysis results presented in this report are separated into immediate settlements (from the construction stage of the model) and consolidation settlements (from the post-construction stage of the model).

Separating the settlement analysis into three stages also allowed for assignment of the moduli developed for immediate settlement, shown in Figure 5-8, to be assigned during the construction stage of the analyses. For all other stages of the analyses, the moduli developed from the compression indices and the Mohr-Coulomb strengths listed in Table 5-1 were assigned to the clay strata. During the construction stage, the strength of the subsurface clay layers was increased to prevent failure in the foundation during placement of the levee lifts. Because the lift placement is modeled in discrete layers, the potential exists for weak zones to fail during the convergence process, as FLAC iterates to bring the forces to equilibrium in the ‘load’ step. After the new levee construction was complete, but before the flow was turned on in the model, the

strength in the subsurface clay layers was reset to the values in Table 5-1 to allow for any permanent displacements that would occur due to the load of the new levee fill.

The tensile strength of the soil and DMM zone were set to zero to allow for the potential formation of tension cracks. No tension cracks occurred in any of the analyses.

5.3.2. Base Case Settlement Analysis

A base case settlement analysis was completed using the best estimate consolidation properties listed in Table 5-1 and the analysis section shown in Figure 5-1. The analysis was completed using a model with a permeable boundary at the base of the levees, isotropic permeability for the full height of the subsurface strata, and a free-draining layer at the base of the model at El -130 ft.

The results of the immediate settlement (construction) stage portion of the analysis are shown in Figure 5-12. These results correspond to the conditions immediately after the new levee is constructed, before the excess pore pressures generated by the loading begin to dissipate. The pore pressure contours in Figure 5-12a indicate that pore pressures in excess of hydrostatic are concentrated in and under the DMM zone and in the upper and middle clay layer under the protected-side slope of the new levee. The displacement vectors in Figure 5-12b and the settlement contours in Figure 5-12c show the magnitude and direction of the immediate settlement and indicate that distortion is occurring in the subsurface clay layers.

The maximum displacement in the model during the construction stage is 3.6 in. This maximum displacement includes horizontal and vertical components and occurs in the portion of the protected slope of the new levee that is not supported by the DMM zone. The maximum vertical component of displacement during construction is 3.3 in. The levee-foundation contact above the DMM shear walls settles about 2 inches during construction. As discussed above, immediate settlements are not important for estimating the post-construction settlement of the levee crest because immediate settlements occur before the final grading of the levee crest.

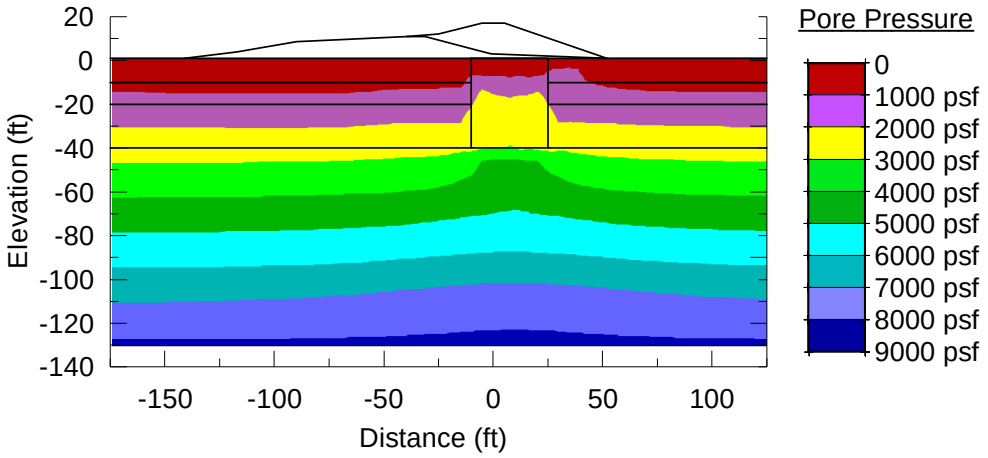

Figure 5-12a. Pore Pressure Contours

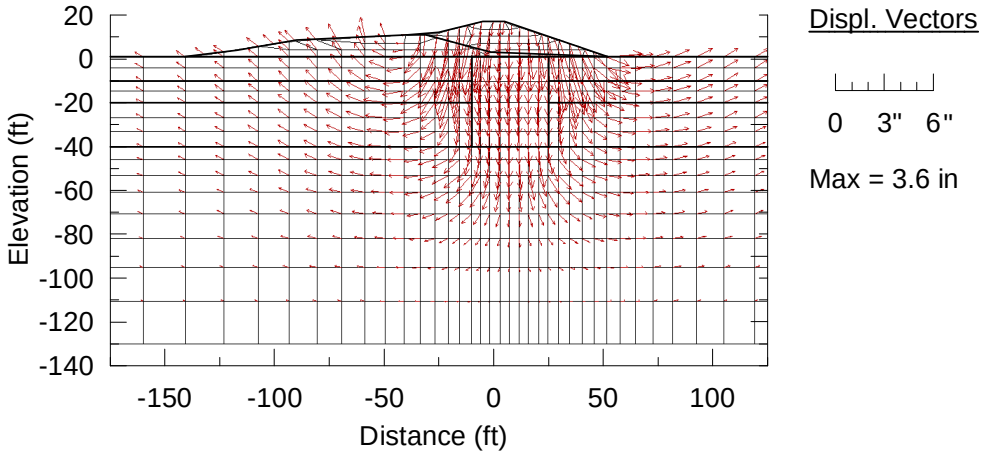

Figure 5-12b. Displacement Vectors

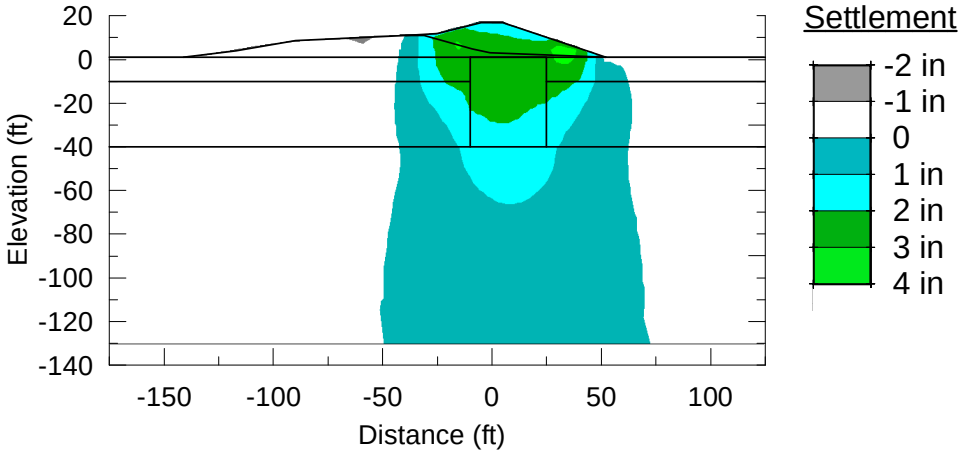

Figure 5-12c. Settlement Contours

Figure 5-12. Pore Pressures and Immediate Settlement at End of Construction

Base Case Settlement Analysis

The results for the consolidation (post-construction) stage of the base case settlement analyses are presented in Figures 5-13, 5-14, and 5-15. The predicted settlement of the levee crest at the centerline is included in the time-rate settlement curves shown in Figure 5-13. Figure 5-13a shows the settlement versus time plot and lists the calculated settlements at 1, 3, 10, and 30 years, as well as the predicted ultimate settlement value for the end of consolidation. Figure 5-13b shows the percent consolidation versus time and provides the predicted time to 50% and 90% consolidation. The calculated settlements are reported to the nearest tenth of an inch in this report to allow for comparison of subtle differences between the results from different analyses cases, but the results should not be inferred to have this much accuracy due to uncertainties in material property values and modeling details. The maximum time interval used in the base case analysis was 1000 years, at which time the pore pressures in the model had returned to hydrostatic and the change in settlement for the last 200 years of the analysis was less than 0.01%. The results presented in Figure 5-13 are limited to the first 600 years of the analyses to allow for better resolution of the curves in the first 30 years. For the base case conditions, the ultimate settlement of the P24 levee with DMM shear walls is on the order of 7 inches and the time to 90% consolidation is 127 years.

Pore pressure contours are presented in Figure 5-14 for 3, 10, 30 and 1000 years after construction. These contours illustrate the dissipation of the excess pore pressures that were generated during construction of the new levee. The pore pressures at 1000 years after construction are hydrostatic.

Settlement contours are presented in Figure 5-15 for 3, 10, 30 and 1000 years after construction is complete. These contours show that the predicted settlements on the flood side of the new levee are slightly less than those predicted for the protected side. This trend in the P24 settlement pattern reflects the effect of the old levee, which causes asymmetry in the geometry of the new levee fill and provides a surcharge to increases the stiffness of the subsurface soils on the flood side of the new levee. The maximum settlement of 7.6-in occurs in the portion of the protected-side slope of the new levee beyond the DMM zone. At this location, the levee load causes settlement due to consolidation in the upper and middle clay layers, in addition to the settlement occurring due to consolidation of the lower clay below the elevation of the bottom of

the DMM zone. The amount of differential settlement between the central portion of the new levee and the portions of the new levee on the flood- and protected-side slopes located beyond the DMM zone is limited on both sides by the decreased compressibility of the of the shallow soil layers due to pre-compression from existing levee loads.

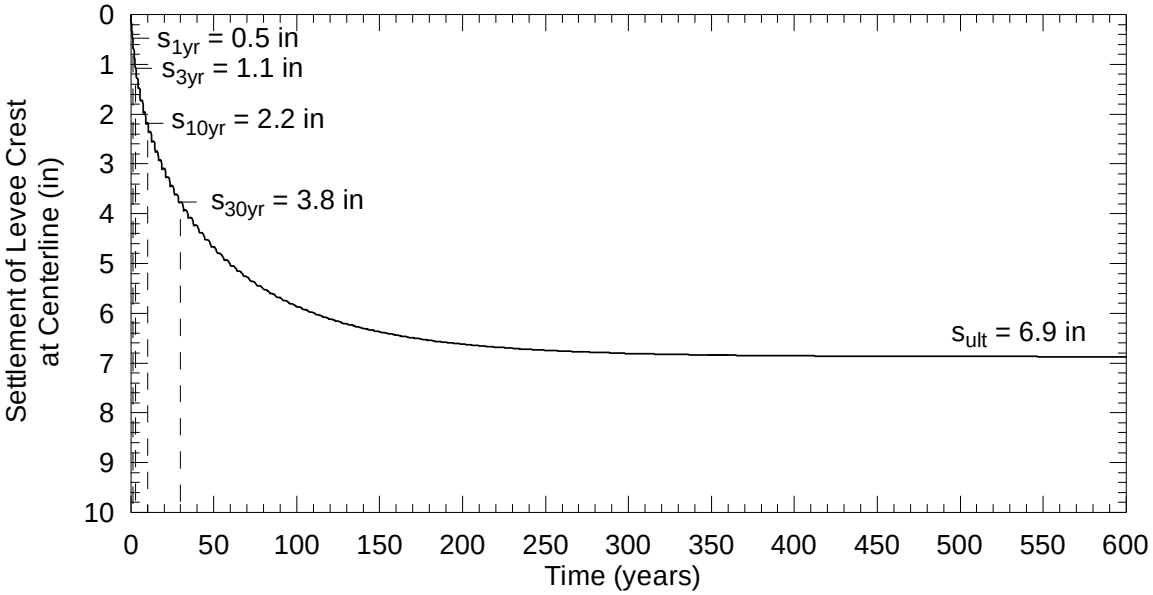

Figure 5-13a. Settlement versus Time

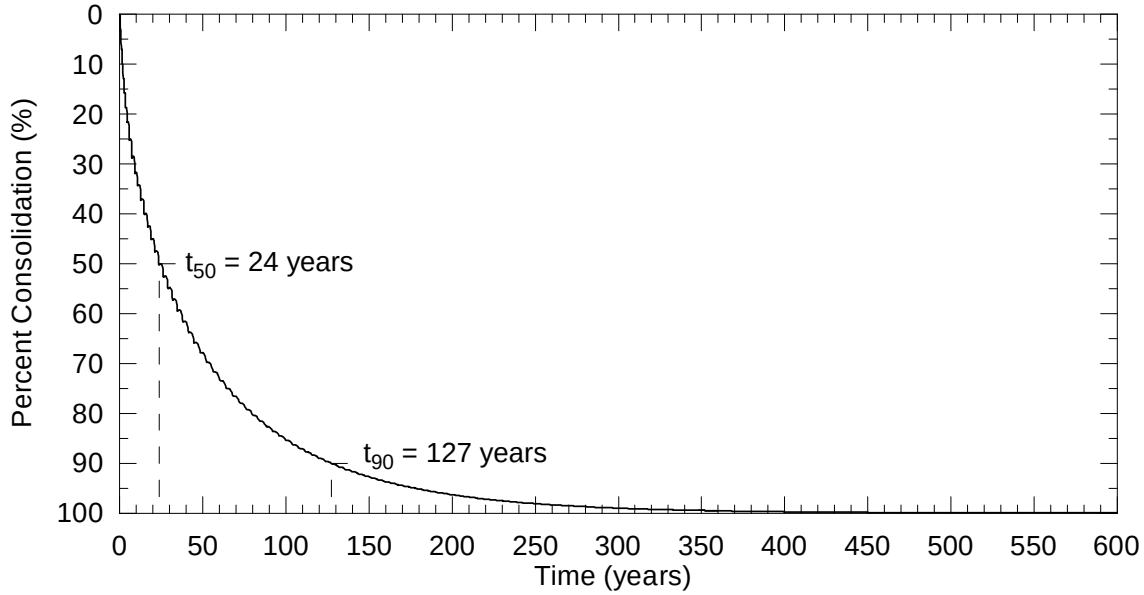

Figure 5-13b. Percent Consolidation versus Time

Figure 5-13. Consolidation Settlement of Levee Crest Centerline for Base Case Settlement Analysis

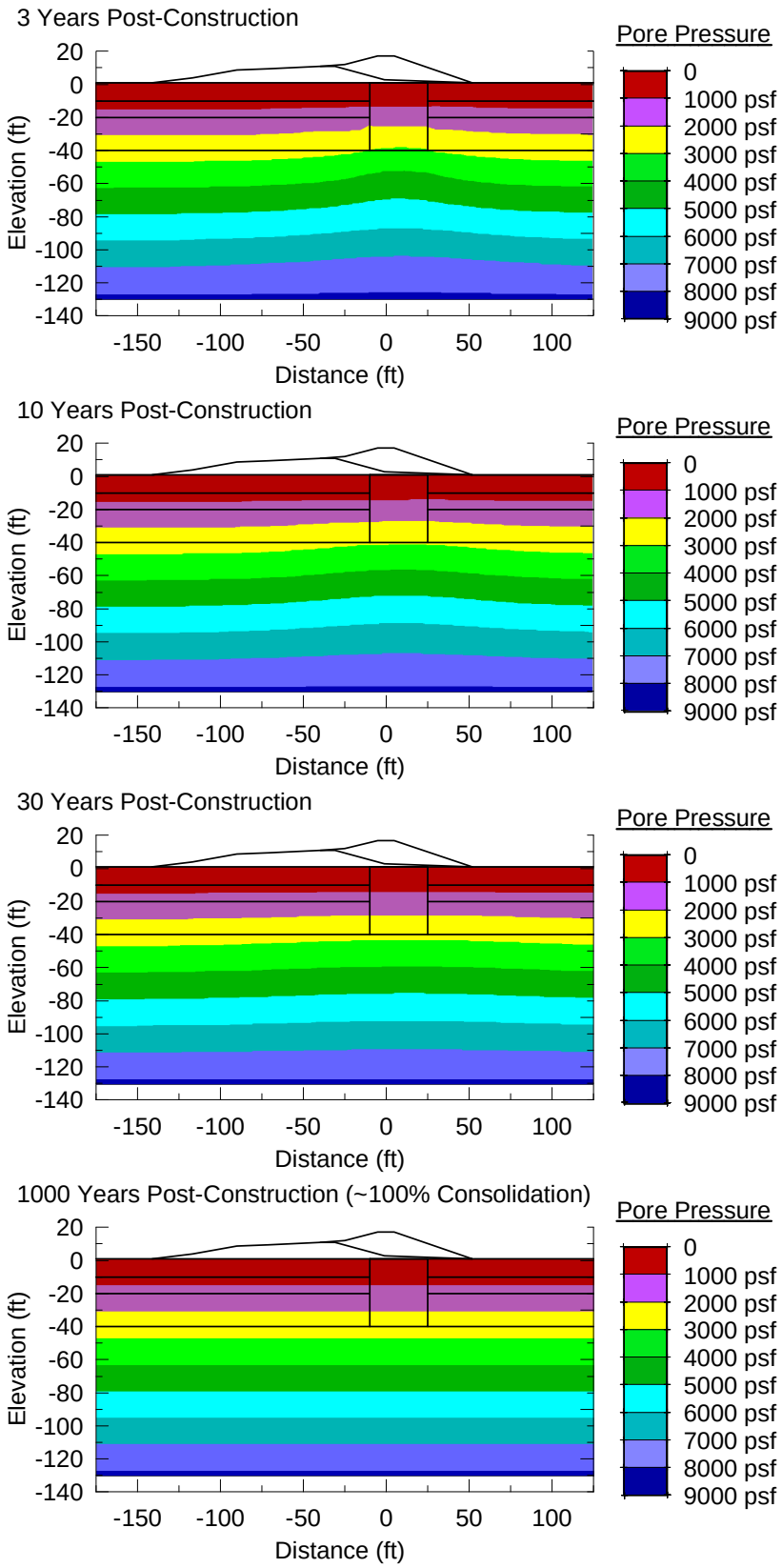

Figure 5-14. Pore Pressure Contours During Consolidation for Base Case Settlement Analysis

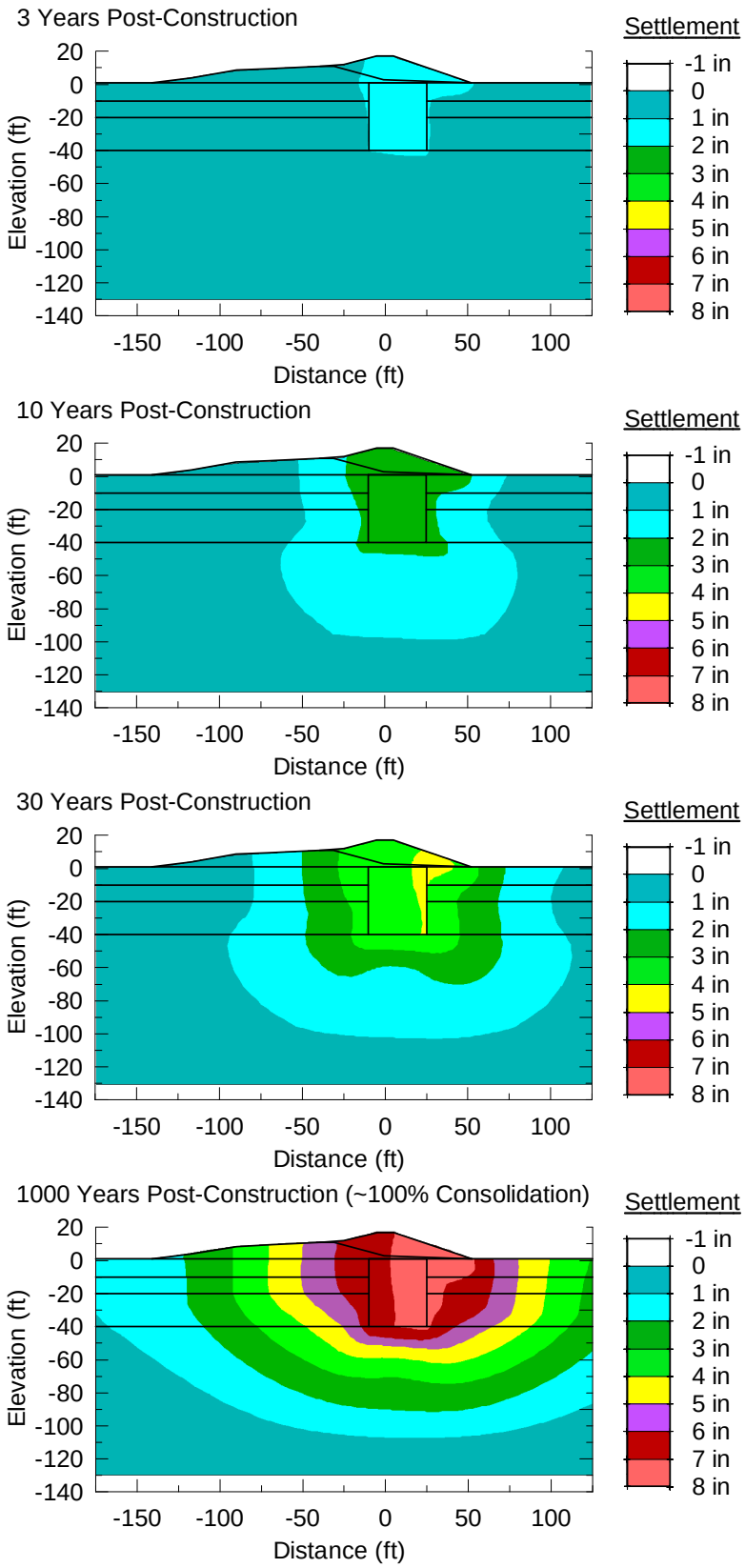

Figure 5-15. Settlement Contours During Consolidation for Base Case Settlement Analysis

5.3.3. Settlement Analyses with Best Estimate Material Properties

Settlement analyses were completed using best estimate consolidation property values for 8 cases to determine the effect of model boundary conditions and increased horizontal permeability on the settlement behavior for the P24 levee. The eight cases were generated by variations in three factors: 1) the seepage boundary conditions at the base of the new and old levee; 2) the potential for increased horizontal permeability in the portions of the subsurface strata with sand and silt lenses; and 3) the depth to the free-draining nearshore gulf deposits. The effect of the seepage boundary conditions was evaluated by modeling the base of the levee as a fully permeable, free-draining boundary, or as an impermeable boundary. The effect of the potential for increased horizontal permeability where sand and silt lenses were observed was evaluated by assigning isotropic permeability to all of the subsurface strata ($k_h = k_v$), or assigning horizontal permeabilities that were 4 times the vertical permeabilities ($k_h = 4k_v$) in the upper portions of the middle and lower clay layers, as shown in Figure 5-1. The effect of the depth to the nearshore gulf deposits was evaluated by modeling the top of the free-draining nearshore gulf deposits at El -130 ft, or at El -150 ft. Analyses for all eight cases were completed using the best estimate material properties listed in Table 5-1 and the best estimate pre-consolidation pressure profile shown in Figure 5-6.

The results from the consolidation portion of the base case analysis are shown with the results for the other three cases with the top of the nearshore gulf deposits at El -130 ft in Figure 5-16. Settlement of the new levee crest at the centerline versus time is shown in Figure 5-16a and percent consolidation versus time is shown in Figure 5-16b.

As can be seen in Figure 5-16, changes in the boundary conditions along the base of the old and new levees and increased horizontal permeability in the portions of the subsurface clay strata with sand and silt lenses have only a small effect on the predicted settlement of the levee. The analysis cases with a permeable boundary along the base of the old and new levee fill resulted in slight increases in the rate of consolidation when compared to the cases with an impermeable boundary. Similarly, the cases with higher horizontal permeability in the upper portions of the middle and lower clay layers resulted in slight increases in the rate of consolidation when compared to those with isotropic permeability.

For all of the analyses cases with the top of the nearshore gulf deposits at El -130 ft, the ultimate settlement of the new levee crest at the centerline is about 7 in., with a calculated settlement at 3 years of about 1 to 2 in. The predicted time to 90% consolidation is in the range of 100 to 165 years.

The results from the consolidation analyses for the cases with the top of the nearshore gulf deposits at El -150 ft are shown in Figure 5-17. Calculated settlements of the new levee crest at the centerline are shown versus time in Figure 5-17a, and percent consolidation versus time is shown in Figure 5-17b.

As can be seen in Figure 5-17, changes in the boundary conditions along the base of the old and new levees and increased horizontal permeability in the portions of the subsurface clay strata with sand and silt lenses have only a small effect on the predicted settlement of the levee for the cases with the top of the nearshore gulf deposits at El -150ft. Consistent with the trends from the cases with the top of the nearshore gulf deposits at El -130 ft, the rate of consolidation is slightly higher when a permeable boundary is specified along the base of the old and new levee fill or an increased horizontal permeability is assigned in the upper portions of the middle and lower clay layers. The results for the cases with the top of the nearshore gulf deposits at El-150 ft also reflect slight increases in ultimate settlement when compared with the analyses for the top of the nearshore gulf deposits at El -130ft. Because the lower boundary of the model is free-draining, the range of predicted settlements for the model with the top of the nearshore gulf deposits at El -150 ft is slightly smaller in the first 150 years after construction.

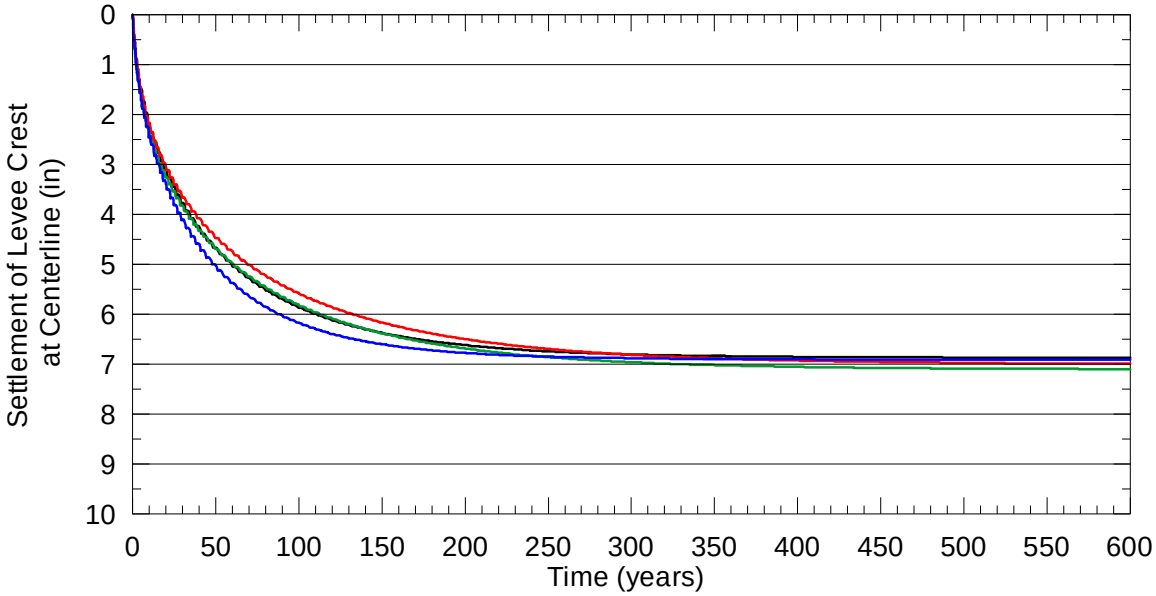

Figure 5-16a. Settlement versus Time

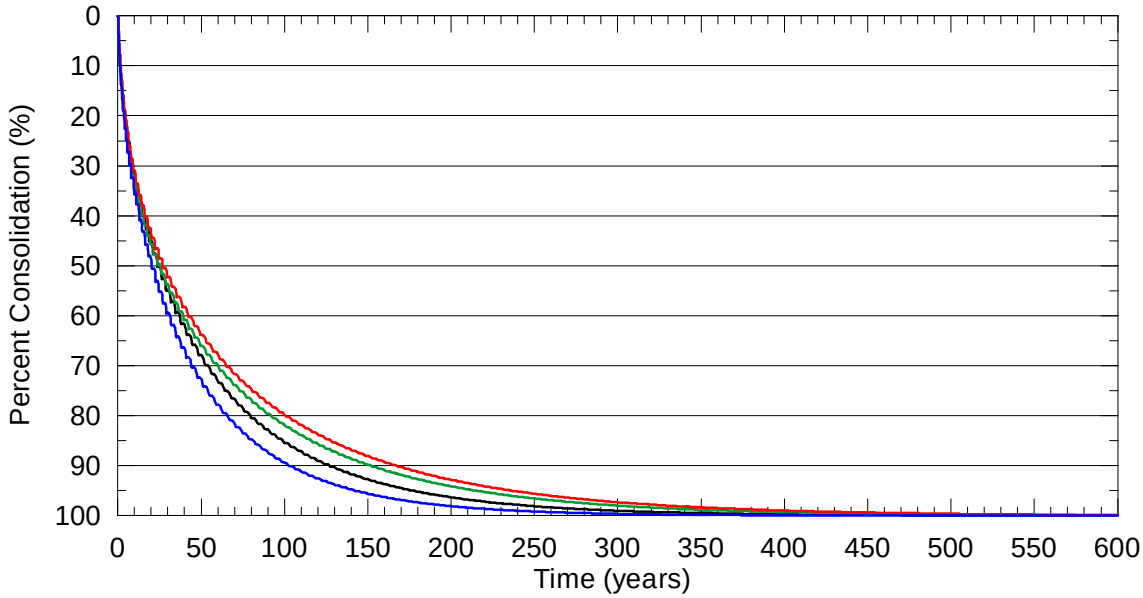

Figure 5-16b. Percent Consolidation versus Time

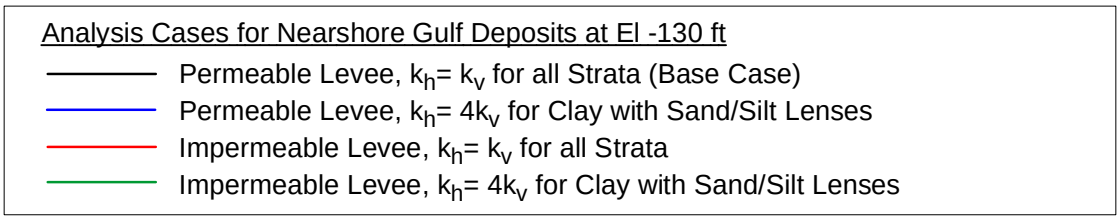

Figure 5-16. Consolidation Settlement of Levee Crest at Centerline with Best Estimate Properties and Top of Nearshore Gulf Deposits at El -130 ft

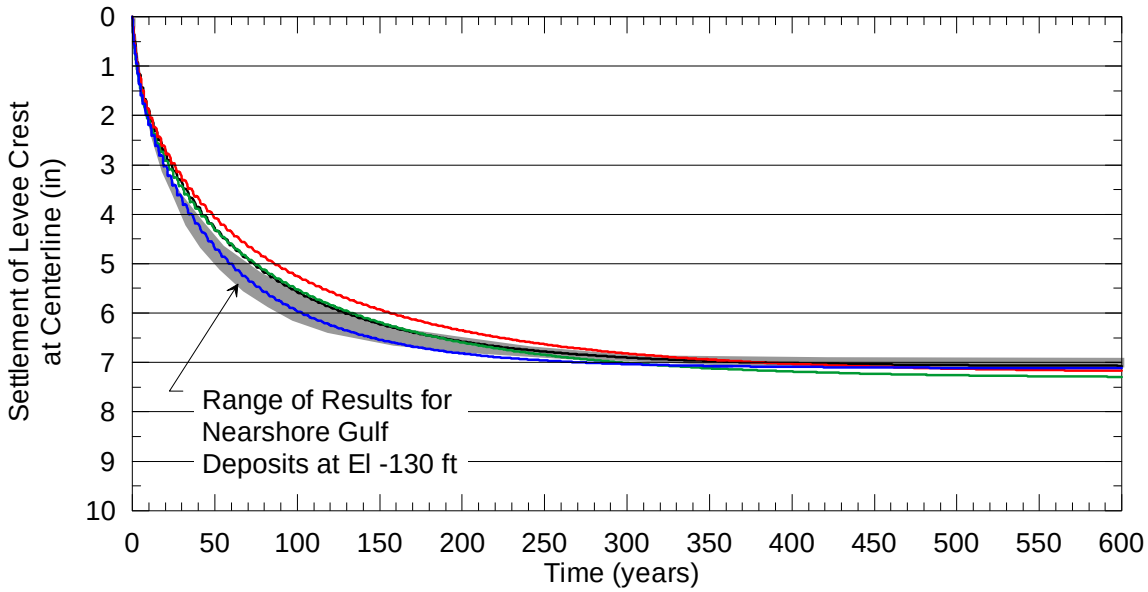

Figure 5-17a. Settlement versus Time

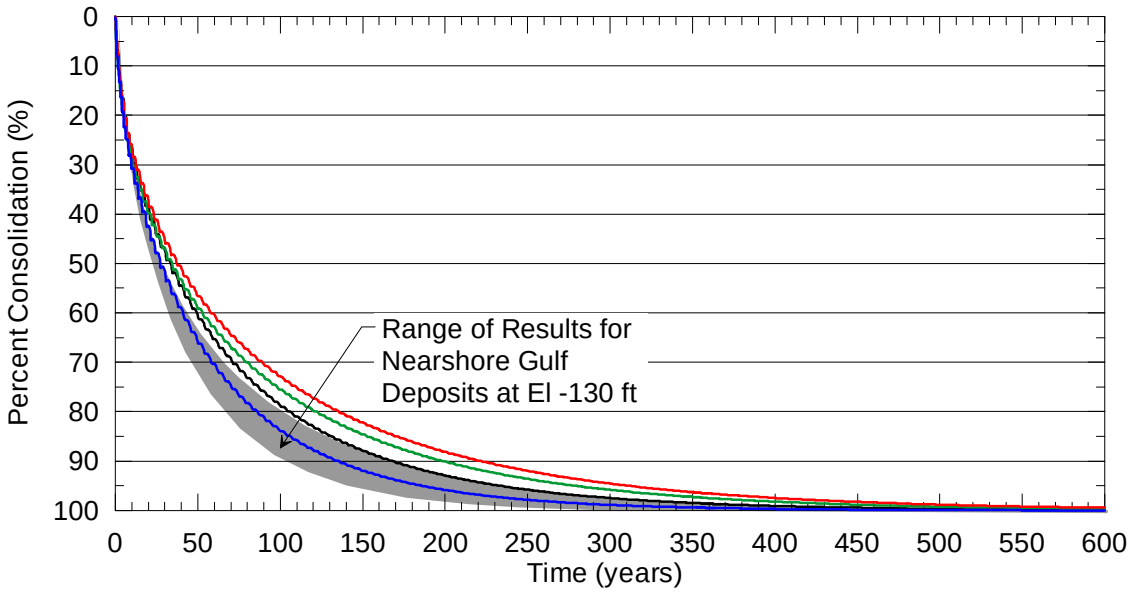

Figure 5-17b. Percent Consolidation versus Time

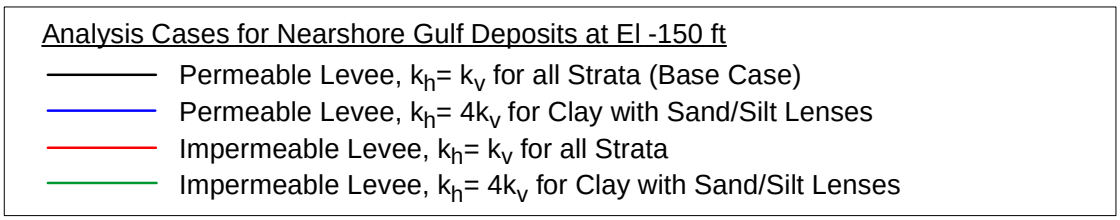

Figure 5-17. Consolidation Settlement of Levee Crest at Centerline for Best Estimate Properties and Top of the Nearshore Gulf Deposits at El -150 ft

Based on the predicted settlements shown in Figures 5-16 and 5-17, the factors investigated in the settlement analyses with best estimate consolidation properties have a minimal effect on the predicted settlement of the levee. For all eight cases, the ultimate settlement of the new levee crest at the centerline is about 7 to 5-in, with a predicted settlement at 3 years of about 1 to 2-in. The predicted time to 90% consolidation is in the range of 100 to 220 years.

The remaining analyses presented in this report were completed using the model with the top of the nearshore gulf deposits at El -130 ft, a permeable boundary at the base of the levees, and isotropic permeabilities for all of the strata.

5.3.4. Settlement Analyses for a Range of Consolidation Material Properties

To determine the effects of variations in the material properties that influence the magnitude and time rate of consolidation settlements, analyses were completed with a range of preconsolidation pressures, compression index values, and coefficient of consolidation values. The range of preconsolidation pressures was based on the lower estimate and upper estimate profiles shown in Figure 5-6. The range of range of compression index and coefficient of consolidation values was based on published values of coefficient of variation (COV) and a 90% confidence interval, as discussed previously.

Eight cases were evaluated to investigate the potential range in predicted settlements based on the lower and upper estimates of the consolidation properties. Preconsolidation pressures, compression index values and coefficient of consolidation values were each varied independently to generate the first six cases. Two additional cases were generated by combining the effect of varying both compression index and coefficient of consolidation to lower and upper estimate values.

The results from the analyses are shown in Figure 5-18. Settlement of the new levee crest at the centerline versus time is shown in Figure 5-18a and percent consolidation versus time is shown in Figure 5-18b. Predicted settlements at 1, 3, 10, and 30 years, as well as the predicted ultimate settlement values for the end of consolidation are listed together with the results from the base case analyses in Table 5-4. The predicted time to 50% and 90% consolidation are also presented in Table 5-4.

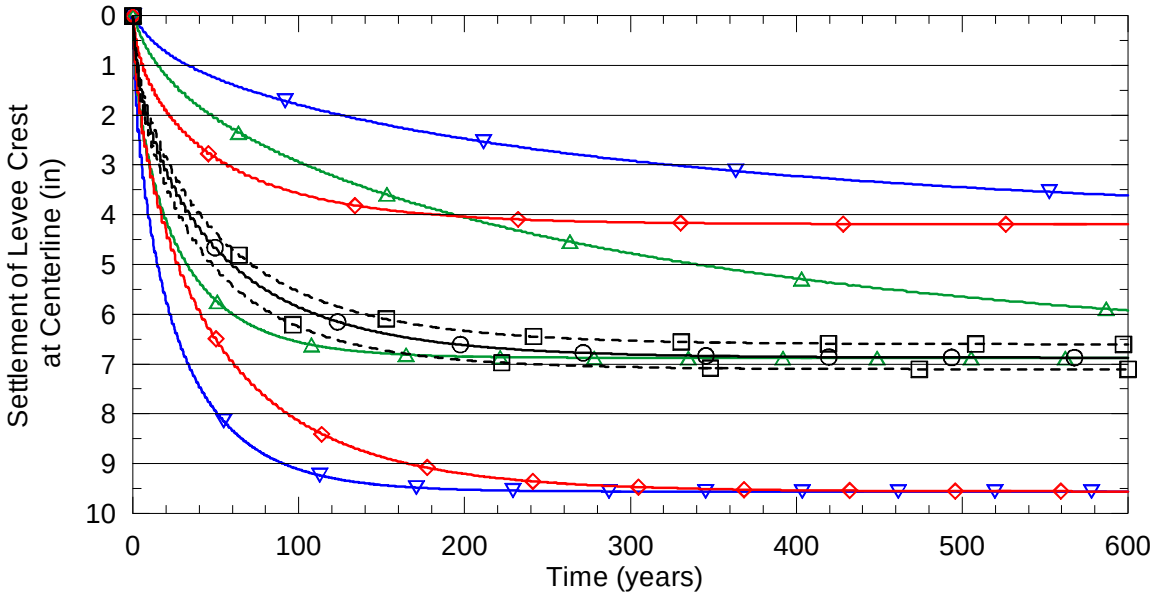

Figure 5-18a. Settlement versus Time

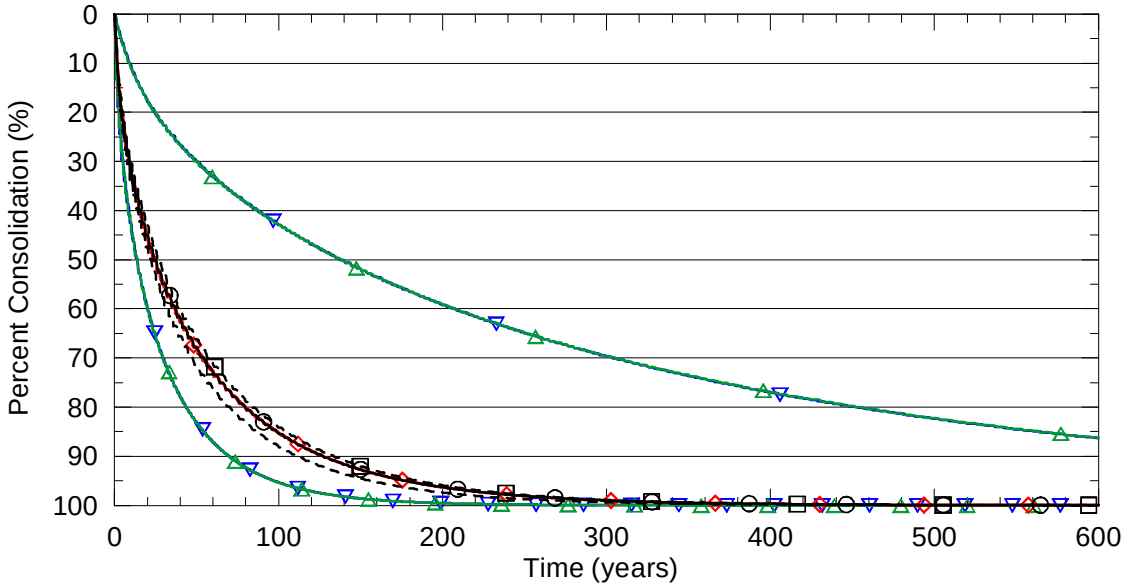

Figure 5-18b. Percent Consolidation versus Time

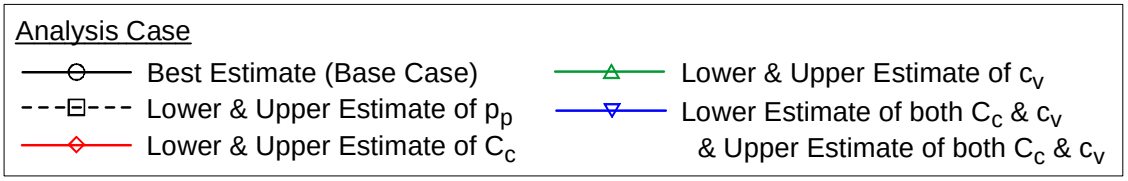

Figure 5-18. Consolidation Settlement of Levee Crest at Centerline for a Range of Consolidation Material Properties

Table 5-4. Results for Settlement Analyses with Range of Consolidation Material Properties

Analysis Case	Settlement of Levee Crest at Centerline (in.)					Time for Consolidation (years)	
	S_{1yr}	S_{3yr}	S_{10yr}	S_{30yr}	S_{ult}	t_{50}	t_{90}
Best Estimate Property Values (Base Case)	0.5	1.1	2.2	3.8	6.9	24	127
Preconsolidation Pressure (p_p) Lower Estimate Values	0.5	1.2	2.4	4.1	7.1	22	111
Preconsolidation Pressure (p_p) Upper Estimate Values	0.4	0.9	2.0	3.5	6.6	26	134
Compression Index (C_c/C_r) Lower Estimate Values	0.3	0.6	1.4	2.3	4.2	24	127
Compression Index (C_c/C_r) Upper Estimate Values	0.7	1.5	2.9	5.2	9.6	25	127
Coefficient of Consolidation (c_v) Lower Estimate Values	0.1	0.3	0.8	1.6	6.9	138	725
Coefficient of Consolidation (c_v) Upper Estimate Values	0.9	1.5	2.9	4.9	6.9	14	69
Both C_c/C_r & c_v Lower Estimate Values	0.02	0.1	0.4	0.9	4.2	137	722
Both C_c/C_r & c_v Upper Estimate Values	1.3	2.3	4.1	6.7	9.6	14	70

As can be seen in Figures 5-18a and 5-18b, changes in preconsolidation pressure profile have a minimal effect on the settlement of the levee. This occurs because the difference between the lower and upper estimate preconsolidation profiles shown in Figure 5-6 is only significant for a limited thickness near the bottom of the middle clay layer. Because the DMM zone extends to the base of the middle clay layer, changes in the compressibility of the soil in this layer have little effect on the settlement of the new levee crest.

The compression index values have a significant effect on the magnitude of the predicted settlement, as shown in Figure 5-18a. For the lower estimate compression index values, which are 40% lower than the best estimate values listed in Table 5-1, the predicted ultimate settlement

of 4.2 in. is 40% lower than the 6.9 in. predicted for the best estimate values. For the upper estimate compression index values, which are 40% higher than the values listed in Table 5-1, the predicted ultimate settlement of 9.6 in. is 40% higher than the 6.9 in. predicted for the best estimate values. The compression index values have no effect on the time-rate of consolidation, as shown in Figure 5-18b.

The coefficient of consolidation values do not affect the magnitude of the predicted ultimate settlement values, as listed in Table 5-4. However, the predicted settlements at intermediate time intervals are affected by the coefficient of consolidation. For the lower estimate c_v values, which are 83% lower than the values listed in Table 5-1, the time to reach 90% consolidation is 725 years. The 127 years predicted for 90% consolidation using the best estimate c_v values listed in Table 5-1 is 83% lower than the calculated time using the lower estimate of c_v values. For the upper bound c_v values, which are 83% higher than the values listed in Table 5-1, the time to reach 90% consolidation is 69 years. The 127-year time to 90% consolidation calculated for the c_v values listed in Table 5-1 is 83% higher than the calculated time using the upper estimate of c_v values.

Based on the range of predicted settlements for all of the analysis cases, the ultimate settlement of the P24 levee crest would be expected to fall in the range from about 4 to 10 inches, with predicted settlement at 3 years in the range from about 0 to 2 inches.

5.3.5. Comparison of Results with Measured Settlements

Settlement monitoring data provided by USACE for the P24 levee consists of surveyed cross-sections at multiple stations along the levee alignment taken on about October 30, 2008. Survey data immediately after construction of the P24 levee was not provided. Based on the nine cross-sections provided for the segment of the P24 levee with DMM shear walls between stations 408+00 and 427+000, the elevation at the centerline of the levee crest in October 2008 ranged between El +17.34 ft and El +17.68 ft. These elevations are higher than the crest elevation of El +17 ft shown the survey profiles at Sta 414+00, as provided to us by USACE as an as-built section for use in the settlement analyses. Without after-construction survey data, a settlement

value cannot be determined for the P24 levee, and precise direct comparisons of the results with measured settlements cannot yet be made.

According to Dr. Pete Cali, the levee was overbuilt by approximately 1 ft and the contractor had a plus/minus 0.25 ft tolerance. Based on the approximate overbuild of the levee and the construction tolerance, the survey data at about 3 years after construction was complete indicates potential settlements in the range from 1 to 11 inches. Considering the basis for this estimated settlement range, it must be considered very approximate.

5.3.6. Comparison of Results with Simplified Settlement Calculation Methods

Simplified hand calculations for consolidation settlement of the levee were made for the base case conditions in the numerical analyses using guidance provided in Skempton and Bjerrum (1957) for applying one-dimensional consolidation calculations to estimate settlement when lateral deformations occur. Lateral deformations develop at the P24 levee site due to the relatively large thickness of compressible clays underneath the levee and DMM zone and the relatively small width of the levee footprint and DMM zone. These deformations are responsible for the immediate settlement during the construction portion of the analyses, and they result in excess pore pressures at the end of construction that are less than the change in vertical stress due to the applied load of the new levee fill. Skempton and Bjerrum provide correlations for determining a correction factor, μ, that can be used to calculate the consolidation settlement for a site where lateral deformations occur based on the conventional one-dimensional settlement calculation, the footing geometry and foundation thickness, and the pore pressure coefficient A of the foundation soil. For the geometry of the P24 levee and the range in pore pressure coefficient A corresponding to normally consolidated clays (0.5 to 1.0), the corrections factor ranges from 0.63 to 1.0.

The following equation was used to calculate the settlement in the lower clay beneath the DMM zone:

$$\rho_c = \mu\rho_{cc} \quad \text{where } \rho_{cc} = H_0 \frac{C_c}{(1+e_0)} \log\left(\frac{p_0 + \Delta p}{p_0}\right) \tag{5.6}$$

ρ_c = Consolidation settlement of the layer

μ = Correction factor from Skempton and Bjerrum (1957)

ρ_{cc} = Conventional one-dimensional consolidation settlement of the layer

H_0 = Initial thickness of the layer

C_c = Compression index for virgin compression

e_0 = Void ratio before construction of new levee

p_0 = Vertical effective stress before construction of new levee

Δp = Change in vertical stress from the load of the new levee fill

The lower clay was subdivided into 4 layers for the settlement calculation. The change in vertical stress in each sublayer due to the applied load of the new levee fill was estimated based, in part, on guidance provided by FHWA (1996) for the settlement of pile group foundations. The applied load on the top of the DMM zone due to the new levee fill was estimated using three different tributary areas: 1) the entire cross-section of the new levee fill; 2) the new levee fill located within 1H:2V tributary lines from the top of the DMM zone; and 3) the new levee fill within vertical tributary lines from the top of the DMM zone. The increase in vertical stress with depth below the DMM zone was estimated for the three load cases using three different load distributions: A) 1H:2V distribution lines beneath an equivalent footing located at the base of the DMM zone; B) 1H:2V distribution lines beneath an equivalent footing located at two-thirds the total DMM zone depth; and C) 1H:2V distribution lines beneath an equivalent footing located at two-thirds the total DMM zone depth with the equivalent footing width determined by a 1H:4V load spread from the top of the DMM zone. Load cases 1 through 3 and distribution cases A through C are shown in Figure 5-19.

The predicted settlements for the hand calculations are listed for each combination of load and distribution case in Table 5-5. The results are presented for a pore pressure coefficient A of 1.0, which is equal to the conventional consolidation settlement, and for a pore pressure coefficient A of 0.5. The calculated settlement ranges from 20.7 in. for the most conservative estimate of Δp (Load Case 1 with Distribution Case A) and A = 1.0, to 6.5 in. for the least conservative estimate of Δp (Load Case 3 with Distribution Case C) and A = 0.5.

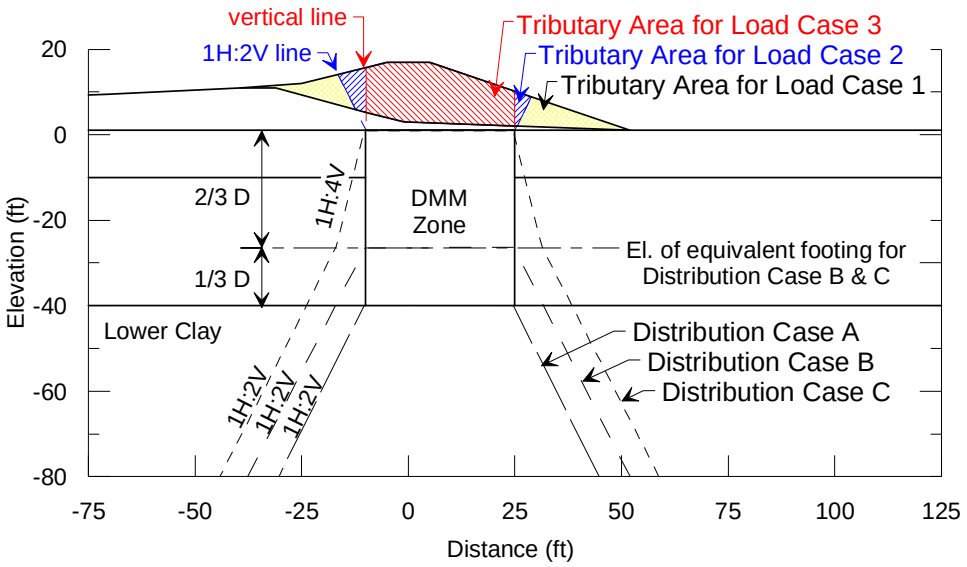

Figure 5-19. Load Tributary Areas and Distribution Lines Used for Calculating the Stress Increase Below the DMM Zone from Placement of New Levee Fill

Table 5-5. Results for Hand Calculation of Settlement for Best Estimate Material Properties

Load Case[1]	Settlement at Top of DMM Zone (in.)					
	Pore Pressure Coefficient A = 1.0[2] (μ = 1.0)			Pore Pressure Coefficient A = 0.5[2] (μ = 0.63)		
	Distribution Case[1]			Distribution Case[1]		
	A	B	C	A	B	C
1	20.7	17.5	15.2	13.0	11.0	9.6
2	16.4	13.8	11.9	10.3	8.7	7.5
3	14.4	12.0	10.4	9.0	7.6	6.5

Notes:
1) Load and distribution cases shown schematically in Figure 5-19.
2) Range in pore pressure coefficient A and correction factor μ determined from guidance in Skempton and Bjerrum (1957).

Considering that not all of the new levee fill will be carried by the DMM zone and some load transfer is likely to occur between the DMM zone and the upper and middle clay layers, Load

Case 2 and Distribution Cases B and C can be considered reasonable approximations for estimating changes in stress due to new levee fill placement for the P24 levee. The results in Table 5-5 show that consolidation settlement of the levee for Load Case 2 and Distribution Case C from hand calculations are 11.9 in. for A = 1.0 and 7.5 in. for A = 0.5. The consolidation settlement of the levee crest from the numerical analyses is 6.9 in., as shown in Table 5-4. Consequently, these results demonstrate that simplified hand calculations provide reasonably good agreement with numerical calculations for the conditions of the P24 levee by using Load Case 2 and Distribution Case C, as illustrated in Figure 5-19, and correcting the conventional consolidation settlement using the guidance provided in Skempton and Bjerrum (1957) with a pore pressure coefficient A = 0.5, which corresponds to $\mu = 0.63$ for this geometry. Conservative calculations can be performed using A = 1, which corresponds to $\mu = 1$ for all geometries.

5.3.7. Stresses in the DMM Zone

To address a question about the potential for settlement-related residual stress in the DMM walls compromising their integrity and function, contours were generated to illustrate the ratio of mobilized shear stress, τ_{xy}, to available shear strength, s, in the DMM zone. Because the FLAC contouring algorithm for stresses interpolates between values at the center of each FLAC zone, the contours were generated using the fine mesh FLAC model shown in Figure 5-11b to provide better resolution at the edges of the DMM zone, where the transition between the relatively strong DMM zone material and the relatively weak native clay results in an abrupt change in stress ratio. The contours shown in Figure 5-20a reflect the stress ratio immediately after construction is complete, before consolidation begins. The shear stresses induced in the DMM zone at the end of construction range from 5 to 35% of the shear strength of the DMM zone, with the highest ratio occurring at the lower flood side corner of the DMM zone. The contours shown in Figure 5-20b reflect a slight decrease in stress ratio during consolidation, with induced shear stresses ranging from 5% to 30% of the shear strength. These results indicated that settlement-induced stress should not compromise the integrity of the DMM walls.

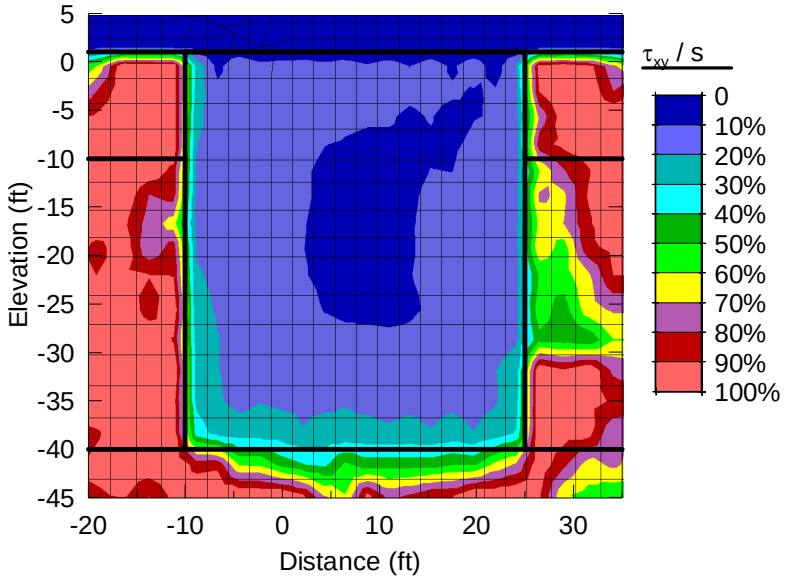

Figure 5-20a. Stress/Strength Ratio at the End of Construction (0% Consolidation)

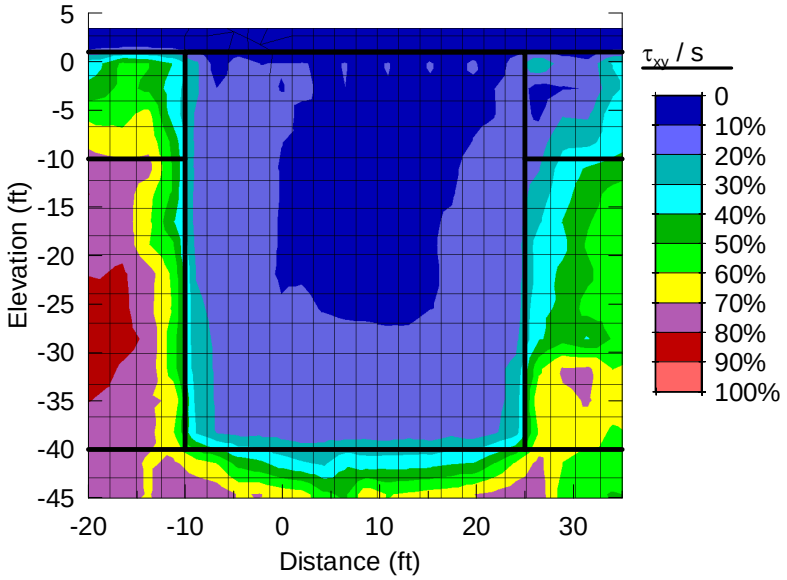

Figure 5-20b. Stress/Strength Ratio at 1000 Years Post-Construction (~100% Consolidation)

Figure 5-20. Shear Stress to Shear Strength Ratio in the DMM Zone

5.4. Conclusions

The following conclusions can be drawn from this study, for the conditions used to represent the P24 Levee:

- The range of ultimate settlement of the P24 levee crest predicted from the settlement analyses is in the range from about 4 to 10 inches, with predicted settlement at 3 years in the range from about 0 to 2 inches. This range was determined using upper and lower estimates of consolidation material property values, as supported by the available data.

- The existing levee reduced the amount of differential settlement of the new levee slopes beyond the flood and protected side boundaries of the DMM shear walls by decreasing the compressibility of the shallow soil layers due to pre-compression from existing levee loads. The potential for longitudinal cracking due to differential settlement under the protected and flood side slopes of the levee beyond the limits of the DMM shear walls should be considered during design. A conservative estimate of differential settlement in this area could be made using simplified hand calculations to predict the settlement in the upper strata (adjacent to the DMM zone) due to the load from the portion of the levee slope that extends beyond the DMM zone.

- Predicted settlement values for the P24 levee crest are not highly sensitive to the depth range investigated for the nearshore gulf deposits, the boundary conditions specified at the base of the old and new levee fill, or the ratio of horizontal to vertical permeability in the portions of the subsurface clay strata with sand and silt lenses. Predicted settlement values also remain relatively constant for the range of preconsolidation pressure profiles investigated in these analyses.

- The compression index values have a significant effect on the magnitude of the predicted ultimate settlement, as well as the predicted settlement for intermediate time intervals. The coefficient of consolidation values do not affect the ultimate settlement magnitude, although they do affect the predicted settlement at intermediate time intervals.

- Survey data from October 2008 provide crest elevations at the centerline of the levee ranging between El +17.34 ft and El +17.68 ft in the segment of the levee with DMM shear walls. These elevations are higher than the crest elevation of El +17 ft shown on the survey profile at Sta 414+00, which was provided to us by USACE as an as-built section for use in the settlement analysis. Without after-construction survey data, a precise settlement value cannot be determined for the P24 levee, which means that reliable direct comparisons between measured and calculated settlements cannot be made. However, based on information from Dr. Pete Cali about overbuild requirements and tolerances, a very approximate estimate is that the levee crest settlement during the first three years after construction may be between 1 and 11 inches. The calculated settlements are at the low end of this range. If subsequent survey data becomes available, more direct comparisons of settlement rates can be made.

- Simplified hand calculations for settlement that calculate the stress increase due to the new levee load using Load Case 2 and Load Distribution Case C, as illustrated in Figure 5-19, and correcting the conventional consolidation settlement using the guidance provided in Skempton and Bjerrum (1957) and a pore pressure coefficient of 0.5 provide reasonable agreement with the numerical analyses for the conditions used to represent the P24 levee.

- None of the analyses produced tensile failure in the levee due to differential settlements.

CHAPTER 6

STABILITY ANALYSES OF THE GAINARD WOODS PUMP STATION T-WALL

This case study included stability analysis of the segment of the U.S. Army Corps of Engineers (USACE)'s Gainard Woods Pump Station T-wall project that included deep-mixed shear walls in the design. Numerical stability analyses were completed and the results were compared with those obtained from the limit equilibrium-based method used by the USACE in their design process. Details of the T-wall design section, material properties, analysis methods, and results are discussed in this chapter. Also provided in this chapter are the conclusions and recommendations specific to this case study.

6.1. Introduction

6.1.1. Purpose and Scope

The primary purposes of the stability analysis case study for the Gainard Woods Pump Station T-wall are to (1) evaluate the stability of the T-wall and DMM system using numerical analyses under the same conditions as used by USACE in their stability analyses, (2) compare the analysis results with the target factor of safety used by USACE to develop the Gainard Woods T-wall design, and (3) make recommendations for future stability evaluations of T-walls with deep-mixed columns.

The scope of work completed for this study includes:

- Reviewing the method-of-planes (MOP) analyses completed by USACE as part of the T-wall design.
- Completing numerical analyses to estimate the T-wall deflections and loads in the piles under design loads.
- Completing numerical analyses to estimate the factor of safety for the system.
- Completing numerical analyses to evaluate the effect of different DMM soil-cement column configurations.

The analyses were completed using the T-wall cross-section, flood level, stratigraphy, unit weights, and strength property values provided by USACE. The project drawings provided by

USACE, as well as the results from their Method of Planes stability analyses and the contractor's documentation of the DMM soil-cement column installation and strength testing are included as Figures A-6 through A-13 in Appendix A.

6.1.2. Project Description

USACE completed reconstruction of flood protection walls adjacent to the Gainard Woods Pump Station along the Mississippi River in Plaquemines Parish, Louisiana. The project included a 90 ft long section of new T-wall construction west of the pump station, between stations 438+40.72 and 439+30.72. The T-wall consists of a reinforced-concrete flood wall supported on two rows of steel H-piles. The flood side piles were installed at a 1H:4V batter to a tip elevation of -71 ft, and the protected side piles were installed at a 1H:3V batter to a tip elevation of -93 ft. The design includes a sheet-pile cutoff underneath the T-wall to elevation -10.5 ft for seepage control. A zone of deep-mixed soil-cement shear walls was installed on the protected side of the T-wall, between the wall and an existing drainage canal, to improve the stability of the system. The shear walls, which are oriented perpendicular to the wall alignment, were constructed using the deep-mixing method (DMM) by overlapping wet-mixed, triple-axis columns. The shear walls are 30 ft long, and positioned at a 6 ft center-to-center spacing in the direction of the levee alignment. Based on the contractor's installation notes, the columns are 36-in. diameter, and the overlap between adjacent columns is 12 in., which produces a center-to-center spacing of 24 in. and a chord length of 26.8 in. at the overlap. The vertical flood side limit of the DMM shear walls was located 30 ft away from the protected side toe of the T-wall at the ground surface to provide a minimum of 10 ft of clearance between the bottom of the shear walls at elevation -55 ft and the battered piles. This geometry leaves a gap between the DMM shear walls and the pile-supported T-wall, which created uncertainty about the effectiveness of the shear walls in improving stability of the T-wall. The effectiveness of the shear walls, considering the gap, can be assessed by numerical analyses.

Deep-mixed shear walls were also installed on the flood side of two segments of existing I-wall between stations 438+10.72 and 438+40.72 and between stations 441+31.00 and 442+54.60. The scope of work for this study did not include evaluation of the I-wall.

The levee geometry and the subsurface conditions used in the analyses are described in the next section.

6.2. Analysis Section and Material Characterization

A design cross-section for the segment of T-wall with DMM soil-cement columns (between stations 438+40.72 and 439+30.72) was provided by USACE. The geometry of the section was established by USACE, and it included the configuration of the soil-cement columns as shown in Section C (Figure A-7 in Appendix A).

The section used for analyses is shown in Figure 6-1, and material property values used in the analyses are listed in Table 6-1. "Stratum 1" is the floodwater on the flood side and the standing water in the drainage canal on the protected side. "Stratum 2" consists of the levee embankment constructed at the base of the T-wall and a stability berm that was constructed on the protected side of the wall. "Stratum 4" through "Stratum 13" are existing layers of soil at the site. Stratum 9 from USACE's MOP analysis section is a thin layer located directly below Stratum 8 that allows USACE to analyze failure surfaces that pass just below the ML layer in MOP analyses. Similarly, Stratum 11 is a thin layer located directly below Stratum 10 that allows USACE to analyze failure surfaces that pass through the top of Stratum 12. These strata are not included in the analysis section used for this study, as the continuous strength assignment options in the limit equilibrium and numerical analysis software allow surfaces to develop at the top of Strata 10 and 12 without the need to insert a distinct layer.

The subsurface profile includes one layer whose strength depends on effective, rather than total, normal stresses. This is an ML layer that is 5 ft thick and located 36 to 41 ft below the base of T-wall. The piezometric surface used by USACE in their MOP analyses to calculate pore pressures in the ML layer coincides with the flood water elevation of +17 ft on the flood side of the T-wall and with the ground surface on the protected side down to the standing water in the drainage canal at elevation -7 ft. In the location of the T-wall, the MOP analyses used a piezometric surface that coincided with the base of the flood wall at elevation +1 ft. This creates unrealistic hydraulic gradients moving from the flood side to the protected side in the ML layer. Instead, we used a smooth hydraulic gradient that varies linearly between the flood elevation on the flood

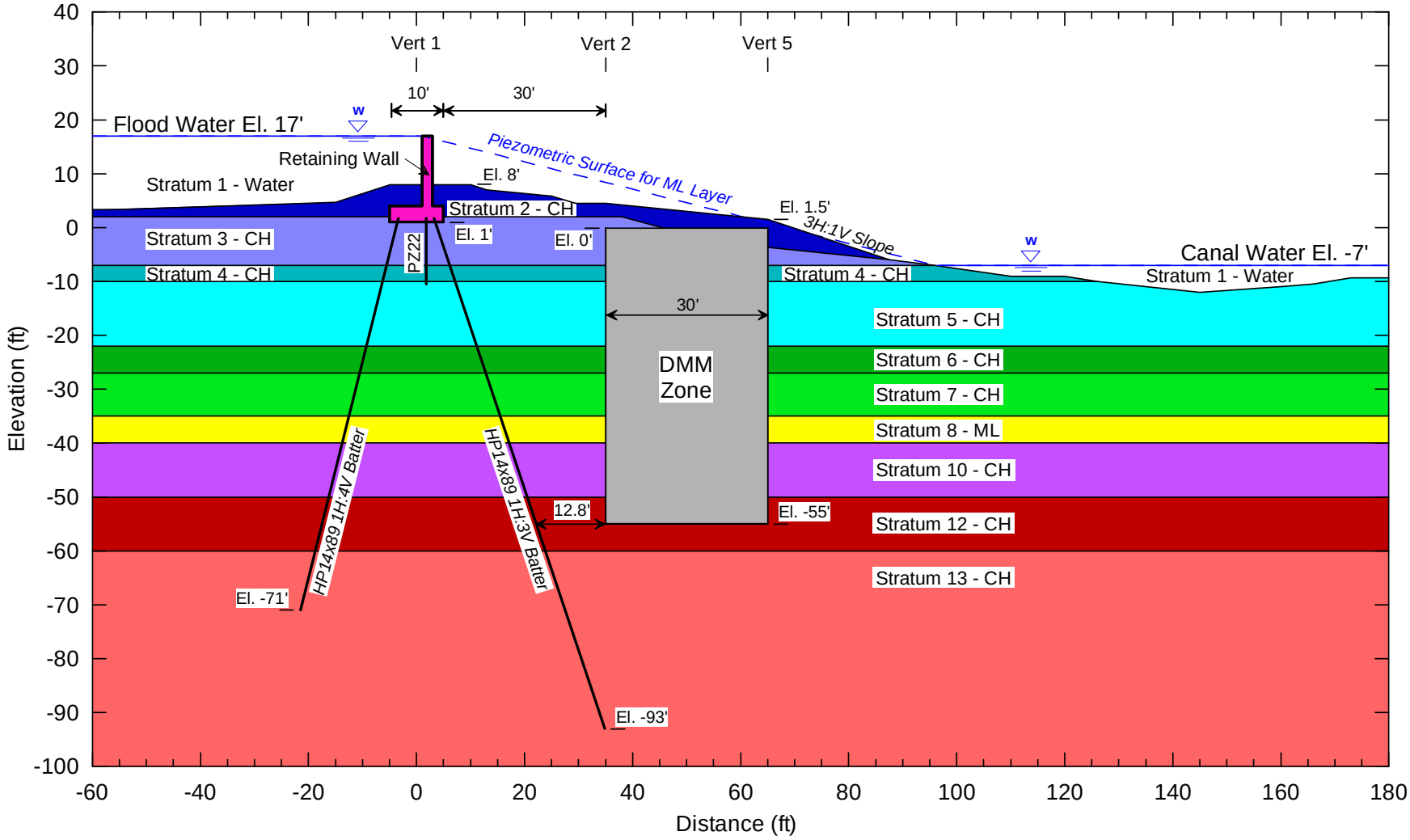

Figure 6-1. Analysis Cross-Section for Stability Analyses of the Gainard Woods Pump Station T-wall

Table 6-1. Summary of Material Property Values for Stability Analyses of the Gainard Woods Pump Station T-wall

Stratum	Elevations (ft)	Unit Weight (pcf)			c[2] (psf)			ϕ (deg)	PMT G/s_u[4]	TXT G/s_u[5]	ν[7]
		Vert 1	Vert 2	Vert 5	Vert 1	Vert 2	Vert 5				
Stratum 1 – Water	-12 to 17	62.4			--			--	--	--	--
Stratum 2 – CL	-6 to 8	110			400			0	130	30.7	0.49
Stratum 3 – CL	-7 to 2	86			300	215	150	0	100	16	0.49
Stratum 4 – CL	-10 to -7	98	86	98	300	215	150	0	130	30.7	0.49
Stratum 5 – CL	-22 to -10	100	92	100	300 to 420	215 to 335	150 to 270	0	130	30.7	0.49
Stratum 6 – CL	-27 to -22	115	100	100	420 to 470	335 to 385	270 to 320	0	130	30.7	0.49
Stratum 7 – CL	-35 to -27	115	100	100	470 to 550	385 to 465	320 to 400	0	130	30.7	0.49
Stratum 8 – ML	-40 to -35	117			200			15	130[6]	30.7[6]	0.49
Stratum 10 – CL	-50 to -40	115	100	100	600 to 700	515 to 615	450 to 550	0	160	30.7	0.49
Stratum 12 – CL	-60 to -50	105			700 to 800	615 to 715	550 to 650	0	160	30.7	0.49
Stratum 13 – CL	Below -60	105			800+	715+	650+	0	160	30.7	0.49
DMM Zone	-55 to 0	Same as existing[1]			1000[3]			0	103[8]		0.45[8]

Notes:

1) The unit weight was unchanged from that assigned to the existing soil layers.
2) Cohesion for the CL layers increases with depth below El -10 ft at a rate of 10 psf/ft.
3) Representative DMM cohesion is a weighted average for the column/soil matrix within the DMM zone, see discussion in text.
4) Stiffness ratios from pressuremeter tests (PMT) based on representative values from the Geomatrix (2007) report.
5) Stiffness ratios from triaxial tests (TXT) based on representative values from the Geomatrix (2007) report. Triaxial G/s_u converted from Geomatrix E/s_u values using a Poisson's ratio of 0.5, such that $G = E/3$.
6) Stiffness assigned to ML layer computed using $s_u = \sigma_v' \tan\phi + c$.
7) Poisson's ratios based on representative values from the Geomatrix (2007) report.
8) Values from Navin (2005) and Navin and Filz (2005).

side of the flood wall stem and the elevation of the water in the drainage canal to calculate pore pressures in the ML layer. This piezometric surface is shown in Figure 6-1. Pore pressures in the other strata were set to zero and shear strengths in these strata were based on a $\phi = 0$ representation to model undrained conditions.

The material property values for the limit equilibrium analyses were provided by USACE in the summary of their MOP analyses, included as Figure A-11 in Appendix A. Liner interpolation was used to model the horizontal variation in soil strengths and unit weights between verts 1 and 2 and between verts 2 and 5. As shown in Figure 6-1, vert 1 is located in the center of the flood wall footprint (X = 0) and verts 2 and 5 are located along the flood side (X = 35) and protected side (X = 65) edges of the DMM zone. Verts 3 and 4 from the Corp's MOP analysis were located along the edges of the DMM zone, just inside of verts 2 and 5, and were used to assign the DMM strength to that segment of the strata. These verts are not included in the cross-section or property table for this study, as the DMM zone is identified as a distinct material. The cohesion assigned to soil strata 5 through 7 and 10 through 13 reflect a 10 psf/ft increase in cohesion with depth below elevation -10 ft. Some of the cohesion values assigned based on this characterization varied slightly from those used in USACE's MOP analyses to standardize the linear increase in cohesion with depth for these strata. The MOP analyses modeled impounded water as a zero strength material. For the limit equilibrium and numerical analyses in this study, impounded water is modeled as an applied pressure on the ground surface.

Additional material property values required for the deformation analyses were determined based on the representative properties for deformation analyses of T-wall structures in New Orleans provided in the Geomatrix Report titled "Soil-Structure Interaction and Load Transfer Mechanisms of Pile Supported T-wall for New Orleans Levees" (Geomatrix 2007). These values are included in Table 6-1. The Geomatrix report provides two sets of representative modulus values for use in the numerical analyses of T-walls in the New Orleans area: one set of shear modulus/shear strength ratios, G/s_u, derived from pressuremeter field tests (PMT), and one set of Young's modulus/shear strength ratios, E/s_u, derived from triaxial laboratory tests (TXT). Additional discussion of the PMT and TXT modulus values is in the Geomatrix (2007) report.

The TXT modulus ratios listed in Table 6-1 were converted to G/s_u ratios using the Poisson's ratio corresponding to undrained behavior of 0.5, to provide for direct comparison with the PMT G/s_u ratios. Stratum 3 was assigned Geomatrix's G/s_u ratio for peat based on the low unit weight of this material. Other strata above and below elevation -40 were assigned PMT G/s_u ratios of 130 and 160, respectively, similar to the characterization in the Geomatrix report. For the numerical analyses, a Poisson's ratio of 0.49 was assigned to all of the soil strata, similar to the characterization in the Geomatrix report. The Poisson's ratios listed in Table 6-1 are reduced from the theoretical upper limit value of 0.5 for undrained behavior to avoid numerical instability in the FLAC finite difference model.

6.2.1 T-wall Properties

The T-wall consists of a pile-supported concrete flood wall with a sheetpile seepage cutoff. The configuration of the wall, piles, and sheetpile were provided by USACE. According to USACE, the dimensions shown on the typical T-wall details of Figure A-10 in Appendix A correspond to the as-built conditions for the Gainard Woods T-wall. Pile dimensions shown on Detail C-1 of Figure A-7 in Appendix A were preliminary and do not reflect the as-built conditions. The as-built conditions shown in Figure A-10 were used for this study, as directed by the USACE.

The concrete flood wall was modeled with elastic elements and assigned a unit weight of 150 pcf, a shear modulus of 1.84×10^8 psf and a bulk modulus of 3.07×10^8 psf. This characterization was taken directly from the Geomatrix (2007) report. Elastic elements are not compatible with FLAC's (Itasca 2005) automated factor-of-safety procedure that was used for some of the numerical analyses described in this report. When FLAC's automated factor-of-safety procedure was used, the flood wall was characterized with a Mohr-Coulomb cohesion of 1020 psf and a somewhat lower shear and bulk moduli to allow the procedure to run.

The HP14x89 piles were modeled using pile elements and assigned a unit weight of 491 pcf, a Young's modulus of 29 x 106 psi, a moment of inertia of 0.04360 ft^4 , a cross-sectional area of 0.1813 ft^2, an exterior perimeter of 4.75 ft and pile spacing of 5 ft. The pile springs used in the FLAC analyses were developed based on the methodology for calculating shear and normal pile springs from empirical p-y and t-z curves discussed in the Geomatrix (2007) report.

The sheet pile cutoff wall was modeled using beam elements. According to Mark Woodward from USACE, the existing sheetpile wall shown on the design drawings consisted of PZ22 units. The beam was assigned a unit weight of 491 pcf, Young's modulus of 29 x 10^6 psi, moment of inertia of 4.1 x10^{-3} ft^4, and cross-sectional area of 0.04618 ft^2/ft. This characterization was taken directly from the Geomatrix (2007) report.

6.2.2 DMM Zone Properties

The cohesion value of 1000 psf listed in Table 6-1 for the DMM zone is based on the area replacement ratio in the DMM zone. This strength value was provided by USACE, and it was based on an unconfined compressive strength for the DMM treated soil of 80 psi (11520 psf) and a 40% replacement ratio. The representative strength calculated by USACE includes two partial factors of safety, each equal to 1.5, which are part of USACE's design process for DMM material. USACE conservatively did not include the strength of the soil between DMM walls in its evaluation of the strength of the DMM zone because of the much higher strain to failure expected for the untreated soil compared to the DMM material. The resulting calculation of the shear strength of the DMM zone is ((0.4)(11520 psf))/((2)(1.5)(1.5)) = 1024 psf, which is approximately equal to USACE's value of 1000 psf listed in Table 6-1.

Unconfined compressive strength tests were performed on core samples taken from the DMM soil-cement columns in the field. Statistical analyses were performed on the 28-day-break strength test data provided by USACE in Figure A-13 in Appendix A, and a summary of the results for the Gainard Woods Pump Station DMM test results is included in Table 6-2. For all of the test data, the average unconfined compressive strength of the DMM mixture was much greater than the 80 psi strength used by USACE for design.

A stiffness ratio, E/s_u, of 300 and a Poisson's ratio of 0.45 were estimated for the wet-mix DMM columns based on guidelines provided by Navin (2005) and Filz and Navin (2006). These values are listed in Table 6-1, after converting E to G using a Poisson's ratio of 0.45 to provide for direct comparison with the other G/s_u ratios.

Table 6-2. Summary of Strength Test Results for Gainard Woods Pump Station Columns

Test Group	No. of Tests	UCS (psi)		
		Mean	Median	St. Dev
DMM west of pump station (Sta. 438+10.72 ~ Sta. 439+30.72)	140	331.8	273	168.5
DMM east of pump station (Sta. 441+31.00 ~ Sta. 442+54.60)	140	273.1	247	128.9
All Tests	280	302.4	255	152.6

In the numerical analyses, vertical joints were included in the DMM improved zone to model potential weak joints between columns. The possibility of weak vertical joints at column overlaps is discussed in the Japanese and Scandinavian literature (CDIT 2002, Broms 2003) and is also recognized in U.S. practice (Sehn 2005). DMM shear walls constructed by overlapping columns are weaker along vertical planes at the column overlaps due to the reduced width of the shear wall at these locations. In addition to this reduction of the composite strength inherent to the design layout, the strength at the column overlap could be further reduced by misalignment during construction. The influence of strength achieved at the column overlap on stability of the system can be evaluated by varying the joint strength over a range extending from that corresponding to the full design mixture strength applied to the full design column overlap (100% efficiency) and that corresponding to no overlap between the columns (0% efficiency).

A vertical joint strength corresponding to 100% efficiency was determined based on the width of the shear wall at the location of the design column overlap (26.8 in.) versus the average width of the shear wall (33.1 in). Because of the reduced width, the replacement ratio for a vertically aligned shear plane located at the joint is 20% less than that for a horizontal shear plane through the wall. Therefore, the composite strength for vertical shearing through the DMM zone along the joints for the case of full design column overlap (100% efficiency) can be estimated as 80% of the composite strength for horizontal shearing through the DMM zone of 1000 psf.

The joint strength corresponding to 0% efficiency was set equal to a representative soil strength of 367 psf in the DMM treated zone, based on a weighted average of soil strengths along the

vertical joints. This condition corresponds to no overlap between columns. The vertical joint strength for intermediate efficiencies can be obtained by interpolation between the values for 0% and 100% efficiencies.

The joints were modeled by assigning FLAC's "Ubiquitous Joint" model to selected columns of elements within the DMM improved zone and assigning a vertical orientation for the reduced strength. On any other plane within the Ubiquitous Joint elements, the full composite shear strength of 1000 psf applies. The DMM improved material between vertical joints was modeled using the full composite strength of 1000 psf in all directions. The modulus of the joint material was not reduced for shearing on the vertical plane from the representative characterization for the DMM zone listed in Table 6-1. While the Ubiquitous Joint model does allow for a different strength assignment along a specified plane, it does not allow for the assignment of a different modulus for shearing on that plane. According to the FLAC manual, modulus values typically have an insignificant effect on factor of safety calculations. For these analyses, the shear walls were assumed to have four equally spaced vertical joints, corresponding to the number of joints between triple-axis installations at the Gainard Woods site.

6.3. Numerical Analyses

Numerical analyses for the Gainard Woods T-wall were completed using the finite difference computer code FLAC (ITASCA 2005). This section describes the analysis methods, model validation, and results.

6.3.1. Analysis Methods

The mesh used for the numerical analyses extended approximately 140 ft beyond the T-wall on the flood side, 150 ft beyond the DMM zone on the protected side, and 50 ft below the tip of the piles. The extent of the model is shown schematically in Figure 6-2 and the discretized mesh in the vicinity of the levee is shown in Figure 6-3. No lateral displacements were allowed on the left- and right-hand sides of the mesh, and no lateral or vertical displacements were allowed on the bottom of the mesh.

For the model validation study, the tensile strength of the elements was set to a high number to prevent tensile failure and allow for direct comparison with the limit equilibrium analyses. For the remainder of the numerical analyses, the tensile strength of the soil and DMM zone were set to zero to allow for the formation of tension cracks.

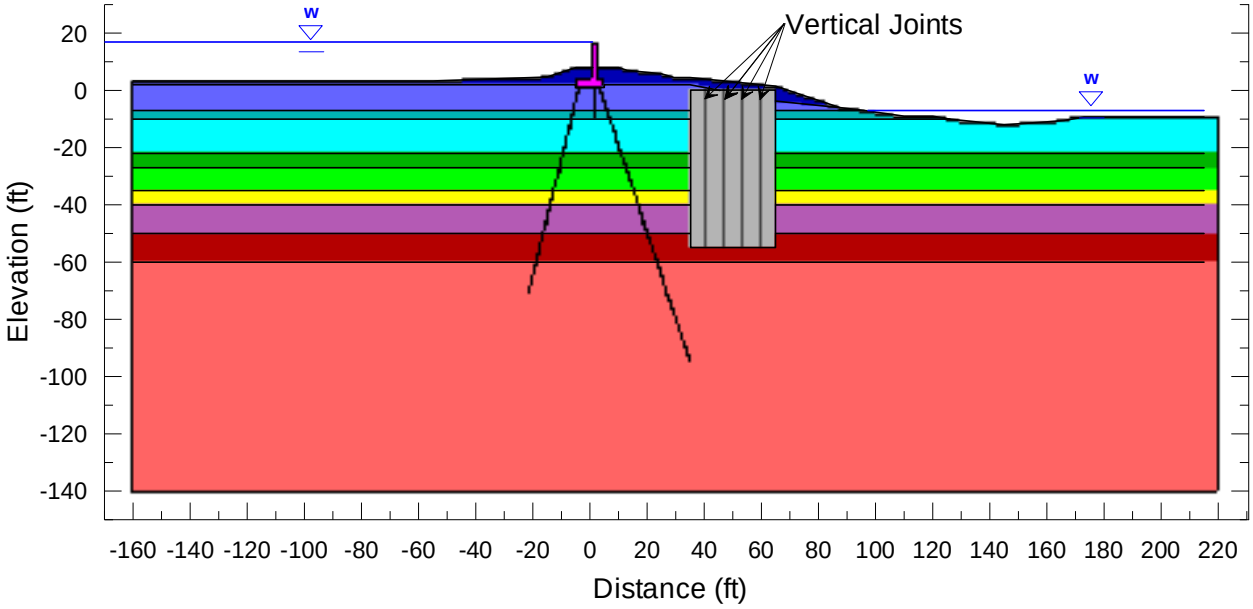

Figure 6-2. Extent of FLAC Model

6.3.2. Model Validation

The numerical model was validated by comparing the results of stability analyses from the numerical model with those from limit equilibrium stability analyses, completed using UTEXAS4 (Wright 2007). The numerical stability analyses were completed using the FLAC mesh and material properties described above. The validation analyses were completed without the HP piles and sheetpile cutoff below the flood wall to provide for direct comparison of the numerical and limit equilibrium results. In addition, the lateral water pressures on the back of the flood wall from the impounded flood water were not included, to avoid a lateral sliding failure of the wall, which would otherwise occur for the wall without pile support.

To avoid complications in the validation analyses and facilitate comparisons between UTEXAS4 and FLAC, the UTEXAS4 analyses were performed without allowing tension cracks to form,

and the FLAC analyses were performed with high tensile strengths to prevent tensile failure of the elements. For the validation section, which does not include the T-wall piles, tension cracks would form on the flood side of the wall and would be filled with water. Because of the difficulty in modeling water-filled tension cracks in FLAC at locations and depths that would *result from* the FLAC analyses rather than be *assumed prior to* the FLAC analyses, the validation study was completed for the case without tension cracks. This was considered a reasonable approach for validation because the tendency for tension cracks to form on the flood side of the wall is considerably less when piles are present. In fact, tension cracks did not develop on the flood side of the wall for the remainder of the Gainard Woods analyses, which did include the T-wall piles and did allow for tensile failure of the soil.

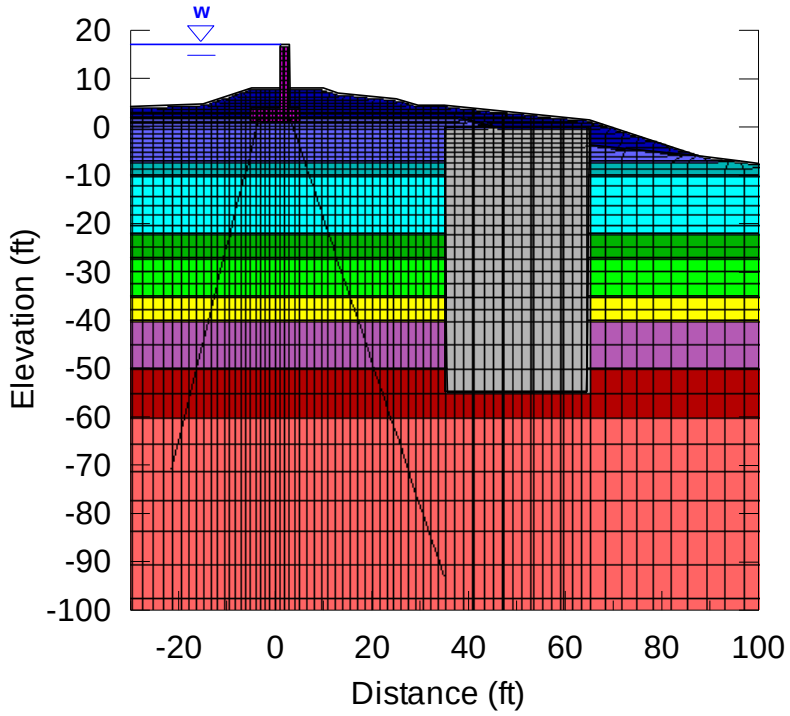

Figure 6-3. FLAC Mesh Discretization near T-wall and DMM Zone

FLAC's automatic factor of safety routine was used to calculate the factor of safety for the validation geometry. This procedure reduces the shear strength of all of the materials in the model by a uniform reduction factor until the program is not able to satisfy convergence criteria in a limited number of iterations. The factor of safety is the largest strength reduction factor (SRF) at which convergence is still achieved within the limited number of iterations. Because

the procedure will not operate with elastic elements, the flood wall was assigned Mohr-Coulomb properties with very high strengths.

Both shallow and deep failure modes were investigated in the numerical analyses. When the factor of safety for shallow failure surfaces was less than the factor of safety for deep failure surfaces, it was necessary to increase the shear strength of a block of soil crossing the shallow failure surface to investigate deeper failure modes. In these cases, a shear strength of 1000 psf was applied to the foundation soils in the area of the shallow failure to permit investigation of deeper failure surfaces. This approach is analogous to the technique often employed in limit equilibrium analyses to avoid shallow failure surfaces when using automated search routines. The computed factors of safety and shear strain contours that illustrate the modes of failure are shown in Figure 6-4. The critical failure mode, shown in Figure 6-4a, is a complex mode consisting of shallow failures on the flood and protected sides of the DMM zone as well as rotation of the DMM zone. The factor of safety for this predominately shallow failure mode is 1.38. For a deeper failure mode that passes beneath the DMM zone, the estimated factor of safety is 1.49, as shown in Figure 6-4b.

The computer program UTEAXS4 was used to search for critical circular and non-circular surfaces. The analyses were performed using Spencer's procedure. The critical surfaces are shown in Figure 6-4. For relatively shallow circular failure surfaces, the minimum calculated factor of safety is 1.58 for a failure surface located on the flood side of the DMM zone, as shown in Figure 6-4a. A search for shallow circular failure surfaces on the canal side of the DMM zone resulted in a minimum calculated value of factor of safety equal to 1.85. For relatively shallow non-circular failure surfaces, the minimum values of factor of safety for failure surfaces on the flood side and canal side of the DMM zone are 1.35 and 1.58, respectively. For deeper failure surfaces passing underneath the DMM columns, the minimum computed values of factor of safety are 1.45 for circular and non-circular failure surfaces, as shown in Figure 6-4b.

Although the critical failure mode from the FLAC numerical analyses for a predominately shallow surface is complex, it can be seen in Figure 6-4 that the factor of safety calculated by FLAC for a predominately shallow failure (FS = 1.38) is similar to the UTEXAS4 limit equilibrium results for the non-circular surface between the flood wall and the DMM zone (FS =

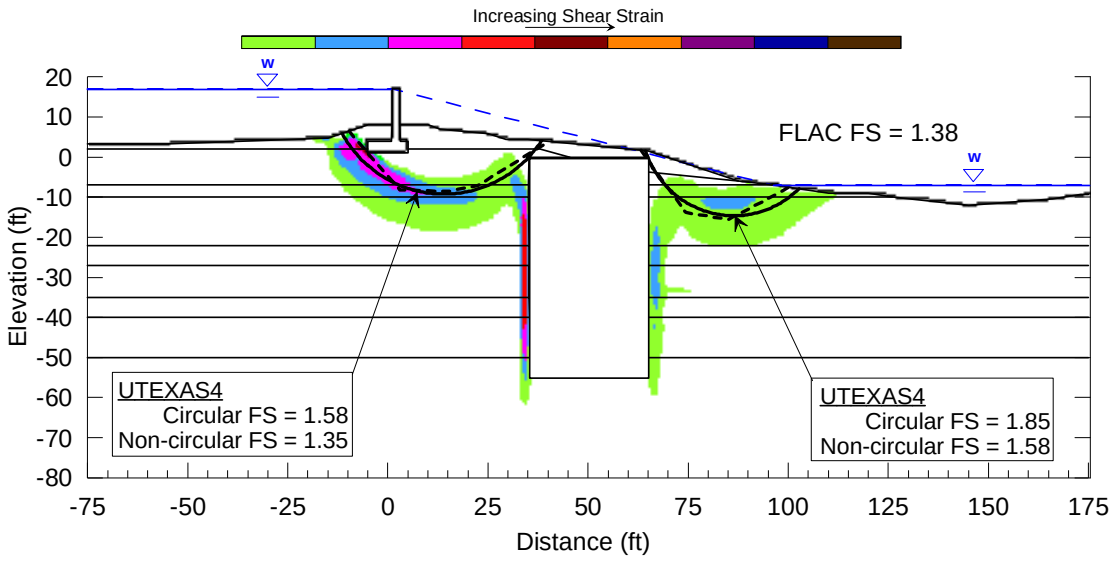

Figure 6-4a. Predominately Shallow Surfaces

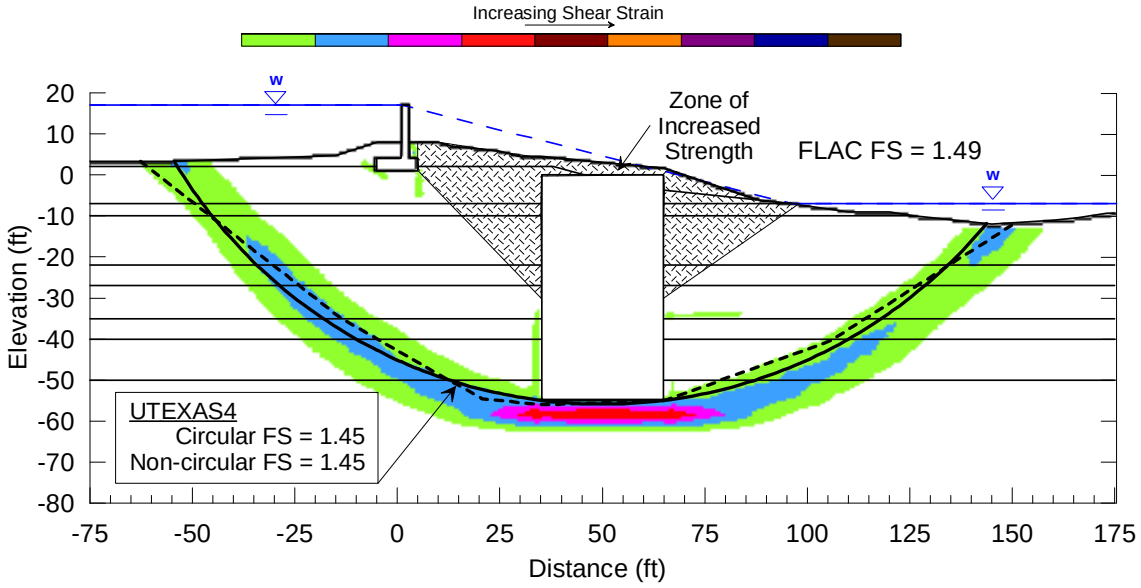

Figure 6-4b. Deep Surfaces

Figure 6-4. Comparison of Results from Limit Equilibrium and Numerical Stability Analyses

1.35), for the conditions of the validation analyses. For the deep failure mode, the shape of the failure surface illustrated by the shear strain contours from the numerical analyses is similar to that determined using limit-equilibrium analyses, and the computed factor of safety from FLAC (FS = 1.49) is in good agreement with that from UTEXAS4 (FS = 1.45).

6.3.3. Deformation Analyses of Pile-Supported T-wall

Deformation analyses were completed for the PMT and TXT stiffness values under the design loading with no reduction of soil strengths (SRF = 1.0) for the case of 100% efficiency of the DMM vertical joints. For these and subsequent numerical analyses described in this report, tensile failure of soil and DMM materials was allowed, with tensile strengths set equal to zero. The resulting shear strain contours and soil displacement vectors in the vicinity of the T-wall and DMM zone are shown in Figures 6-5 and 6-6. The shear strain contours show the initial stages

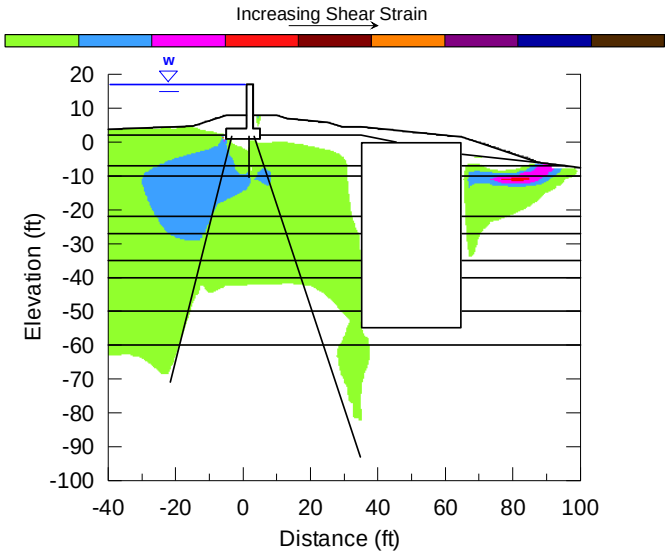

Figure 6-5a. PMT G/s_u

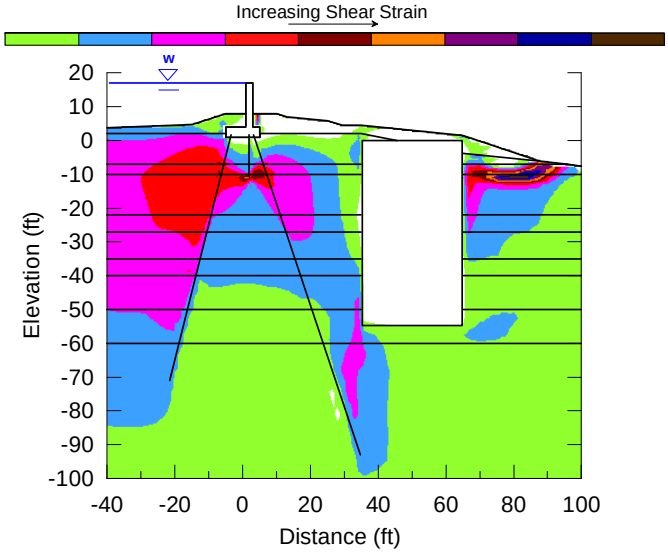

Figure 6-5b. TXT G/s_u

Figure 6-5. Shear Strain Contours for Design Loads with SRF = 1.0, 100% Efficiency of Joints

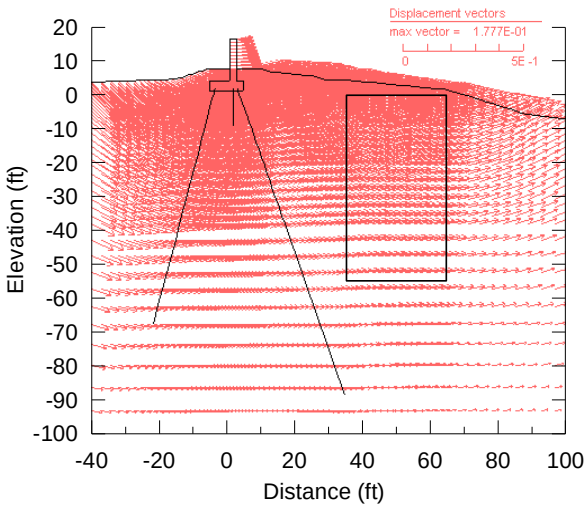

Figure 6-6a. PMT G/s_u

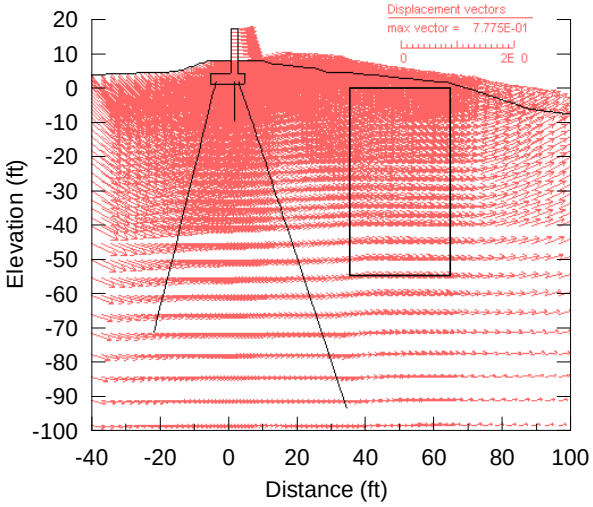

Figure 6-6b. TXT G/s_u

Figure 6-6. Displacement Vectors for Design Loads with SRF = 1.0, 100% Efficiency of Joints

of development of a shallow rotational failure on the canal side of the DMM zone, similar to the shallow failure surfaces at this location from the validation analyses. The displacement vectors indicate that the T-wall and the DMM zone generally move laterally towards the canal. While the shear strain and displacement patterns are similar for both models, the magnitudes are significantly greater for the TXT stiffnesses. The maximum displacement for any gridpoint in the model is 2.1 in. for PMT G/s_u and 9.3 in. for TXT G/s_u.

Monitoring points were selected at the locations shown in Figure 6-7 to permit better understanding of the movement of the T-wall, DMM zone, and the shallow failure surface on the

canal side of the DMM zone. Horizontal and vertical displacements for these points are listed in Tables 6-3 and 6-4 to allow for relative comparison between analyses cases. For 100% efficiency of DMM joints, deformation analyses under design loads with SFR = 1.0 for the model with PMT stiffnesses show a lateral displacement of the base of the flood wall of 1.68 in. and a slight uplift of the top of the wall equal to 0.05 in. For the model with TXT stiffnesses, the calculated lateral displacement of the base of the flood wall is 6.89 in. and the uplift of the top of the wall is 0.04 in. Results for other cases listed in Tables 6-3 and 6-4 are discussed in the following sections.

The larger lateral displacements calculated for the model with TXT stiffness are also reflected in the pile response curves shown in Figure 6-8. The movement of the piles, shear force, and moment are all greater for the model with TXT stiffnesses. The sign convention for axial and normal pile displacements is shown in Figure 6-7. The axial and normal pile displacements for the flood side and protected side piles are total displacements, not the relative movements between the pile and the soil. For the TXT stiffnesses, the axial forces in the flood side pile indicate that the upper 15 ft of the pile is in tension, while the lower 60 ft of the pile is in compression. For the PMT stiffnesses, the entire flood side pile is in compression. The protected side pile is in compression for the entire length of the pile for both stiffnesses.

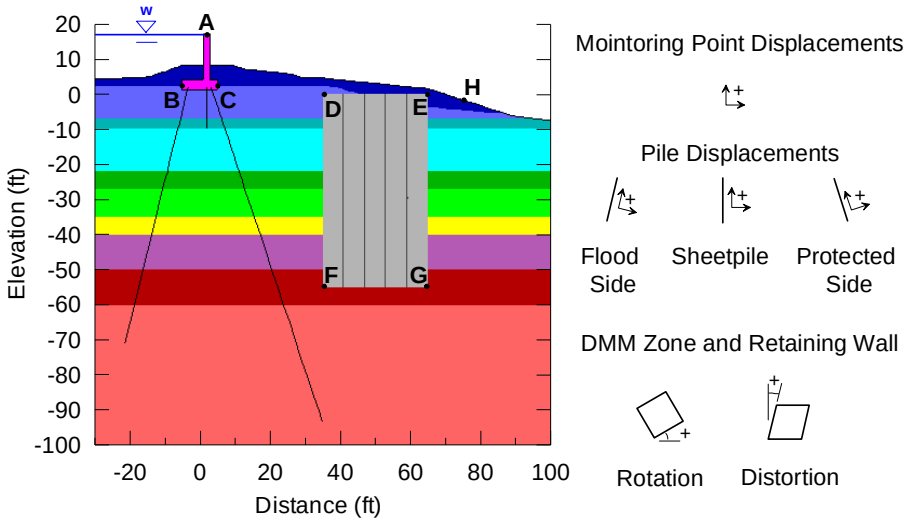

Figure 6-7. Location of Monitoring Points and Sign Convention for Displacements

Table 6-3. Horizontal Displacements of Monitoring Points for Design Loads with SRF = 1.0

Analysis Case	Horizontal Displacement (in.)							
	Pt. A	Pt. B	Pt. C	Pt. D	Pt. E	Pt. F	Pt. G	Pt. H
100% Efficiency, PMT G/s_u	0.83	1.68	1.68	1.46	1.36	1.05	0.88	1.31
100%, Efficiency, TXT G/s_u	3.82	6.89	6.89	6.38	6.23	5.25	4.85	6.02
0%, Efficiency, PMT G/s_u	0.83	1.68	1.68	1.47	1.36	1.05	0.88	1.32
0%, Efficiency, TXT G/s_u	3.83	6.90	6.90	6.37	6.22	5.23	4.84	6.02
No DMM Zone, PMT G/s_u	0.93	1.83	1.83	1.64	1.48	1.05	0.85	1.42
No DMM Zone, TMT G/s_u	4.69	7.87	7.87	7.33	6.72	5.39	4.35	6.51

Table 6-4. Vertical Displacements of Monitoring Points for Design Loads with SRF = 1.0

Analysis Case	Vertical Displacement (in.)							
	Pt. A	Pt. B	Pt. C	Pt. D	Pt. E	Pt. F	Pt. G	Pt. H
100% Efficiency, PMT G/s_u	0.05	-0.38	0.23	0.45	0.24	0.12	0.16	0.42
100% Efficiency, TXT G/s_u	0.04	-1.46	0.68	1.49	0.79	0.88	0.66	1.85
0% Efficiency, PMT G/s_u	0.05	-0.38	0.23	0.45	0.24	0.12	0.16	0.42
0% Efficiency, TXT G/s_u	0.04	-1.46	0.68	1.48	0.81	0.87	0.66	1.87
No DMM Zone, PMT G/s_u	0.06	-0.39	0.25	0.58	0.52	0.04	0.19	0.51
No DMM Zone, TMT G/s_u	0.02	-1.54	0.68	2.57	2.58	0.15	1.02	2.58

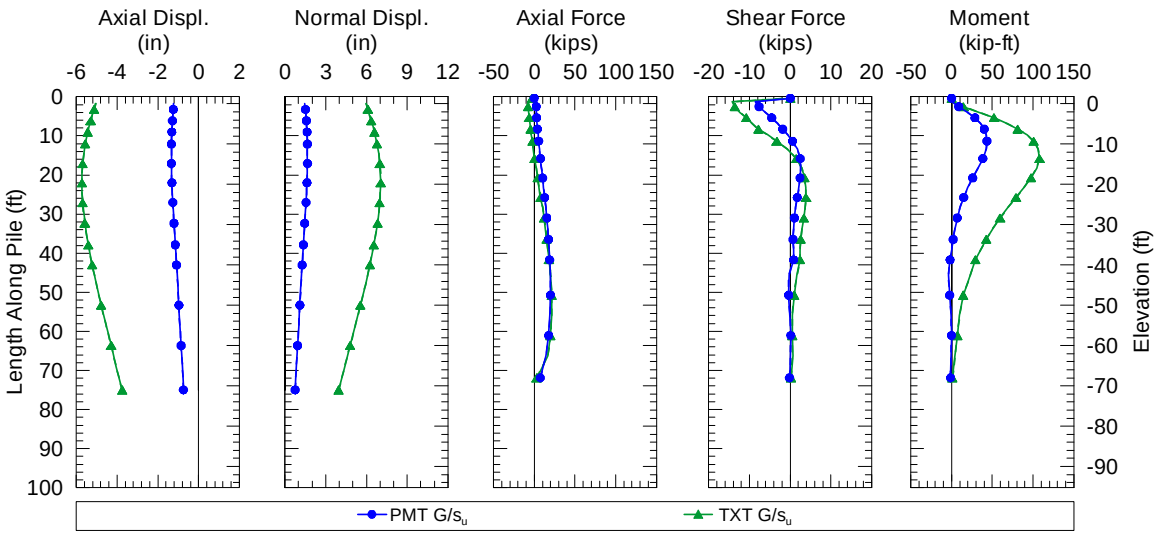

Figure 6-8a. Flood Side Pile (Tip El -71 ft, 1H:4V Batter, 5 ft Spacing)

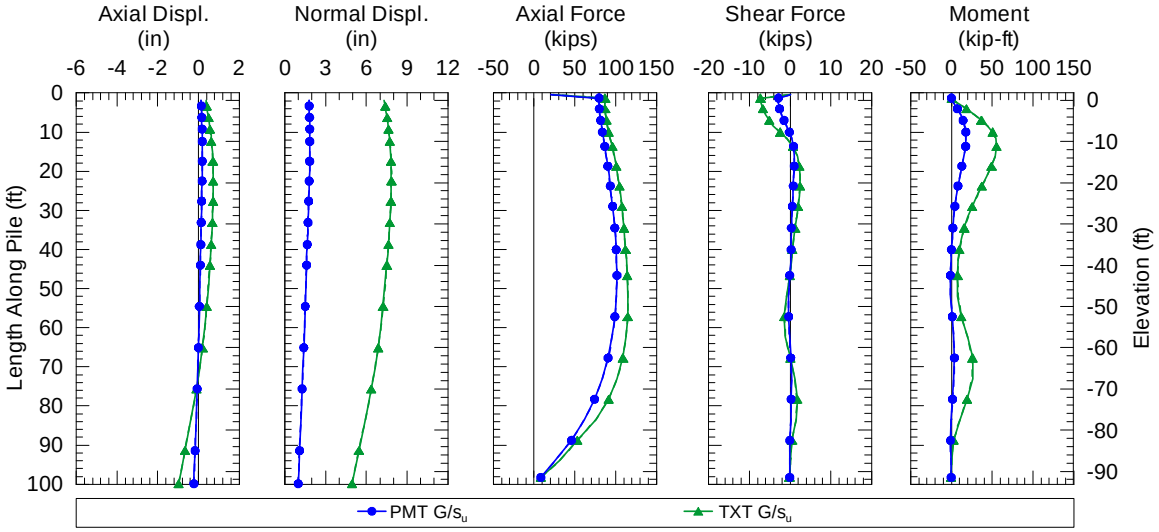

Figure 6-8b. Protected Side Pile (Tip El -93 ft, 1H:3V Batter, 5 ft Spacing)

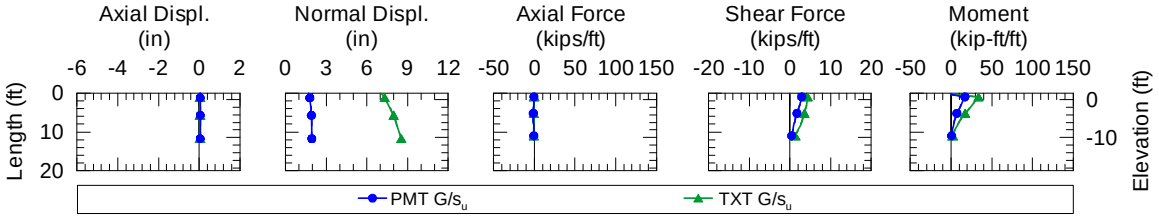

Figure 6-8c. Sheetpile (Tip El -10.5 ft, Vertical)

Figure 6-8. Pile Response for Design Loads (SRF=1.0)

6.3.4. Factor of Safety Analyses of Pile-Supported T-wall

Factors of safety were initially calculated using an automated procedure in the FLAC program. As discussed previously, this procedure reduces the shear strength of all of the materials in the model by a uniform reduction factor until the program is not able to satisfy convergence criteria in a limited number of iterations. The factor of safety is the largest strength reduction factor at which convergence is still achieved within the limited number of iterations. The automated procedure can be used with Mohr-Coulomb and ubiquitous joint strength characterizations, but it will not operate with elastic, two-dimensional, elements in the model. The procedure does function with elastic structural elements in the model, such as piles. However, the strength reduction factor in FLAC's automated procedure is not applied to the strength of the pile coupling springs that connect the pile to the two-dimensional soil elements.

Because the automated procedure does not reduce the strength of the pile coupling springs, a manual procedure was developed for calculating the factor of safety of the Gainard Woods T-wall section. In this procedure, the automated procedure was first run on a base model that had reached equilibrium under design loads with design soil and pile coupling spring strengths to determine the number of additional iterations FLAC allowed for convergence to be achieved in its automated procedure. The additional step cutoff for the automated factor of safety procedure was calculated by subtracting the number of steps required to reach the initial equilibrium state for the base model from the total number of steps allowed in the automated factor of safety analysis. Individual deformation analyses were then run using the same base model for a range of strength reduction factors, with the strength reduction factor applied to the soil elements and the pile coupling springs. The number of additional steps required for convergence for each strength reduction factor in the manual procedure was compared with the additional step cutoff from the automatic factor of safety analyses, and the factor of safety is the largest strength reduction factor for which the convergence ratio is less than or equal to 1.0.

This procedure was applied to the models with 100% efficiency of the DMM joints for PMT and TXT stiffnesses. The factor of safety calculated by the automated procedure for these cases is 1.67. The results for the manual factor of safety analyses that include reduction of the pile spring strengths are plotted in Figure 6-9. Also included in Figure 6-9 are the results for manual factor

of safety analyses that did not include reduction of the pile spring strengths, which provide for direct comparison with the automated factor of safety procedure.

Figure 6-9 shows that, for the analyses that included reduction of the pile spring strength, the factor of safety is about 1.61 for the PMT G/su and about 1.59 for the TXT G/su. These values are slightly less than the value of FS = 1.67 from FLAC's automated procedure, which is reasonable considering that FLAC's automated procedure does not apply strength reduction to the pile coupling spring strengths. It can also be seen in Figure 6-9 that the manual factor of safety values generally coincide with the break point on the convergence curve, after which small increases in SRF result in large increases in the number of iterations required to reach convergence. Calculated horizontal and vertical displacements for monitoring point A (the top of the T-wall stem) are also included in Figure 6-9. These plots show a trend of increasing rate of displacement at SRF values near the factor of safety.

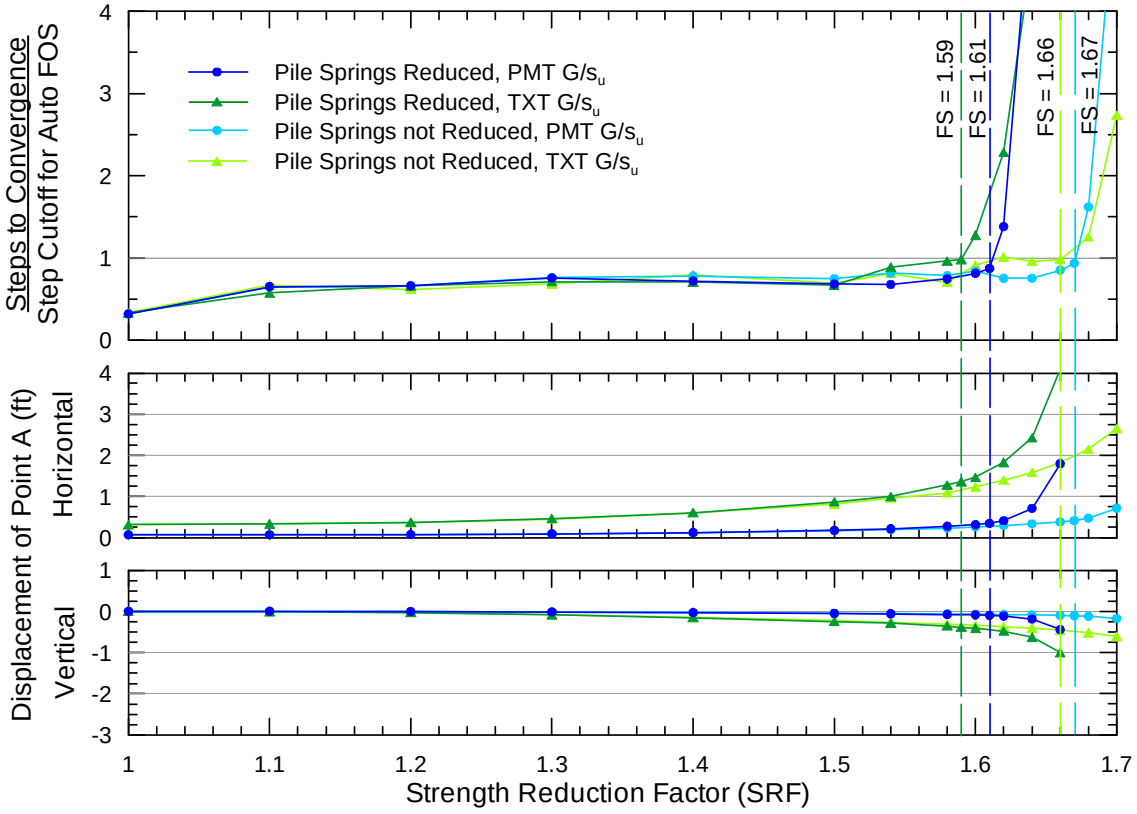

Figure 6-9. Manual Factor of Safety, 100% Efficiency of Joints

For the manual factor of safety analyses without reduction of the pile spring strength, the trends are similar, but the convergence criterion was reached at strength reduction factors of 1.67 for the PMT G/s_u and 1.66 for the TXT G/s_u. These values are in good agreement with that obtained from the automated factor of safety procedure (FS = 1.67).

The shear strain contours corresponding to failure for 100% efficiency of vertical joints are shown in Figure 6-10 for the PMT and TXT models. The contours indicate that the failure mode is complex, with shearing along the flood side pile, rotation of the DMM zone as a rigid block, and a shallow rotational failure on the canal side of the DMM zone. Again, the shear strain patterns exhibit similarities for both models. The magnitudes of the displacements are significantly greater for the TXT stiffnesses, as shown in Figures 6-9, 6-11, and 6-12.

The pile response curves at failure for the model with PMT stiffnesses are shown in Figure 6-11, and the curves for the model with TXT stiffnesses are shown in Figure 6-12. For comparison, the pile response curves for the design loads with SRF = 1.0 are also included in Figures 6-11 and 6-12. For both stiffnesses, the axial forces in the flood side pile become more tensile for failure conditions. For the PMT stiffness, the upper 35 ft of the pile is in tension and for TXT stiffnesses the entire length of the pile is in tension. The percentage change in axial force for the protected side pile is relatively minor.

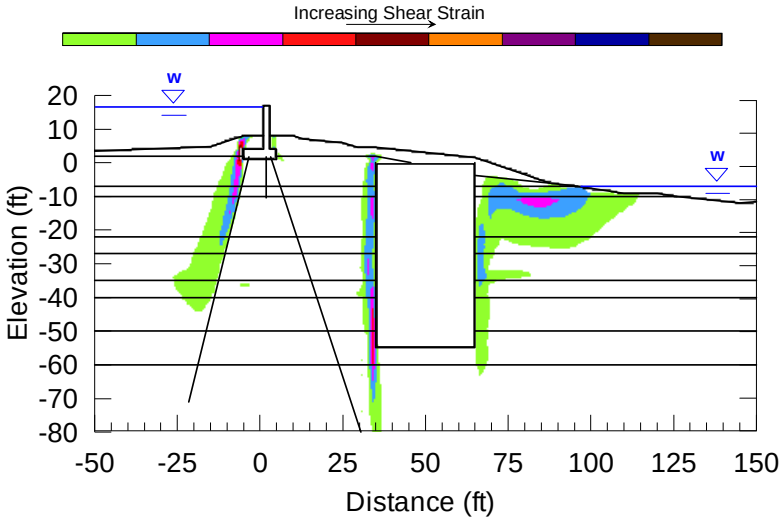

Figure 6-10a. PMT G/s_u, SRF = 1.61

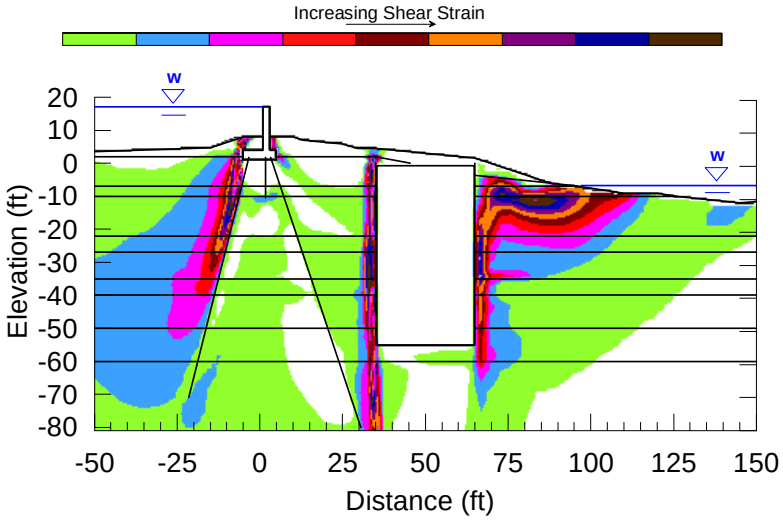

Figure 6-10b. TXT G/s_u, SRF = 1.59

Figure 6-10. Shear Strain Contours at Failure, 100% Efficiency of Joints

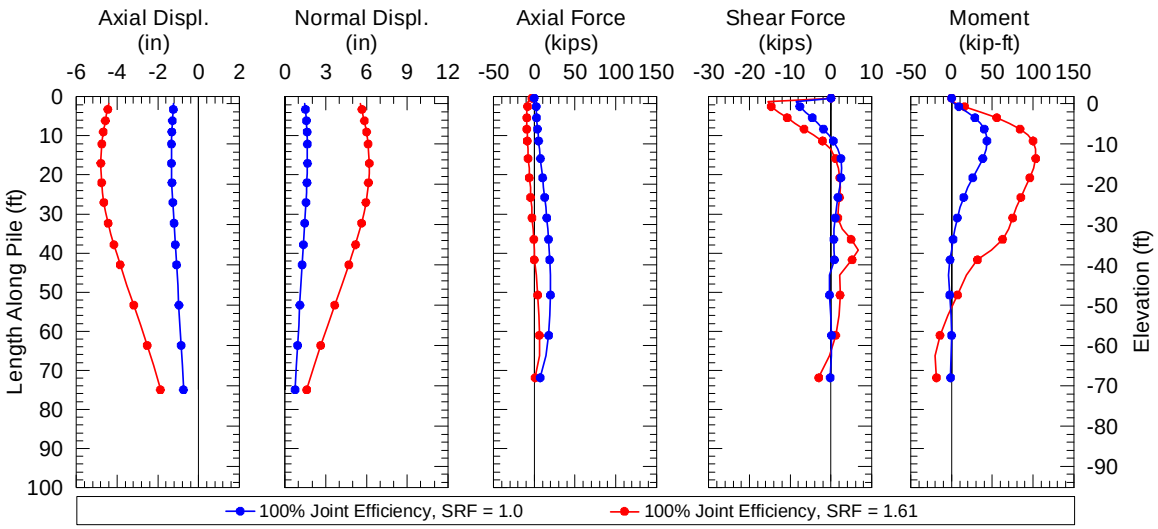

Figure 6-11a. Flood Side Pile (Tip El -71 ft, 1H:4V Batter, 5 ft Spacing)

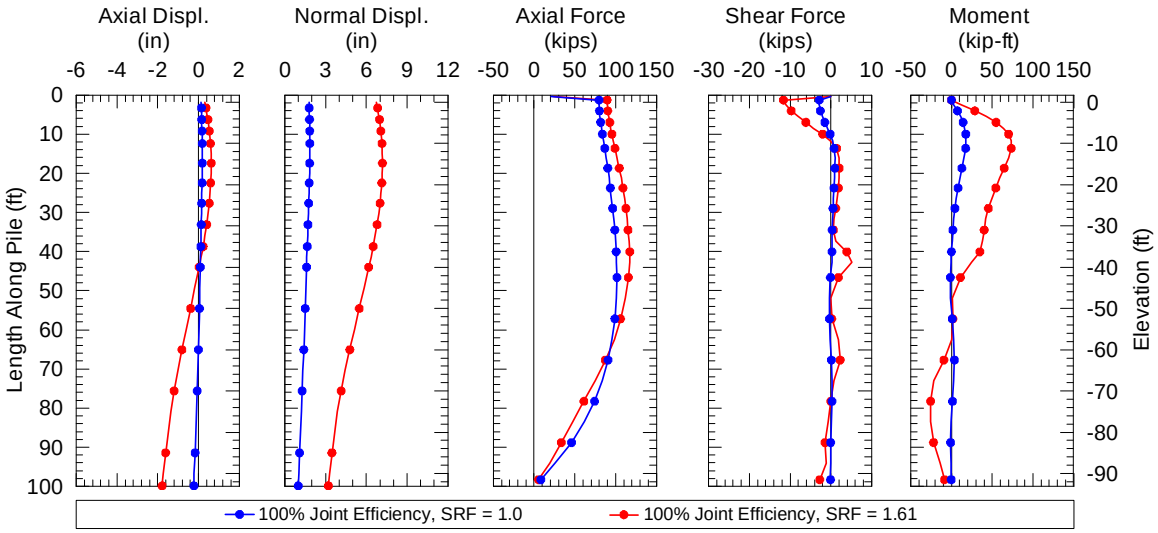

Figure 6-11b. Protected Side Pile (Tip El -93 ft, 1H:3V Batter, 5 ft Spacing)

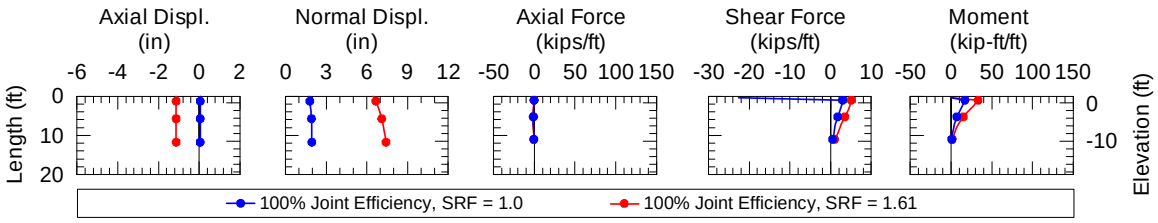

Figure 11c. Sheetpile (Tip El -10.5 ft, Vertical)

Figure 6-11. Pile Response for SRF = 1.0 and 1.61,
100% Efficiency of Vertical Joints, PMT G/s_u

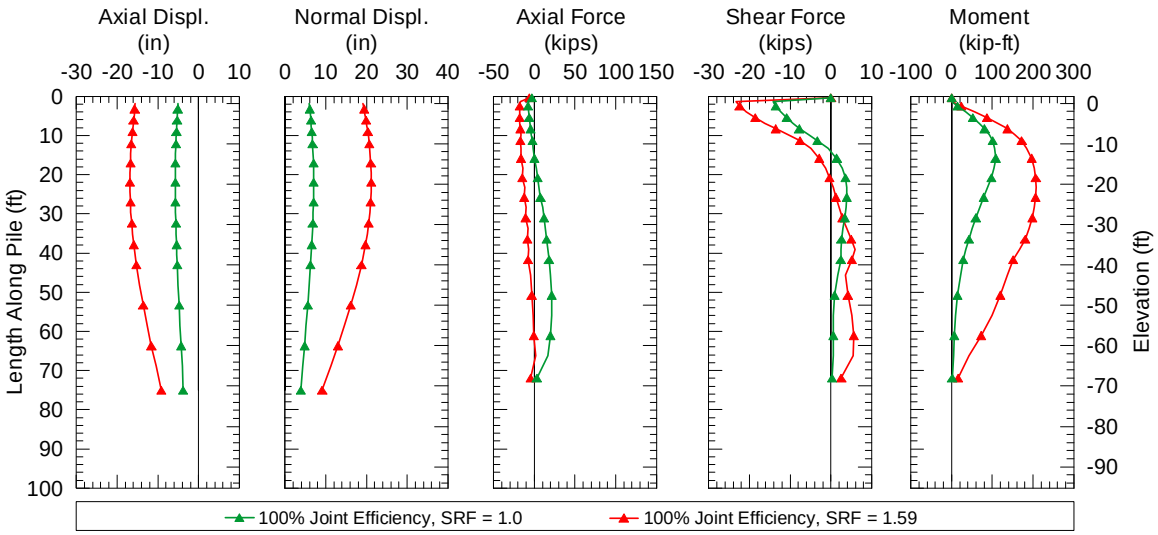

Figure 6-12a. Flood Side Pile (Tip El -71 ft, 1H:4V Batter, 5ft Spacing)

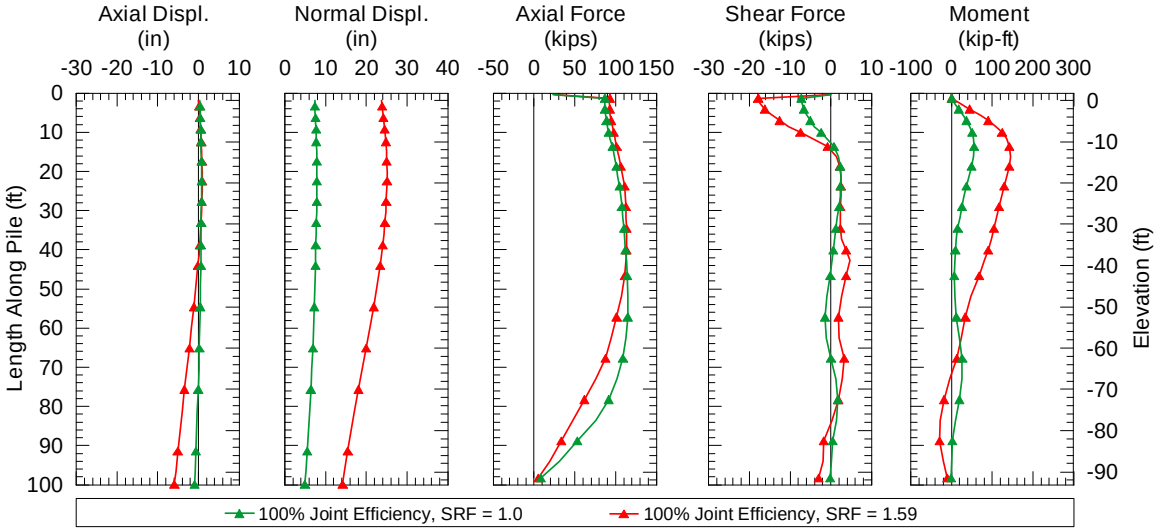

Figure 6-12b. Protected Side Pile (Tip El -93 ft, 1H:3V Batter, 5ft Spacing)

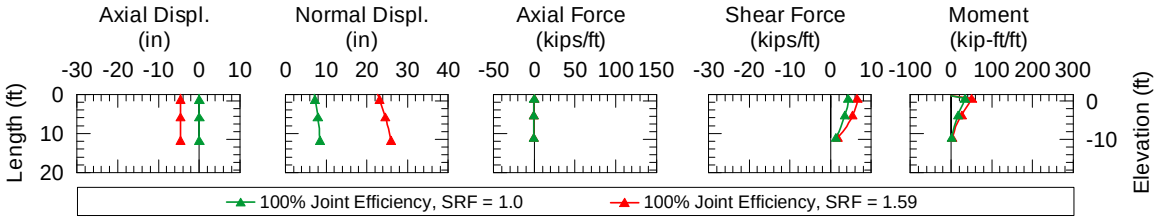

Figure 6-12c. Sheetpile (Tip El -10.5 ft, Vertical)

Figure 6-12. Pile Response for SRF = 1.0 and 1.59,
100% Efficiency of Vertical Joints, TXT G/s_u

6.3.5. Effect of DMM Vertical Joint Efficiency

Deformation and stability analyses were completed for 0% efficiency of vertical joints to assess the effects of vertical joints within the shear wall. Deformation analyses for design loads with SRF = 1.0 showed that the shear strain contours, displacements, and pile loads were essentially the same as those shown in Figures 6-5, 6-6, and 6-8 for 100% efficiency of vertical joints. As such, separate plots of shear strain contours and pile response curves are not included for 0% efficiency of joints for SRF = 1.0. Displacements of the monitoring points for 0% efficiency joints are listed in Tables 6-3 and 6-4 to show their close agreement with the values from 100% efficiency of joints.

The results for the manual factor of safety analyses that include reduction of the pile coupling spring strengths with 0 % joint efficiency are plotted in Figure 6-13. The results for 100% joint efficiency are also included in Figure 6-13 to allow for comparison. For 0% efficiency joints, the factor of safety is about 1.60 for the PMT G/s_u and about 1.57 for the TXT G/s_u. These values are slightly smaller than the corresponding values for 100% efficiency joints. Calculated horizontal and vertical displacement for monitoring point A (the top of the T-wall stem) are also included in Figure 6-13. These plots show a trend of increasing rate of displacements at SRF values near the factor of safety based on convergence criteria.

The shear strain contours corresponding to failure for 0% efficiency of vertical joints are shown in Figure 6-14 for the PMT and TXT models. While the SRF values corresponding to failure are only slightly smaller than those for 100% efficiency of joints, the shear strain contours for 0% efficiency of joints show movement along the joints, indicating that an internal racking failure between DMM installations occurs in the shear walls. The failure mode for 0% efficiency of joints also includes the same shearing along the flood side pile and shallow rotational failure on the canal side of the DMM zone that were seen in the failure modes for the 100% efficiency of joints.

The presence of racking can also be seen in the degree of distortion of the DMM zone over a range of SRF values, as shown in Figure 6-15. For the analyses with 100% efficiency of vertical joints, distortion is negligible for all values of SRF, indicating that the DMM zone rotates as a

rigid block. For the analyses with 0% efficiency of vertical joints, the distortion increases with increasing SRF. However, the distortion at design loads with SRF = 1.0 is negligible for all efficiencies, indicating that the DMM zone moves as a rigid body when SRF = 1.0, regardless of joint efficiency.

The effect of DMM joint efficiency on pile response for PMT and TXT stiffnesses are shown in Figures 6-16 and 6-17. For design loads with SRF = 1.0, the response curves for 0% joint efficiency and 100% joint efficiency are essentially the same. For the PMT stiffnesses under failure conditions, the 0% joint efficiency analyses resulted in somewhat larger pile displacements, loads, and moments than the 100% joint efficiency analyses. The differences in pile response due to differences in joint efficiency were less pronounced for the TXT stiffnesses.

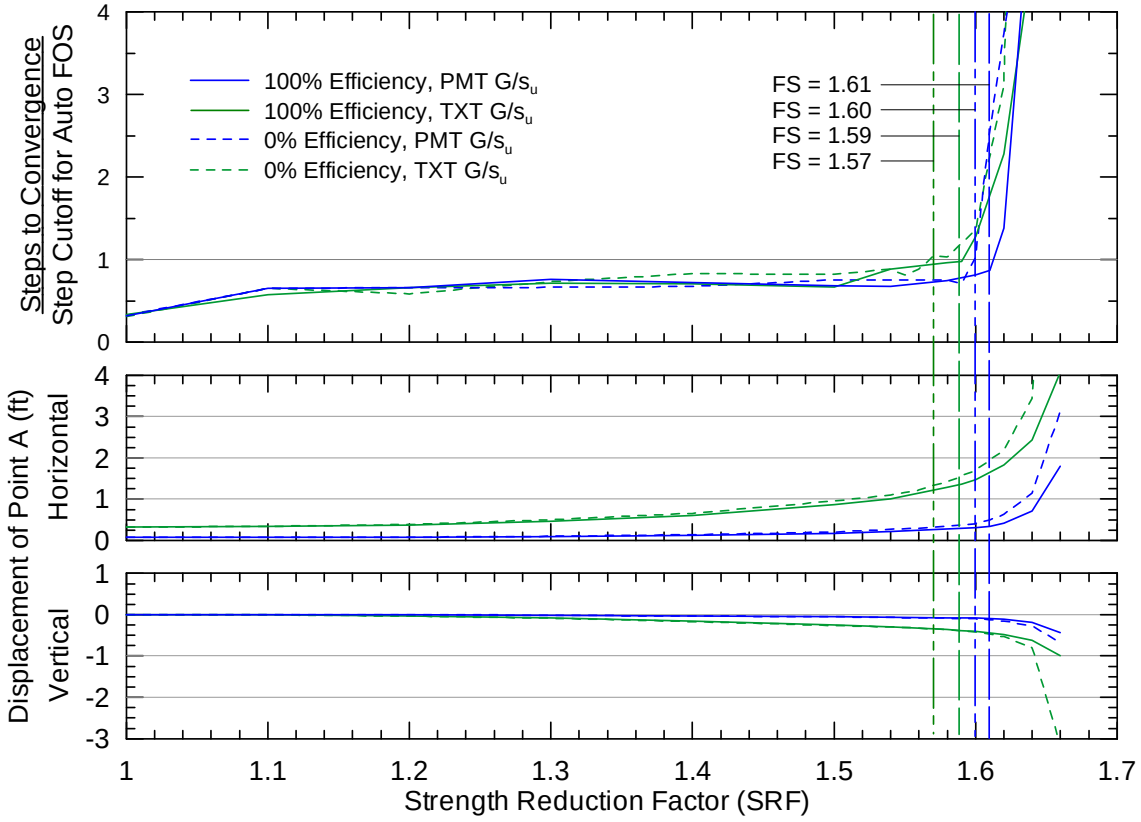

Figure 6-13. Manual Factor of Safety, Variable Efficiency of Joints

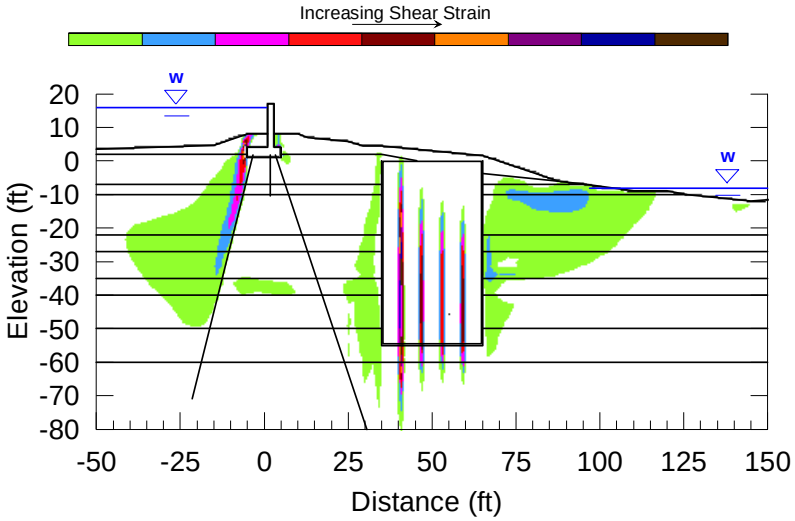

Figure 6-14a. PMT G/s_u, SRF = 1.60

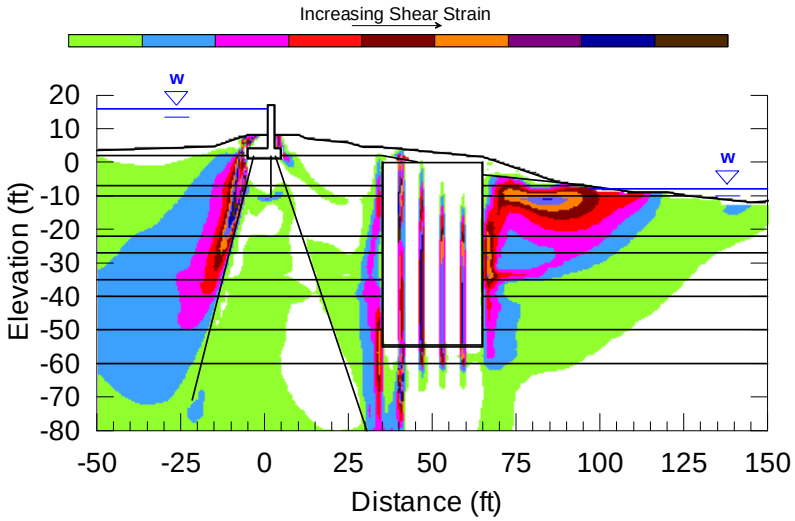

Figure 6-14b. TXT G/s_u, SRF = 1.57

Figure 6-14. Shear Strain Contours at Failure, 0% Efficiency of Joints

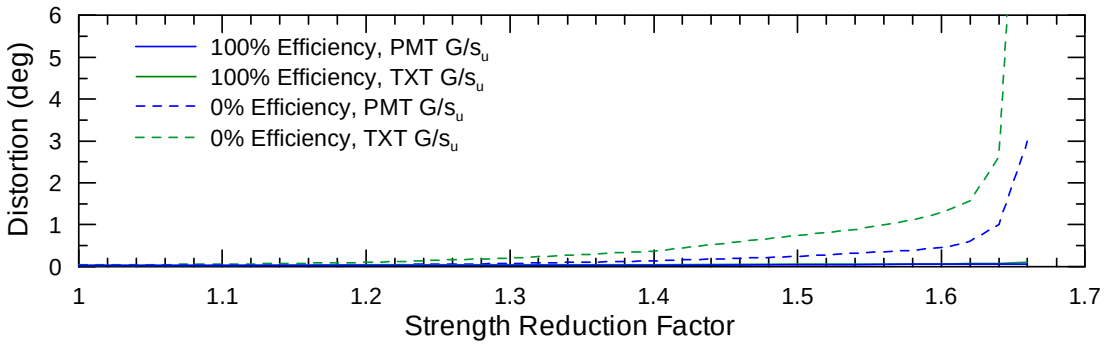

Figure 6-15. Distortion of DMM Zone, Variable Efficiency of Joints

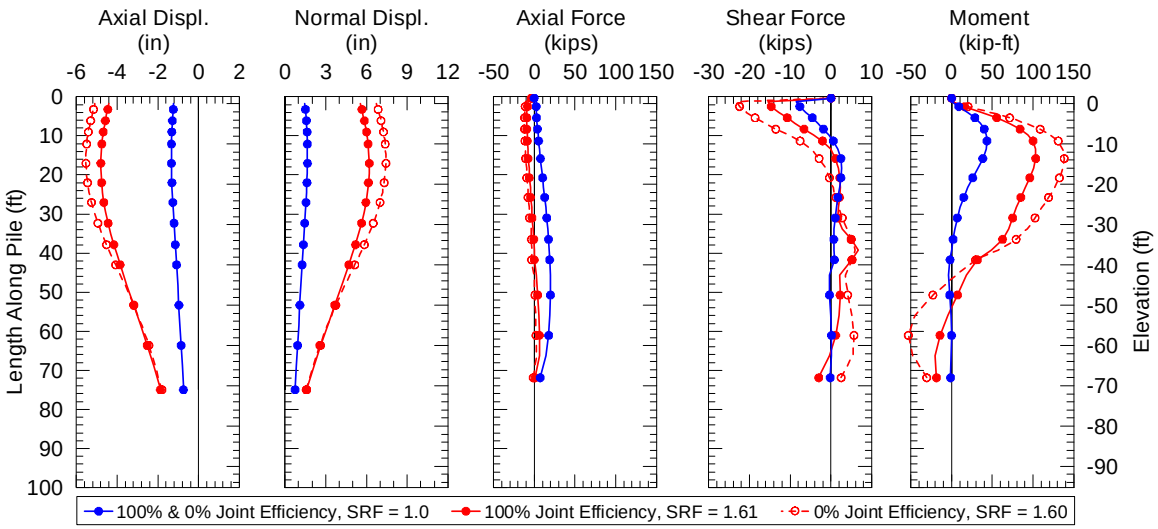

Figure 6-16a. Flood Side Pile (Tip El -71 ft, 1H:4V Batter, 5 ft Spacing)

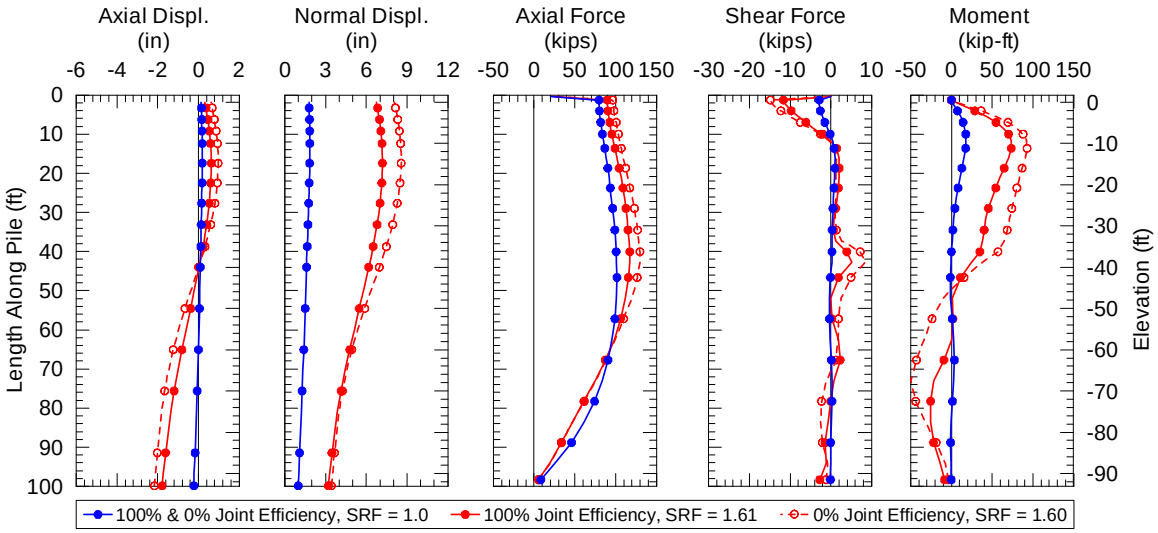

Figure 6-16b. Protected Side Pile (Tip El -93 ft, 1H:3V Batter, 5 ft Spacing)

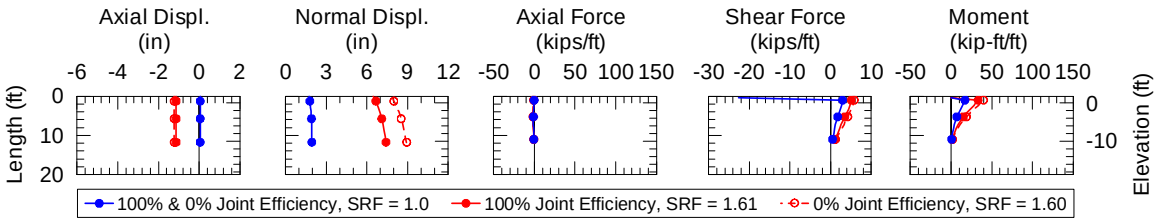

Figure 16c. Sheetpile (Tip El -10.5 ft, Vertical)

Figure 6-16. Pile Response at SRF = 1.0 and at Failure, 0% and 100% Efficiency of Vertical Joints, PMT G/s_u

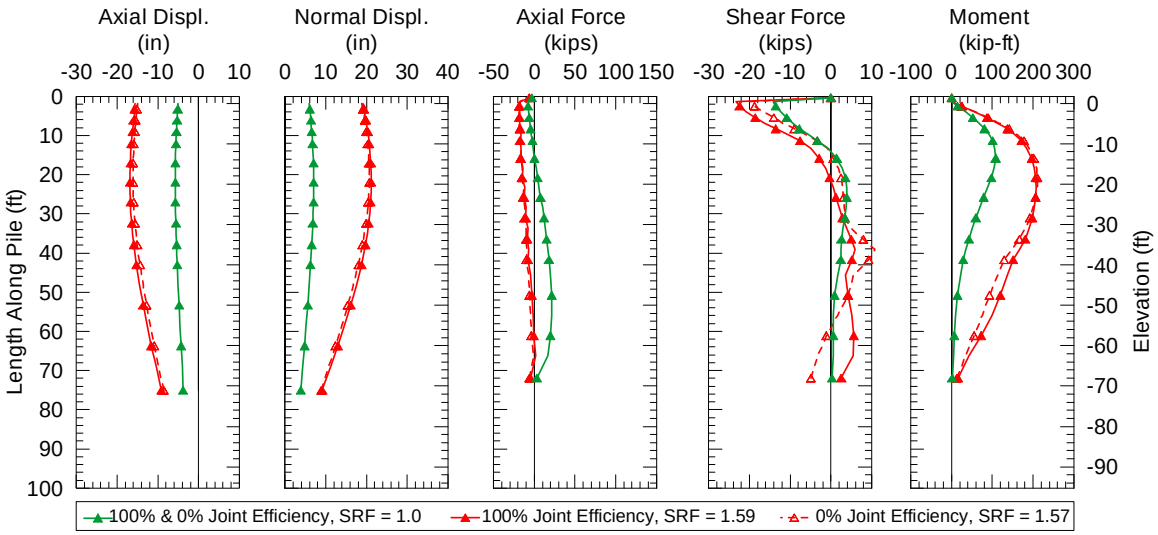

Figure 6-17a. Flood Side Pile (Tip El -71 ft, 1H:4V Batter, 5 ft Spacing)

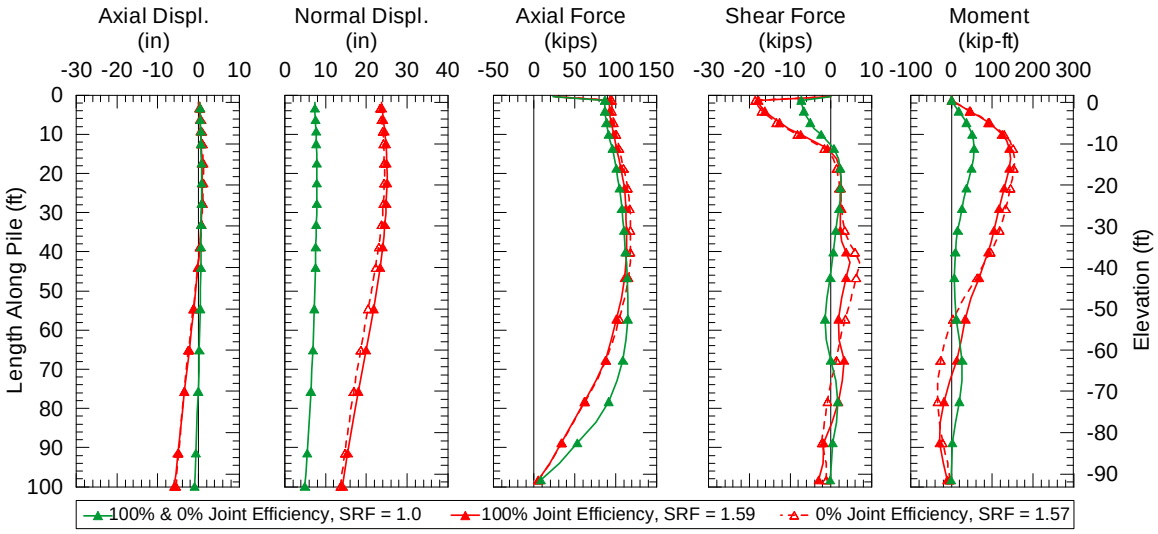

Figure 6-17b. Protected Side Pile (Tip El -93 ft, 1H:3V Batter, 5 ft Spacing)

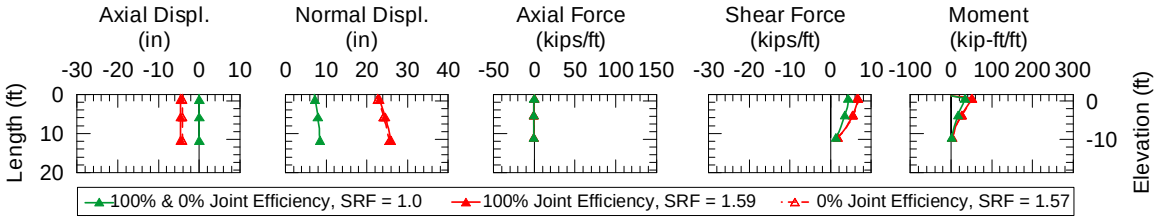

Figure 6-17c. Sheetpile (Tip El -10.5 ft, Vertical)

Figure 6-17. Pile Response at SRF = 1.0 and at Failure, 0% and 100% Efficiency of Vertical Joints, TXT G/s_u

6.3.6. Comparison of Numerical Results with USACE's Analyses

The analyses used by USACE to design the T-wall and DMM system at Gainard Woods employed Method of Planes (USACE 2002) slope stability analyses for a cross-section that did not include the T-wall, coupled with structural analyses of the T-wall using loads derived from the MOP stability analyses. USACE's MOP stability analyses for this project are summarized in Figure A-11 in Appendix A. USACE's analyses show a minimum factor of safety of 1.3. Based on conversations with USACE personnel, the Gainard Woods T-wall was designed to meet a target factor of safety of 1.3 for MOP global stability analyses and 1.4 for MOP slip surfaces that pass through the DMM zone.

The numerical analyses show that the factor of safety for the T-wall and DMM design section at Gainard Woods is about 1.6. This value is substantially higher than the target factor of safety values of 1.3 and 1.4 that USACE used in the MOP analyses to develop the design section.

6.3.7. Optimization of DMM Zone Geometry

Before attempting to optimize the geometry of the DMM zone, analyses were completed to better understand the effect of the DMM geometry used in the design provided by USACE.

Deformation analyses were completed for the PMT and TXT stiffness values under the design loading with SRF = 1.0 for the case without DMM shear walls. The resulting shear strain contours are shown in Figure 6-18. The shear strain contours for both stiffnesses show initial stages of development of the same shallow rotational failure of the slope near the canal as was seen for the analyses with the DMM zone, as illustrated in Figure 6-5. The displacements of the monitoring points are listed in Tables 6-3 and 6-4. Comparison of the horizontal displacement of the T-wall (Points A, B, and C) for the case with and without the DMM zone shows that the DMM zone slightly reduces the calculated wall displacements for design loads with SRF = 1.0.

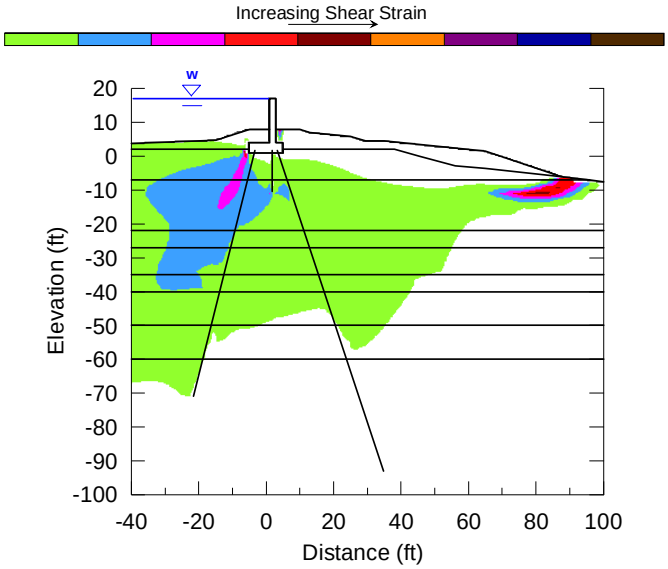

Figure 6-18a. PMT G/s_u

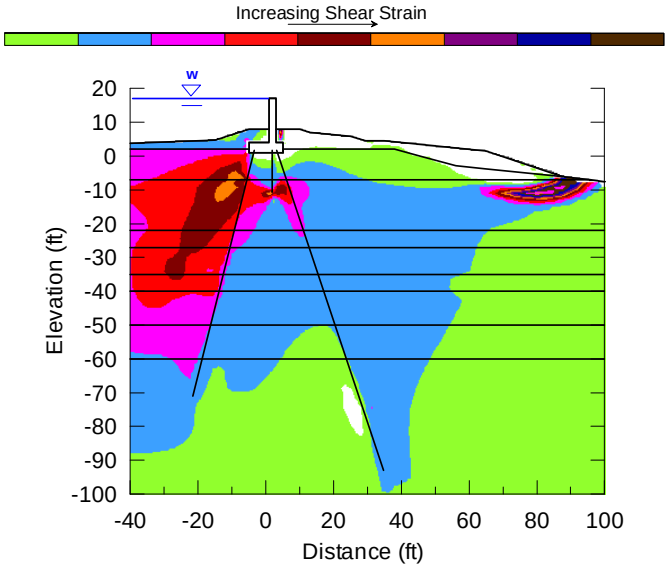

Figure 6-18b. TXT G/s_u

Figure 6-18. Shear Strain Contours for Design Loads with SRF = 1.0, No DMM Zone

Manual factor of safety analyses with reduction of the pile spring strengths for the case with no DMM zone and PMT G/s_u result in a factor of safety of 1.24. The shear strain contours shown in Figure 6-19a indicate that this factor of safety corresponds to a shallow failure of the slope near the drainage canal. The shear strain contours at failure for the case with the DMM zone, PMT G/s_u, and 100% efficiency of vertical joints, originally shown in Figure 6-10a, are included again in Figure 6-19b for comparison. The addition of the DMM zone to the Gainard Woods analysis

section shifts the critical failure mode from a shallow failure of the slope near the drainage canal to one that engages the T-wall, increasing the factor of safety of the analysis section from 1.24 to 1.61. Without the DMM zone, the slope near the canal fails before the full capacity of the pile-supported T-wall is engaged.

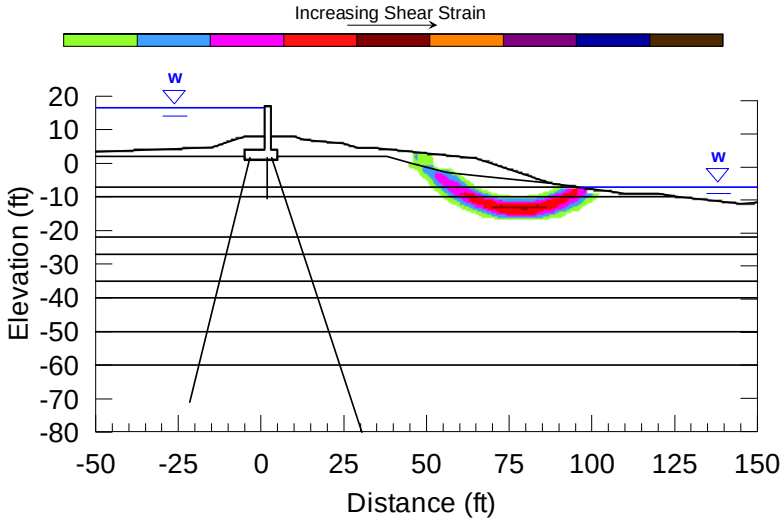

Figure 6-19a. Without DMM Zone, FS = 1.24

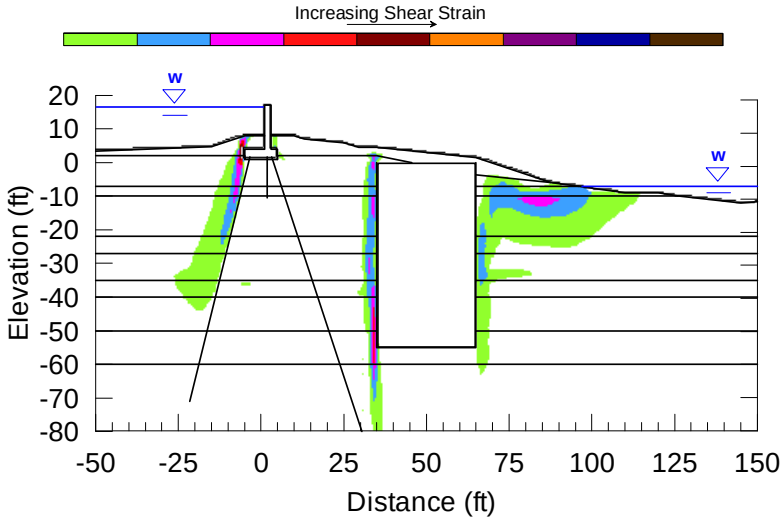

Figure 6-19b. With DMM Zone, FS = 1.61

Figure 6-19. Comparison of Shear Strain Contours and Factor of Safety Values, with and without DMM Zone, PMT G/s_u

To assess whether the DMM zone as designed provides a stabilizing force on the T-wall in addition to helping stabilize the shallow slope failure near the canal, factor of safety analyses

were completed with a shallow zone of increased strength elements at the ground surface near the canal. Analyses were performed with and without the DMM zone as originally designed. For both cases, the PMT G/s_u values were used. For the analyses with the DMM zone, 100% efficiency vertical joints were used. The shallow strengthened zone was 5 ft deep, and the edge of the zone farthest from the T-wall extended to the toe of the deep failure surface from the validation analyses. The edge of the shallow strengthened zone closest to the T-wall extended to the top of the 3H:1V slope of the stability berm (X = 65) for the case without the DMM zone. For the case with the DMM zone, a 10 ft gap was left between the DMM zone and the shallow zone of increased strength, to avoid effects of connectivity between these two zones. Manual factor of safety analyses with reduction of the pile spring strengths result in a factor of safety of 1.62 for the case with no DMM zone and 1.64 for the case with the DMM zone, when shallow failure of the stability berm slope is prevented in both cases by the shallow strengthened zone. The shear strain contours corresponding to failure are shown in Figure 6-20. For the case with no DMM Zone, the failure mode consists of shearing along the floodside pile and partial development of a slip surface along the slope near the canal. For the case with the DMM zone, the failure mode consists of shearing along the floodside pile and rotation of the DMM zone as a rigid block, with very little movement of the slope near the canal.

Based on the results of the analyses shown in Figures 6-19 and 6-20, it appears that the increase in factor of safety due to the addition of the existing DMM zone is largely due to stabilization of the slope near the canal. Considering the importance of stabilizing this slope, the alternate DMM geometries considered in the optimization study were located immediately upslope from the canal to stabilize that slope.

For the optimization study, the canal side of the DMM zone was fixed at the edge of the canal (X = 96). Automatic factor of safety analyses were run for DMM zone widths of 10, 20, and 30 ft with base elevations ranging from El -18 ft to El -60 ft. The factor of safety increased with increasing depth of the zone until the bottom of the DMM zone reached elevation -37.5 ft, after which the factor of safety remained essentially constant. For a 10 ft wide DMM zone with tip elevations at or below elevation -37.5 ft, the factor of safety from the automated procedure was 1.61, and the shear strain contours showed a shallow slope failure on the flood side of the DMM

zone. For 20 ft and 30 ft wide zones, the factor of safety from the automated procedure for DMM zone tip elevations at or below elevation -37.5 ft was 1.69 and the shear strain contours showed that the shallow slope failure had been arrested. Based on these analyses, a DMM zone 20 ft wide with a base elevation of -37.5 ft was selected as the minimum size of DMM zone for stabilizing the shallow slope failure. A manual factor of safety analysis with reduction of the pile spring strengths resulted in a factor of safety of 1.62 for the overall levee and slope system. The shear strain contours corresponding to failure are shown in Figure 6-21.

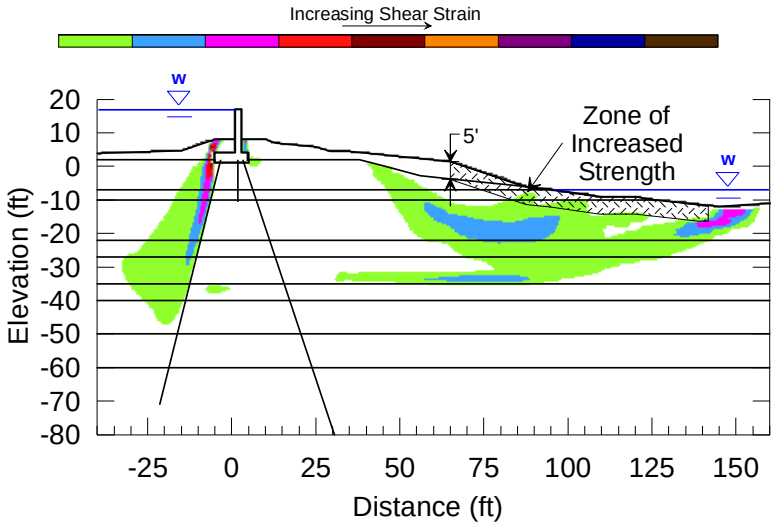

Figure 6-20a. Without DMM Zone, FS = 1.62

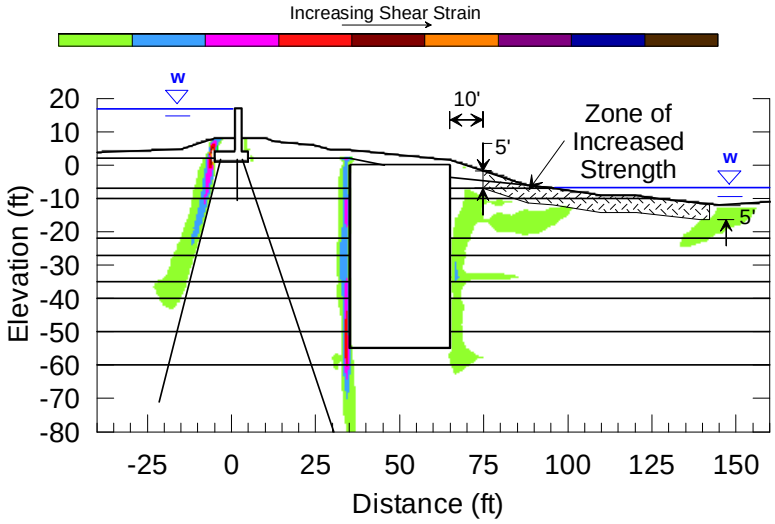

Figure 6-20b. With DMM Zone, FS = 1.64

Figure 6-20. Comparison of Shear Strain Contours and Factor of Safety Values, with and without DMM Zone, PMT $G/s_{u,}$ Shallow Failure of Stability Berm Slope Prevented

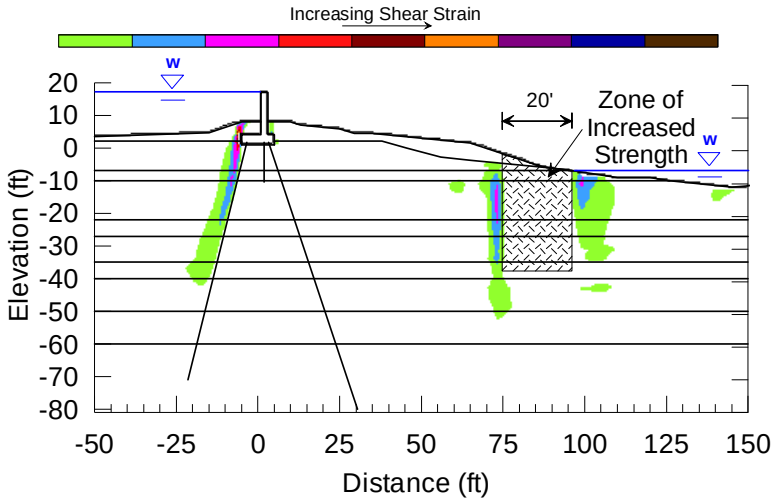

Figure 6-21. Shear Strain Contours at Failure, Alternate DMM Zone, PMT G/s_u, FS = 1.62

Neither increases in width in the direction towards the T-wall of the DMM treated zone shown in Figure 6-21, nor increases in the depth of the DMM treated zone, caused appreciable increases in the factor of safety. Furthermore, Figure 6-21 shows that high shear strains do not connect the T-wall movement and the DMM zone movement. These facts indicate that the DMM zone in Figure 6-21 stabilizes the slope next to the canal, and it is not directly stabilizing the T-wall. It can be concluded that the factor of safety for the pile-supported T-wall itself is at least 1.62, once the slope near the canal is stabilized, according to these FLAC numerical analyses.

6.4. Conclusions and Recommendations

The following conclusions can be drawn from this study, for the conditions used to represent the Gainard Woods pile-supported T-wall.

- Calculated displacements of the T-wall are strongly dependent on soil stiffness. The lateral displacement of the base of the T-wall using the soil stiffnesses obtained from field pressuremeter tests (PMT G/s_u) is 1.68 in. under design loads without reduction of the soil or pile coupling spring strengths, i.e., using a strength reduction factor (SRF) equal to unity. For soil stiffnesses obtained from the laboratory triaxial compression tests (TXT G/s_u), lateral displacement of the base of the T-wall is more than four times as large. The difference in calculated displacements for these two representative stiffness

profiles underscores the importance of obtaining site-specific soil modulus information to calculate accurate displacements for T-wall design.

- Displacements of the T-wall at design loads with SRF = 1.0 are independent of DMM vertical joint efficiency. Racking does not occur in the DMM zone for SRF = 1.0 regardless of vertical joint efficiency.

- The factor of safety for the pile-supported T-wall with the DMM zone is about 1.6, according to the numerical calculations. The factor of safety value is only slightly dependent on soil stiffness and vertical joint efficiency. For 100% vertical joint efficiency, the factor of safety is 1.61 for pressuremeter stiffnesses and 1.59 for triaxial stiffnesses. For 0% vertical joint efficiency, the factor of safety is 1.60 for pressuremeter stiffnesses and 1.57 for triaxial stiffnesses.

- The failure mode is dependent on the joint efficiency. For 100% efficiency of joints, the DMM zone rotates as a rigid block at failure. For 0% efficiency of joints, racking of the DMM shear walls occurs along the vertical joints at failure. The racking failure mode occurs for both pressuremeter stiffnesses and triaxial stiffnesses for 0% efficiency vertical joints. This change in failure mode occurs even though the drop in the factor of safety value is very small due to a decrease in vertical joint efficiency from 100% to 0%, i.e., a drop of 0.01 for pressuremeter stiffnesses and a drop of 0.02 for triaxial stiffnesses.

- Numerical analyses of the pile-supported T-wall under design loads with SRF = 1.0, but without DMM treatment, showed that the horizontal displacement of the base of the T-wall is only slightly increased by removal of the DMM treatment, from 1.68 in. with the DMM zone to 1.83 in. without the DMM treatment, for the pressuremeter soil stiffnesses.

- The factor of safety for the case with no DMM zone is 1.24, which corresponds to a shallow failure of the slope near the drainage canal. The addition of the DMM zone to the Gainard Woods analysis section shifts the critical failure mode from a shallow failure of the slope near the drainage canal to one that engages the T-wall, increasing the factor

of safety of the analysis section from 1.24 to 1.61. Without the DMM zone, the slope near the canal fails before the full capacity of the pile-supported T-wall is engaged.

- The increase in factor of safety due to the design DMM zone appears to be due primarily to stabilization of the shallow slope failure near the canal. Analyses were performed without the designed DMM treatment zone, but with a shallow zone of strengthened ground at the location of the slope near the canal, and the resulting factor of safety is 1.62.

- An alternate DMM zone geometry consisting of 20 ft wide shear walls with a base elevation of -37.5 ft located immediately upslope of the canal was analyzed, and the calculated factor of safety value of the overall levee and slope system is 1.62. This block of treated material is about 55 ft from the protected side pile and about 70 ft from the T-wall. At failure, high shear strain contours do not connect the T-wall to the alternate DMM zone. Furthermore, moderate increases in the size of the alternate DMM zone extending deeper and closer to the T-wall do not appreciably increase the factor of safety of the system. These facts support the conclusion that the factor of safety of the pile-supported T-wall at Gainard Woods is about 1.6, even without additional support from DMM treatment, once the shallow slope near the canal on the protected side is stabilized.

- The factor of safety of about 1.6 for the T-wall and DMM system at Gainard Woods from the numerical analyses is substantially higher than the target factor of safety of 1.3 used by USACE in their MOP analyses to develop the design section.

The following recommendations are made:

- Until an alternate reliable design procedure is developed, it is recommended that numerical analyses be performed for design of pile-supported T-walls. There is a large difference between the target factor of safety value of 1.3 used by USACE to develop the design section and the value of 1.6 from the numerical analyses. More cost effective, yet still reliable designs could be produced by employing properly performed numerical analyses in the design process.

- Additional studies should be performed to assess the potential for DMM to help stabilize pile-supported T-walls. In such studies, it will be useful to analyze a cross-section on approximately level ground to avoid the complications introduced by the slope next to the canal at Gainard Woods. The analyses performed for the Gainard Woods cross-section indicate that the designed DMM zone may not be helping to stabilize the T-wall substantially, although it does help stabilize the slope near the canal. For a level ground cross-section, alternate DMM treatment locations that should be explored include regions close to the T-wall on both the flood side and the protected side of the T-wall.

- Although the numerical deformation and stability analyses for the Gainard Wood Pump Station T-wall did not indicate that a tension crack or gap would form at this site, the potential for formation of tension cracks and gaps should continue to be considered for design of T-wall and levee systems.

CHAPTER 7

STABILITY ANALYSES OF A T-WALL ON LEVEL GROUND

This case study included stability analysis of a T-wall analysis section with level ground conditions. The analysis section was developed based on the U.S. Army Corps of Engineers (USACE)'s Gainard Woods Pump Station T-wall analysis section described in the previous case study. Numerical stability analyses were completed to optimize the size and location of the DMM zone relative to the T-wall. Details of the T-wall analysis section, material properties, analysis methods, and results are discussed in this chapter. Also provided in this chapter are the conclusions specific to this case study.

7.1. Introduction

7.1.1. Background Information

The results of the stability analyses of the T-wall at Gainard Woods Pump Station (discussed in Chapter 6) concluded that the increase in factor of safety due to the addition of DMM columns on the protected side of the T-wall was primarily due to stabilization of a shallow slope near the existing drainage canal. A recommendation was made to perform additional studies to assess the potential for DMM to help stabilize pile-supported T-walls with approximately level ground conditions to avoid the complications introduced by the slope next to the canal at Gainard Woods.

7.1.2. Purpose and Scope

The primary purpose of this study is to develop a level ground cross-section and perform additional numerical analyses of the T-wall and DMM system to identify DMM configurations that would be effective in improving the stability of the T-wall system.

The scope of work completed for this study includes:

- Developing a level ground T-wall cross-section with a factor of safety of approximately 1.2 without DMM soil-cement columns.

- Completing numerical analyses to evaluate the effect of different DMM soil-cement column configurations on the factor of safety.

7.2. Analysis Section and Material Characterization

The design cross-section provided by USACE for the segment of the Gainard Woods Pump Station T-wall with DMM soil-cement columns was adjusted to create a level ground analysis section for the optimization study. A target factor of safety of 1.2 was suggested by USACE for developing the level ground T-wall cross-section without DMM soil-cement columns. Using the same material property characterization as provided by USACE for the Gainard Woods Pump Station with a level ground surface elevation of +2 ft, a factor of safety of 1.2 was achieved without DMM columns by raising the flood side and protected side pile tip elevations to El -70' and raising the height of the flood wall and flood water to El. +27', as shown in Figure 7-1. This analysis section was reviewed and approved by Neil Schwanz of the St. Paul District for use in the optimization study.

The location of the DMM soil-cement columns (DMM zone) relative to the T-wall, as designed for the Gainard Woods Pump Station T-wall, is shown in Figure 7-1. The design drawings for the Gainard Woods soil-cement columns are also included as Figures A-7 and A-8 in Appendix A. The material property values used in the analyses were taken from the Gainard Woods Pump Station analyses and are listed in Table 7-1. Horizontal variation in soil strengths and unit weights is modeled using linear interpolation between verts 1 and 2 and between verts 2 and 5. As shown in Figure 7-1, vert 1 is located in the center of the flood wall footprint (X = 0) and verts 2 and 5 are located along the flood side (X = 35) and protected side (X = 65) edges of the DMM zone. The analyses for the optimization study were completed using the set of shear modulus/shear strength ratios, G/s_u, derived from pressuremeter field tests. For these analyses, the representative strength for the DMM zone was considered to be the same as that used for the Gainard Woods analyses, and the potential for slippage along vertical joints was not modeled. General discussion of the analysis section and material property characterization is included in Chapter 6, Stability Analysis of the Gainard Woods Pump Station T-wall.

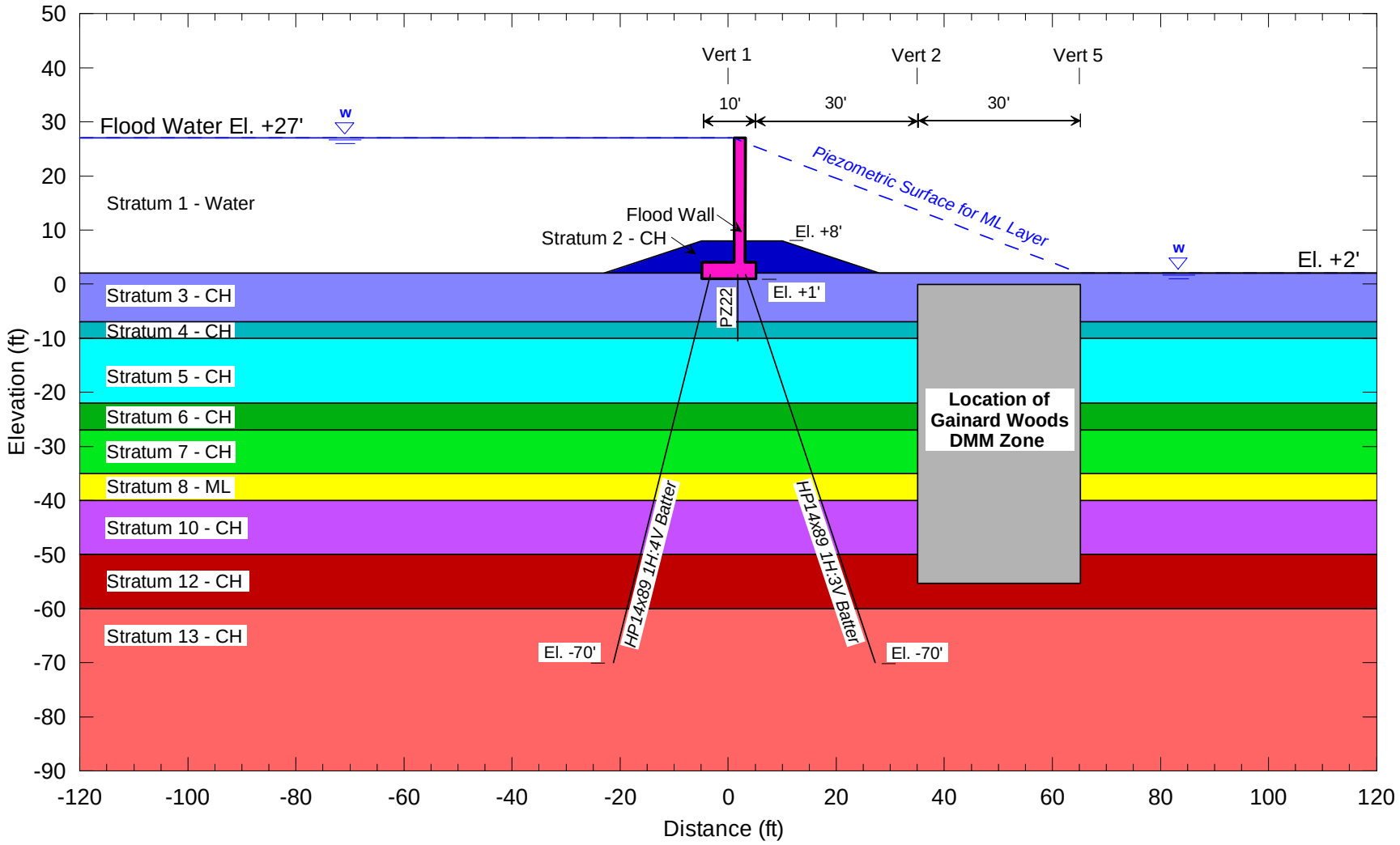

Figure 7-1. Analysis Cross-Section for Stability Analyses of a T-wall on Level Ground

Table 7-1. Summary of Material Property Values for Stability Analyses of a T-wall on Level Ground

Stratum	Elevations (ft)	Unit Weight (pcf)			c[3] (psf)			ϕ (deg)	G/s_u[5]	ν
		Vert 1[1]	Vert 2[1]	Vert 5[1]	Vert 1[1]	Vert 2[1]	Vert 5[1]			
Stratum 1 – Water	-12 to 17	62.4			--			--	--	--
Stratum 2 – CH	-6 to 8	110			400			0	130	0.49
Stratum 3 – CH	-7 to 2	86			300	215	150	0	100	0.49
Stratum 4 – CH	-10 to -7	98	86	98	300	215	150	0	130	0.49
Stratum 5 – CH	-22 to -10	100	92	100	300 to 420	215 to 335	150 to 270	0	130	0.49
Stratum 6 – CH	-27 to -22	115	100	100	420 to 470	335 to 385	270 to 320	0	130	0.49
Stratum 7 – CH	-35 to -27	115	100	100	470 to 550	385 to 465	320 to 400	0	130	0.49
Stratum 8 – ML	-40 to -35	117			200			15	130[6]	0.49
Stratum 10 – CH	-50 to -40	115	100	100	600 to 700	515 to 615	450 to 550	0	160	0.49
Stratum 12 – CH	-60 to -50	105			700 to 800	615 to 715	550 to 650	0	160	0.49
Stratum 13 – CH	Below -60	105			800+	715+	650+	0	160	0.49
DMM Zone	-55 to 0	Same as existing[2]			1000[4]			0	103	0.45

Notes:

1) Horizontal variation in soil strengths and unit weights is modeled using linear interpolation between verts 1 and 2 and between verts 2 and 5. The locations of the verticals are shown in Figure 7-1.
2) The unit weight was unchanged from that assigned to the existing soil layers.
3) Cohesion for the CH layers increases with depth below El -10 ft at a rate of 10 psf/ft.
4) Representative DMM cohesion is a weighted average for the column/soil matrix within the DMM zone based on an unconfined compressive strength for the DMM treated soil of 80 psi, a 40% replacement ratio, and two partial factors of safety, each equal to 1.5.
5) Stiffness ratios from pressuremeter tests.
6) Stiffness assigned to ML layer computed using $s_u = \sigma_v' \tan\phi + c$, where σ_v' = initial vertical effective stress.

7.3. Numerical Analyses

Numerical analyses for the level ground analysis section were completed using the finite difference computer code FLAC (ITASCA 2005) and the analysis methods developed for the Gainard Woods case study, as described in Chapter 6.

The finite difference mesh from the Gainard Woods Pump Station stability analyses was modified to reflect the level ground surface in Figure 7-1. The mesh used for the numerical analyses extended approximately 140 ft beyond the T-wall on the flood side, 220 ft beyond the T-wall on the protected side, and 70 ft below the tip of the piles. The extent of the model is shown schematically in Figure 7-2. No lateral displacements were allowed on the left- and right-hand sides of the mesh, and no lateral or vertical displacements were allowed on the bottom of the mesh.

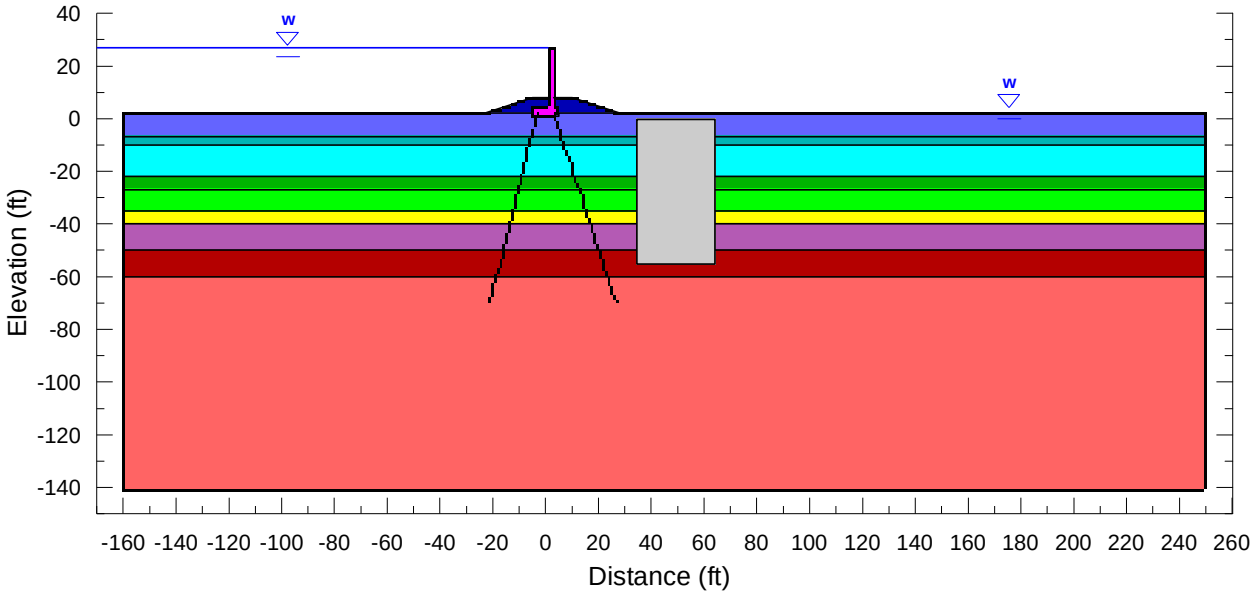

Figure 7-2. Extent of FLAC Model with Location of Gainard Woods DMM Zone

The discretized mesh in the vicinity of the T-wall is shown in Figure 7-3. The FLAC mesh zone size was gradually increased with distance from the T-wall to achieve accurate displacements in the vicinity of the wall, without exceeding the memory limitations of the FLAC program. Alternate DMM zone geometries were explored by varying the width of the DMM zone at the

ground surface and the clearance between the DMM zone and the T-wall piles. Discretization of the mesh did not always allow for the edge of the DMM zone to be located exactly at the x-coordinate corresponding to the specified nominal width of the DMM zone or the specified nominal clearance between the DMM zone and the T-wall piles. The widths discussed in this report are actual values unless specified otherwise.

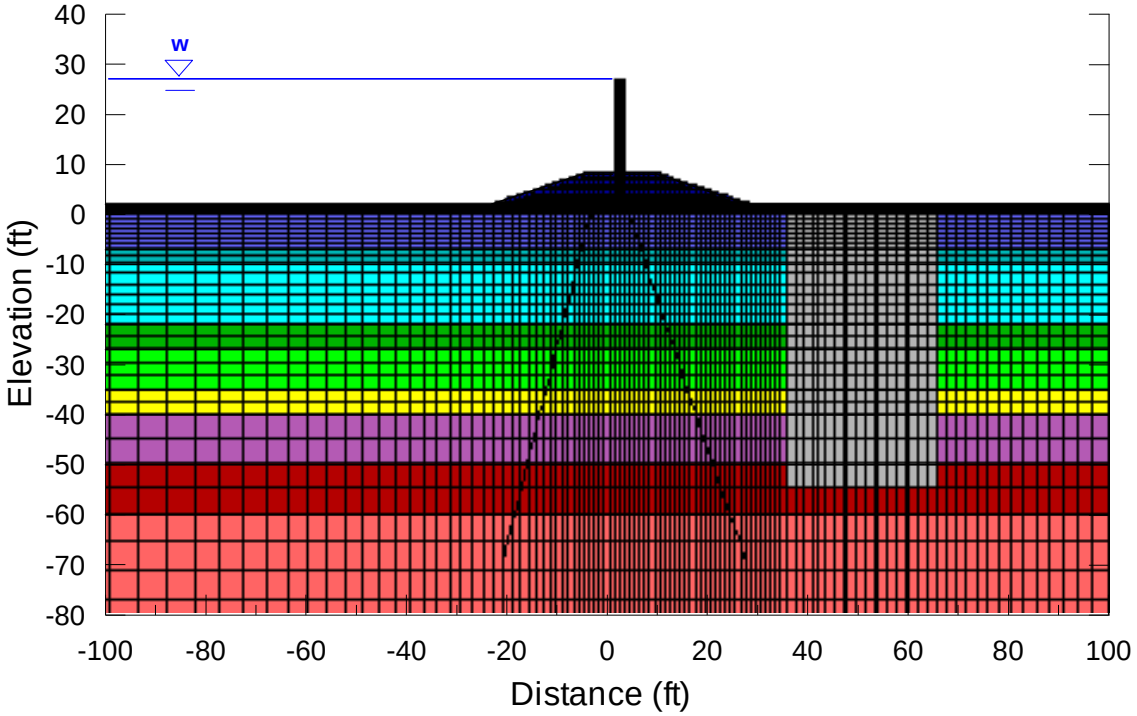

Figure 7-3. FLAC Mesh Discretization Near T-wall

The analyses described here were completed using the automated factor of safety procedure in FLAC. Analyses completed for several sections using the manual factor of safety procedure for the Gainard Woods case study (described in Chapter 6) resulted in factors of safety that were consistently about 0.06 lower than those determined using the automated procedure. Because the differences between the automated and manual procedures were relatively small and shown to be consistent for the Gainard Woods analyses, and because it was necessary to perform a large number of analyses for the level-ground case, the quicker automated procedure was used for these analyses.

7.3.1. Analyses without DMM Zone

As stated above, the level ground analysis section was developed to provide a factor of safety of about 1.2 without DMM soil-cement columns. For the analysis section presented in Figure 7-1, the factor of safety obtained from the automated factor of safety procedure in FLAC is 1.21. The shear strain contours corresponding to failure are shown in Figure 7-4. The failure mode is complex, with shear occurring around the piles and in soil masses adjacent to piles.

While the contours in Figure 7-4 do indicate some shear strain in the soil between the flood side and protected side piles, the spring connection of the piles to the FLAC mesh does not allow for slip surfaces to cross the piles without failing the pile-soil springs. Three-dimensional modeling would be needed to capture the full potential for soil movement between the piles.

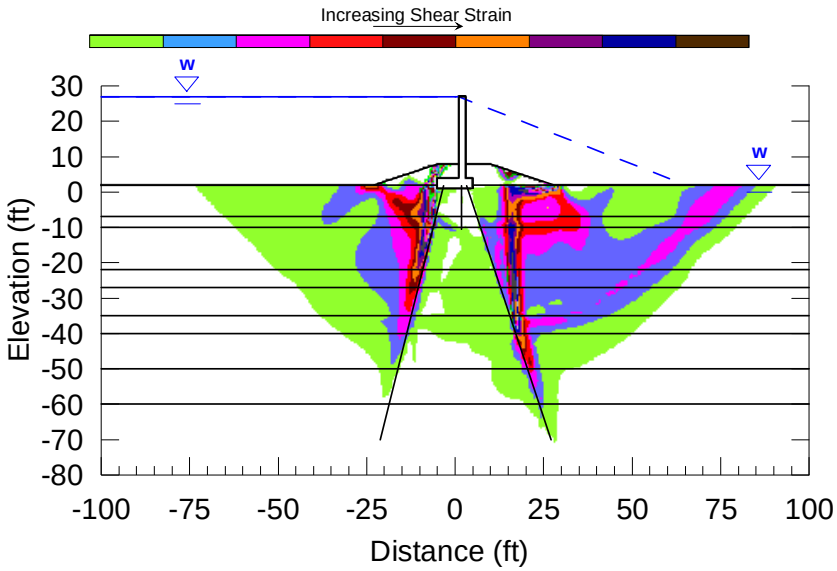

Figure 7-4. Shear Strain Contours at Failure, Without DMM Zone, FS = 1.21

7.3.2. Analyses with DMM Zone from Gainard Woods Pump Station T-wall

Factor of safety analyses for the DMM zone used for the Gainard Woods Pump Station T-wall, as shown in Figure 7-1, resulted in a factor of safety of 1.34. The shear strain contours corresponding to failure are shown in Figure 7-5, and they indicate a significant amount of shear strain in the soil between the T-wall and the DMM zone, with some shearing along the pile as well as lateral squeezing of the soil between the T-wall and DMM zone.

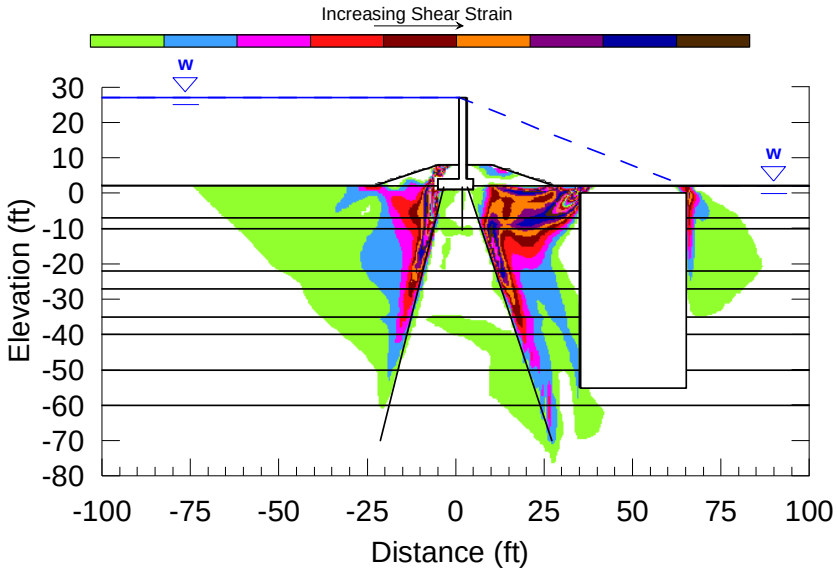

Figure 7-5. Shear Strain Contours at Failure, DMM Zone Location from Gainard Woods Pump Station T-wall Design, FS = 1.34

7.3.3. Analyses with Protected Side DMM Zone

To investigate the ability of the DMM zone to limit the amount of shear strain in the soil between the DMM zone and the T-wall, the DMM zone configurations on the protected side of the wall were modified to include a stepped configuration near the protected side pile, and the top of the DMM zone was raised to El +1ft. To be consistent with the specifications used in the Gainard Woods Pump Station T-wall design, the first set of analyses were completed for a minimum horizontal clearance between the protected side pile and the DMM soil-cement columns of 10 ft. The results of these analyses are presented in Figure 7-6. Automatic factor of safety analyses were run for DMM zone widths of 45 ft, 65 ft, and 85 ft with base elevations of El -18 ft, El -35 ft and El -71 ft. The factor of safety for each case is plotted at the lower right corner of the DMM zone in Figure 7-6a. As an illustration of one of the results in Figure 7-6a, the DMM zone configuration and factor of safety for a DMM zone with base elevation of -55 ft and width of 65 ft is shown in Figure 7-6b. Figure 7-6a shows that the factor of safety increases with increasing depth and width of the DMM zone.

To investigate the effect of placing the DMM zone closer to the T-wall, a second set of analyses was completed with the minimum horizontal clearance between the protected side pile and the

DMM zone reduced to 5 ft. The results of these analyses are presented in Figure 7-7. The factor of safety for each case is plotted in Figure 7-7a at the lower right corner of the DMM zone. Figure 7-7b shows the DMM zone configuration and factor of safety for a base elevation of -55 ft and a DMM zone width of 70 ft.

The shear strain contours shown in Figures 7-8 and 7-9 correspond to failure for the DMM zone configurations shown in Figures 7-6b and 7-7b. The shear strain contours for both models indicate a significant amount of shear strain in the soil between the T-wall and the DMM zone, with shearing along the pile and shallow lateral sliding failure of the berm in front of the flood wall.

The results for different configurations and clearances for DMM zones located on the protected side of the T-wall are shown in Figure 7-10. The factors of safety are plotted versus the width of the DMM zone to allow for clear comparison between the analyses with 5 ft clearance and the analyses with 10 ft clearance. The factor of safety increases with increasing DMM zone width and depth for a given clearance, although the benefit of additional depth below El -55 ft is relatively small. The factors of safety for 5 ft clearance are generally slightly higher than for 10 ft clearance, indicating a relatively small benefit of placing the soil-cement columns closer to the T-wall piles. Based on the shear strain contours in Figures 7-4, 7-8 and 7-9, reducing the gap between the T-wall piles and the DMM zone increases the factor of safety by minimizing the extent of shear strain in the soil between the T-wall and the DMM zone. Protection of piles and DMM columns should be considered in establishing minimum clearance distances.

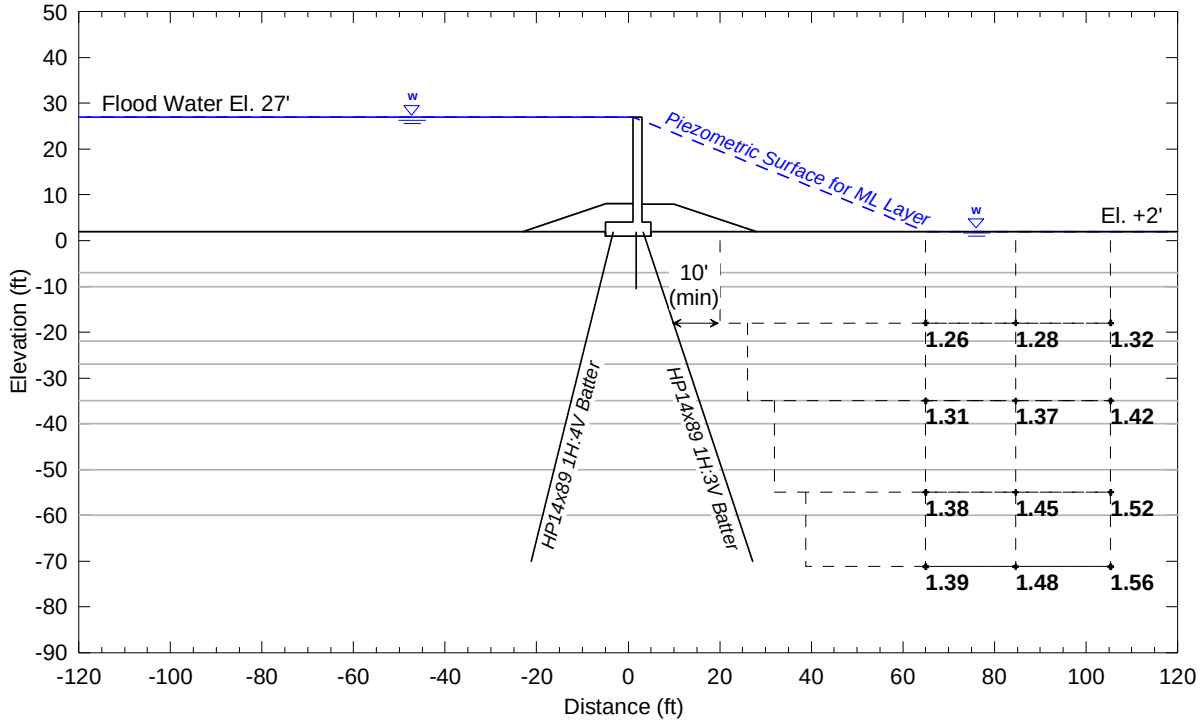

Figure 7-6a. Factors of Safety for Multiple DMM Zone Widths and Depths

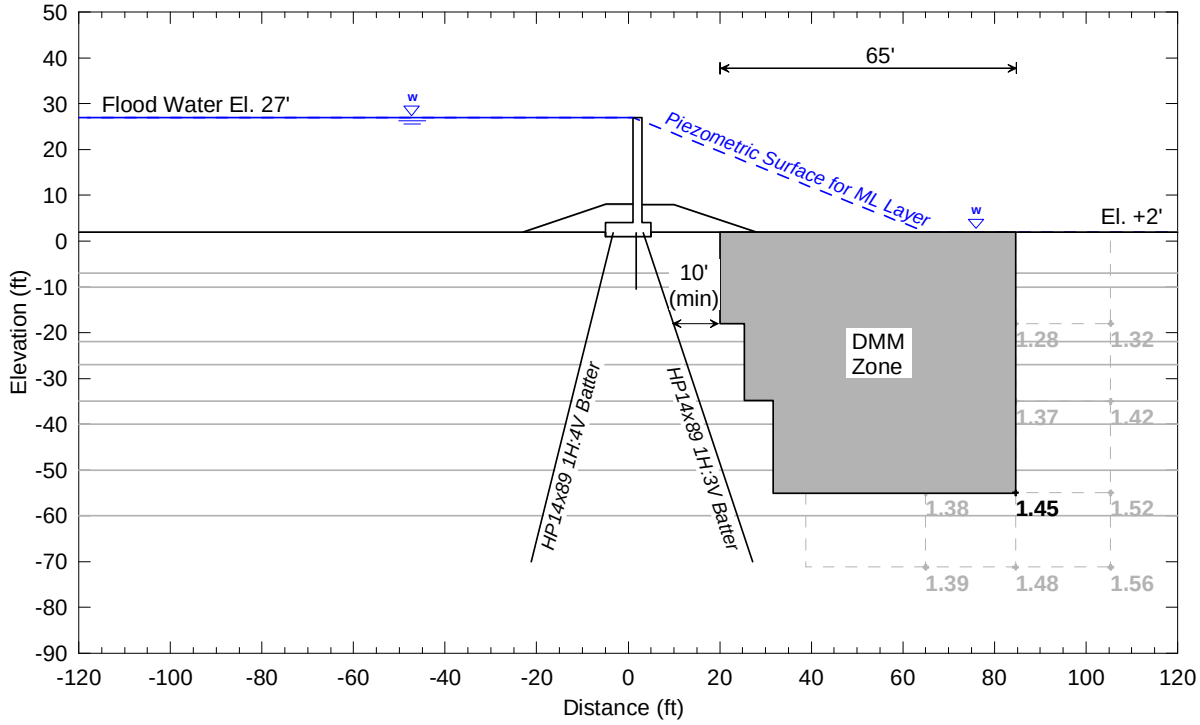

Figure 7-6b. Factor of Safety for 65 ft Wide DMM Zone with Tip El. -55 ft

Figure 7-6. Factors of Safety for Single DMM Zone on Protected Side
10’ (min) Clearance Between DMM Zone and Protected Side Pile

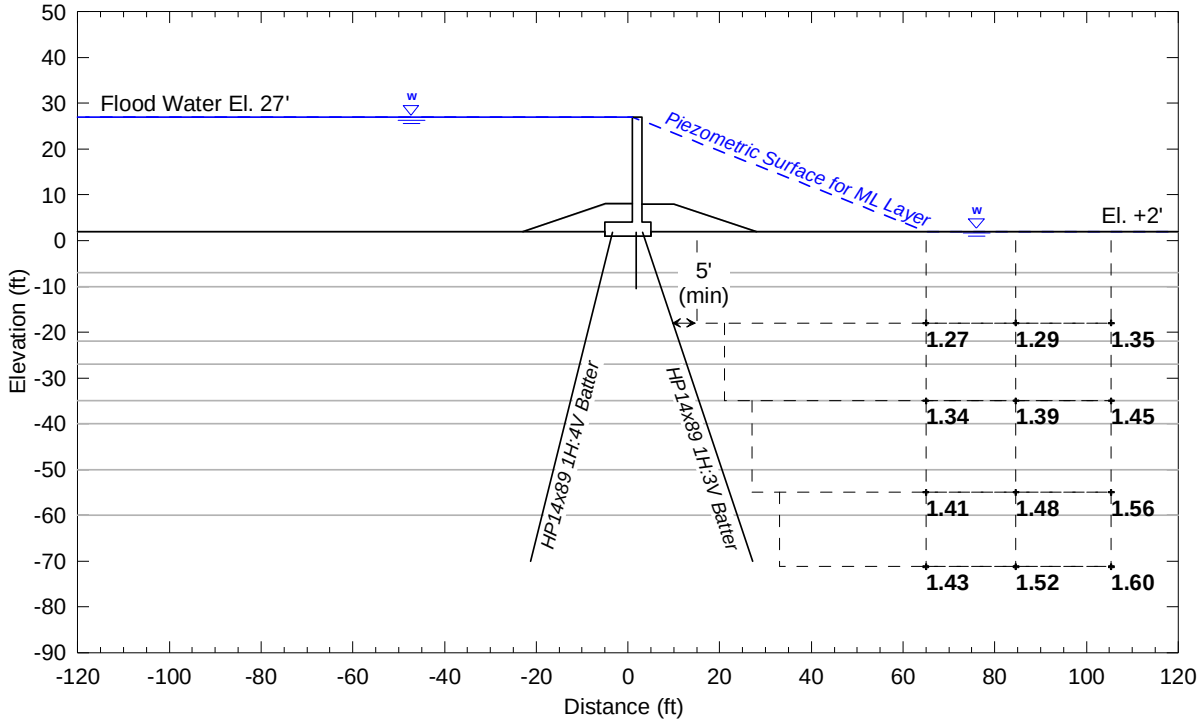

Figure 7-7a. Factors of Safety for Multiple DMM Zone Widths and Depths

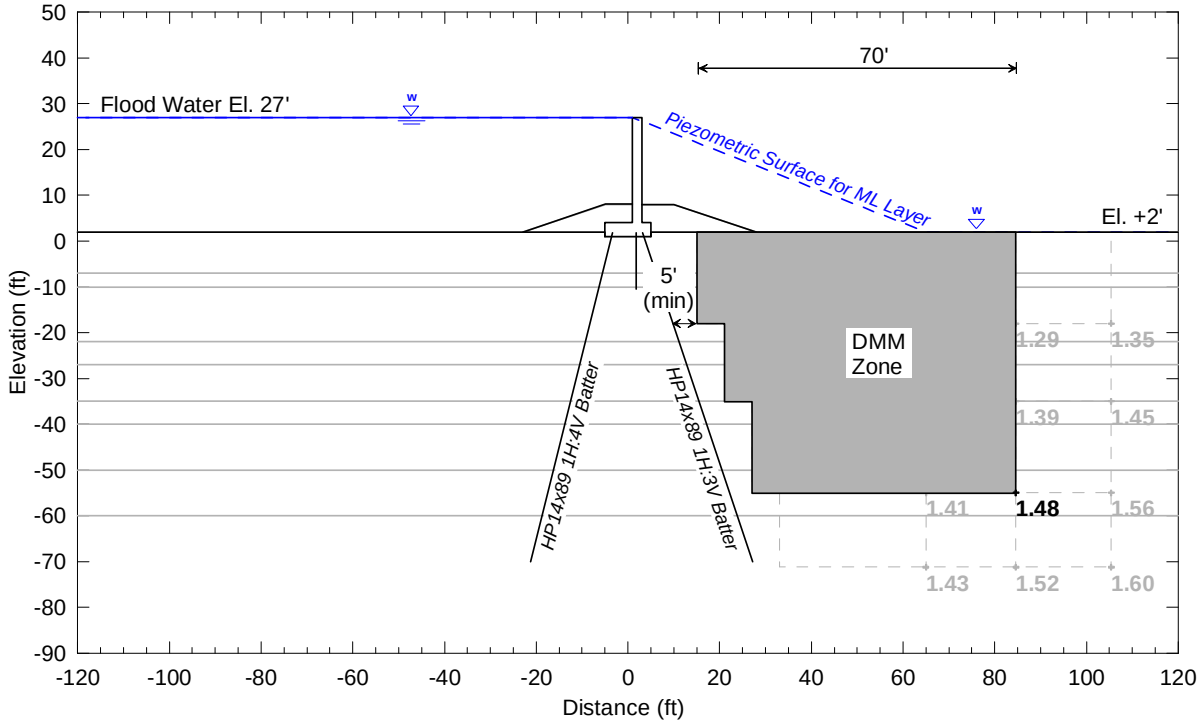

Figure 7-7b. Factor of Safety for 70 ft Wide DMM Zone with Tip El. -55 ft

Figure 7-7. Factors of Safety for Single DMM Zone on Protected Side
5' (min) Clearance Between DMM Zone and Protected Side Pile

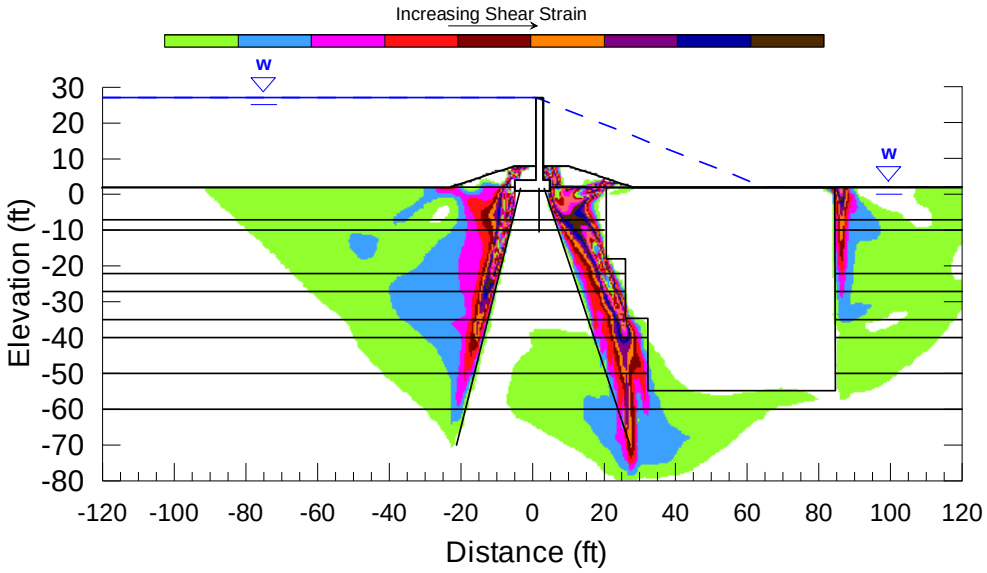

Figure 7-8. Shear Strain Contours at Failure, Single 65 ft Wide DMM Zone with Tip El. -55 ft on Protected Side, 10' (min) Clearance Between DMM Zone and Protected Side Pile, FS = 1.45

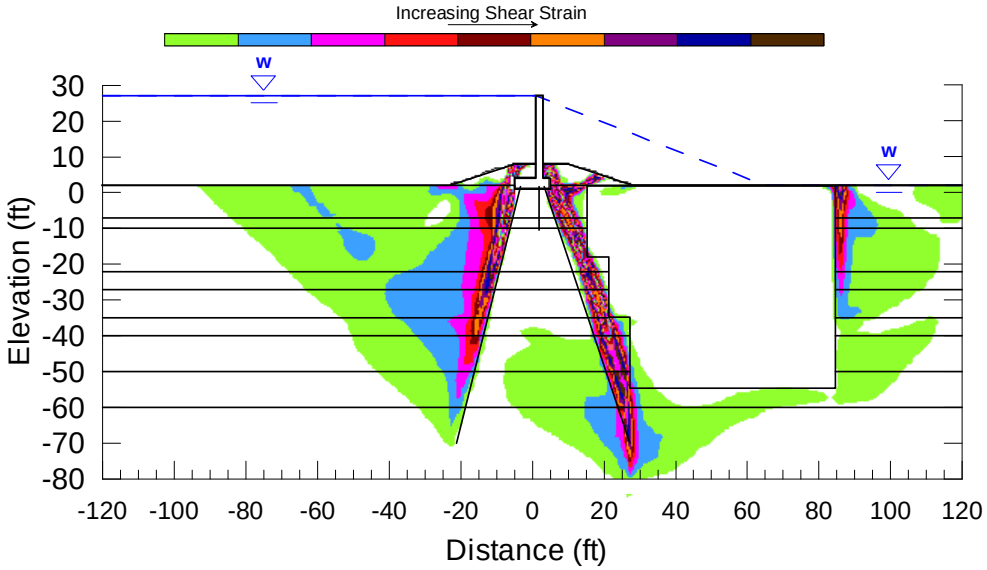

Figure 7-9. Shear Strain Contours at Failure, Single 70 ft Wide DMM Zone with Tip El. -55 ft on Protected Side, 5' (min) Clearance Between DMM Zone and Protected Side Pile, FS = 1.48

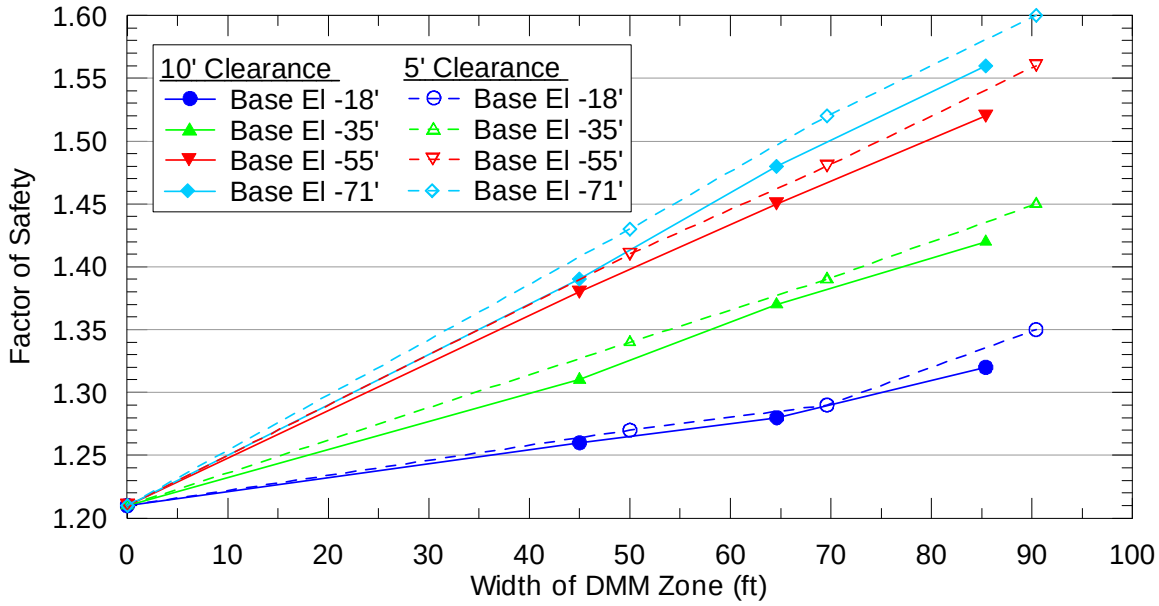

Figure 7-10. Comparison of Factors of Safety for Single DMM Zone on Protected Side 5 ft and 10 ft Clearance Between DMM Zone and Protected Side Pile

7.3.4. Analyses with a Flood Side DMM Zone

The effect of placing the DMM zone on the flood side of the T-wall was investigated for a range of DMM zone configurations. The first set of analyses was completed for a minimum horizontal clearance between the flood side pile and the DMM soil-cement columns of 10 ft. The results of these analyses are presented in Figure 7-11. Automatic factor of safety analyses were run for DMM zone widths of 26 ft, 44 ft, 68 ft, and 86 ft with base elevations of El -18 ft, El -35 ft, -55 ft and El -71 ft. The factor of safety for each case is plotted at the lower left corner of the DMM zone in Figure 7-11a. Figure 7-11b shows the DMM zone configuration and factor of safety for a DMM zone base elevation of -55 ft and width of 68 ft.

To investigate the effect of placing the DMM zone closer to the T-wall, a second set of analyses was completed for a minimum horizontal clearance between the protected side pile and the DMM zone of 5 ft. The results of these analyses are presented in Figure 7-12. The factor of safety for each case is plotted in Figure 7-12a at the lower left corner of the DMM zone. Figure 7-12b shows the DMM zone configuration and factor of safety for a base elevation of -55 ft and a DMM zone width of 74 ft.

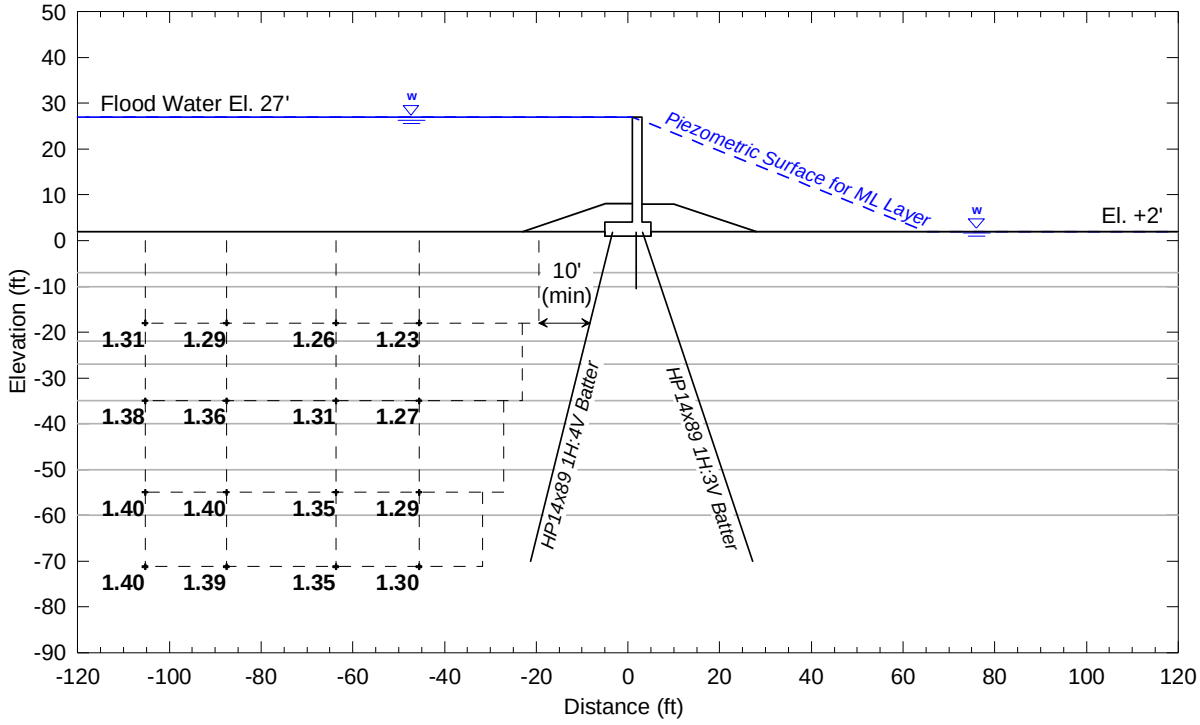

Figure 7-11a. Factors of Safety for Multiple DMM Zone Widths and Depths

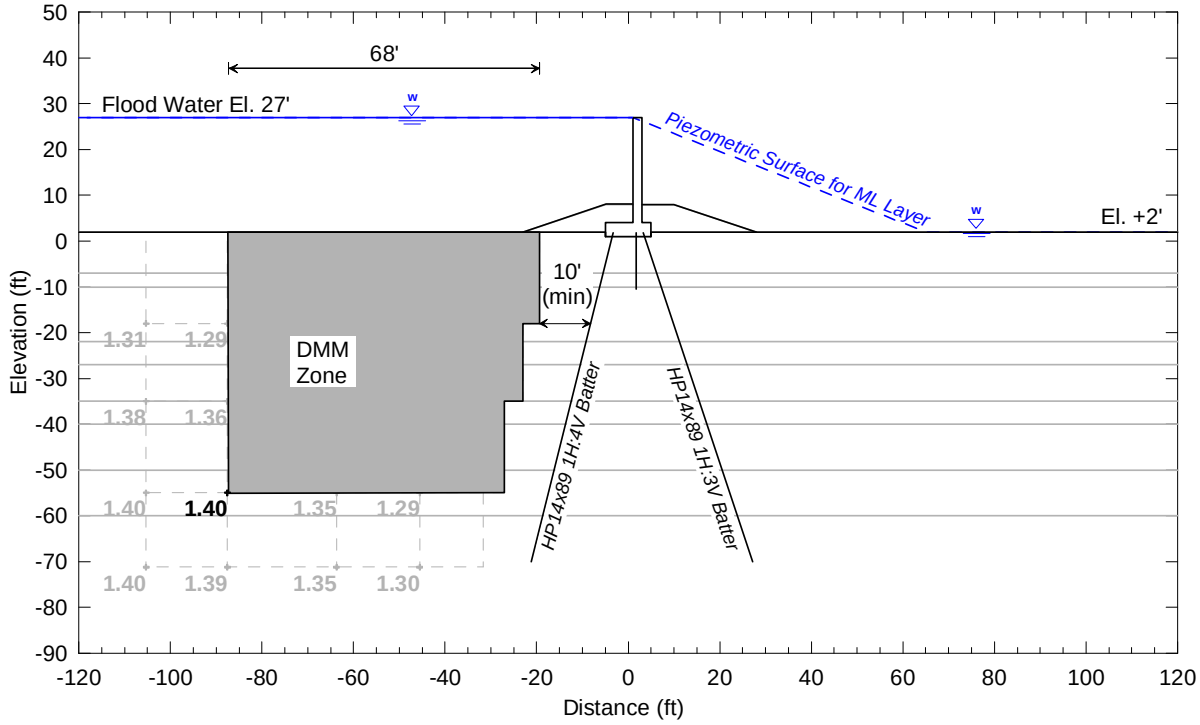

Figure 7-11b. Factor of Safety for 68 ft Wide DMM Zone with Tip El. -55 ft

Figure 7-11. Factors of Safety for Single DMM Zone on Flood Side
10’ (min) Clearance Between DMM Zone and Flood Side Pile

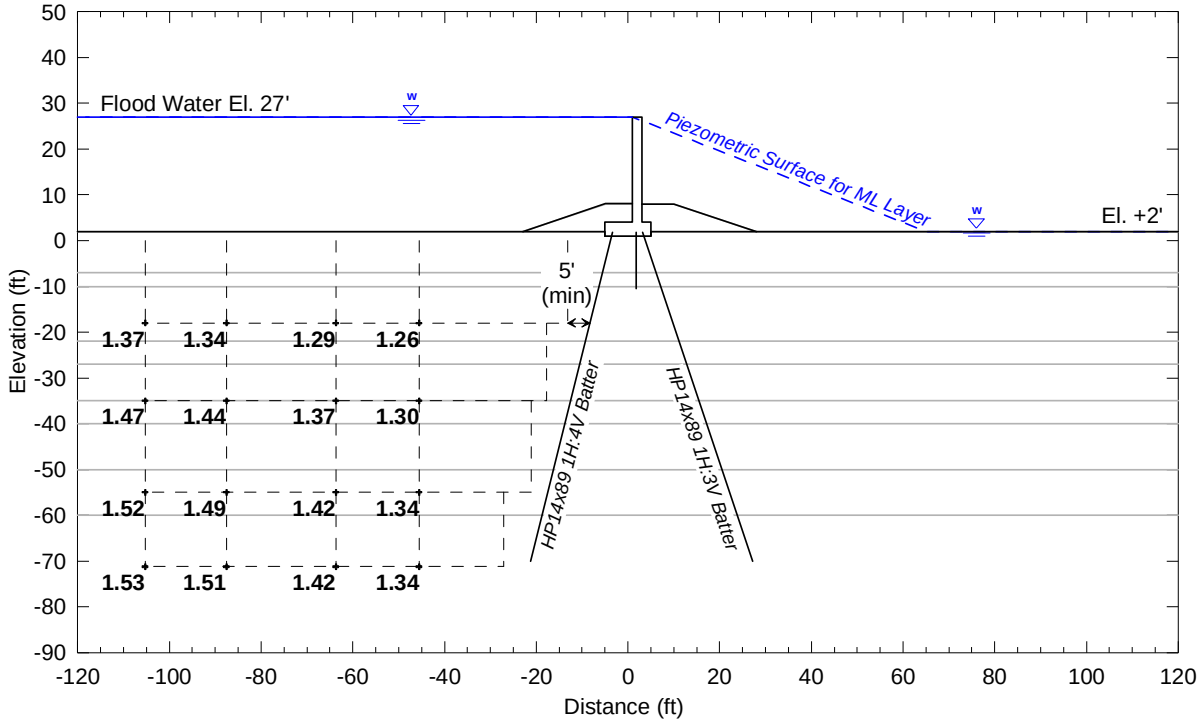

Figure 7-12a. Factors of Safety for Multiple DMM Zone Widths and Depths

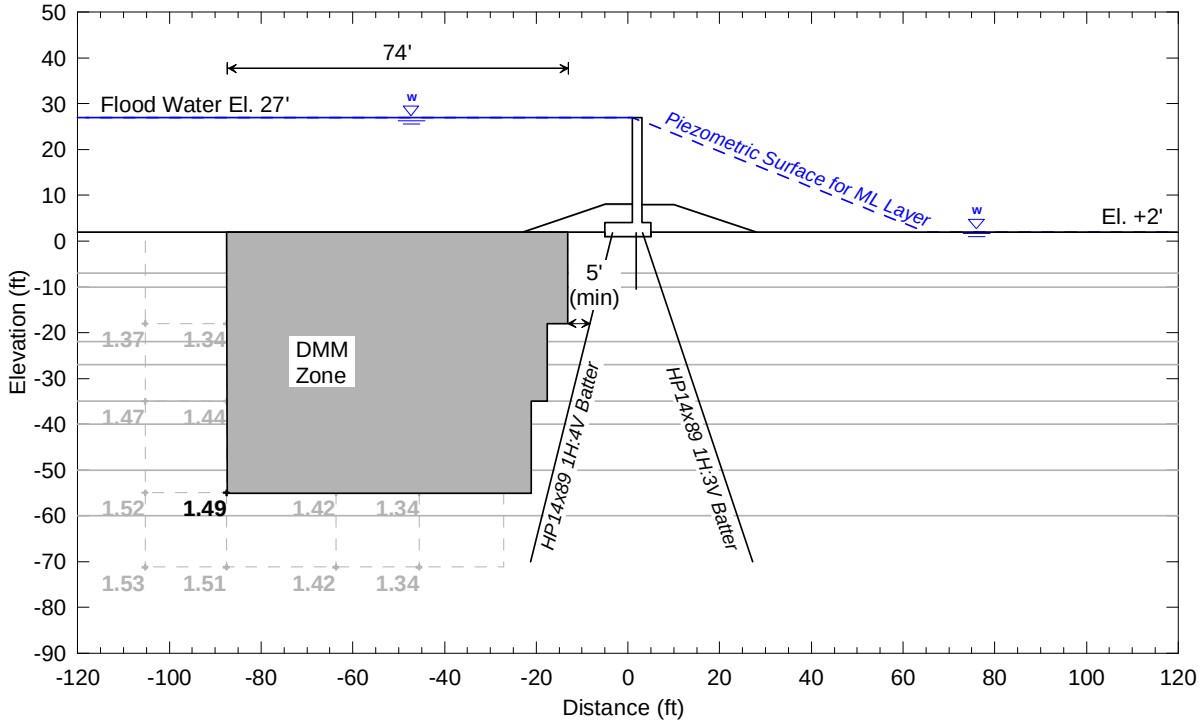

Figure 7-12b. Factor of Safety for 74 ft wide DMM Zone with Tip El. -55 ft

Figure 7-12. Factors of Safety for Single DMM Zone on Flood Side
5’ (min) Clearance Between DMM Zone and Protected Side Pile

The shear strain contours shown in Figures 7-13 and 7-14 correspond to failure for the DMM zone configurations shown in Figures 7-11b and 7-12b. The shear strain contours for 10 ft of clearance between the DMM zone and the flood side piles, shown in Figure 7-13, indicate shearing along the upper half of the flood side pile as well as shear strain in the soil between the DMM zone and the T-wall. Similar trends are present in the shear strain contours for 5 ft of clearance, shown in Figure 7-15, with increased shearing along the pile and decreased shear strain in the soil between the DMM zone and the piles.

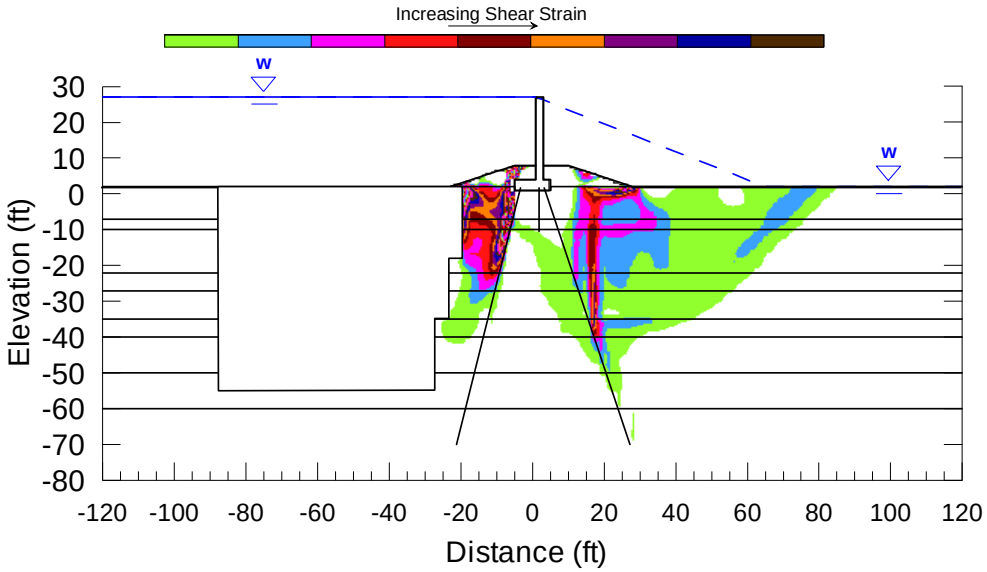

Figure 7-13. Shear Strain Contours at Failure, Single 68 ft Wide DMM Zone with Tip El. -55 ft on Flood Side, 5' (min) Clearance Between DMM Zone and Protected Side Pile, FS = 1.40

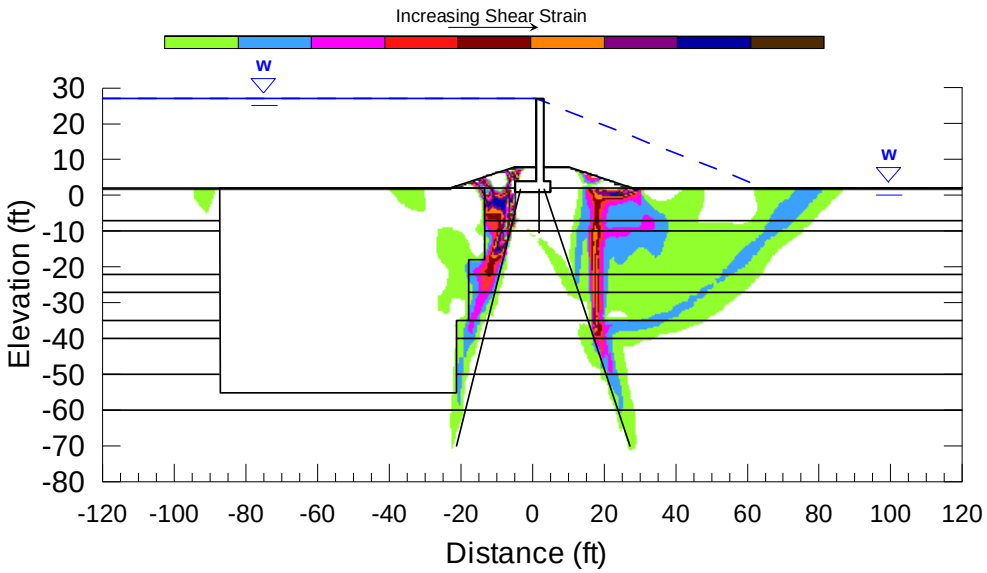

Figure 7-14. Shear Strain Contours at Failure, Single 74 ft Wide DMM Zone with Tip El. -55 ft on Flood Side, 5' (min) Clearance Between DMM Zone and Protected Side Pile, FS = 1.49

The results for different configurations and different clearances for a DMM zone located on the flood side of the T-wall are shown in Figure 7-15. The factor of safety generally increases with increasing DMM zone width and depth for a given clearance; however, the trend lines show little additional benefit as the base elevation decreases from El -55' to El -71'. In contrast to the results for DMM zones located on the protected side, the factors of safety for 5 ft clearance are significantly higher than for 10 ft clearance for DMM zones on the flood side. Based on the shear strain contours in Figures 7-13 and 7-14, reducing the gap between the T-wall piles and the DMM zone increases the factor of safety by minimizing the extent of shear strain in the soil between the T-wall and the DMM zone. Decreases in clearance for the flood side DMM zone configuration result in larger increases in factor of safety than for protected side DMM zones because the reduced clearance for the upstream DMM zone extends this block underneath the driving loads of the impounded water, allowing for more of this load to be taken up by the DMM zone instead of being carried by the T-wall.

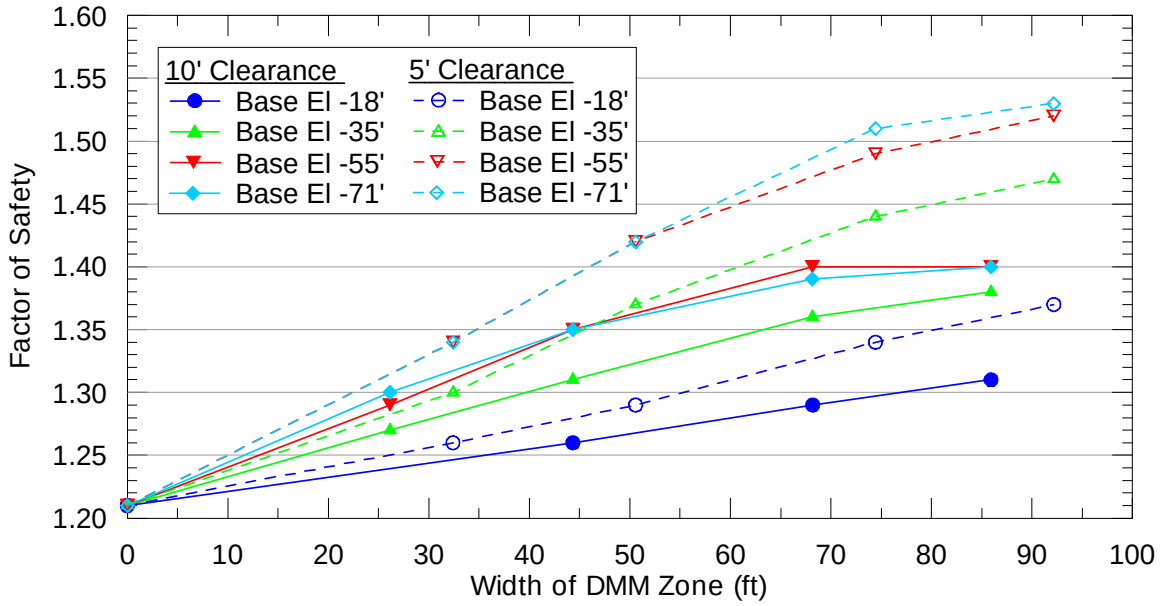

Figure 7-15. Comparison of Factors of Safety for Single DMM Zone on Flood Side 5 ft and 10 ft Clearance Between DMM Zone and Flood Side Pile

7.3.5. Analyses with Symmetric Flood and Protected Side DMM Zones

The effect of placing symmetric zones of DMM soil-cement columns on the flood side and protected side of the T-wall was investigated for a range of zone configurations. The analyses were completed for a minimum horizontal clearance between the T-wall piles and the DMM soil-cement columns of 10 ft. The results of these analyses are presented in Figure 7-16. Each automatic factor of safety analysis was run with two DMM zones. The DMM zones had combined widths of 89 ft, 133 ft, or 171 ft with base elevations of El -18 ft, El -35 ft, El -55 ft, or El -71 ft. The factor of safety for each case is plotted at the lower left corner of the flood side DMM zone and at the lower right corner of the protected side DMM zone in Figure 7-16a. Figure 7-16b shows the DMM zone configuration and factor of safety for a DMM zone base elevation of -55 ft and combined DMM zone width of 133 ft.

The shear strain contours shown in Figure 7-17 correspond to failure for the DMM zone configuration shown in Figure 7-16b. The shear strain contours show shear strain on the protected side consistent with the single protected side DMM zone in Figure 7-8 and shear strain on the flood side consistent with the single flood side DMM zone in Figure 7-13.

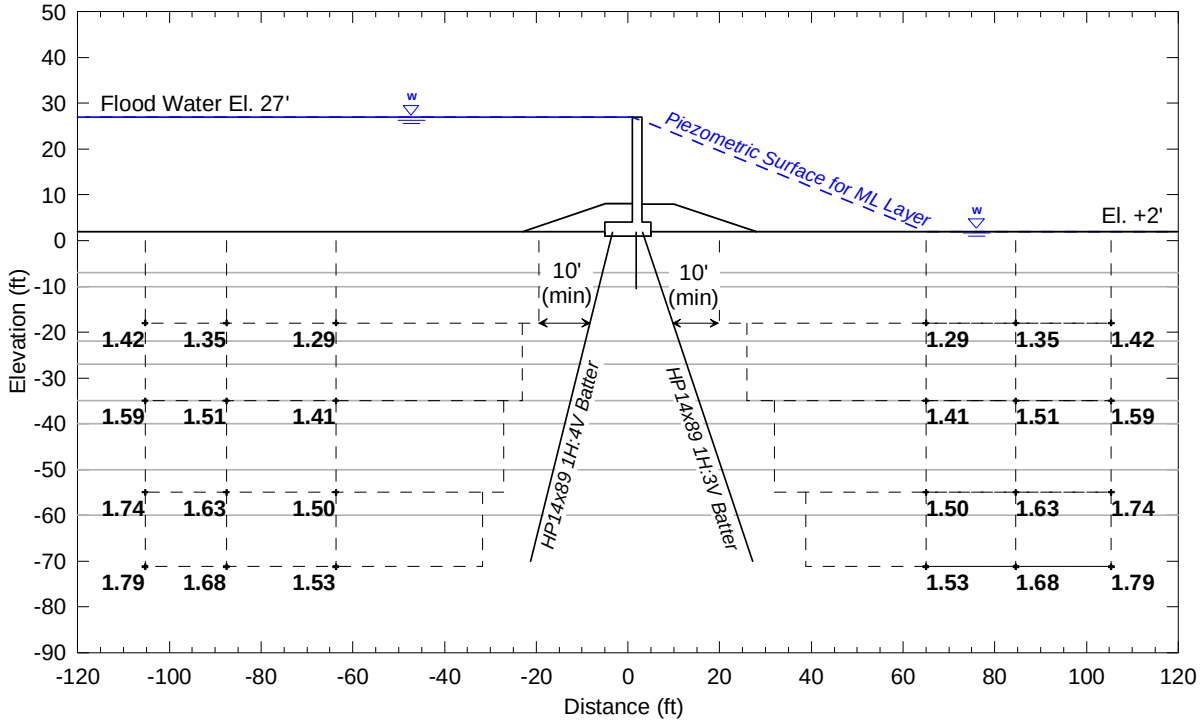

Figure 7-16a. Factors of Safety for Multiple DMM Zone Widths and Depths

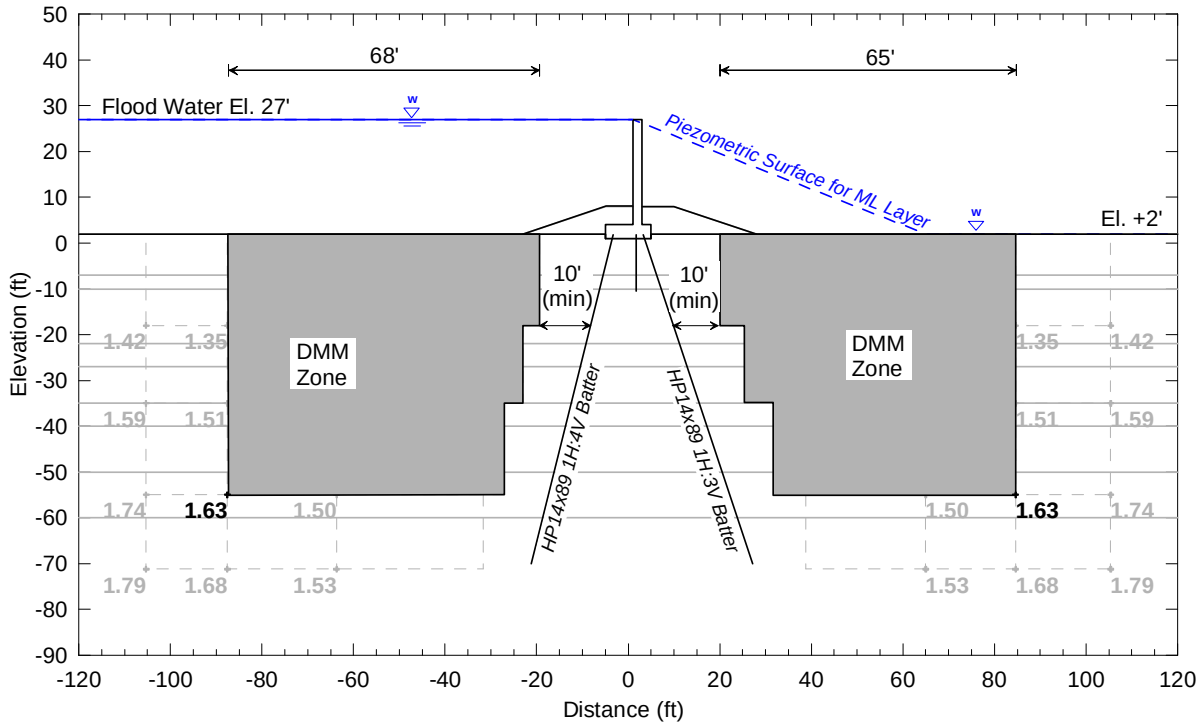

Figure 7-16b. Factor of Safety for Combined DMM Zone Width of 133 ft with Tip El. -55 ft

Figure 7-16. Factors of Safety for Symmetric DMM Zones
10’ (min) Clearance Between DMM Zone and T-wall Piles

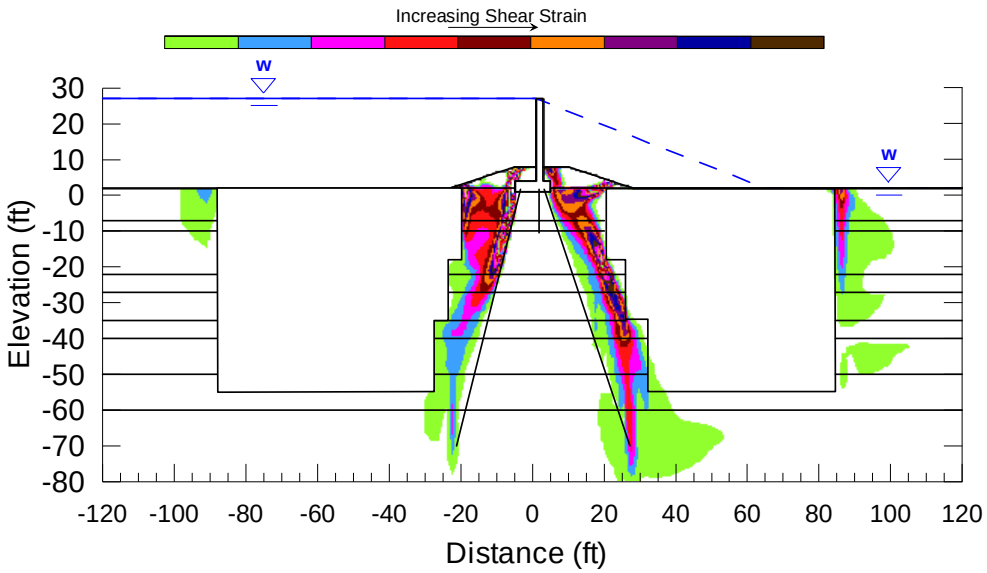

Figure 7-17. Shear Strain Contours at Failure, Combined DMM Zone Width of 133 ft with Tip El. -55 ft , 10' (min) Clearance Between DMM Zones and Piles, FS = 1.63

The results for different configurations of symmetric DMM zones located on the flood side and protected side of the T-wall are shown in Figure 7-18. The factor of safety shows a fairly linear increase with increasing DMM zone width. There is relatively little improvement in the factor of safety when the base elevation of the DMM zones is lowered from El -55 ft to El -71 ft, which is consistent with the trends noted for the previous analyses.

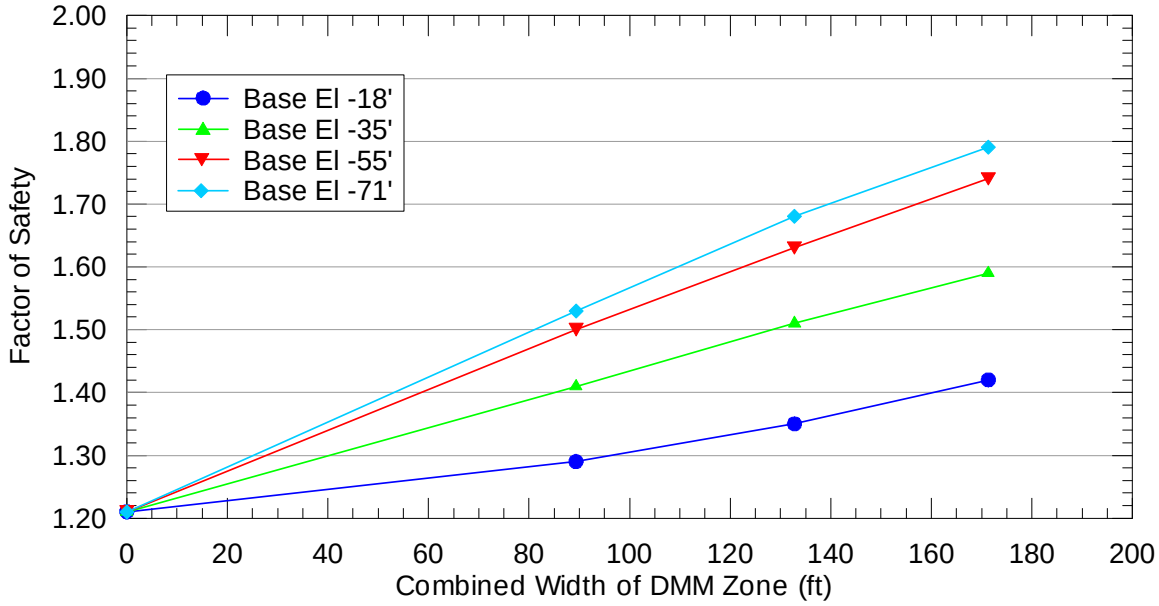

Figure 7-18. Comparison of Factors of Safety for Symmetric DMM Zones

10 ft Clearance Between DMM Zone and Flood Side Pile

7.3.6. Analyses with a Single DMM Zone Centered Underneath the T-wall

The effect of placing a single zone of DMM soil-cement columns, centered underneath the T-wall, was investigated for a range of zone configurations. For these analyses, the representative DMM cohesion and stiffness was applied to the DMM zone soil elements, but the pile coupling springs that attach the pile to the mesh were based on the strength of the native, untreated soil. This characterization may underestimate the movement of the piles, as they would be embedded in the native soil in between the DMM shear walls, and the deformations in the soil could be higher than those calculated for the composite DMM zone elements. A three dimensional model would be needed to model the deformations in the native soil and shear walls to more accurately predict the displacement of the piles.

The analyses considered a continuous DMM zone centered underneath the T-wall and did not include a joint in the DMM shearwall at the sheetpile. As such, these analyses correspond either to the case where the shearwalls are constructed before the sheetpile is installed and the sheetpile is driven into the shearwalls before the wet-mix DMM soil-cement columns set up, or where the soil-cement columns are installed after the sheetpile and jet grout columns are installed to

connect the protected and flood side portions of the DMM zones to the sheetpile. If the shear walls are not continuous, relative movement between the flood side and protected side DMM zones and the concrete flood wall would cause stress concentrations at the connection between the DMM zones and the wall. The results of these analyses would likely be dependent on the relative locations of the DMM zone corners to the concrete flood wall, and additional analyses would be needed to evaluate this DMM zone configuration. According to Hayward Baker personnel, they have been able to install dry-mixed soil-cement columns within a few inches of buried structures, which would minimize the width of the joint in the DMM panels at the sheetpile.

The results of the analyses for centered DMM zones are presented in Figure 7-19. Automatic factor of safety analyses were run for DMM zone widths of 31 ft, 50 ft, 72 ft, 90 ft, and 133 ft with base elevations of El -18 ft, El -35 ft, El -55 ft, and El -71 ft. The factor of safety for each case is plotted at the lower left corner and lower right corner of the DMM zone in Figure 7-19a. Figure 7-19b shows the DMM zone configuration and factor of safety for a DMM zone base elevation of -35 ft and width of 72 ft.

The shear strain contours shown in Figure 7-20 correspond to failure for the DMM zone configuration shown in Figure 7-19b. The shear strain contours show a complex failure mode, with a rotational failure underneath the DMM zone, shearing around the piles, and shearing through the DMM zone.

The results for different configurations of centered DMM zone are shown in Figure 7-21. The trend lines are plotted relative to the total width of the DMM zone. For base elevations of -55 ft and below, there is a sharp increase in the factor of safety as the DMM zone width increases from 50 ft to 72 ft.

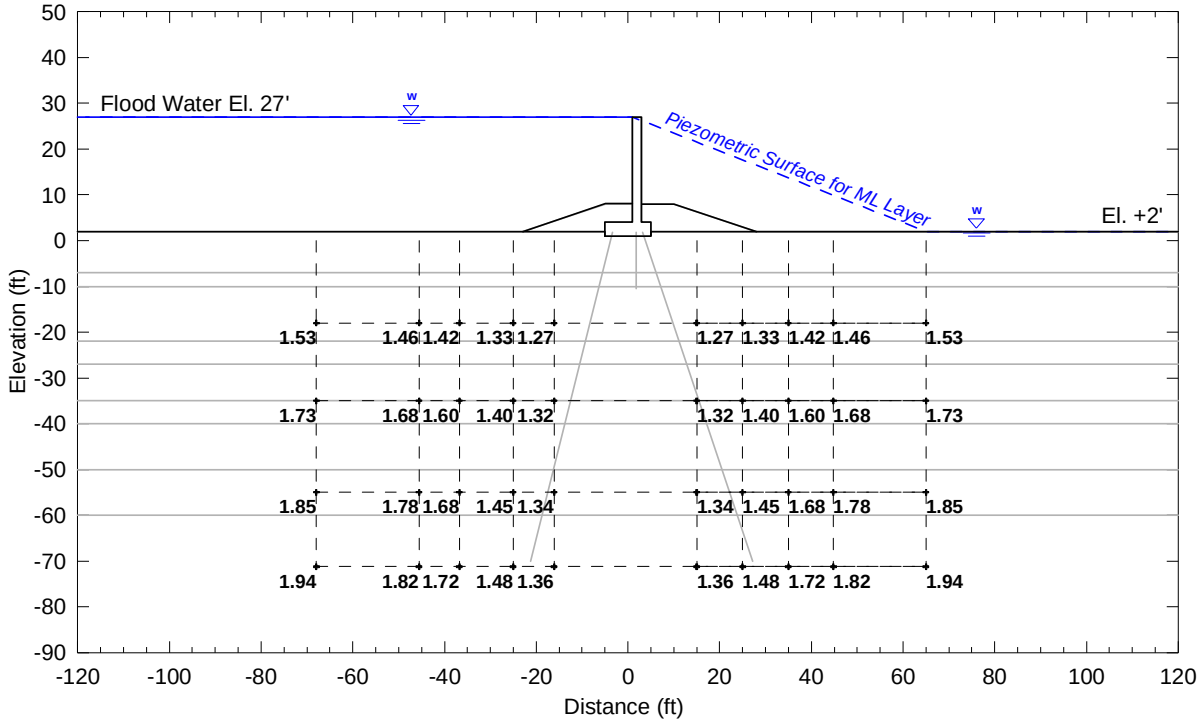

Figure 7-19a. Factors of Safety for Multiple DMM Zone Widths and Depths

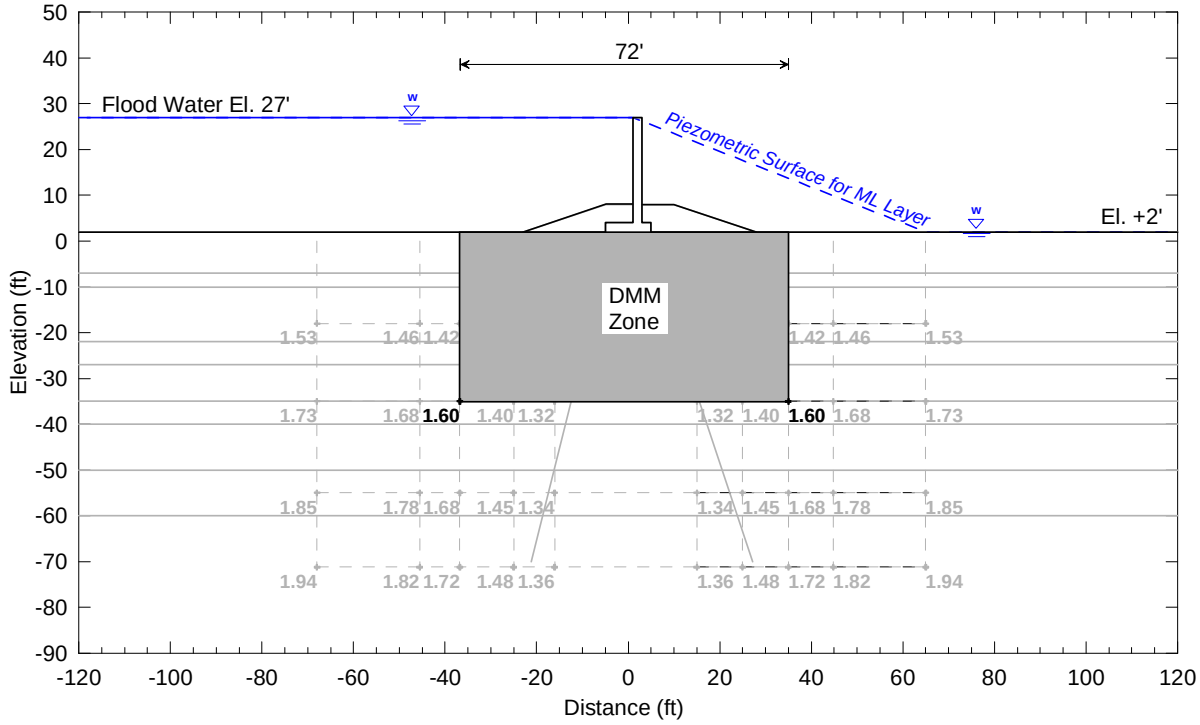

Figure 7-19b. Factor of Safety for Centered 72 ft Wide DMM Zone with Tip El. -35 ft

Figure 7-19. Factors of Safety for Centered DMM Zone

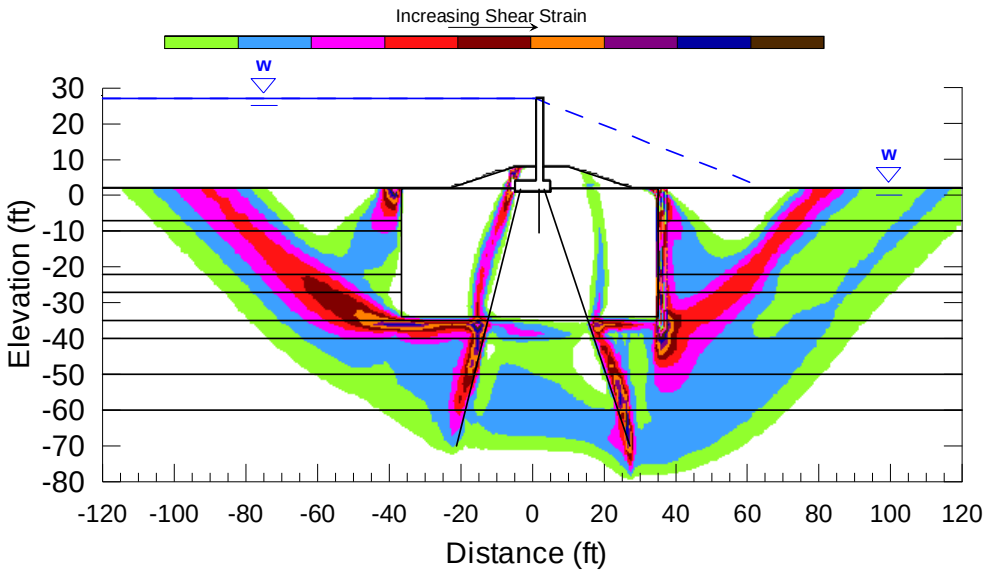

Figure 7-20. Shear Strain Contours at Failure, Centered 72 ft Wide DMM Zone with Tip El. -35 ft , FS = 1.60

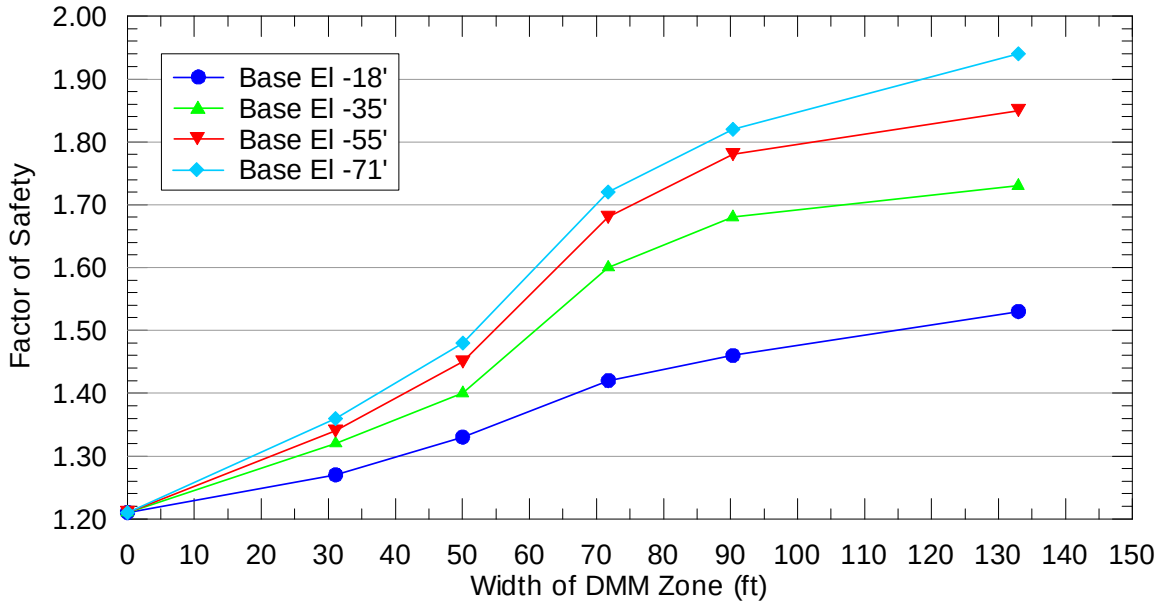

Figure 7-21. Comparison of Factors of Safety for Centered DMM Zone

7.3.7. Efficiency of DMM Zone Configurations

The optimum DMM zone configuration would be the one that meets the design criteria for factor of safety with the smallest DMM zone, considering that the cost of installing the DMM zone is a function of the total treated volume. The efficiency of each DMM zone configuration can be evaluated by dividing the increase in factor of safety by the volume of improved ground. For this study, the increase in factor of safety is determined by subtracting the factor of safety of 1.21 for the T-wall without a DMM zone from the factor of safety obtained for each DMM configuration. Because the replacement ratio is constant for this study, the cross-sectional area of the DMM zone is used instead of the volume of improved ground. For the single protected side DMM zone that is 45 ft wide with a tip elevation at -18 ft and 10 ft clearance between the DMM columns and the T-wall piles, the resulting calculation for the efficiency of the DMM zone is $(1.27\text{-}1.21)/((45')(19')) = 5.85 \times 10^{-5} / ft^2$.

The efficiencies for each of the DMM zone configurations are presented in Figures 7-22 through 7-25. For DMM zones on the protected side, the efficiency of the DMM zones with 5 ft of clearance between the soil-cement columns and the protected side pile are only slightly higher than those with 10 ft of clearance, as shown in Figure 7-22. The increase in efficiencies for the reduced clearance is more pronounced for the case of DMM zones on the flood side of the T-wall, as shown in Figure 7-23. In general, for DMM zone base elevations lower than El -18 ft, the efficiency of a DMM zone on either the protected side or the flood side of the T-wall decreases with increasing width and increasing depth. The DMM zones on the flood side with 10 ft of clearance tend to have lower efficiencies than the other configurations shown in Figures 7-22 and 7-23, and the DMM zones on the flood side with 5 ft of clearance tend to have higher efficiencies than the other configurations.

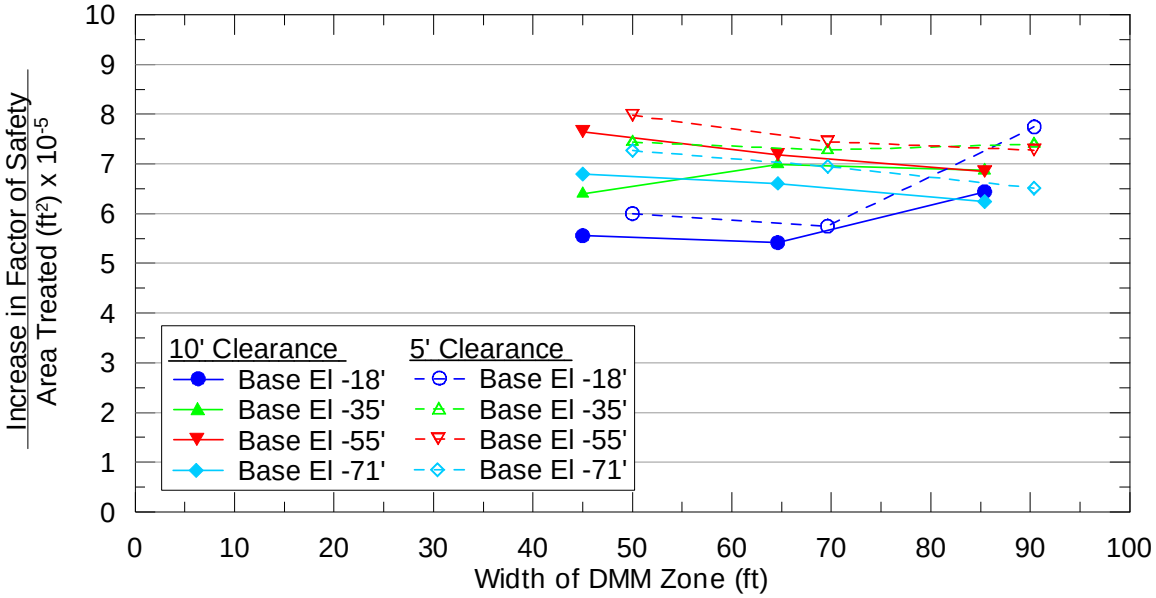

Figure 7-22. Comparison of Efficiencies for Single DMM Zone on Protected Side with 5 ft and 10 ft Clearance Between DMM Zone and Protected Side Pile

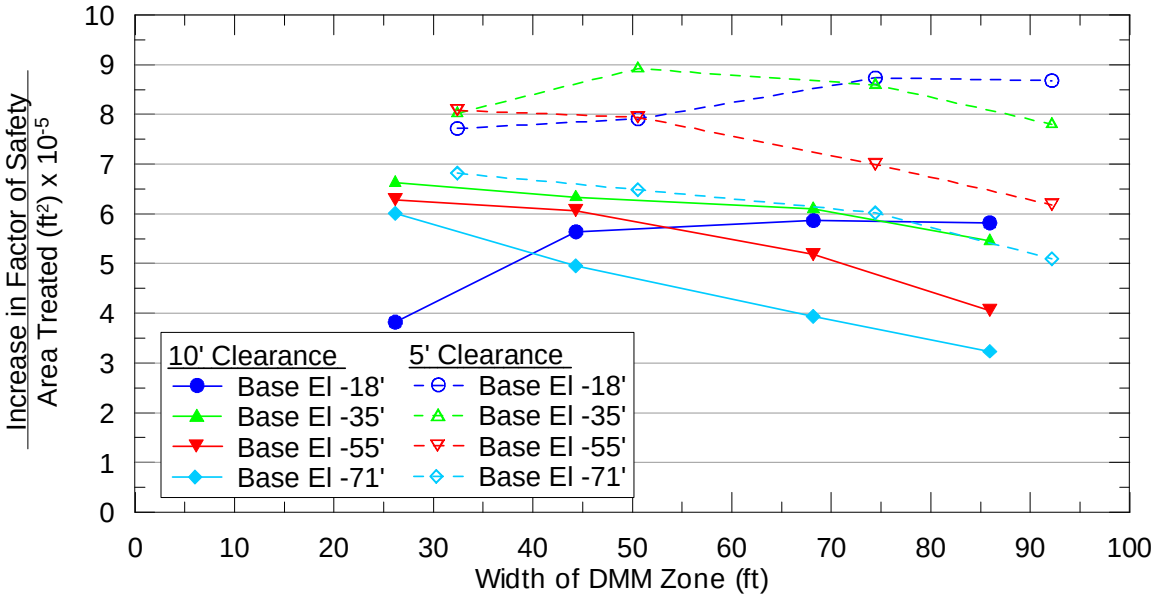

Figure 7-23. Comparison of Efficiencies for Single DMM Zone on Flood Side with 5 ft and 10 ft Clearance Between DMM Zone and Flood Side Pile

The efficiencies for symmetric DMM zones with 10 ft of clearance, which are shown in Figure 7-24, fall generally in the same range as those for single DMM zones with 10 ft of clearance on the flood side, and they are slightly less than those obtained for a single DMM zone on the protected side with 10 ft of clearance. For DMM zone base elevations lower than El -18 ft, the efficiency for the symmetric DMM zones decreases with increasing width and increasing depth, which is consistent with the trends noted for the previous analyses. The overall increases in factor of safety for the symmetric zone configurations, which use a large total volume of deep mixed material to improve both the flood and protected sides of the T-wall, are significantly greater than increases in factor of safety obtained for the single zone configurations, as can be seen by comparing Figures 7-15 and 7-18. Symmetric DMM zones may be useful if the computed factors of safety for single zone configurations do not meet the design criteria.

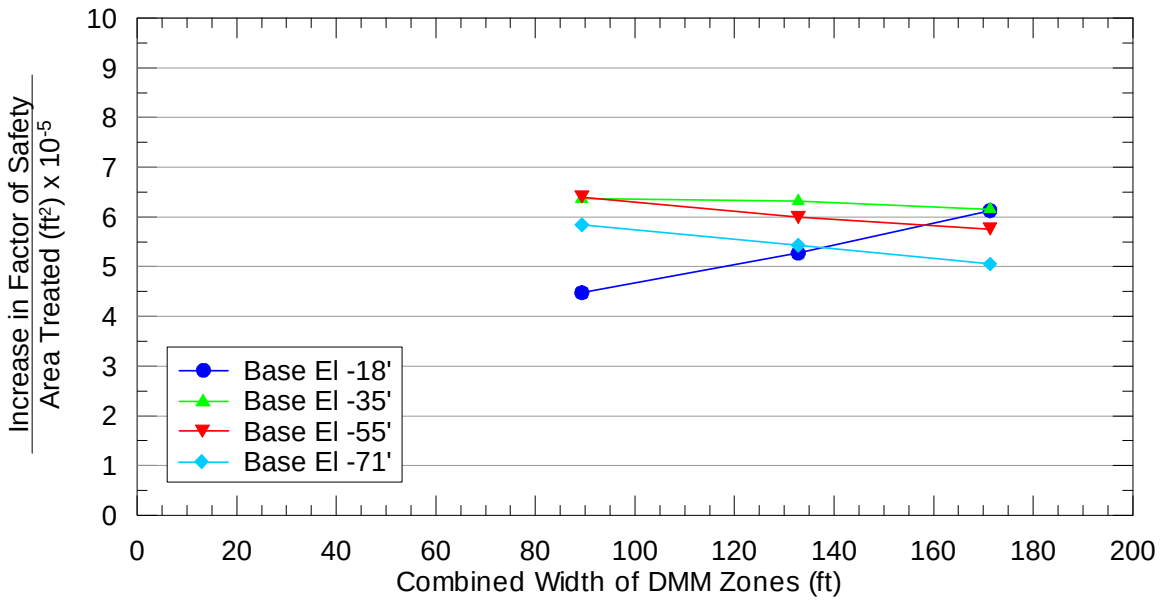

Figure 7-24. Comparison of Efficiencies for Symmetric DMM Zones

10 ft Clearance Between DMM Zone and T-wall Piles

The efficiencies of single DMM zones centered beneath the T-wall, which are shown in Figure 7-25, are significantly greater than those obtained for the other configurations, indicating that a single DMM zone centered underneath the T-wall is the most effective at stabilizing the T-wall.

The efficiencies for the single DMM zone decrease with increasing treatment depth. For all DMM zone depths, the peak efficiency corresponds to a zone width of 72 ft.

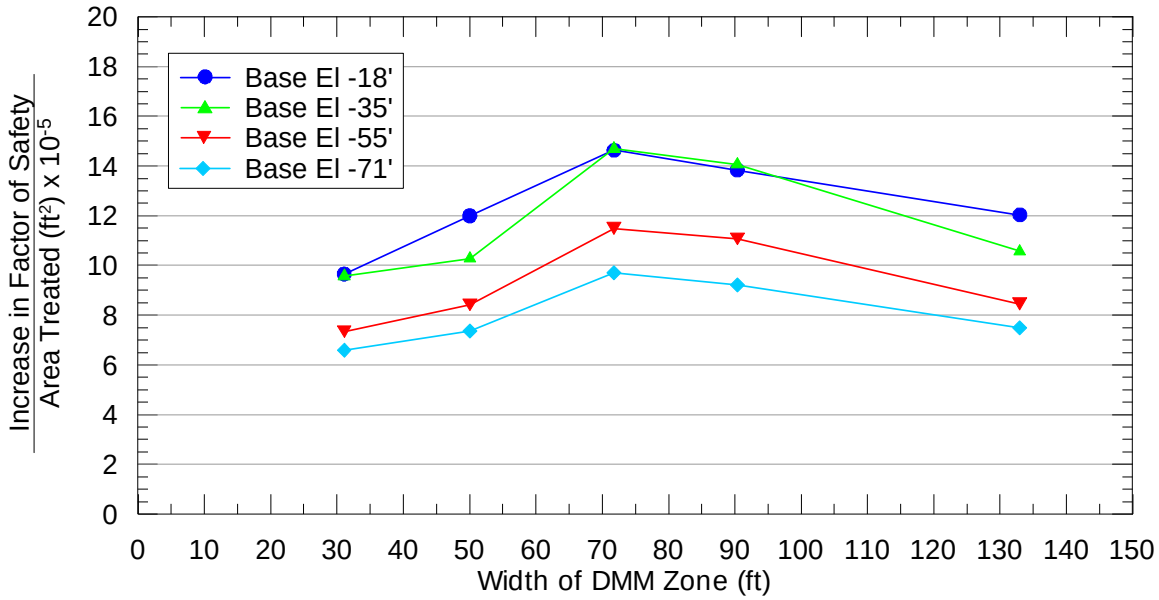

Figure 7-25. Comparison of Efficiencies for Centered DMM Zone

While the trends shown in Figures 7-22 through 7-25 provide a basis for comparing the efficiency of different DMM zone configurations, they do not reflect the ability of the different configurations to achieve acceptable factors of safety. Selecting an optimum DMM section for a given design would require considering both the desired factor of safety and the efficiency. For example, if the desired factor of safety is 1.5 for the centered DMM zones shown in Figure 7-19, then Figure 7-21 can be used to obtain minimum widths of 115 ft, 61 ft, 55 ft, and 52 ft for base elevations of El -18 ft, El -35 ft, El -55 ft, and El -71 ft, respectively. Figure 7-25 shows that the most efficient of these four configurations is the one that is 115 ft wide with a base elevation of El -18 ft. The shape of the curves in Figure 7-25 also suggest that base elevations between El-18 ft and El -35 ft should also be investigated and would likely produce greater efficiency while still achieving the desired factor of safety for the given site conditions. Because all the efficiency peaks in Figure 7-25 occur at a width of 72 ft, a near optimum design could be found by finding the base elevation of a 72 ft wide DMM zone that produces a factor of safety of 1.5. Interpolating in Figure 7-21, the optimum 72 ft wide DMM zone would have a base elevation of

about El -25 ft or El -26 ft. In practice, the final elevation should be confirmed by analyses to reflect the details of stratigraphy and system geometry.

7.4. Conclusions

The following conclusions can be drawn from this study, for the conditions used to represent the level ground T-wall section.

- DMM soil-cement column configurations that minimize or eliminate the gap between the DMM and the T-wall result in higher factors of safety. The analyses show that the effect of a gap on the flood side is more pronounced than the effect of a gap on the protected side.

- Of the configurations included in this study, a continuous DMM zone centered underneath the T-wall is the most efficient configuration for stabilizing the wall. This configuration considers the flood side and protected side portions of the DMM zone to be connected to the sheetpile, requiring the sheetpile to be installed after the shear walls or installation of jet grout columns to connect the flood and protected side DMM panels to the sheetpile. In addition, the potential for pile driving to damage the DMM columns or for the DMM column installation to damage the piles should be carefully considered and evaluated.

- If the DMM columns cannot be installed continuously to depth across the sheetpile, but a DMM zone centered underneath the T-wall with a joint at the sheetpile is desired, additional analyses would be necessary to evaluate the effect of a full depth joint in the panel at the location of the sheetpile. Relative movement between the flood side and protected side DMM zones and the concrete flood wall would cause stress concentrations at the connection between the DMM zones and the wall. The results of analyses to investigate these stress concentrations would likely be dependent on the relative locations of the DMM zone corners to the concrete flood wall. According to Hayward Baker personnel, they have been able to install dry-mixed soil-cement columns within a few

inches of buried structures, which would minimize the width of the joint in the DMM panels at the sheetpile.

- For the continuous DMM zones centered underneath the T-wall, the highest efficiency is produced by a 72 ft wide zone. However, both efficiency and achieving the desired factor of safety should be considered in selecting an optimum design configuration.

- Alignment of the piles and DMM shear walls would have to be carefully considered before implementing a centered DMM zone in practice.

- If a single DMM zone centered underneath the T-wall is not feasible, and if a 10 ft gap must be maintained between the DMM columns and the piles, then the most effective configuration for stabilizing the T-wall is a single block on the protected side of the T-wall.

- If the design criteria for factor of safety cannot be achieved with a single DMM zone on the protected side of the wall, and if a continuous DMM zone centered underneath the T-wall is not feasible, then symmetric DMM zones on the protected side and the flood side of the wall can be used to raise the factor of the safety.

CHAPTER 8

STABILITY ANALYSES OF THE INNER HABOR NAVIGATION CANAL REACH III B-IA I-WALL

This case study included stability analysis of a segment of the U.S. Army Corps of Engineers (USACE)'s Inner Harbor Navigation Canal Reach III B-1A project that was designed by Burns Cooley Dennis (BCD) and included deep-mixed shear walls in the design. Numerical stability analyses were completed and the results were compared with those obtained from the limit equilibrium-based simplified design method used during design. Details of the I-wall design section, material properties, analysis methods, and results are discussed in this chapter. Also provided in this chapter are the conclusions and recommendations specific to this case study.

8.1. Introduction

8.1.1. Purpose and Scope

The primary purposes of the stability analysis case study for the IHNC Reach III B-1A I-wall are to: 1) evaluate the stability of the I-wall and DMM system; 2) assess the potential influence of a water-filled gap behind the I-wall; 3) estimate the potential displacements of the I-wall during construction loading; and 4) compare the results from the numerical analyses with factors of safety calculated for the Reach III B-1A I-wall using a simplified analysis and design procedure.

The scope of work completed for this study includes:

- Completing numerical analyses to estimate the factor of safety for the I-wall system.
- Completing a parametric study using numerical analyses to evaluate the effects of the DMM zone strength and the efficiency of vertical joints at column overlaps on the performance of the I-wall system.
- Evaluating the potential for a water-filled gap to form during loading of the I-wall sheetpile and completing numerical analyses, if appropriate, to evaluate the effect of a water-filled gap on the factor of safety of the I-wall system.

- Completing deformation analyses for construction conditions to make a conservative estimate of I-wall deflection during installation of the DMM shear walls.

- Comparing the results of the numerical analyses with the factors of safety calculated for the Reach III B-1A I-wall using a simplified design procedure described in "Design Guide for Levee and Floodwall Stability Using Deep-Mixed Shear Walls" (Filz and Templeton 2009).

The I-wall cross-section, flood level, stratigraphy, unit weights, and strength property values for stability analyses are shown in Sheet C-17, "Alternative 3, Typical Section," and in Figure B-2, "Global Stability by Method of Planes", included as Figures A-14 and A-15 in Appendix A. The design factors of safety calculated using the simplified analyses for the Reach III B-1A cross-section were obtained from the IHNC Reach III B-1A example calculations in Appendix B of the Design Guide for Levee and Floodwall Stability Using Deep-Mixed Shear Walls (Filz and Templeton 2009).

8.1.2. Project Description

To improve the stability of the IHNC West Reach III B-1A existing levee and I-wall, BCD was retained by the USACE to design DMM shear walls for the protected side of the I-wall. The I-wall consists of a concrete wall founded on a sheet-pile cutoff that extends to a tip elevation of -17 ft for stability and seepage control. The sheetpile cutoff consists of PZ-27 sections. The shear walls were constructed with overlapping DMM soil-cement columns. The original design of the shear walls for the Reach III B-1A section, shown in Figure A-14 in Appendix A, included 14-ft-long shear walls that extended down to elevation -16 to -30 ft. Based on a post-award analysis performed by BCD, the length of the shear walls was increased to 18 ft and the depth of the shear walls extended to elevation -32 ft, as shown in Figure A-15 in Appendix A. Although we understand that the construction contract was not modified from the 14-foot long panels due to right-of-way constraints, the numerical analyses were performed using the dimensions shown in Figure A-15 to permit comparison with the results of BCD's post-award analyses. The limit of the DMM shear wall in the flood-side direction is located 4 ft away from the I-wall sheetpile. The contract specifications for the project required that the individual soil-cement columns be at

least 31.5 in. in diameter and have a minimum horizontal overlap between any two adjacent columns of at least 20% of the area of a single column. An overlap distance of 9.9 in. produces a 20% overlap area for 31.5-in.-diameter columns. The area replacement ratio was also specified as 30%, which corresponds to a center-to-center panel spacing of 8 ft for 31.5-in.-diameter columns with a 9.9-in. overlap. The top of the DMM columns are 3 ft below the existing grade of the earthen embankment.

8.2. Analysis Section and Material Characterization

A design cross-section for the Reach III B-1A I-wall with DMM shear walls was provided by BCD. The geometry of the section includes the configuration of the DMM zone shown in Figure A-15 of Appendix A.

The section used for the analyses in this study is shown in Figure 8-1, and material property values are listed in Table 8-1. The material property values for the limit equilibrium analyses were provided by BCD in Figure A-15 of Appendix A. Linear interpolation was used to model the horizontal variation in soil strength for Layer 4 between verts 1 and 5. As shown in Figure 8-1, vert 1 is located along the flood side edge of the DMM zone (X = 4) and vert 5 is located near the toe of the existing earthen embankment, 8 ft from the protected edge of the DMM zone (X = 30). Verts 2 through 4 were used in the BCD characterization to assign the DMM zone material properties in Method of Planes (MOP) analyses. These verts were not necessary for assigning DMM zone properties in the FLAC model and are not shown in Figure 8-1. The cohesion assigned to Layer 5 reflects an 11.25 psf/ft increase in cohesion with depth below elevation -15 ft. For the numerical analyses, impounded water is modeled as an applied pressure on the ground surface and I-wall.

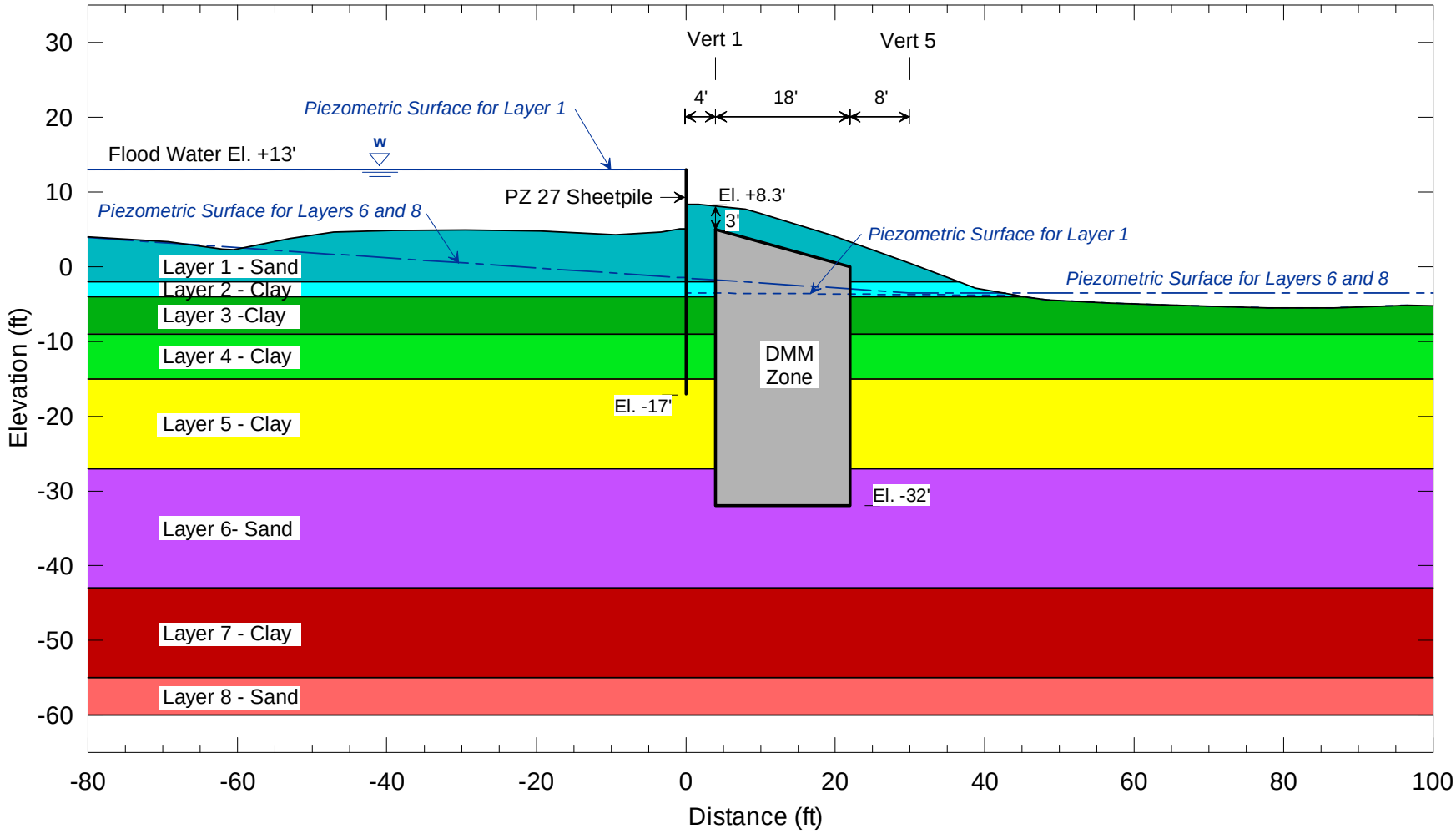

Figure 8-1. Analysis Cross-Section for Stability Analyses of the Reach III B-1A I-wall

Table 8-1. Summary of Material Property Values for Stability Analyses of the Reach III B-1A I-wall

Soil Layer	Description	Elevations (ft)	Unit Weight[1] (pcf)	c[1] (psf)		ϕ[1] (deg)	E[2] (psf)		ν[2]
				Vert 1	Vert 5		Vert 1	Vert 5	
1	Sand	-2 to +8.5	122	0		30	5600000[6]		0.33[10]
2	Clay	-4 to -2	116	250		0	75000[7]		0.45[11]
3	Clay	-9 to -4	116	200		0	60000[7]		0.45[11]
4	Clay	-15 to -9	105	325	275	0	97500[7]	82500[7]	0.45[11]
5	Clay	-27 to -15	105	325 to 460[4]		0	97500 to 138000[7,8]		0.45[11]
6	Sand	-43 to -27	122	0		30	5600000[6]		0.33[10]
7	Clay	-55 to -43	115	900		0	270000[7]		0.45[11]
8	Sand	-60 to -55	122	0		33	5600000[6]		0.32[10]
--	DMM Zone	-32 to +4.9	Same as existing[3]	Varies[5]		0	500c[9]		0.45[9]

Notes:

1) These parameter values were provided by BCD.
2) These parameter values were estimated for use in the numerical analyses.
3) The unit weight was unchanged from that assigned to the existing soil layers.
4) Cohesion for Layer 5 increases with depth below El -15 ft at a rate of 11.25 psf/ft.
5) Corresponds to a weighted average for the column/soil matrix within the DMM zone, see discussion in text. A DMM zone strength of 1300 psf was provided by BCD for use in the base case analyses.
6) Young's modulus for sand layers based on the correlation $E'_s = 700(N_1)_{60}$ tsf (Duncan and Bursey 2007) and a representative SPT $(N_1)_{60}$ value of 4 for loose sand.
7) Young's modulus for clay layers based on a shear modulus/shear strength ratio $E/s_u = 300$ (Duncan and Bursey 2007).
8) Young's Modulus, E, increases with depth below El -15 ft at a rate of 3375 psf/ft.
9) Values from Navin (2005) and Navin and Filz (2005).
10) Poisson's ratio for sand layers estimated based on the effective stress friction angle, $\nu = (1 - \sin \phi')/(2 - \sin \phi')$.
11) Poisson's ratio for clay layers reduced from theoretical upper limit value of 0.5 for undrained behavior to avoid numerical instability in the numerical analyses.

The subsurface profile includes three sand layers whose strength depends on effective, rather than total, normal stresses. The piezometric surfaces used for these layers were provided by BCD and are shown in Figure 8-1. The piezometric surface used for the Layer 1 sand coincides with the flood water elevation of +13.0 ft on the flood side of the I-wall sheetpile and falls below the bottom of Layer 1 on the protected side of the I-wall sheetpile. The piezometric surface used for the sand in Layers 6 and 8 varies linearly from an elevation of + 6.3 ft approximately 116 ft from the flood side of the I-wall sheetpile to an elevation of -3.5 ft approximately 30 ft from the protected side of the I-wall sheetpile. Pore pressures in the other strata were set to zero and shear strengths in these strata were based on a $\phi = 0$ representation to model undrained conditions.

Additional material property values were required for the numerical analyses. Values for Young's Modulus, E, were estimated from published correlations for soil modulus. The undrained moduli for the clay layers were based on soil plasticity and undrained shear strength (Duncan and Bursey 2007). For the sand layers, the drained moduli were based on the relative density of the sand, using a representative standard penetration test $(N_1)_{60}$ value of 4 for loose sand (Duncan and Bursey 2007).

For the FLAC analyses, a Poisson's ratio of 0.45 was assigned to all of the clay layers. The Poisson's ratios listed in Table 8-1 for clays are reduced from the theoretical upper limit value of 0.5 for undrained behavior to avoid numerical instability in the FLAC finite difference model. For the sand layers, the Poisson's ratio was related to the effective stress friction angle, $\nu = (1 - \sin \phi')/(2 - \sin \phi')$

8.2.1. I-wall Properties

The I-wall consists of a concrete flood wall constructed on top of a sheetpile. The configuration of the wall, as shown in Figure A-14 in Appendix A, was provided by BCD. In the FLAC analyses, the concrete flood wall and the sheeetpile are both represented using beam elements with the sheetpile properties extending from the top of the I-wall at elevation +13 ft to the tip elevation of the sheetpile at -17 ft. Based on the analysis section provided by BCD, the stick up of the I-wall sheetpile above existing grade is approximately 4.7 ft. According to Eddie Templeton of BCD, the sheetpile consists of PZ-27 units. The beam elements were assigned a

unit weight of 491 pcf, Young's modulus of 29 x 10^6 psi, moment of inertia of 8.9 x10^{-3} ft^4/ft, and cross-sectional area of 5.5 x10^{-2} ft^2/ft. This characterization was developed based on published values for PZ-27 sheetpiles (Bethlehem Steel 1998).

8.2.2. DMM Zone Properties

The cohesion value for the DMM zone is a weighted average for the column/soil matrix. The composite cohesion used for the DMM zone is a function of area replacement ratio and the strengths of the DMM soil-cement mixture and the untreated native soils between the shear walls. Because peak strengths in the DMM treated ground would be expected to develop at much smaller strains than those corresponding to peak strength in the existing site soils between the shear walls, the strength of the existing site soils is neglected in establishing the composite DMM zone strength.

The base-case shear strength value of 1300 psf for the composite DMM zone, as listed in the notes of Table 8-1, was established by BCD at the start of this case study. This value was selected by BCD to provide an adequate factor of safety for non-vertical shear based on Method of Planes (USACE 2002) limit equilibrium stability analyses. BCD also established that a replacement area ratio of 30%, which is required by the project specifications for Reach III B, should be used in the analyses. Based on a 30% area replacement ratio and a composite DMM zone strength of 1300 psf, the corresponding design strength for the deep-mixed soil-cement ground is (1300 psf)/(.3) = 4333 psf.

A parametric study completed to investigate the effects of the composite DMM zone strength and vertical joint efficiency used cohesion values for the composite DMM zone that ranged from 800 to 5300 psf. After the parametric study had been completed, the simplified design calculations for the Reach III B-1A project were provided. The simplified design calculations established a design shear strength of 6428 psf for the deep-mixed ground. Based on the same 30% area replacement ratio, the composite shear strength of the DMM zone corresponding to a 6428 psf strength of the deep mixed-ground is (0.3)(6428 psf) = 1928 psf. Because this composite DMM zone strength is within the range of strengths used for the parametric study, no additional analyses were completed using the updated design strength, and the comparison of the

numerical stability results with the simplified design procedure was done using factors of safety interpolated from the results of the parametric study.

A stiffness ratio, E/s_u, and a Poisson's ratio were estimated for the DMM columns based on guidelines provided by Navin (2005) and Filz and Navin (2006). The reported range in E/s_u values is 100 to 500 for DMM column installed using the dry method, and 150 to 2000 for DMM columns installed using the wet method. According to the FLAC manual, modulus values typically have an insignificant effect on factor of safety calculations. The numerical analyses were completed using an E/s_u ratio of 500 and a Poisson's ratio of 0.45. These values are listed in Table 8-1.

In the numerical analyses, vertical joints were included in the DMM improved zone to model potential weak joints between columns. The possibility of weak vertical joints at column overlaps is discussed in the Japanese and Scandinavian literature (CDIT 2002, Broms 2003) and is also recognized in U.S. practice (Sehn 2005). DMM shear walls constructed by overlapping columns are weaker along vertical planes at the column overlaps due to the reduced width of the shear wall at these locations. In addition, the strength of the shear wall at the column overlap could be further reduced by misalignment of columns during construction. The influence of strength achieved at the column overlap on stability of the system can be evaluated by varying the joint strength over a range extending from that corresponding to the full design mixture strength applied to the full design column overlap (100% efficiency) and that corresponding to no overlap between the columns (0% efficiency).

A vertical joint strength corresponding to 100% efficiency was determined based on the area replacement ratio and the area overlap ratio specified for the project. For an area replacement ratio of 30% and an area overlap ratio of 20%, the chord length of the column overlap at the joint between columns is 79.5% of the average width of the wall. Therefore, the composite strength on a vertical plane along the joint between adjacent DMM columns is 79.5% of the composite strength on any other plane, when the full design column overlap is achieved. For the base case analyses with a DMM zone strength of 1300 psf, the vertical joint strength for 100% vertical joint efficiency is (0.795)(1300psf) = 1033 psf.

The joint strength corresponding to 0% efficiency was set equal to a representative soil strength of 320 psf in the DMM treated zone, based on a weighted average of soil strengths of the clay layers along the vertical joints. This condition corresponds to no overlap between columns. The vertical joint strength for intermediate efficiencies can be obtained by interpolation between the values for 0% and 100% efficiencies.

8.3. Numerical Analyses

Numerical analyses for the Reach III B-1A I-wall were completed using the two-dimensional finite difference computer code FLAC (ITASCA 2005). This section describes the analysis methods, model validation, and results.

8.3.1. Analysis Methods

The mesh used for the numerical analyses extended approximately 100 ft beyond the I-wall on the flood side, 150 ft beyond the I-wall on the protected side, and to the bottom of the Layer 8 sand at elevation -60 ft. The extent of the model is shown schematically in Figure 8-2. For the analyses, no lateral displacements were allowed on the left- and right-hand sides of the mesh, and no lateral or vertical displacements were allowed on the bottom of the mesh.

Four equally spaced vertical joints were included in the DMM Zone at the locations indicated in Figure 8-2. The joints were modeled by assigning FLAC's "Ubiquitous Joint" model to these columns of elements within the DMM improved zone and assigning a vertical orientation for the reduced strength. On any other plane within the Ubiquitous Joint elements, the full composite DMM zone shear strength applies. The DMM improved material between vertical joints was modeled using the full composite DMM zone strength in all directions. The modulus of the joint material was not reduced for shearing on the vertical plane from the representative characterization for the DMM zone listed in Table 8-1. While the Ubiquitous Joint model does allow for a different strength assignment along a specified plane, it does not allow for the assignment of a different modulus for shearing on that plane. According to the FLAC manual, modulus values typically have an insignificant effect on factor of safety calculations.

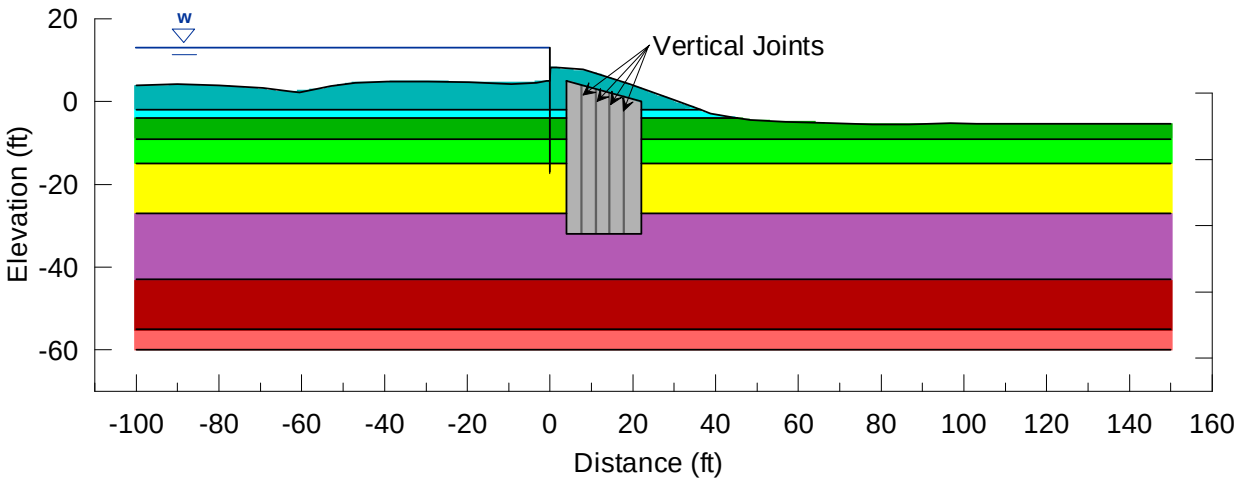

Figure 8-2. Extent of FLAC Model

Two meshes were developed for the Reach III B-1A analyses. The standard mesh has zone widths in the vicinity of the I-wall and DMM zone in the range of 0.5 to 1.5 ft. The discretized standard mesh in the vicinity of the I-wall and DMM zone is shown in Figure 8-3a. A second mesh was developed with finer spacing to verify that the factors of safety computed using the standard mesh were independent of mesh size. The fine mesh has zone widths in the vicinity of the I-wall and DMM zone in the range of 0.5 to 0.9 ft. The discretized fine mesh in the vicinity of the I-wall and DMM zone is shown in Figure 8-3b. Analyses completed for several cases using the fine mesh resulted in factors of safety that were 0.01 to 0.03 lower than those determined using the standard mesh. Because the differences between the standard and fine mesh analyses were relatively small, and because stability analyses completed using the fine mesh took 4 times as long as stability analyses using the standard mesh, the quicker standard mesh was used for the stability analyses presented in this report. The fine mesh was used for the deformation analyses for construction conditions to allow for greater accuracy in the calculated I-wall displacements under construction loading.

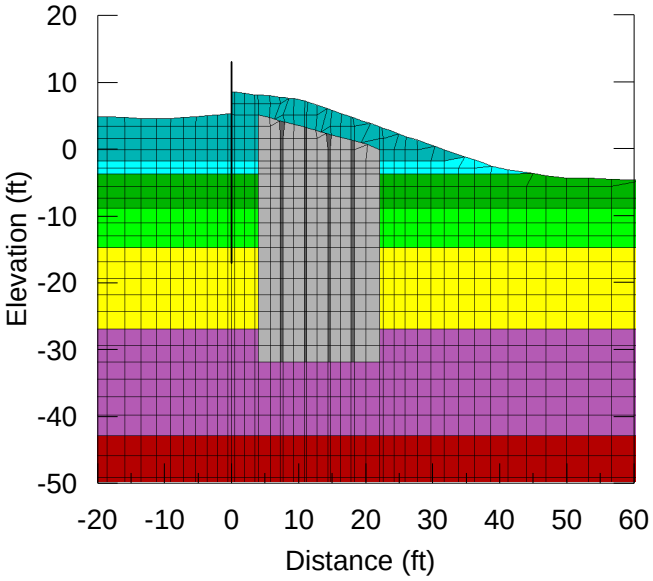

Figure 8-3a. Standard Mesh

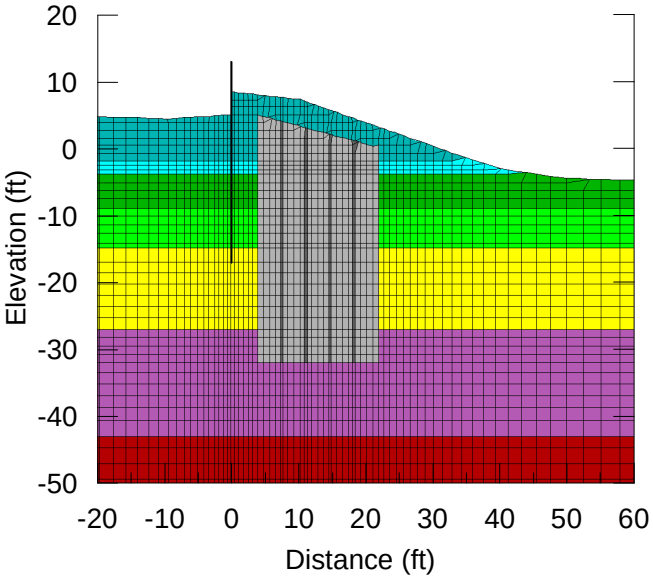

Figure 8-3b. Fine Mesh

Figure 8-3. FLAC Mesh Discretization near I-wall and DMM Zone

FLAC's automatic factor of safety routine was used to calculate the factors of safety for this report. This procedure reduces the shear strength of all of the materials in the model by a uniform reduction factor until the program is not able to satisfy convergence criteria in a limited number of iterations. The factor of safety (FS) is the largest strength reduction factor (SRF) at which convergence is still achieved within the limited number of iterations.

The factor of safety for an infinite slope failure of the protected side slope of the sand embankment is 1.64. To prevent this type of slope failure from occurring in the FLAC analyses, a shear strength of 50 psf was applied to the elements along the embankment slope to permit investigation of deeper failure surfaces.

The tensile strength of the soil and DMM zone were set to zero for all of the numerical analyses to allow for the formation of tension cracks.

8.3.2. Stability Analyses for DMM Zone Strength of 1300 psf

Stability analyses were completed using the composite DMM zone strength of 1300 psf initially provided by BCD for the base case. As discussed previously, this shear strength was selected to provide an adequate factor of safety for non-vertical shear (FS = 1.4) based on BCD's Method of Planes limit equilibrium stability analyses. For 100% efficiency of vertical joints, the computed factor of safety from the numerical analyses was 1.38. The shear strain contours corresponding to failure are shown in Figure 8-4a. The contours indicate a complex failure mode, with shearing along the flood side of the I-wall sheetpile, rotation of the DMM zone, shear failure through the DMM zone at approximate elevation -23 ft, and multiple zones of shearing on the protected side of the DMM zone.

For 0% efficiency of vertical joints, i.e., only the native soil strength due to no overlap between columns, the computed factor of safety from the numerical analyses was 1.15. The shear strain contours corresponding to failure are shown in Figure 8-4b. The contours show movement along the joints, indicating that an internal racking failure between DMM columns occurs in the shear walls. The failure mode for 0% efficiency of the joints also includes shearing along the flood side of the I-wall sheetpile and multiple zones of shearing on the protected side of the DMM zone.

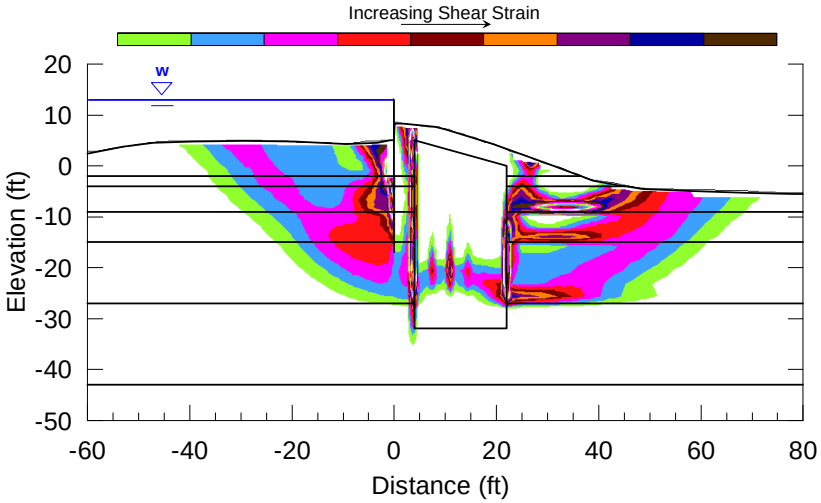

Figure 8-4a. Shear Strain Contours at Failure for 100% Efficiency of Vertical Joints, FS = 1.38

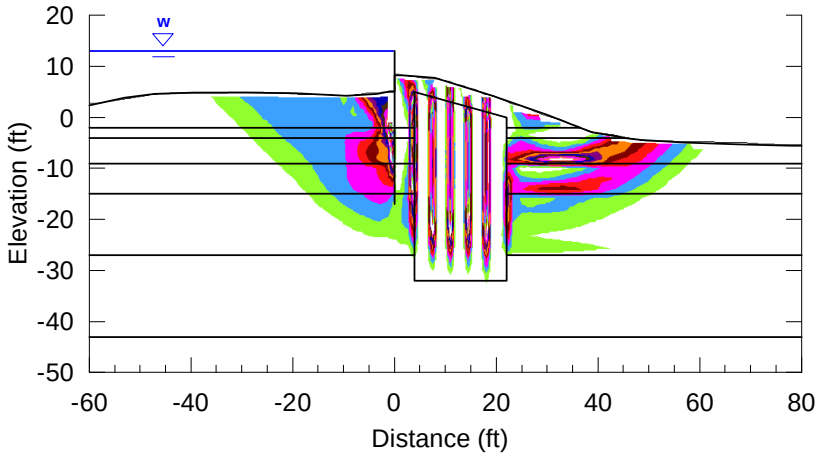

Figure 8-4b. Shear Strain Contours at Failure for 0% Efficiency of Vertical Joints, FS = 1.15

Figure 8-4. Comparison of Results for 0% and 100% Efficiency of Vertical Joints

DMM Zone Strength = 1300 psf

Stability analyses were completed for vertical joint strengths corresponding to different efficiencies ranging from 0 to 100%. The results are summarized in Figure 8-5, and they show a decrease in the value of factor of safety as the efficiency of the vertical joints decreases. This occurs because racking failure of the joints becomes more likely as the vertical joint efficiency decreases. The racking failure mechanism ceases to control performance at vertical joint efficiencies greater than or equal to about 70%, which corresponds to a vertical joint strength of about 820 psf. The factor of safety for a vertical joint efficiency of 50% is 1.33.

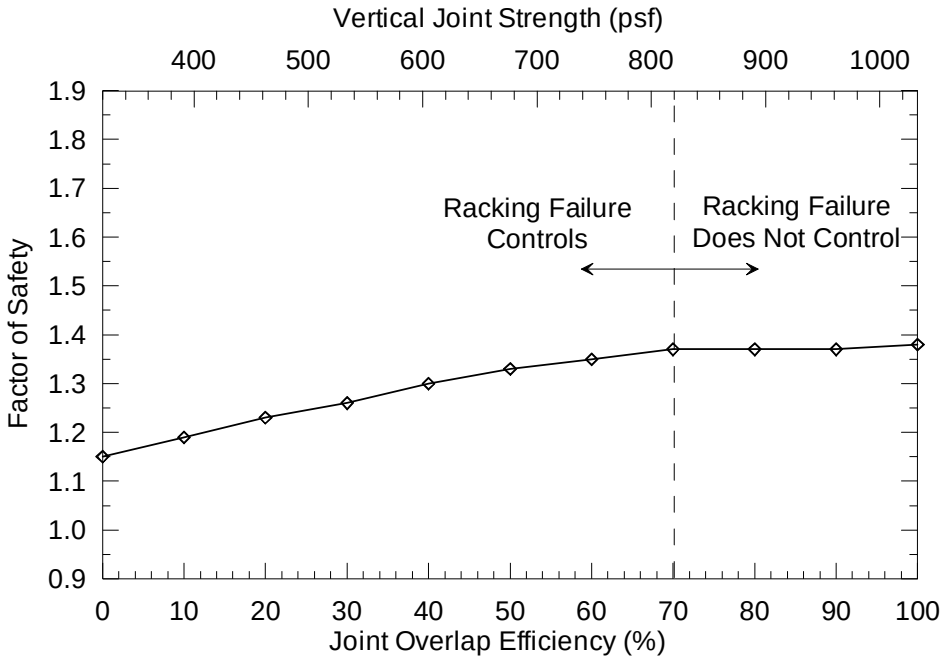

Figure 8-5. Factor of Safety Versus the Efficiency of Vertical Joints

DMM Zone Strength = 1300 psf

8.3.3. Parametric Study for DMM Zone Strength and Vertical Joint Efficiency

A parametric study was completed to investigate the effects of DMM zone strength and vertical joint efficiency on the stability of the Reach III B–1A I-wall. The stability analyses were performed using the analysis section shown in Figure 8-1 and the material properties in Table 8-1. For this study, analyses were completed for DMM zone strengths of 800, 1300, 1800, 2300, 2800, 3300, 3800, 4300, and 5300 psf. For each DMM zone strength, analyses were completed for vertical joint strengths corresponding to joint efficiencies of 0% to 100% to investigate the effect of both variables on the system response. Some of the DMM Zone strength values used in the parametric study are in excess of the values typically used by USACE for levee design in Louisiana. This range was selected to allow for a comprehensive understanding of the system behavior for the Reach III B-1A analysis section.

The results of the analyses are presented in Figure 8-6. The factors of safety are shown as a function of vertical joint strength in Figure 8-6a, and as a function of DMM zone strength in

Figure 8-6b. Also included in Figure 8-6a are the factors of safety for analyses completed without vertical joints. These analyses provide an upper bound factor of safety for each DMM zone strength.

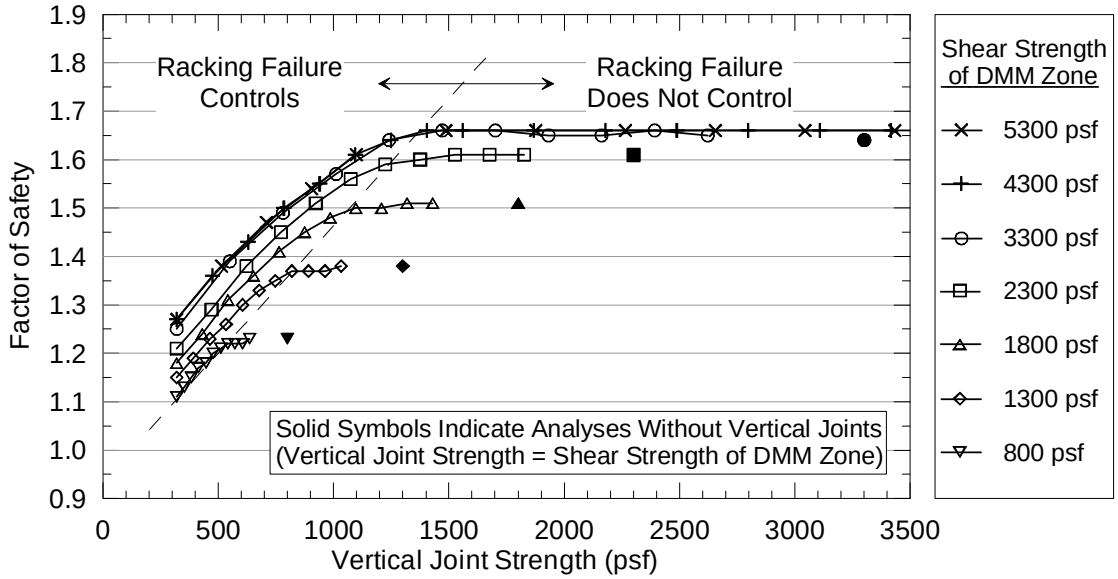

Figure 8-6a. Factor of Safety Versus Vertical Joint Strength

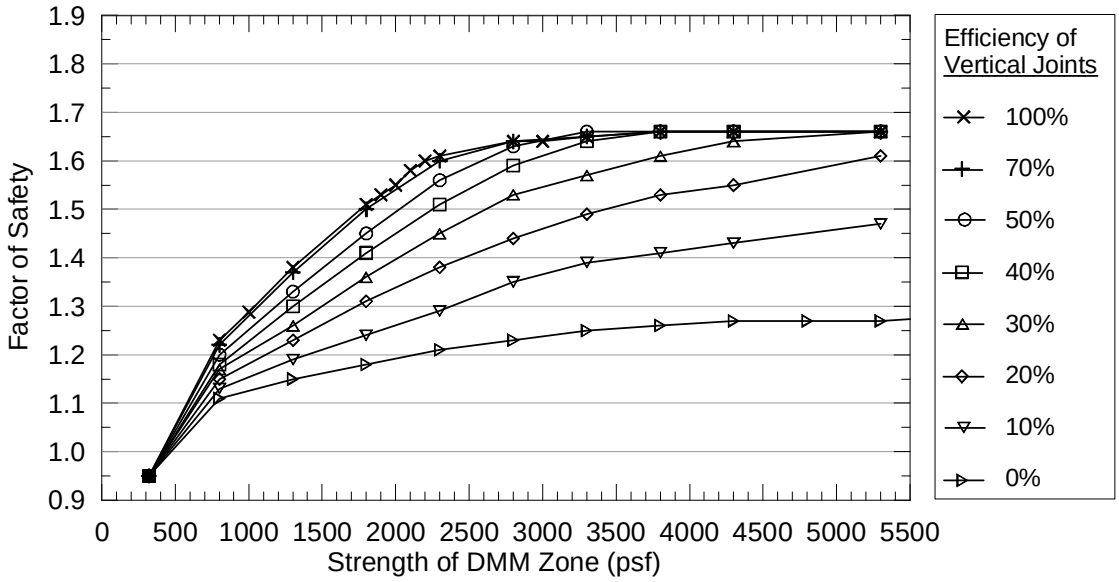

Figure 8-6b. Factor of Safety Versus Shear Strength of DMM Zone

Figure 8-6. Factors of Safety for the Reach III B-1A Parametric Study

The results presented in Figure 8-6a indicate that system response depends on both the DMM zone strength and the vertical joint strength. The curves for DMM zone strengths of 4300 and 5300 psf shown in Figure 8-6a nearly coincide, indicating that the factor of safety is uniquely a function of vertical joint strength for high DMM zone strengths. For DMM zone strengths less than 4300 psf, the factor of safety decreases with decreasing DMM zone strength, even at the same vertical joint strength, which indicates that an internal failure other than shearing along vertical joints is occurring in the DMM zone for low DMM zone strengths. The vertical joint strength at which the racking failure mechanism ceases to control is also a function of DMM zone strength, as illustrated in Figure 8-6a.

The results presented in Figure 8-6b show how the system response varies with vertical joint efficiency. The curves for vertical joint efficiencies of 70% and 100% shown in Figure 8-6b nearly coincide, indicating that a racking failure does not control the system performance for joint efficiencies greater than 70%. In this figure, racking failure controls for combinations of DMM zone strength and efficiency that fall below the curves for 70% and 100% joint efficiency.

For conditions where the racking failure mode does not control, the decrease in factor of safety with decreasing DMM zone strength can be explained by three distinct DMM zone failure modes that occur at higher joint efficiencies. These failure modes are illustrated by the shear strain contours at failure for DMM zone strengths 1300, 2300, and 4300 psf with 100% efficiency of vertical joints, as shown in Figure 8-7. The shear strain contours for all three cases indicate complex failure modes with common elements, including shearing along the flood side of the I-wall sheetpile, rotation of the DMM zone, and multiple zones of shearing on the protected side of the DMM. The contours for a DMM zone strength of 1300 psf, originally presented in Figure 8-4a and repeated for comparison in Figure 8-7a, indicate a near-horizontal shear failure across the DMM zone above the top of the Layer 6 sand. The contours for a DMM zone strength of 2300 psf, shown in Figure 8-7b, indicate shearing in the Layer 6 sand below the DMM zone as well as a small zone of shearing in the DMM zone at the toe, which is indicative of a crushing failure at the toe of the DMM zone. The failure modes shown in 8-7a and 8-7b involve internal failure of the DMM zone other than shearing on non-vertical planes, which accounts for the decrease in factor of safety with decreasing DMM zone strength shown in Figure 8-6b for DMM zone

strengths less than 4300 psf and vertical joint efficiencies high enough to prevent racking (70% or greater). The contours for a DMM zone strength of 4300 psf, shown in Figure 8-7c, indicate shearing in the Layer 6 sand below the DMM zone with no internal shear in the DMM zone. This failure mode corresponds to the case where the DMM zone strength is high enough to prevent shear failure on non-vertical planes and the DMM zone rotates as a rigid block. Because there is no internal failure of the DMM zone, the factor of safety shown in Figure 8-6b is independent of DMM zone strength for DMM zone strengths equal to or greater than 4300 psf when the vertical joint strength is high enough to prevent racking (approximately 1200 psf or greater, in this case).

For conditions where the racking failure mode does control, the decrease in factor of safety with decreasing DMM zone strength can be explained by two distinct racking failure modes that occur at lower joint efficiencies. These failure modes are illustrated by the shear strain contours and the deformed shape of the FLAC mesh at failure for DMM zone strengths 1300, 2300, and 4300 psf with 0% efficiency of vertical joints. The shear strain contours are shown in Figure 8-8 and the deformed mesh in the vicinity of the DMM zone and the Layer 6 sand are shown in Figure 8-9. The shear strain contours for all three DMM zone strengths show movement along the joints, indicating that an internal racking failure between the DMM columns occurs in the shear walls. The contours for DMM zone strengths of 1300 and 2300 psf, shown in Figures 8-8a and 8-8b, also indicate some non-vertical shearing in the DMM zone just above the Layer 6 sand at El -27 ft. The contours for a DMM zone strength of 4300, shown in Figure 8-8c, show only vertical shearing within the DMM zone, and they indicate shearing in the Layer 6 sand below the DMM zone. Additionally, the shear strain contours shown in Figures 8-8a and 8-8b indicate that shearing along the vertical joints does not extend all the way through the bottom of the DMM zone and into the Layer 6 sand. The shear strain contours shown in Figure 8-8c indicate shearing along the joints extends to the bottom of the DMM zone and into the Layer 6 sand.

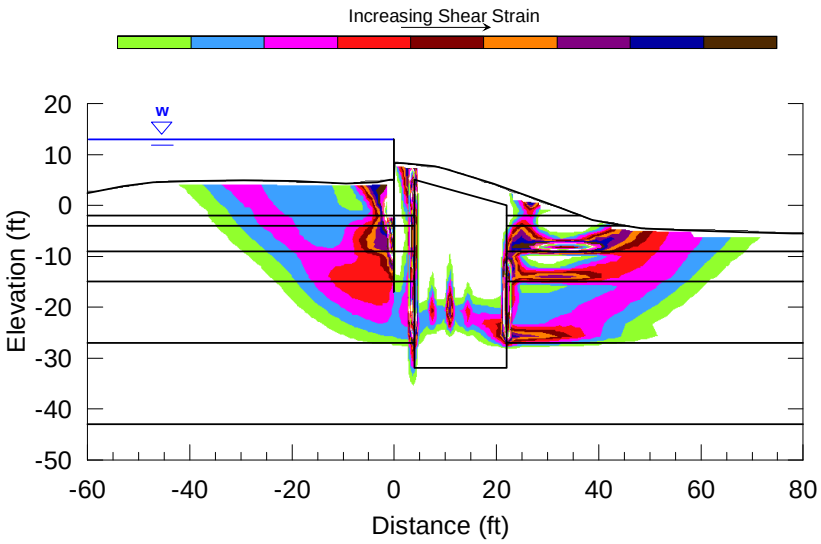

Figure 8-7a. Shear Strain Contours at Failure for DMM Zone Strength = 1300 psf, FS = 1.38

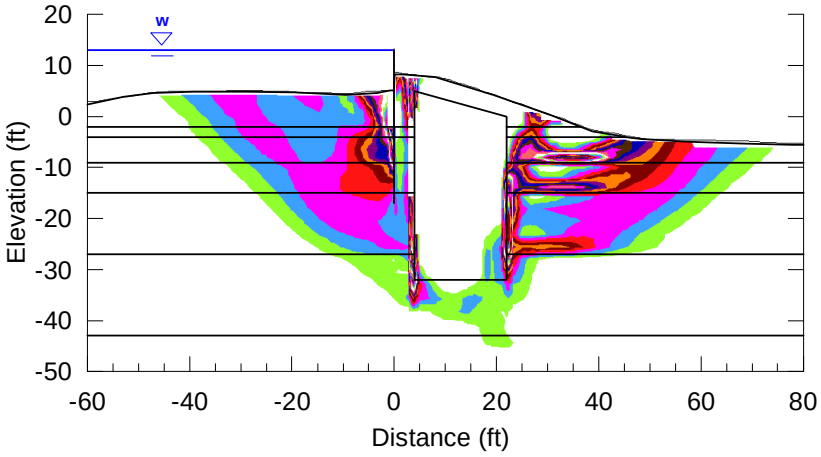

Figure 8-7b. Shear Strain Contours at Failure for DMM Zone Strength = 2300 psf, FS = 1.61

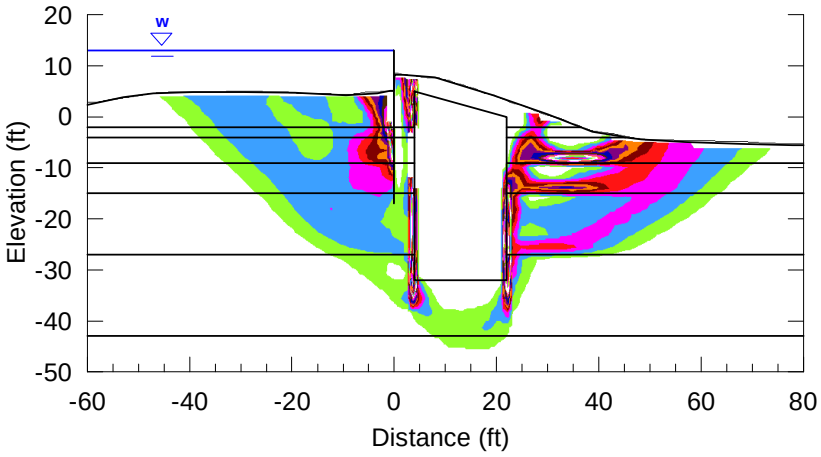

Figure 8-7c. Shear Strain Contours at Failure for DMM Zone Strength = 4300 psf, FS = 1.66

Figure 8-7. Comparison of Results for 100% Efficiency of Vertical Joints

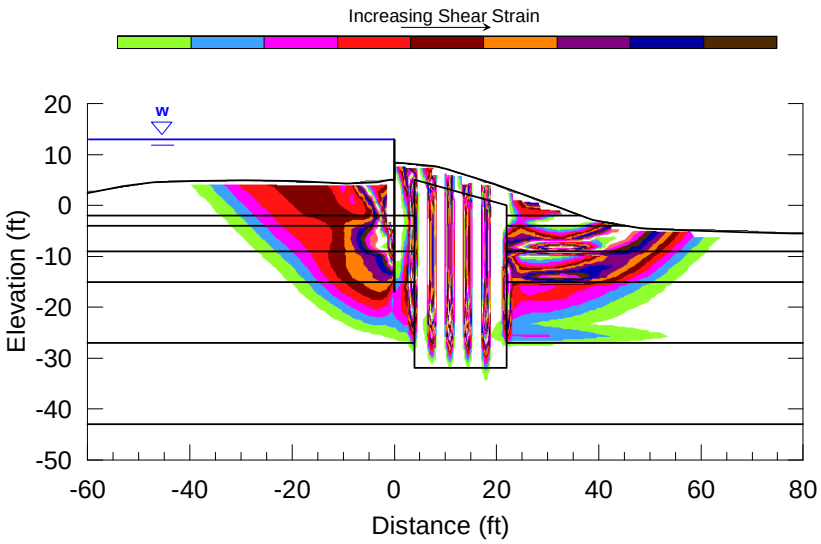

Figure 8-8a. Shear Strain Contours at Failure for DMM Zone Strength = 1300 psf, FS = 1.15

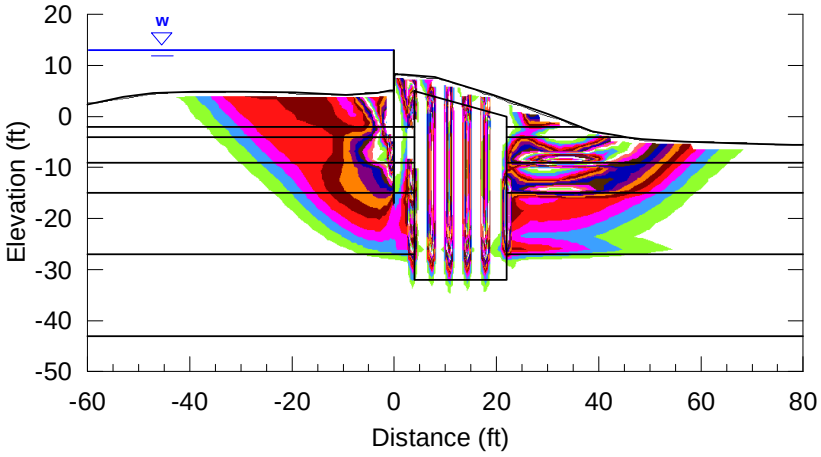

Figure 8-8b. Shear Strain Contours at Failure for DMM Zone Strength = 2300 psf, FS = 1.21

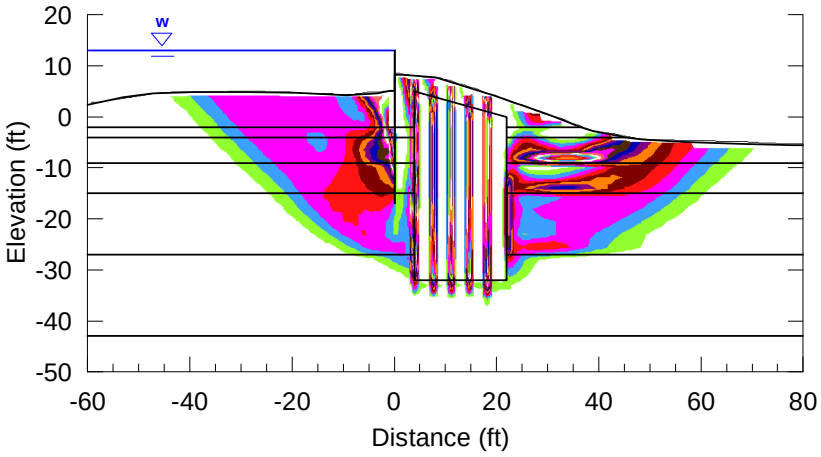

Figure 8-8c. Shear Strain Contours at Failure for DMM Zone Strength = 4300 psf, FS = 1.27

Figure 8-8. Comparison of Results for 0% Efficiency of Vertical Joints

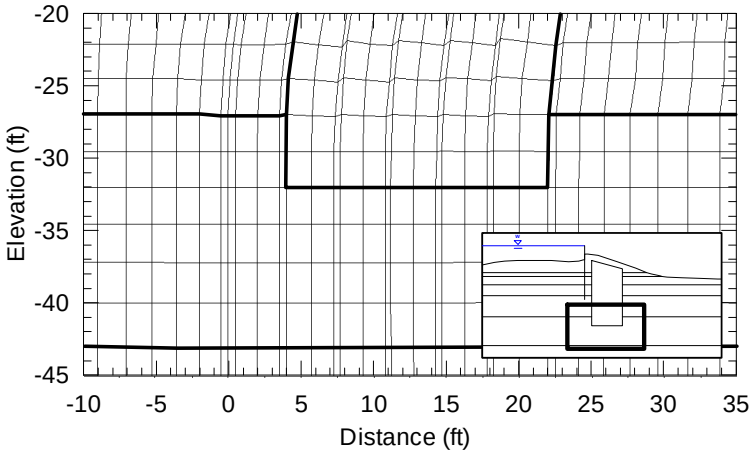

Figure 8-9a. Deformed Mesh for DMM Zone Strength = 1300 psf

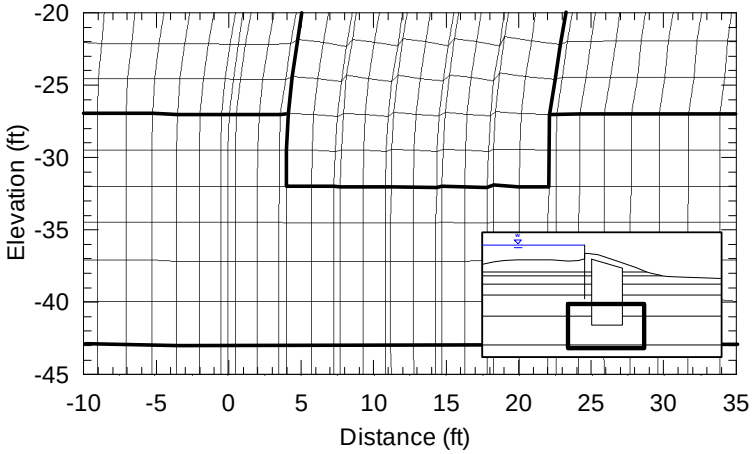

Figure 8-9b. Deformed Mesh for DMM Zone Strength = 2300 psf

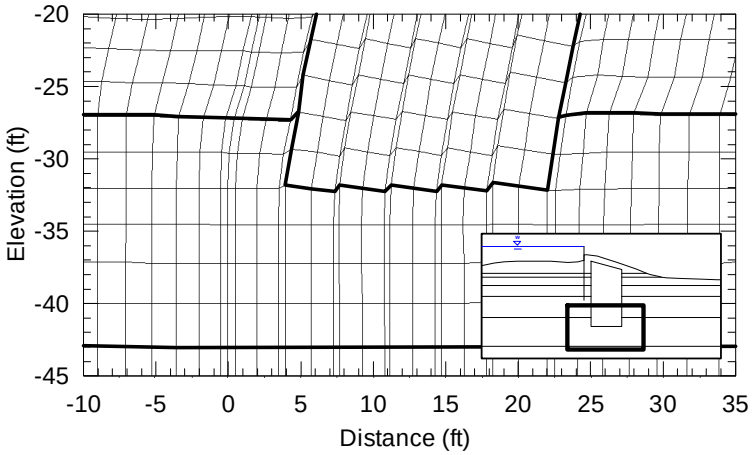

Figure 8-9c. Deformed Mesh for DMM Zone Strength = 4300 psf

Figure 8-9. Comparison of Deformations in the DMM Zone for 0% Efficiency of Vertical Joints Displacements Magnified 2x

The importance of the subtle differences in the shear strain contours at and below elevation -27 ft in Figure 8-8 is also illustrated by the deformed meshes at failure in Figure 8-9 for each of the DMM zone strengths. The deformed meshes for DMM zone strengths of 1300 and 2300 psf, shown in Figures 8-9a and 8-9b, indicate minimal deformations in the portion of the DMM zone that is socketed into the Layer 6 sand, with the deformed shape of the DMM zone indicating a bending-type failure at the elevation of the top of the sand layer. Because the deformations of the vertical joints are not consistent with a racking failure along the full depth of the joints, this is considered a partial-depth racking failure. The deformed mesh for a DMM zone strength of 4300 psf, shown in Figure 8-9c, indicates deformations of the vertical joints that are consistent with a racking failure in the portion of the DMM zone that is socketed into the Layer 6 sand, as well as deformations in the Layer 6 sand below and beside the DMM zone. Because the deformations of the vertical joints are consistent with a racking failure along the full depth of the joints, this is considered a full-depth racking failure.

The conditions that control the failure modes for different combinations of DMM zone strength and vertical joint strength are shown by the failure envelopes and shaded regions shown in Figure 8-10. The failure envelopes and regions are shown as functions of vertical joint strength in Figure 8-10a, and as functions of DMM zone strength in 8-8-10b. The linear failure envelope for full-depth racking failure shown in Figure 8-10a indicates that the factor of safety for the full-depth racking failure mode is a unique function of the vertical joint strength for the conditions at Reach III B-1A. Similarly, the linear failure envelopes for near-horizontal shear failure and crushing failure shown in Figure 8-10b, indicate that, for each of these modes, the factor of safety depends only on the DMM zone strength. The rotation failure envelope is linear and horizontal on both figures, indicating that the factor of safety for this mode is independent of vertical joint strength and DMM zone strength. The conditions corresponding to partial-depth racking failure are shown by shaded regions on both figures, indicating that the factor of safety for this mode is a function of both vertical joint strength and DMM zone strength.

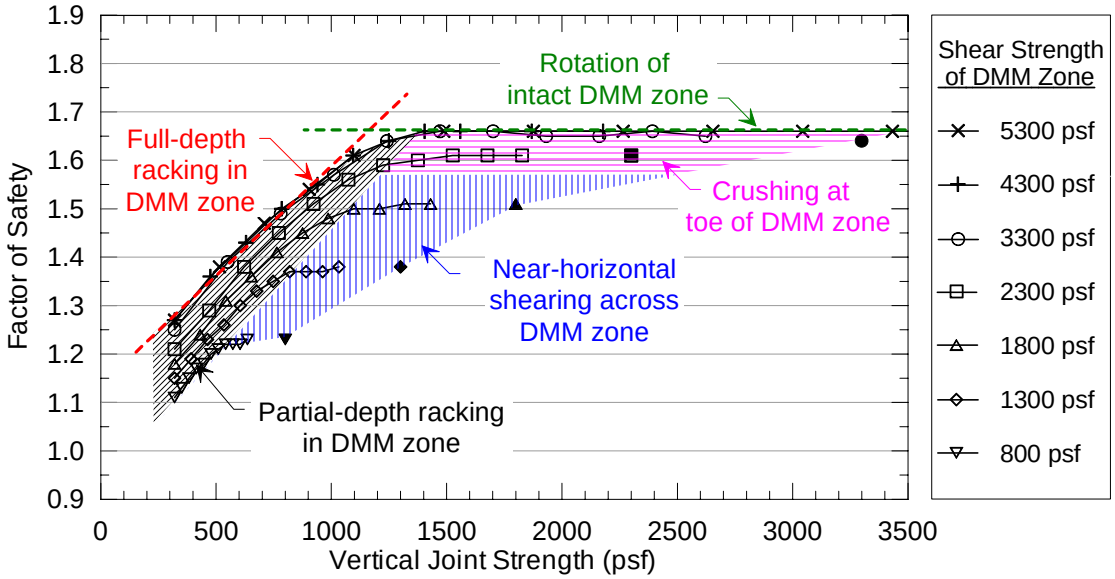

Figure 8-10a. Factor of Safety Versus Vertical Joint Strength

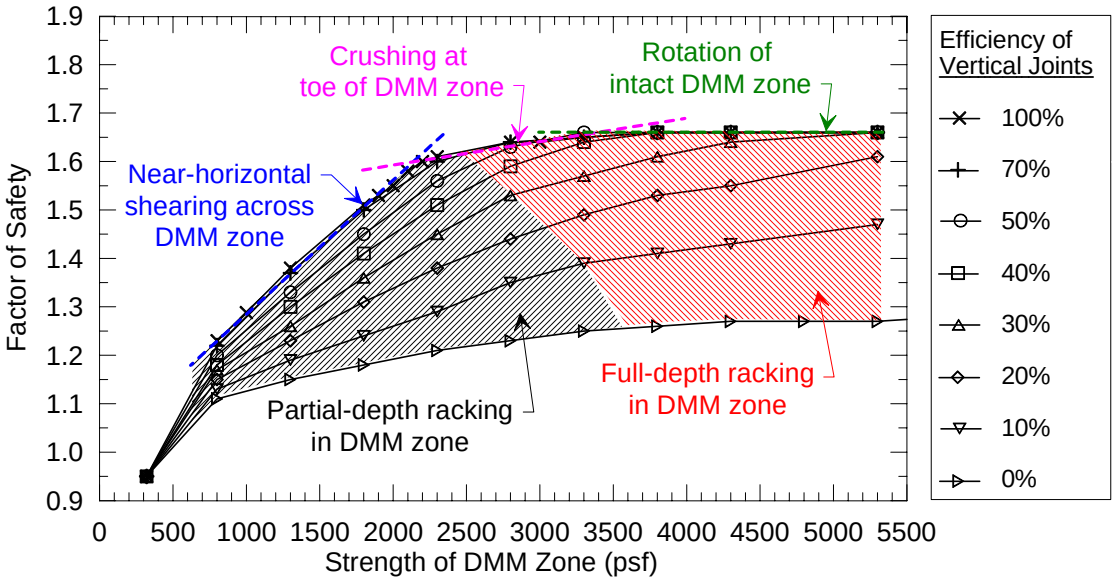

Figure 8-10b. Factor of Safety Versus Shear Strength of DMM Zone

Figure 8-10. DMM Zone Failure Modes for the Reach III B-1A Parametric Study

The failure modes shown in Figures 8-7 through 8-9 for the Reach III B-1A analysis section are complex, including the DMM zone failure modes of rotation, near-horizontal shearing, racking, or crushing, as well as shearing along the flood side of the sheetpile and multiple zones of shearing on the protected side of the DMM zone. At higher DMM zone strengths, rotation and full-depth racking DMM zone failure modes control. At lower DMM zone strengths, the system performance is controlled by failure modes that include shearing through the DMM zone on non-

vertical planes, such as near-horizontal shearing failure, crushing, and partial-depth racking. If the DMM shear walls were not socketed into the relatively strong Layer 6 sand, rotation and full-depth racking failure modes would likely control for all DMM zone strengths, similar to the results from the P24 levee and Gainard Woods Pump Station T-wall numerical analyses (as discussed in Chapters 4 and 6).

8.3.4. Evaluation of Potential for Gap Formation Behind I-wall Sheetpile

Some I-wall structures have been shown to develop gaps behind the sheetpile as the unbalanced lateral load of the floodwater causes the sheetpile to deflect. The potential for gap formation at the Reach III B-1A I-wall is reduced by the presence of the Layer 1 sand, which increases the vertical overburden stresses in the underling soft clay. Based on a simple Rankine evaluation of the stresses in the Layer 2 clay on the flood side of the sheetpile, the potential exists for a water-filled gap to extend from the top of the Layer 2 clay at elevation -2 to approximately elevation -3.6 ft, for a total vertical gap depth of only 1.6 ft. Because a water-filled gap along the flood side of the sheetpile in the Layer 2 clay would be entirely contained within the failure mass for any of the potential failure modes disclosed by these analyses, the net lateral destabilizing effect of hydrostatic water pressures in the open gap would be zero. In addition, tension cracks did not develop on the flood side of the I-wall sheetpile for any of the numerical analyses, which did allow for tensile failure of the soil elements. For these reasons, additional analyses were not performed to investigate the effect of a water filled gap on the back of the Reach III B-1A I-wall.

8.3.5. Deformation Analyses of I-wall for Construction Loading

Deformation analyses were completed using FLAC to evaluate potential displacements of the I-wall during construction of the DMM shear walls. Construction access limitations required a large crane to install the soil-cement columns while sitting on the flood side of the existing I-wall. In addition, disturbance of the native soils during mixing of the soil-cement columns might produce a soil-cement mixture with a lower strength than the native soil until the cement cures and gains strength. Limit-equilibrium stability analyses were completed by BCD to determine the factor of safety during construction conditions for a preliminary, 14 ft wide, DMM zone configuration. Based on these analyses, BCD recommended that not more than 10% of the soil within the DMM zone be mixed within a 12-hour period. BCD's two-dimensional stability

analyses for this case were modeled using a 250 psf surcharge load to represent the crane, extending over a 24-ft wide strip immediately adjacent to the flood side of the I-wall. The shear strength of the native soils within the extent of the DMM zone geometry was reduced by 10% to model the temporary weakening of the soil during mixing.

The cross-section geometry used for the FLAC deformation analyses of construction loading was consistent with the analysis section shown in Figure 8-2, except that the water level and the piezometric surface for the Layer 1 sand on the flood side of the I-wall were lowered from +13 ft to +3.5 ft, and the crane load was added on the flood side of the I-wall, as shown in Figure 8-11. The construction-case piezometric surface for Layers 6 and 8 is the same as shown in Figure 8-2. The material properties for the analyses were consistent with the characterization in Table 8-1, except that the strength and moduli of the soil elements within the extent of the DMM zone were assigned soil strength and moduli values that were reduced by 10% from the material properties listed in Table 8-1 for the native soils. The fine mesh shown in Figure 8-3b was used for the construction loading analyses to allow for greater accuracy in the calculated I-wall displacements.

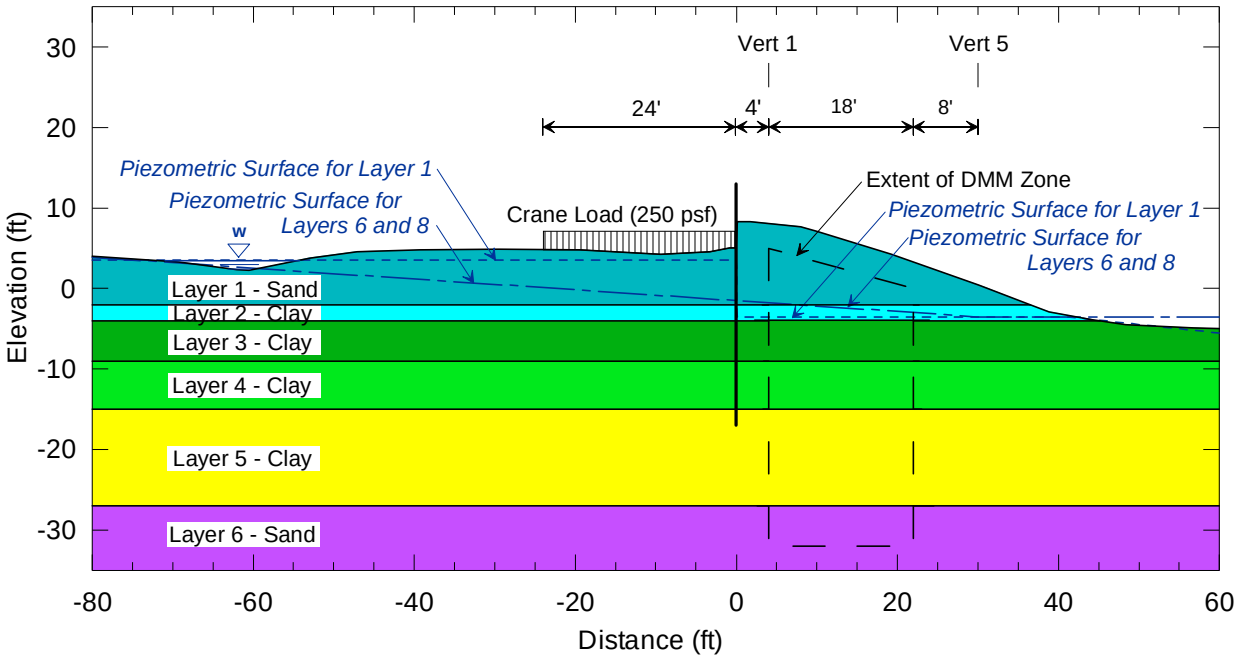

Figure 8-11. Modifications to the Analyses Section for Construction Loading

To delineate the effects of the crane loading and the potential weakening of the soil during soil cement mixing, three deformation analyses were completed for construction loading: 1) no strength reduction in the DMM zone with the crane loading applied; 2) 10% strength reduction in the DMM zone with the crane loading applied; and 3) 10% strength reduction without the crane loading applied. For all of the cases, the calculated lateral displacements of the top of the I-wall are less than 0.1 in., and vertical settlements are less than 0.25 in., as indicated in Table 8-2.

Table 8-2. Displacements at Top of I-wall for Construction Conditions

Analysis Case	Displacement of Top of I-wall (in.)	
	Horizontal[(1)]	Vertical[(2)]
No Strength Reduction in DMM Zone, with Crane Loading	-0.02	-0.14
10% Strength Reduction in DMM Zone, with Crane Loading	0.05	-0.21
10% Strength Reduction in DMM Zone, without Crane Loading	0.02	-0.03

Notes:
1) Negative horizontal displacements indicate movement towards the flood side of the I-wall and positive horizontal displacements indicate movement towards the protected side of the I-wall.
2) Negative vertical displacements indicate settlement of the top of the wall.

Factor of safety analyses were also completed for each of the cases listed in Table 8-2, as well as for the case with no strength reduction in the DMM zone and no crane loading, which corresponds to the conditions before construction of the DMM shear walls. The results for the cases with crane loading are shown in Figure 8-12. The factor of safety for the case with no strength reduction in the DMM zone is 1.09 and the factor safety for the case with a 10% reduction in shear strength in the DMM zone is 1.04. For both cases, the shear strain contours for the critical surface indicate a rotational failure through embankment fill and into the underlying foundation on the protected side of the I-wall sheetpile. The stability analyses for the cases without the crane loading resulted in nearly identical shear strain contours at failure, with a factor of safety for no strength reduction in the DMM zone of 1.09 and a factor of safety for a 10% reduction in shear strength of 1.04. Based on these results, the presence of the 250 psf

crane load does not significantly affect the factor of safety for the critical failure mode during construction loading.

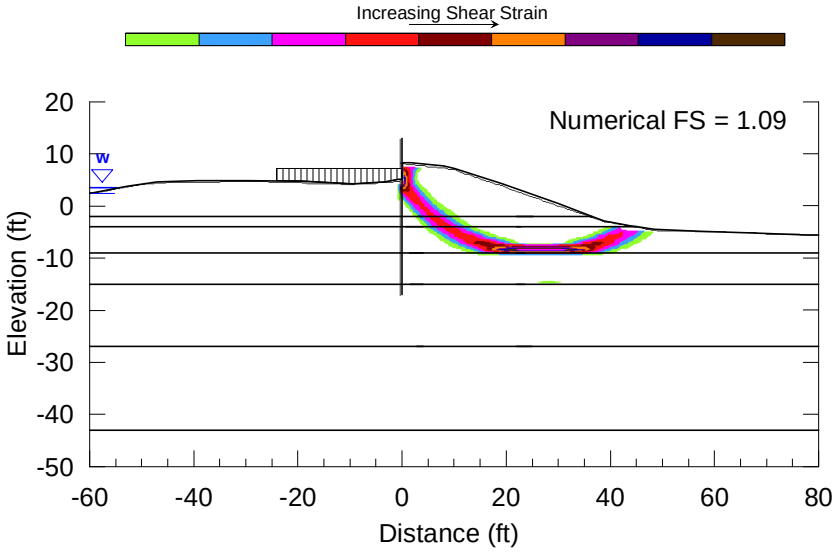

Figure 8-12a. Shear Strain Contours at Failure for No Strength Reduction in DMM Zone

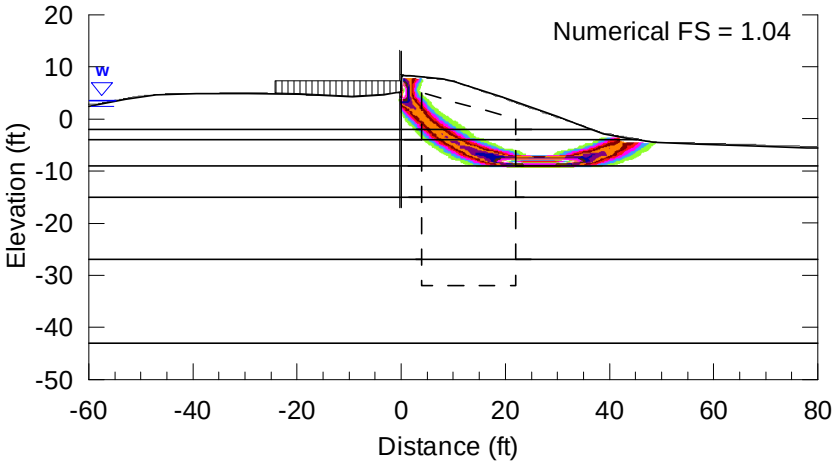

Figure 8-12b. Shear Strain Contours at Failure for 10% Strength Reduction in DMM Zone

Figure 8-12. Results for Numerical Stability Analyses for Construction Conditions with Crane Loading

Limit equilibrium stability analyses were completed for the construction cases using UTEXAS3 (Wright 1991). The analyses were completed using Spencer's procedure and searches were performed for circular surfaces. The critical surfaces from the limit equilibrium analyses with crane loading are superimposed on the shear strain contours at failure from the numerical

analyses in Figure 8-13. For the limit equilibrium stability analyses, the factor of safety for the case with no strength reduction in the DMM zone was 1.06 and the factor of safety for the case with 10% reduction in shear strength was 1.01. The critical failure surfaces and the factors of safety from the limit equilibrium analyses and numerical analyses are in relatively good agreement. The critical failure surfaces and the factors of safety for the limit equilibrium analyses without crane loading were identical to those determined for the cases with crane loading.

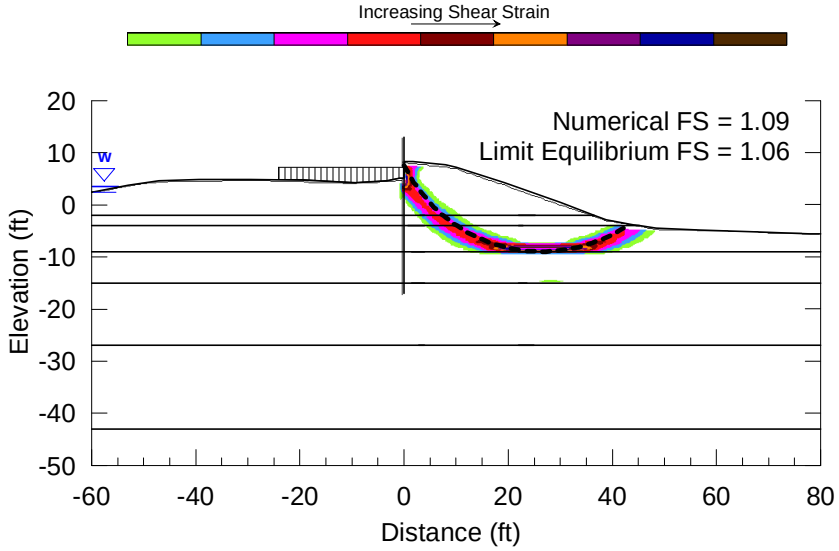

Figure 8-13a. Shear Strain Contours at Failure for No Strength Reduction in DMM Zone

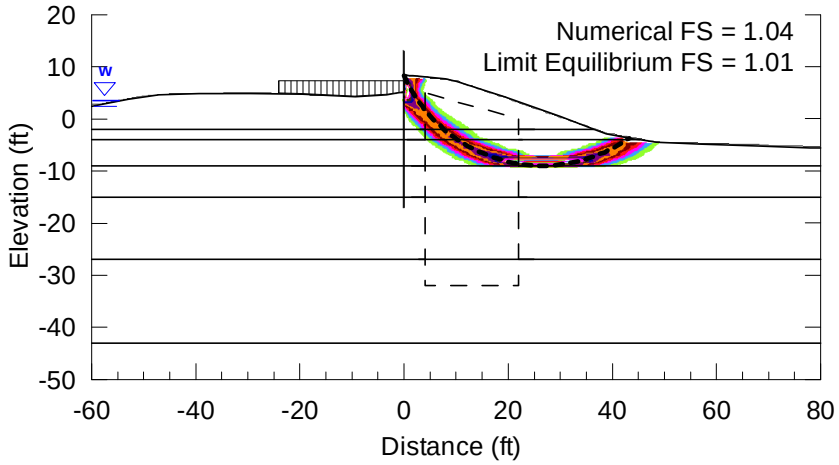

Figure 8-13b. Shear Strain Contours at Failure for 10% Strength Reduction in DMM Zone

Figure 8-13. Comparison of Results from Limit Equilibrium and Numerical Stability Analyses for Construction Conditions with Crane Loading

The factors of safety calculated for all of the analyses of the construction condition load case are between 1.0 and 1.1, indicating the need for care during construction and that a restriction on the extent of mixing, as proposed by BCD, was appropriate. For limit equilibrium and numerical stability analyses, the reduction in factor of safety due to a 10% reduction in shear strengths in the DMM zone is about 5%. There is no reduction in the calculated factor of safety for the critical surface associated with the 250 psf crane loading, although the addition of the crane load may reduce the factor of safety for other failure surfaces. Provided that the actual factor of safety during construction was not lower than the calculated value, the results of these deformation analyses indicate that the displacements of the top of the I-wall would not exceed about ¼ in.

8.3.6. Comparison of Numerical Results with Simplified Analyses

The results of the numerical analyses were compared with those developed using the simplified design procedure discussed in the "Design Guide for Levee and Floodwall Stability Using Deep-Mixed Shear Walls" (Filz and Templeton 2009). The factors of safety determined for the various failure modes using both procedures are summarized in Table 8-3, along with the design criteria from the design guide.

As discussed previously, the factors of safety listed for the numerical analyses in Table 8-3 for non-vertical shearing and for crushing were interpolated for the DMM zone strength of 1928 psf that was established during the design calculations provided by BCD. The factor of safety for vertical shearing was interpolated for a vertical joint strength of 1526 psf, which is based on the DMM zone strength of 1928 psf and an area overlap ratio of 20%. The factors of safety calculated for global stability, sliding, overturning and extrusion are independent of the DMM zone strength.

Table 8-3. Comparison of Factors of Safety from the Numerical Analyses and the Simplified Procedure from the Design Guide

Mode of Failure	Factor of Safety		
	Numerical Analyses	Simplified Procedure	Design Criteria
Global Stability, F_g			
Limit Equilibrium using Spencer's Method / Numerical Analyses	> 1.66 (1)	> 1.5	1.4
Limit Equilibrium using Method of Planes		> 1.5	1.3
Non-Vertical Shearing, F_n			
Limit Equilibrium using Spencer's Method / Numerical Analyses	1.53(2)	> 1.4 (9)	1.4
Limit Equilibrium using Method of Planes		> 1.3 (9)	1.3
Sliding, F_s	> 1.66 (1)	1.61	1.3
Overturning (Rotational Failure), F_o	1.66 (3)	1.45	1.4
Vertical Shearing , F_v			
Full-Depth Racking Failure			
100% Efficiency of Vertical Joints	> 1.66 (4)	1.6	1.4
Partial-Depth Racking Failure			
50% Efficiency of Vertical Joints	1.48 (5)	Not calculated (10)	1.4
0% Efficiency of Vertical Joints	1.19 (6)	Not calculated (10)	1.4
Extrusion, F_e	n/a (7)	> 2.0	1.4
Crushing, F_c	> 1.53 (8)	Not calculated (11)	1.4

Notes:

1) Based on the highest factor of safety obtained from numerical analyses for all modes of failure. Because this failure mode was not encountered in the numerical analyses, the factor of safety for this mode would be greater than or equal to 1.66.
2) Based on Figure 8-10b for a DMM zone strength of 1928 psf and joint efficiency of 100%.
3) Based on rotation of intact DMM zone failure envelopes in Figures 8-10a and 8-10b.
4) Based on the highest factor of safety reported for the full-depth racking failure mode in Figure 8-10a. Because the 1526 psf vertical joint strength is greater than the range of strengths for which this mode was observed, the factor of safety would be greater than or equal to 1.66.
5) Based on Figure 8-10b for a DMM zone strength of 1928 psf and joint efficiency of 50%.
6) Based on Figure 8-10b for a DMM zone strength of 1928 psf and joint efficiency of 0%.
7) The extrusion failure mode is not captured by the two dimensional FLAC model.
8) Based on the factor of safety for the critical, near-horizontal shearing failure mode from Figure 8-10b for a DMM zone strength of 1928 psf. The factor of safety for crushing would be greater than or equal to 1.53.
9) Limit equilibrium analyses completed using DMM zone strengths of 1100 psf and 1300 psf, see discussion in text.
10) The partial depth racking failure mode is not included in the simplified design procedure.
11) The design example in Appendix B of the design guide (Filz and Templeton 2009) does not include a calculation for the factor of safety against crushing.

The factors of safety listed for the simplified procedure in Table 8-3 are taken directly from the example design calculations for the Reach III B-1A I-wall, as presented in Appendix B of the design guide (Filz and Templeton 2009). Based on the calculations for the non-vertical shearing failure mode, a minimum DMM zone strength of 1100 psf was needed to achieve the design factor of safety of 1.4 using Spencer's method and a minimum DMM zone strength of 1300 psf was needed to achieve the design factor of safety of 1.3 using Method of Planes. Because the factors of safety using the design DMM zone strength of 1928 psf would be greater than those completed using DMM zone strengths of 1100 psf and 1300 psf, the example design calculations do not include limit equilibrium analyses results for a DMM zone strength of 1928 psf.

The factors of safety listed in Table 8-3 for the simplified design procedure are lower than those listed for the numerical analyses for all of the cases that were evaluated using both procedures. The factor of safety for vertical shearing calculated in the simplified design procedure is for a full-depth racking failure mode with 100% joint efficiency. Based on the results of the numerical analyses, the partial-depth racking failure mode controls the system behavior for a DMM zone strength of 1928 psf and joint efficiencies less than 70%. For these conditions, the factor of safety for vertical shearing from numerical analyses would be smaller than from the simplified design procedure.

The factor of safety for a partial depth racking failure could be calculated using the simplified design procedure by calculating the factor of safety for vertical shearing in the portion of the DMM zone above the strong layer.

The factors of safety listed in Table 8-3 for both the numerical analyses and the simplified design procedure meet the design criteria for every case except a partial-depth racking failure with a vertical joint efficiency of 0%. Sources in the literature suggest that vertical joint efficiencies on the order of 50% should be considered in design (CDIT 2002, Broms 2003). The factors of safety for vertical shearing listed in Table 8-3 for joint efficiencies equal to or greater than 50% meet the design guide criteria.

It should be noted, however, that specifying the required column overlap as a distance or area ratio when the column diameter is not specified, as was done at IHNC Reach III B, is important

for maintaining an adequate vertical joint strength for large diameter columns. If the requirement for column overlap had been specified as a minimum distance instead of an area overlap ratio, the factor of safety against racking failure at 50% joint efficiency could have been significantly lower than the design criteria if larger column diameters had been selected for construction. This issue is illustrated by considering a DMM column diameter of 5 ft with a minimum column overlap distance of 6 in. For an area replacement ratio of 30%, the DMM zone strength would still be 1928 psf, but the chord length of the column overlap at the joint between columns for this geometry would only be 53.1% of the average width of the wall. The factor of safety for a vertical joint efficiency of 100% would be 1.5, based on Figure 8-10a for a DMM zone strength of 1928 psf and a vertical joint strength of 1024 psf (equal to 53.1% of 1928 psf). For a vertical joint efficiency of 50%, the vertical joint strength for 5 ft diameter columns with a 6 in. minimum column overlap distance would be 528 psf and the corresponding factor of safety from Figure 8-10a would be about 1.31. This issue can be addressed by specifying the minimum overlap between columns as a ratio of the column diameter or area, which allows the ratio of the design joint strength to DMM zone strength to remain constant over a wide range of column diameters for a fixed area replacement ratio.

8.4. Conclusions and Recommendations

The following conclusions can be drawn from this study, for the conditions used to represent the Reach III B-1A I-wall, which include an 18-ft-long panel width, as indicated in Figure 8-1.

- The factors of safety from the numerical stability analyses for the base case DMM zone strength of 1300 psf provided by BCD are 1.38, 1.33, and 1.15 for vertical joint efficiencies of 100%, 50%, and 0%, respectively. The factors of safety from the numerical stability analyses for the design case DMM zone strength of 1928 psf provided by BCD are 1.53, 1.48, and 1.19 for vertical joint efficiencies of 100%, 50%, and 0%, respectively. Racking failure does not control the system performance for vertical joint efficiencies equal to or greater then 70% for either of these DMM zone strengths.

- The potential failure modes for the Reach III B-1A analysis section are complex, including the DMM zone failure modes of rotation, near-horizontal shearing, racking, or

crushing, as well as shearing on the flood side of the sheetpile and multiple zones of shearing on the protected side of the DMM zone.

- Two distinct potential racking failure modes were identified for the Reach III B-1A analysis section. For the full-depth racking failure, the vertical joints in the DMM zone exhibit racking deformations for the full depth of the joints and failure is induced in the Layer 6 sand next to and below the DMM zone. For the partial-depth racking failure, the vertical joints in the DMM zone do not exhibit racking deformations for the full depth of the joints and the DMM zone exhibits a type of bending failure at the top of the Layer 6 sand.

- The controlling failure mode for the Reach III B-1A analysis section depends on the vertical joint efficiency and the strength of the DMM zone. For higher DMM zone strengths (3800 psf and above), rotational failure controls for higher vertical joint efficiencies and full-depth racking failure controls for lower vertical joint efficiencies. For lower DMM zone strengths (2300 psf and below), near-horizontal shear failure and crushing failure control for higher vertical joint efficiencies and partial-depth racking failure controls at lower vertical joint efficiencies. The DMM zone strength where the transition occurs between the "higher" DMM zone strength failure modes and "lower" DMM zone strength failure modes depends on the efficiency of the vertical joints.

- Failure modes that include internal failure of the DMM zone on non-vertical planes control for lower DMM zone strengths. If the DMM shear walls were not socketed into the relatively strong Layer 6 sand, rotation and full-depth racking failure modes would likely control at all DMM zone strengths, similar to the results from the P24 levee and Gainard Woods Pump Station T-wall numerical analyses discussed in Chapters 4 and 6.

- The occurrence of near-horizontal and partial depth racking failures on the system performance for the Reach IIII B-1A I-wall suggests that there is a limit to the increase in factor of safety that can be achieved for these types of systems by extending the deep-mixed shear walls further into a relatively strong bearing layer.

- Based on a simple Rankine evaluation, the potential for formation of a gap on the flood side of the I-wall sheetpile is limited to a total vertical gap depth of only 1.6 ft within the soft clay of Layer 2. Because a water-filled gap of this depth at this location would be entirely contained within the failure mass for any of the potential failure modes disclosed by these analyses, the net lateral destabilizing effect of hydrostatic water pressures in the open gap would be zero. In addition, tension cracks did not develop on the flood side of the I-wall sheetpile for any of the numerical analyses, which did allow for tensile failure of the soil elements.

- The calculated factors of safety for all of the analyses completed for construction conditions are between 1.0 and 1.1, indicating that care was warranted during construction and that a restriction on the extent of mixing, as proposed by BCD, was appropriate. The calculated reduction in factor of safety for a 10% decrease in the shear strengths in the DMM zone is about 5%. There is no reduction in the factor of safety for the critical surface associated with the addition of the 250 psf crane load, although the addition of the crane load may reduce the factor of safety for other failure surfaces.

- Provided that the actual factor of safety during construction was not less than the calculated factor of safety, the results of the deformation analyses indicate that the displacements of the top of the I-wall would not exceed ¼ in.

- For all of the failure modes that were evaluated using both methods, the simplified design procedure resulted in lower factors of safety than those from the numerical analyses. The factor of safety for vertical shearing calculated in the simplified design procedure is for a full-depth racking failure mode with 100% joint efficiency. Based on the results of the numerical analyses, the partial-depth racking failure mode controls the system behavior for a DMM zone strength of 1928 psf and joint efficiencies less than 70%. For these conditions, the factor of safety for vertical shearing from numerical analyses would be smaller than from the simplified design procedure. The factor of safety for a partial-depth racking failure could be calculated using the simplified design procedure by

calculating the factor of safety for vertical shearing in the portion of the DMM zone above the strong layer.

- The factors of safety calculated using both the numerical analyses and the simplified design procedure meet the design criteria for every case except a partial-depth racking failure with a vertical joint efficiency less than about 35%. Sources in the literature suggest that vertical joint efficiencies on the order of 50% should be considered in design (CDIT 2002, Broms 2003). The factor of safety for vertical shearing for a vertical joint efficiency of 50% meets the design guide criteria.

- Specifying the minimum overlap between columns as a ratio of the column diameter or area when the column diameter is not specified is preferred to specifying a fixed overlap distance because specifying an overlap ratio allows the ratio of design joint strength to DMM zone strength to remain constant over a wide range of column diameters for a fixed area replacement ratio.

The following recommendations are made:

- Although the potential for formation of a water-filled gap and its effect on the factor of safety was determined to be insignificant for the Reach III B-1A analysis section, the effect could be significant for other conditions. Water-filled gaps should continue to be considered in stability analyses of I-wall systems with deep-mixed shear walls.

- Although the simplified analyses were conservative for all failure modes that could be compared to the numerical analyses performed for the Reach III B-1A I-wall, it is recommended that numerical analyses be performed for future deep-mixing support of I-walls until a larger set of comparisons can be completed.

- Based on the numerical analyses reported here, two changes are recommended to the simplified procedure: (1) consideration of partial depth racking by evaluating the racking failure mode to the depth of the top of a strong layer, if present in the profile, and (2)

incorporation of less than 100% efficiency vertical joints by a relatively simple modification to the shear strength along vertical joints in the simplified procedure.

- Construction staging should be considered when evaluating the stability of DMM shear wall projects. Disturbance of the native soils during mixing of the soil-cement columns might produce a soil-cement mixture with a lower strength than the native soils until the cement cures and gains strength. Depending on the initial stability of the system and the location of equipment for installation of the DMM shear walls, a restriction on the extent of mixing may be warranted, as was done for the Reach III B-1A I-wall.

CHAPTER 9

SUMMARY AND CONCLUSIONS

9.1. Summary of Work Accomplished

The following summarizes the work accomplished in this study.

- Stability analyses were completed for the P24 levee. Independent limit equilibrium analyses were completed using Spencer's method as implemented in the UTEXAS software and the results were compared with those obtained from the Method of Planes limit equilibrium analyses previously completed by the USACE. Numerical stability analyses were completed using the FLAC software and the results were compared with those from the limit equilibrium analyses. A parametric study was conducted to evaluate the effect of vertical joint efficiency on the factor of safety.

- Settlement analyses were completed for the P24 levee. Numerical settlement analyses were completed using the FLAC software for an estimated range of consolidation properties and conditions. The range of predicted settlement values were compared with settlement monitoring data provided by the USACE and with settlement predictions from simplified (hand calculation) methods.

- Stability analyses were completed for the Gainard Woods Pump Station T-wall. Numerical deformation analyses were completed using the FLAC program to estimate the T-wall deflections and loads in the piles under the design loads and numerical stability analyses were completed to estimate the factor of safety for the system. Parametric studies were conducted to evaluate the effect of vertical joint efficiency on the displacements, pile loads, and factor of safety.

- Stability analyses were completed for a T-wall similar to the Gainard Woods Pump Station T-wall with level ground conditions. Numerical stability analyses were completed using the FLAC program. Six different configurations of DMM shear walls were evaluated for a range of widths and depths to identify the relative effectiveness of

the various configurations for increasing the factor of safety of the system. Guidance was provided for optimizing shear wall geometry during design.

- Stability analyses were completed for the Reach III B-1A I-wall. Numerical stability analyses were completed using the FLAC software and the results were compared with limit equilibrium analyses results obtained by BCD using Method of Planes limit equilibrium analyses. A parametric study was conducted to evaluate the effect of DMM zone strength and vertical joint efficiency on the critical failure mode and factor of safety for the system. The results of these analyses were compared with factors of safety calculated by BCD using a simplified design procedure for DMM shear walls. Numerical stability and deformation analyses were also completed to assess the potential for instability during construction.

9.2. Conclusions

For the conditions evaluated by the five case studies completed for this research, as described in Chapters 4 through 8, the following general conclusions can be made about analyses of stability and settlement of levees and floodwalls supported by DMM shear walls:

- Numerical stability analyses permit quantitative assessment of the complex failure mechanisms that can occur for these systems over a wide range of conditions.

- The controlling failure mode for these systems depends on the efficiency of the vertical joints in the shear walls at the column overlap locations. At lower vertical joint efficiencies, racking failure modes control. At higher vertical joint efficiencies, the DMM zone functions as a block for which sliding, rotation, crushing, or non-vertical shearing failure modes control. The vertical joint efficiency where the transition occurs between the racking failure modes and the sliding, rotation, crushing, or non-vertical shearing failure modes depends on the system geometry and the strength of the DMM zone and in-situ soils.

- Numerical stability analyses can identify new failure modes, such as the partial depth racking failure mode identified in the Reach III B-1A I-wall analyses. This failure mode is not discussed in the DMM literature, and it illustrates the usefulness of numerical analyses in identifying potential failure modes that are not already well understood.

- Limit equilibrium slope stability analyses resulted in factors of safety that were equal to or lower than those obtained from numerical stability analyses for the failure modes that limit equilibrium slope stability methods can capture.

- Because numerical stability analyses indicate that there is an influence of vertical joint efficiency on system performance, it is recommended that column overlap dimensions be given special attention during design and in quality assurance and quality control (QC/QA) operations during construction.

- The simplified design method for DMM shear walls provided by Filz and Templeton (2009) resulted in conservative estimates of factor of safety for the Reach III B-1A I-wall for all modes of failure except for a partial-depth racking failure mode, which can control for some combinations of DMM zone strength and vertical joint efficiency when the DMM zone extends into a strong layer. The partial depth racking failure mode could be evaluated using the simplified design method by calculating the factor of safety for vertical shearing in the portion of the DMM zone above the strong layer.

  [Note: The final version of the "Design Guide for Levee and Floodwall Stability Using Deep-Mixed Shear Walls" by Filz and Templeton was published in April 2011 and incorporates findings from the research in this dissertation. The reader is directed to the April 2011 version for a simplified method of calculating factor of safety against partial depth racking.]

- When the DMM shear walls are socketed into a relatively strong bearing layer, non-vertical shearing and partial depth racking failure modes can occur. At lower DMM zone strengths, non-vertical shearing through the DMM zone can occur at high vertical joint efficiencies, and partial-depth racking failure can occur at low vertical joint efficiencies.

At higher DMM zone strengths, rotational failure of the DMM zone as an intact block can occur at high vertical joint efficiencies, and full depth racking failure can occur at low vertical joint efficiencies. The DMM zone strength where the transition occurs between the "lower" DMM zone strength failure modes and the "higher" DMM zone strength failure modes depends on the system geometry and the strength of the insitu soils, as well as the efficiency of the vertical joints.

- When the DMM column diameter is not specified, the minimum overlap between columns should be specified as a ratio of the column diameter or area instead of specifying a fixed overlap distance because specifying an overlap ratio allows the ratio of vertical joint strength to DMM zone strength to remain constant over a wide range of column diameters at the same area replacement ratio.

- The potential for shearing failure through the DMM zone, crushing at the toe, and partial depth racking should be evaluated whenever the shear walls are socketed into a relatively strong bearing layer. The potential for near-horizontal shearing and partial depth racking failures indicate that, for a given DMM zone strength, there is a limit to the increase in factor of safety that can be achieved for these types of systems by extending the deep-mixed shear walls further into the bearing layer.

- Calculated displacements from deformation analyses are strongly dependent on soil stiffnesses. The results for the Gainard Woods Pump Station T-wall deformation analyses illustrate the importance of obtaining realistic soil modulus information to calculate accurate displacement of T-walls.

- For T-walls, DMM shear wall configurations that minimize or eliminate the gap between the DMM and the T-wall result in higher factors of safety. The effect of a gap on the flood side is more pronounced than the effect of a gap on the protected side.

- Selecting an optimum DMM shear wall configuration for a given design requires considering both the desired factor of safety and the efficiency, where the efficiency of

each DMM shear wall configuration is evaluated by dividing the increase in factor of safety by the volume of improved ground.

- The potential for a water-filled gap on the flood side of an I-wall to affect the wall's stability should be evaluated as a routine part of I-wall design and remediation strategies, including for I-walls remediated with DMM shear walls. For I-walls with sand strata at the ground surface on the flood side of the wall, the potential for a water-filled gap to form in underlying soft clays may be limited to portions of the wall where a gap would not be expected to affect the stability of the wall.

- Simplified hand calculations for settlement of levees supported on DMM shear walls can provide reasonable agreement with numerical analyses when appropriate load concentration and distribution methods are used together with correction factors to account for the effect of shear distortions during load placement.

- For low height levees constructed next to existing levees, the potential for differential settlement of levee slopes beyond the flood and protected side boundaries of the DMM shear walls may be relatively small because of decreased compressibility of the shallow soil layers due to pre-compression from existing levee loads. The potential for longitudinal cracking due to differential settlement under the protected and flood side slopes of the levee beyond the limits of the DMM shear walls should be considered during design. A conservative estimate of differential settlement in this area could be made using simplified hand calculations to predict the settlement in the upper strata (adjacent to the DMM zone) due to the load from the portion of the levee slope that extends beyond the DMM zone.

- Construction loading should be considered when evaluating the stability of DMM shear wall projects. Disturbance of the native soils during mixing of the soil-cement columns might produce a soil-cement mixture with a lower strength than the native soils until the cement cures and gains strength. Depending on the initial stability of the system and the location of equipment for installation of the DMM shear walls, a restriction on the extent

of freshly mixed soil in front of the mixing equipment may be warranted, as was implemented for the IHNC Reach III B-1A I-wall.

- For the P24 levee, the small observed amounts of immediate settlement during construction and consolidation settlement in the 3 years since completing construction are consistent with the small settlements calculated by the numerical analyses.

- No signs of instability have been reported for the sections of the P24 levee, the Gainard Woods Pump Station T-wall, or the Reach III B-1A I-wall that included DMM shear walls. This observation is consistent with the factors of safety calculated by the numerical analyses.

9.3. Recommendations for Further Research

The use of case studies for this research allowed for the evaluation of systems with complex, real-world stratigraphy and material characterization. These complex systems provided valuable insights, highlighting site-specific issues and design factors that were not previously identified. However, the complexity and specificity of these systems also limits the flexibility of the models for conducting a wider range of parametric studies to further develop, refine, and validate robust design procedures. More simplified analysis cross-sections, with less complex levee and floodwall configurations and simplified subsurface layering and characterizations, would enable exploration of these topics.

It is recommended that research be completed on the following topics to facilitate further development, refinement, and validation of generalized design recommendations for DMM support of levees and floodwalls:

- Additional parametric numerical analyses should be performed for a wide range in levee, flood wall, and shear wall geometries to further validate the simplified DMM shear wall design procedures provided by Filz and Templeton (2009) and the simplified settlement procedure described in Chapter 5 for the P24 levee.

- Three-dimensional numerical stability analyses should be conducted to investigate the potential for extrusion of the untreated soil between the shear walls and the potential for differential settlement and transverse cracking in earthen levees between shear walls or at the end of the segment of levee alignment that is supported on deep-mixed shear walls.

- Reliability analyses should be completed to evaluate the probability of failure for these systems. Reliability analyses based on numerical stability analyses of an embankment stabilized using isolated DMM columns showed that a system with a factor of safety equal to 1.4 had a probability of failure equal to 3.2% due to the high variability of the strength of the DMM material (Filz and Navin 2006). The effect of DMM strength variability may not be as significant for support by DMM shear walls as for support by isolated DMM columns, but the effects of such variability should still be investigated for levees and floodwalls supported by DMM shear walls.

- It would be worthwhile to investigate whether current state-of-practice methods for assessing the impact of water-filled tension cracks and water-filled gaps on stability of levees and floodwalls without DMM support are also appropriate and sufficient for levees and floodwalls with DMM support.

REFERENCES

Adams, T.E., Filz, G.M., Cali, P.R., and Woodward, M.L. (2008a). "Stability analyses of a levee on deep-mixed columns, Plaquemines Parish, Louisiana," *Geosustainability and Geohazard Mitigation*, GSP No. 178, ASCE, Reston, VA: 708-715.

Adams, T.E., Filz, G.M., Cali, P.R., and Woodward, M.L. (2008b). "Deformation and stability analyses of a pile supported T-wall with deep mixed shear panels in Plaquemines Parish, Louisiana," *Proc. 2nd Int. Conf. Geotechnical Engineering for Disaster Mitigation & Rehabilitation*, Science Press Beijing and Springer Berlin, 481-486.

Adams, T., Filz, G., and Navin, M. (2009). "Stability of Embankments and Levees on Deep-Mixed Foundations," *Proc. Int. Symp. Deep Mixing & Admixture Stabilization*, Okinawa, Japan, May 19-21, 6 pp.

Baker, S. (2000). "Deformation behaviour of lime/cement column stabilized clay." Chalmers University of Technology.

Barker, R. M., Duncan, J. M., Rojiani, K. B., Ooi, PSK, Tan, C. K., Kim, S. G. (1991). *Manuals for the Design of Bridge Foundations: Shallow Foundations*, NCHRP Report 343, Transportation Research Board, Washington, D.C.

Bethlehem Steel (1988). Bethlehem Steel Sheet Piling, Booklet No. 2001A, Bethlehem Steel Corp, USA.

Broms, B.B. (2003). *Deep Soil Stabilization: Design and Construction of Lime and Lime/Cement Columns*, Royal Institute of Technology, Stockholm, Sweden.

Cali, P.R., Woodward, M., Bruce, D.A., and Forte, E. (2005a). "Levee stability application for deep mixing (1) – design of full scale test section using dry mixed soil cement columns." *International Conference on Deep Mixing*, Swedish Geotechnical Institute, Stockholm Sweden, May 23-25, 8 pp.

Cali, P.R., Woodward, M., Bruce, D.A., and Forte, E. (2005b). "Levee stability application for deep mixing (2) – conclusions from test section using dry mixed soil cement columns." *International Conference on Deep Mixing*, Swedish Geotechnical Institute, Stockholm Sweden, May 23-25, 9 pp.

CDM (Cement Deep Mixing) (1985). Design and Construction Manual for CDM Institute, Partial English Translation

CDIT (Coastal Development Institute of Technology). (2002). "The deep mixing method: Principle, design, and construction." A.A. Balkema: The Netherlands.

Duncan, J. M. (2000). "Factors of Safety and Reliability in Geotechncial Engineering", *Journal of Geotechncial and Environmnetal Engineering*, Vol. 126, No. 4, April, 2000, pp. 307-316.

Duncan, J.M. and Buchignani, A.L. (1987). *An Engineering Manual for Settlement Studies*, Department of Civil Engineering, University of Berkeley, California, 94 pp. (This document is available through the Civil and Environmental Engineering Department at Virginia Tech, Blacksburg).

Duncan, J.M., and Bursey, A.J. (2007). *Soil and Rock Modulus Correlations or Geotechnical Engineering*, Virginia Polytechnic Institute and State University Center for Geotechnical Practice and Research, CGPR #44, Blacksburg.

Duncan, J. M. and Wright, S.G. (2005). *Soil Strength and Slope Stability*, John Wiley and Sons, Inc.: New Jersey.

EuroSoilStab (2002). "Development of design and construction methods to stabilise soft organic soils." Design Guide Soft Soil Stabilization, CT97-0351, Project No.: BE 96-3177.

Fenton, G.A. and Griffiths, D.V. (2008). *Risk assessment in Geotechnical Engineering*, John Wiley & Sons, Hoboken, N.J.

FHWA (Federal Highway Administration). (1996). *Design and Construction of Driven Pile Foundations-Volume 1*, U.S. Department of Transportation, Federal Highway Administration, Publication No. FHWA-HI-97-013.

Filz, G.M. (2009). "Design of Deep Mixing Support for Embankments and Levees." *Proc. Int. Symp. Deep Mixing & Admixture Stabilization*, Okinawa, Japan, May 19-21, 23 pp.

Filz, G.M., Adams, T.E., and Navin, M.P. (2010). Deep mixing to improve the stability of embankments, levees and floodwalls constructed on soft clay. *New Techniques on Soft Soils*, (Almeida M (ed.)) Oficicina de Textos, Sao Paulo, Brazil, pp. 107-122.

Filz, G.M. and Navin, M.P. (2006). *Stability of Column-Supported Embankments*, Virginia Transportation Research Council Report No. 06-CR13, Richmond.

Filz, G.M. and Templeton, E. (2009). *Design Guide for Levee and Floodwall Stability Using Deep-Mixed Shear Walls*, prepared by Burns Cooley Dennis for the U.S. Army Corps of Engineers, report dated February 10, 2009.

Filz, G.M., Templeton, E. and Adams, T.E. (2011). "Stability analysis for levees on deep-mixed shear walls," *Ground Improvement*, 164 August 2011 Issue GI3: 117-126.

Geomatrix. (2007). *Soil Structure Interaction and Load Transfer Mechanism of Pile-Supported T-Wall for New Orleans Levees*, prepared for U.S. Army Engineer Research & Development Center, Project No. 12048.001, March 2007.

Han, J., Chen, J., Hong, Z. (2008a). "Geosynthetic Reinforcement for Riverside Slope Stability of Levees due to Rapid Drawdown," *Proc. 2nd Int. Conf. Geotechnical Engineering for Disaster Mitigation & Rehabilitation*, Science Press Beijing and Springer Berlin, 153-158.

Han, J. Hong, Z. and Shen, S. (2008b). "Stability of Levees over Soft Soil Improved by Deep Mixing Technology," *Geosustainability and Geohazard Mitigation*, GSP No. 178, ASCE, Reston, VA: 716-723.

Han, J. Chen, J., Hong, Z. and Shen, S. (2010). "Mitigation of levee failure using deep mixed columns and geosynthetics," *Geomechanics and Geoengineering: An International Journal*, Vol. 5, No. 1: 49-55.

Holtz, R.D., Jamiolkowski, M.B., Lancellotta, R. and Pderoni, R. (2001) *Prefabricated Vertical Drains: Design and Perfomrmance*, Constrcution Indstry Research and Information Assocaiation Gorund Engineering Report: Ground Improvement, Butterworth-Heinemann: Oxford.

Inagaki, M., Abe, T., Yamamoto, M., Nozu, M., Yanagawa, Y., and Li, L. (2002). "Behavior of cement deep mixing columns under road embankment." Physical Modeling in Geotechnics: ICPMG '02, 967-972.

ITASCA Consulting Group (2005). *FLAC2D Fast Lagrangian Analysis of Continua*, Users Manual, ITASCA Consulting Group, Minneapolis, MN.

Jacobson, J. R., Filz, G. M., and Mitchell, J. K. (2003). Report prepared for the Virginia Transportation Research Council, Virginia Polytechnic Institute and State University.

Jacobson, J. R., Filz, G. M., and Mitchell, J. K. (2005). "Factors Affecting Strength of Lime-Cement Columns Based on a Laboratory Study of Three Organic Soils." Deep Mixing '05: International conference on deep mixing best practice and recent advances.

Japanese Geotechnical Society (2000). "Standard practice for making and curing stabilized soil specimens without compaction (JGS 0821-2000)." Rep. No. Chapter 7 (in Japanese).

Kitazume, M. and Karastanev, D. (1996). "Bearing capacity of improved ground with column type DMM." Grouting and Deep Mixing, Proceedings

Kitazume, M. and Maruyama, K. (2005). "Collapse Failure of Group Column Type Deep Mixing Improved Ground Under Embankment." *International Conference on Deep Mixing*, Swedish Geotechnical Institute, Stockholm Sweden, May 245-254, 10 pp.

Lambe, T.W. and Whitman, R.V. (1969). *Soil Mechanics*, John Wiley and Sons, New York.

McGinn, A. J. and O'Rourke, T. D. (2003). "Performance of deep mixing methods at Fort Point Channel." Cornell University.

Miyake, M., Wada, M., and Satoh, T. (1991). "Deformation and strength of ground improved by cement treated soil columns." Proceedings International Conference on Geotechnical for Coastal Development (GEO-COAST '91), 369-380.

NAVFAC (Naval Facilities Engineering Command) (1982). Soil Mechanics. *Design Manual 7.1, Naval Facilities Engineering Command.*

Navin, M.P. (2005). "Stability of Embankments Founded on Soft-Soil Improved with Deep-Mixing-Method Columns." Doctor of Philosophy Dissertation, Virginia Tech Blacksburg, VA.

Ohishi, K., Katagiri, M., Terashi, M., Ishii, T. and Miyakoshi, Y. (2005). "Physical and Numerical Simulation of Deep Mixed Foundation, Part 2: Revetment on Treated Soil Block Underlain by a Sandy Layer." *International Conference on Deep Mixing*, Swedish Geotechnical Institute, Stockholm Sweden, May 281-288, 8 pp.

Ou, C. Y., Wu, T. S., and Hsieh, H. S. (1996). "Analysis of deep excavation with column type of ground improvement in soft clay." Journal of Geotechnical Engineering, 122(9), 709-716.

Porbaha, A., Ghaheri, F., and Puppala, A. J. (2005). "Soil Cement Properties from Borehole Geophysics Correlated with Laboratory Tests." Deep Mixing '05: International conference on deep mixing best practice and recent advances.

PWRC (Public Work Research Center) (1999). "Design and Construction Manual on Deep Mixing Method for Inland Construction." 326 p. (in Japanese)

Rollins, K., Herbst, M., Adsero, M. and Brown, D. (2009). "Increased Lateral Pile Group Resistance from Soil Mixed and Jet Grout Walls." *Proc. Int. Symp. Deep Mixing & Admixture Stabilization*, Okinawa, Japan, May 19-21, 6 pp.

Sehn, A. L. (2005). Personal communication to Prof. George M. Filz.

Skempton, A.W., and Bjerrum, L. (1957). "A Contribution to the Settlement Analysis of Foundations on Clay", *Geotechnique*, Vol. 7 No. 3 April, 2000, pp. 168-178. (Skempton and Bjerrum's results are summarized in Duncan and Buchignani, 1987).

Smith, M.E. (2005). "Design of Bridge Layers in Geosynthetic-Reinforced Column-Supported Embankments." Doctor of Philosophy Dissertation, Virginia Tech Blacksburg, VA.

Terashi, M. (2003). "The state of practice in deep mixing methods." Grouting and Ground Treatment, Proceedings of the 3rd International Conference, New Orleans, 25-49.

Terzaghi,K. and Peck, R.B. (1968) *Soil Mechanics in Engineering Practice*. John Wiley and Sons, Inc, New York.

USACE (U.S. Army Corps of Engineers) (2002). "Stability with Uplift", Version 2.2, April 2002, FS004, USACE LMVD Method of Planes.

Woodward, M. (2009). "Quality control and verification of New Orleans Hurricane Deep Mixing Projects." *Proc. Int. Symp. Deep Mixing & Admixture Stabilization*, Okinawa, Japan, May 19-21, 4 pp.

Wright, S.G. (1991). *UTEXAS3: A Computer Program for Slope Stability Calculations*, Users Manual, Shinoak Software, Austin, TX.

Wright, S.G. (2007). *UTEXAS4: A Computer Program for Slope Stability Calculations*, Users Manual, Shinoak Software, Austin, TX.

APPENDIX A

BACKGROUND MATERIAL FOR CASE STUDIES

This section provides some of the material provided by U.S. Army Corps of Engineers (USACE) for the P24 Levee and Gainard Woods Pump Station case studies and by Burns Cooley Dennis (BCD) for the Inner Harbor Navigation Canal (IHNC) Reach III B-1A I-wall.

A.1. P24 Levee

Selected documents were provided by the USACE for the segment of the P24 levee that included deep mixed shear walls in the foundation. For the stability analyses case study, the documentation provided by USACE generally pertained to the analysis section used in their design process. Because the objective of the settlement analyses case study was to estimate the expected settlement for the as-built conditions, a second set of documentation was provided for the settlement case study.

A.1.1. Stability Analyses Case Study

Background material provided by the USACE for this case study included:

- Drawing 4a. Contract P24, Typical Section 4 - Deep Mixing
- Drawing 7. Contract P24, Plan/Profile, B/L Sta. 357+00 to B/L Sta. 420+00
- Drawing 8. Contract P24, Plan/Profile, B/L Sta. 420+00 to B/L Sta. 490+00
- A summary of USACE's Method of Planes stability analysis

These documents are included as Figures A-1 through A-4. In addition to the documentation included as figures in this appendix, USACE provided copies of laboratory testing reports with the results of 2081 unconfined compression tests on DMM samples taken during installation of the columns.

A.1.1. Settlement Analyses Case Study

Some of the background material provided by the USACE for the stability analyses were also used in the development of the settlement analyses case study. Additional information provided by the USACE for developing an analysis section for the as-built conditions of the included:

- Survey cross-sections of the pre-construction and post-construction ground surfaces for Sta. 414+00

This document is included as Figure A-5. In addition to the survey cross-sections included in this appendix, USACE provided boring logs and laboratory test results for borings B-1 through B-9 and PSV-10UT through PSV-12UT, located along the P24 alignment, and boring logs R-37, R36-2, and R36.6, located in the vicinity of the P24 levee project.

A.2. Gainard Woods Pump Station T-wall

Selected documents were provided by the USACE for the segment of the Gainard Woods Pump Station T-wall that included deep mixed shear walls in the foundation. Background material provided by the USACE for this case study included:

- Drawing 5. Gainard Woods P.S., Plan
- Drawing 6. Gainard Woods P.S., Typical Sections 1 of 2
- Drawing 7. Gainard Woods P.S., Typical Sections 2 of 2
- Drawing 8. Gainard Woods P.S., Profile
- Drawing 9. Gainard Woods P.S., T-wall Layout
- A summary of USACE's Method of Planes stability analysis
- Contractor's documentation of the DMM soil-cement column installation
- Contractor's documentation of the DMM soil-cement strength testing

These documents are included as Figures A-6 through A-13.

A.3. IHNC Reach III B-1A I-wall

Selected documents were provided by BCD for the segment of the IHNC West Reach III B-1A I-wall that included deep mixed shear walls in the foundation. Background material provided by the BCD for this case study included:

- Sheet C-17. Reach III IHNC West Levee, Alternative 3, Typical Section
- A summary of BCD's Method of Planes stability analysis

These documents are included as Figures A-14 and A-15. In addition to the plates included in this appendix, BCD also provided their calculations for the simplified design procedure they used in their design of the shear walls. These calculations are included in Appendix B of the Design Guide for Levee and Floodwall Stability Using Deep-Mixed Shear Walls (Filz and Templeton 2009).

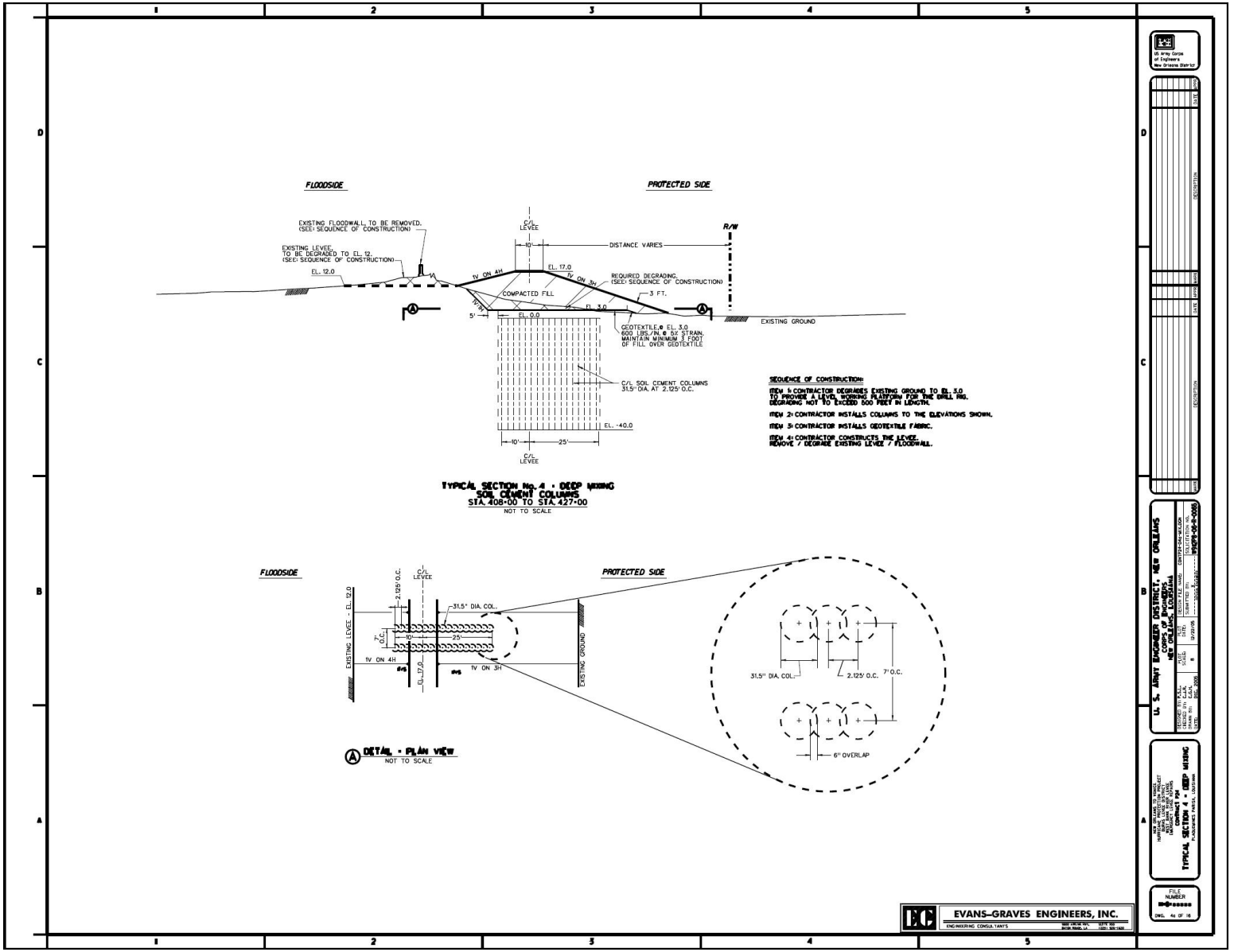

Figure A-1. P24 Levee DMM Typical Section

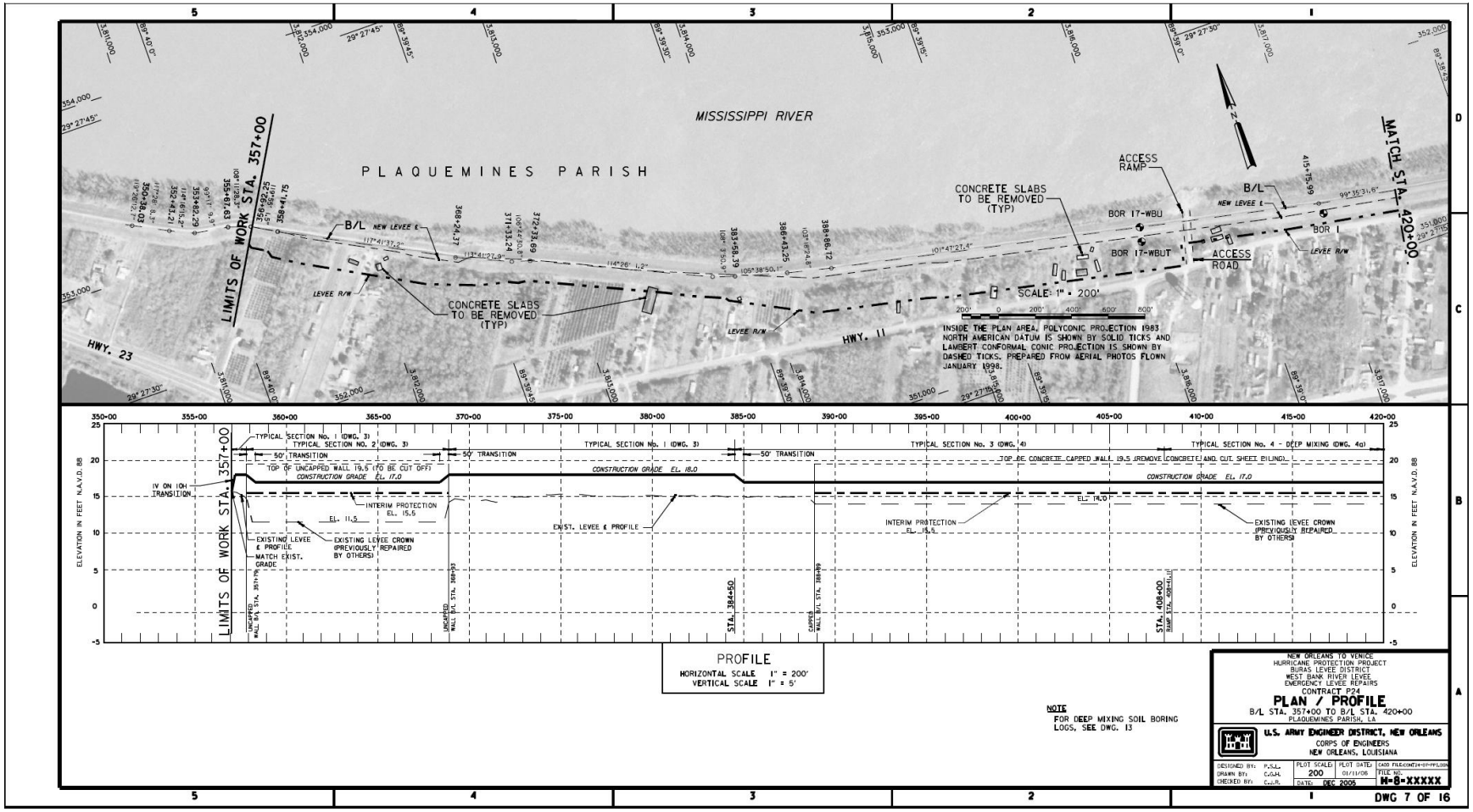

Figure A-2. P24 Levee Plan/Profile Station 357+00 to Station 420+00

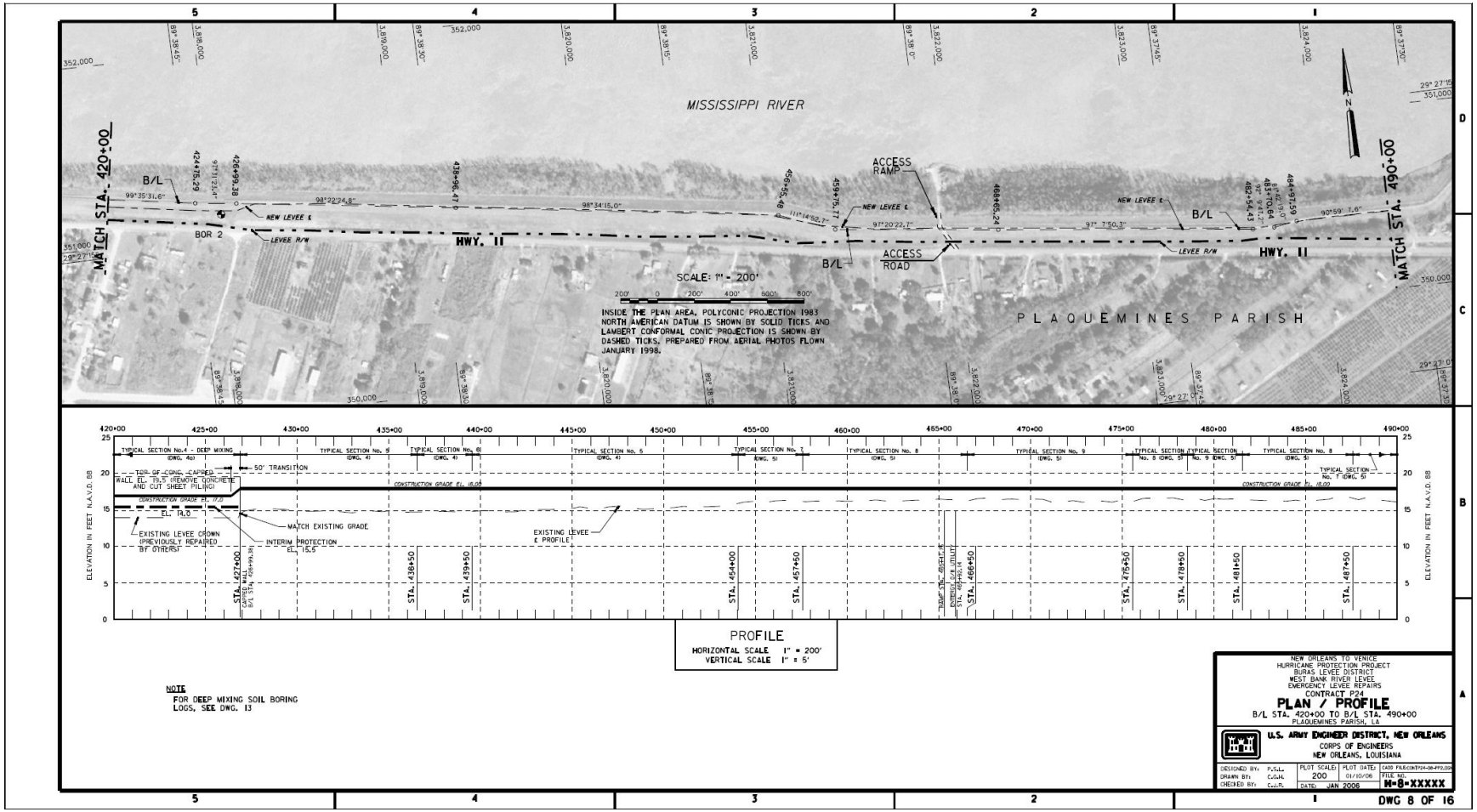

Figure A-3. P24 Levee Plan/Profile Station 420+00 to Station 490+00

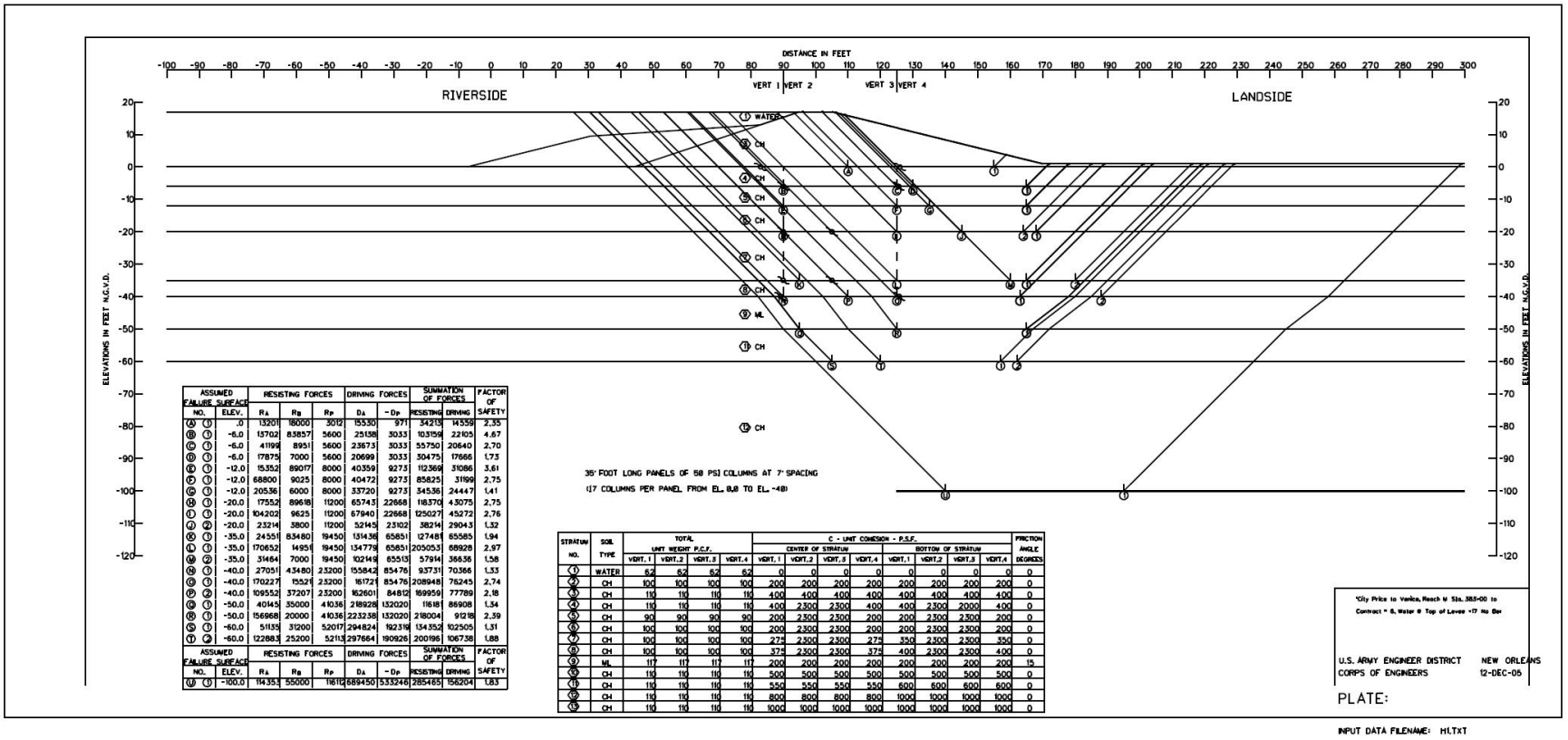

ASSUMED FAILURE SURFACE NO.		ELEV.	RESISTING FORCES R_A	R_B	R_P	DRIVING FORCES D_A	$-D_P$	SUMMATION OF FORCES RESISTING	DRIVING	FACTOR OF SAFETY
A	1	0	13201	18000	3012	15330	971	34213	14359	2.35
B	1	-6.0	13702	83857	5600	25138	3033	103159	22105	4.67
C	1	-6.0	41198	8951	5600	23673	3033	55750	20640	2.70
D	1	-6.0	17875	7000	5600	20699	3033	30475	17666	1.73
E	1	-12.0	15352	89017	8000	40359	9273	112369	31086	3.61
F	1	-12.0	68800	9025	8000	40472	9273	85825	31199	2.75
G	1	-12.0	20536	6000	8000	33720	9273	34536	24447	1.41
H	1	-20.0	17552	89618	11200	65745	22668	118370	43075	2.75
I	1	-20.0	104202	9625	11200	67940	22668	125027	45272	2.76
J	2	-20.0	23214	3800	11200	52145	23102	38214	29043	1.32
K	1	-35.0	24551	83480	19450	131436	65851	127481	65585	1.94
L	1	-35.0	170652	14951	19450	134779	65851	205053	68928	2.97
M	2	-35.0	31464	7000	19450	102149	65513	57914	36636	1.58
N	1	-40.0	27051	43480	23200	155842	85476	93731	70366	1.33
O	1	-40.0	170227	15521	23200	161721	85476	208948	76245	2.74
P	2	-40.0	109552	37207	23200	162601	84812	169959	77789	2.18
Q	1	-50.0	40145	35000	41036	218928	132020	116181	86908	1.34
R	1	-50.0	156968	20000	41036	223238	132020	218004	91218	2.39
S	1	-60.0	51155	31200	52017	294824	192316	134352	102505	1.31
T	2	-60.0	122883	25200	52113	297664	190926	200196	106738	1.88

ASSUMED FAILURE SURFACE NO.		ELEV.	RESISTING FORCES R_A	R_B	R_P	DRIVING FORCES D_A	$-D_P$	SUMMATION OF FORCES RESISTING	DRIVING	FACTOR OF SAFETY
U	1	-100.0	114353	55000	11812	689450	533246	285465	156204	1.83

STRATUM NO.	SOIL TYPE	TOTAL UNIT WEIGHT P.C.F. VERT. 1	VERT. 2	VERT. 3	VERT. 4	C - UNIT COHESION - P.S.F. CENTER OF STRATUM VERT. 1	VERT. 2	VERT. 3	VERT. 4	BOTTOM OF STRATUM VERT. 1	VERT. 2	VERT. 3	VERT. 4	FRICTION ANGLE DEGREES
1	WATER	62	62	62	62	0	0	0	0	0	0	0	0	0
2	CH	100	100	100	100	200	200	200	200	200	200	200	200	0
3	CH	110	110	110	110	400	400	400	400	400	400	400	400	0
4	CH	110	110	110	110	400	2300	2300	400	400	2300	2000	400	0
5	CH	90	90	90	90	200	2300	2300	200	200	2300	2300	200	0
6	CH	100	100	100	100	200	2300	2300	200	200	2300	2300	200	0
7	CH	100	100	100	100	275	2300	2300	275	350	2300	2300	350	0
8	CH	100	100	100	100	375	2300	2300	375	400	2300	2300	400	0
9	ML	117	117	117	117	200	200	200	200	200	200	200	200	15
10	CH	110	110	110	110	500	500	500	500	500	500	500	500	0
11	CH	110	110	110	110	550	550	550	550	600	600	600	600	0
12	CH	110	110	110	110	800	800	800	800	1000	1000	1000	1000	0
13	CH	110	110	110	110	1000	1000	1000	1000	1000	1000	1000	1000	0

Figure A-4. P24 Levee Method of Planes Stability Analyses

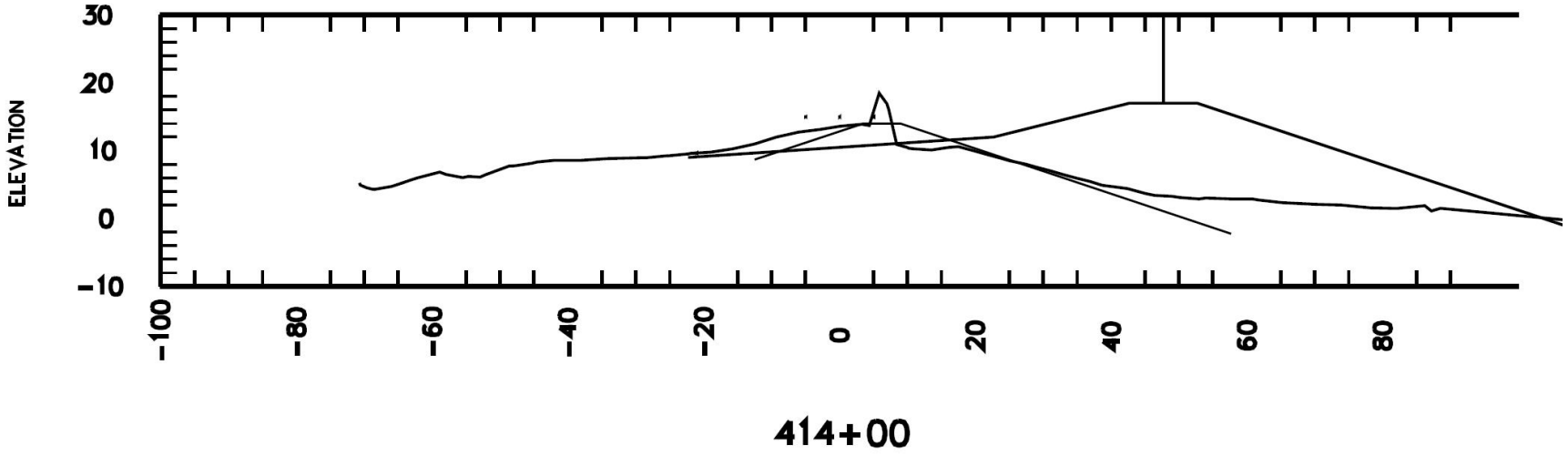

Figure A-5. P24 Levee Survey Cross-Sections at Station 414+00

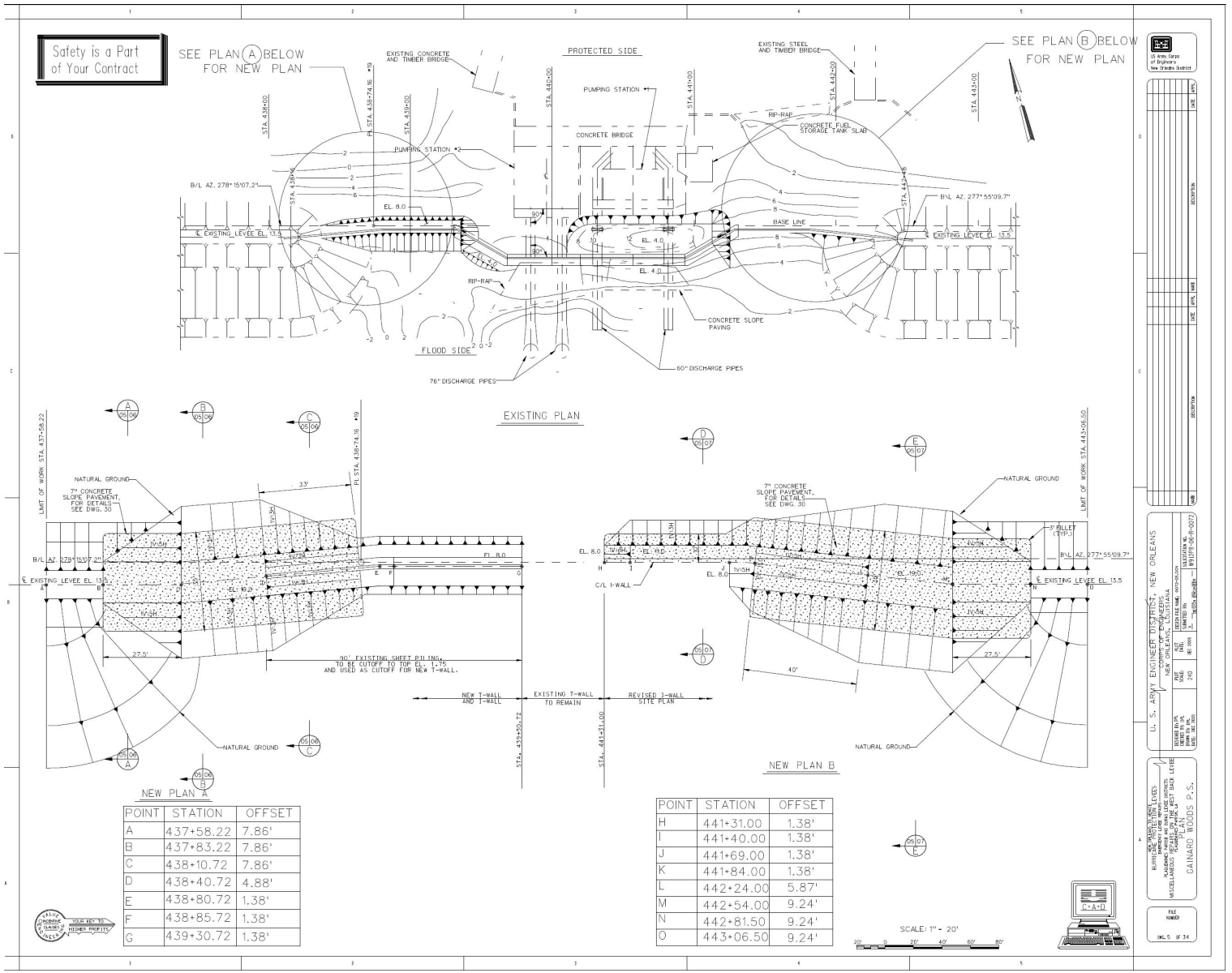

NEW PLAN A

POINT	STATION	OFFSET
A	437+58.22	7.86'
B	437+83.22	7.86'
C	438+10.72	7.86'
D	438+40.72	4.88'
E	438+80.72	1.38'
F	438+85.72	1.38'
G	439+30.72	1.38'

POINT	STATION	OFFSET
H	441+31.00	1.38'
I	441+40.00	1.38'
J	441+69.00	1.38'
K	441+84.00	1.38'
L	442+24.00	5.87'
M	442+54.00	9.24'
N	442+81.50	9.24'
O	443+06.50	9.24'

Figure A-6. Gainard Woods Pump Station T-wall Plan View

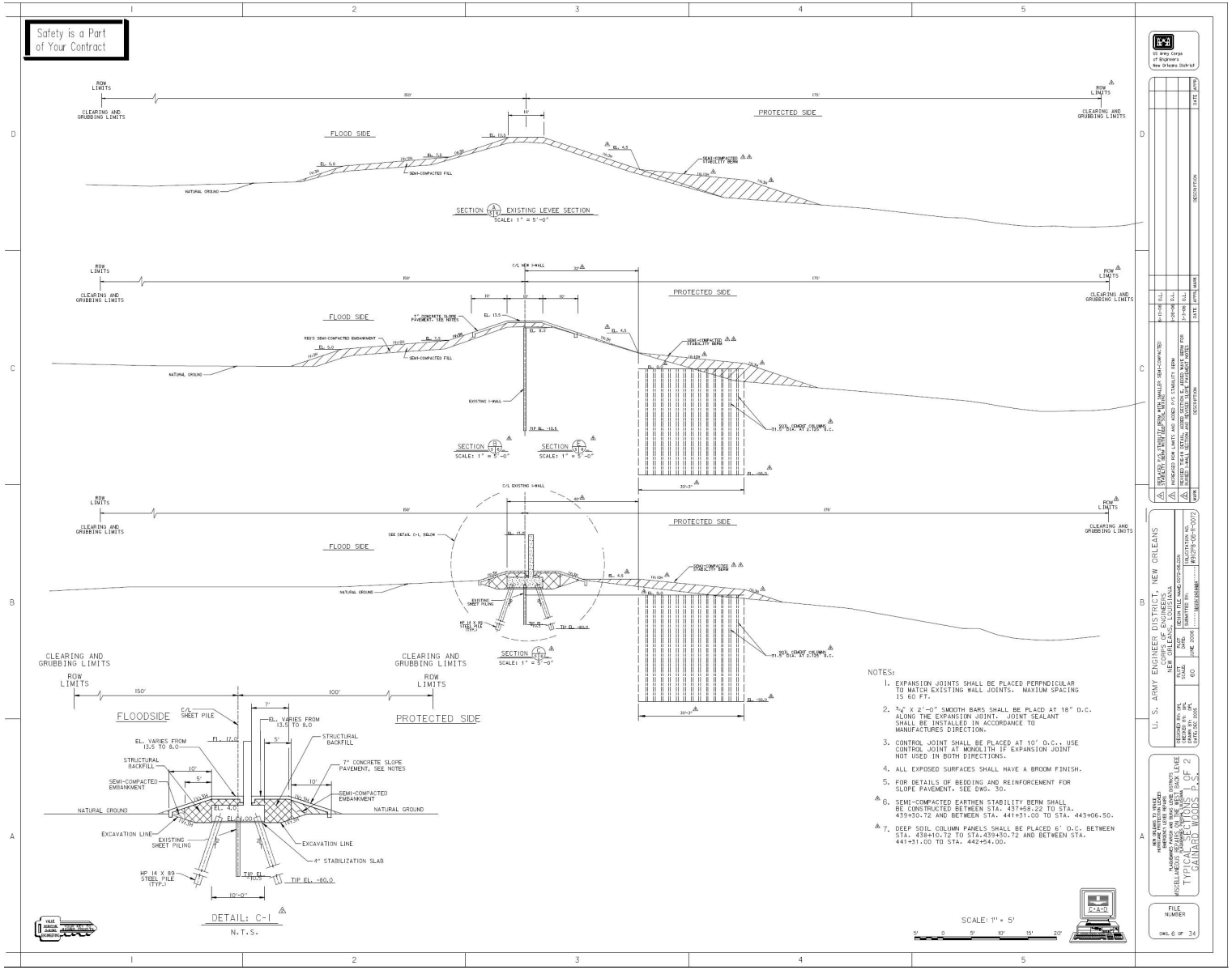

Figure A-7. Gainard Woods Pump Station T-wall Typical Section with DMM Zone Location

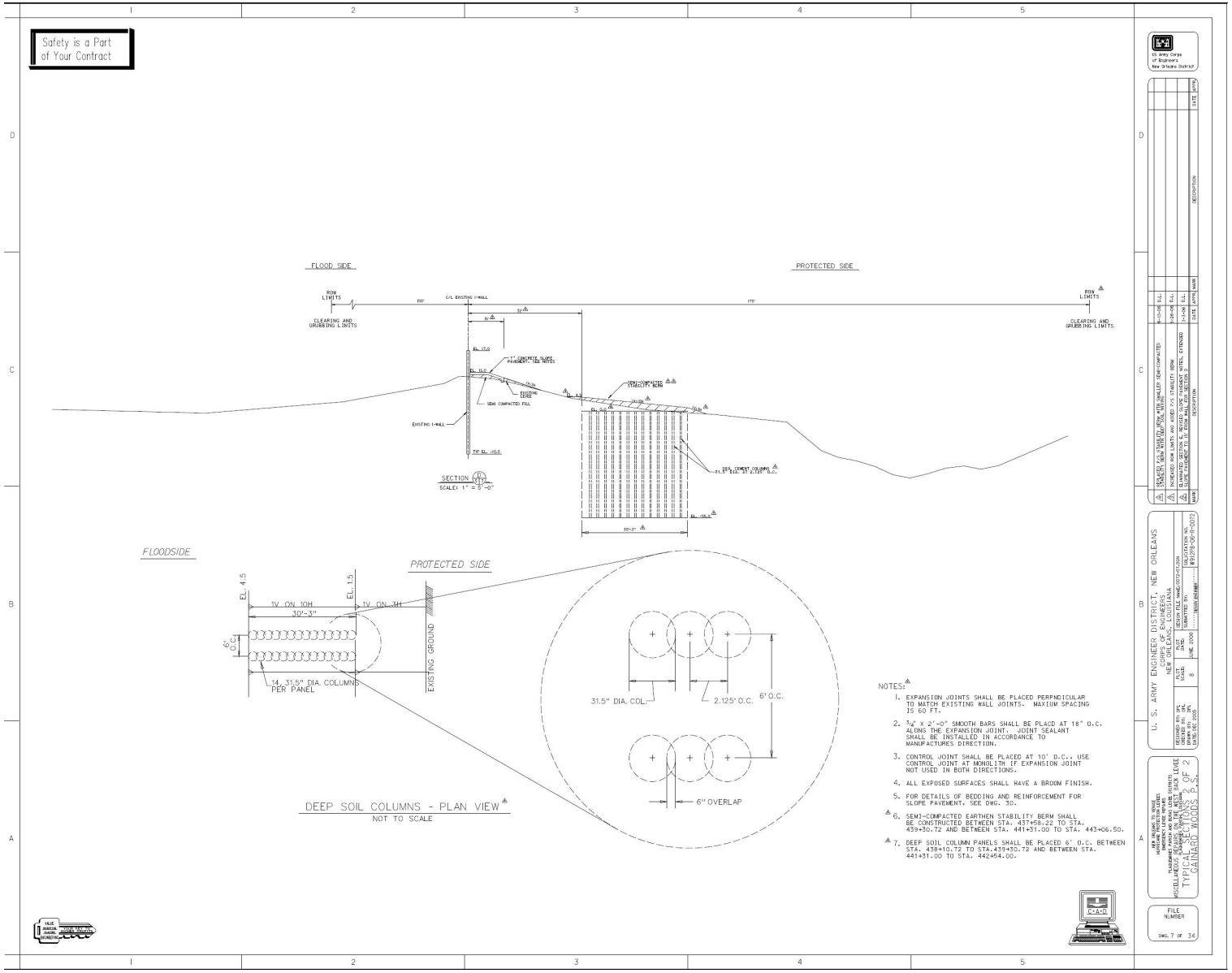

Figure A-8. Gainard Woods Pump Station T-wall DMM Column Layout

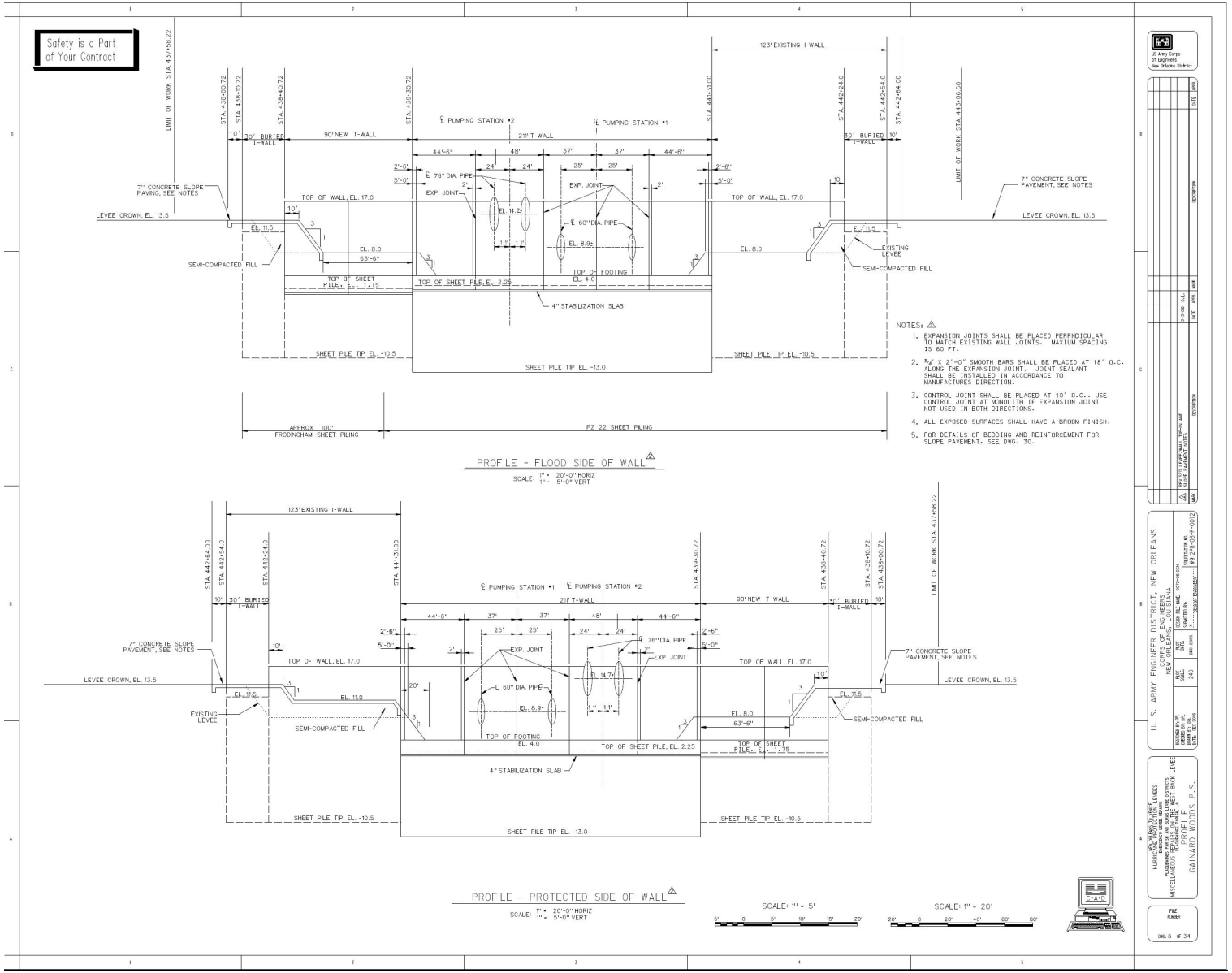

Figure A-9. Gainard Woods Pump Station T-wall Profile View

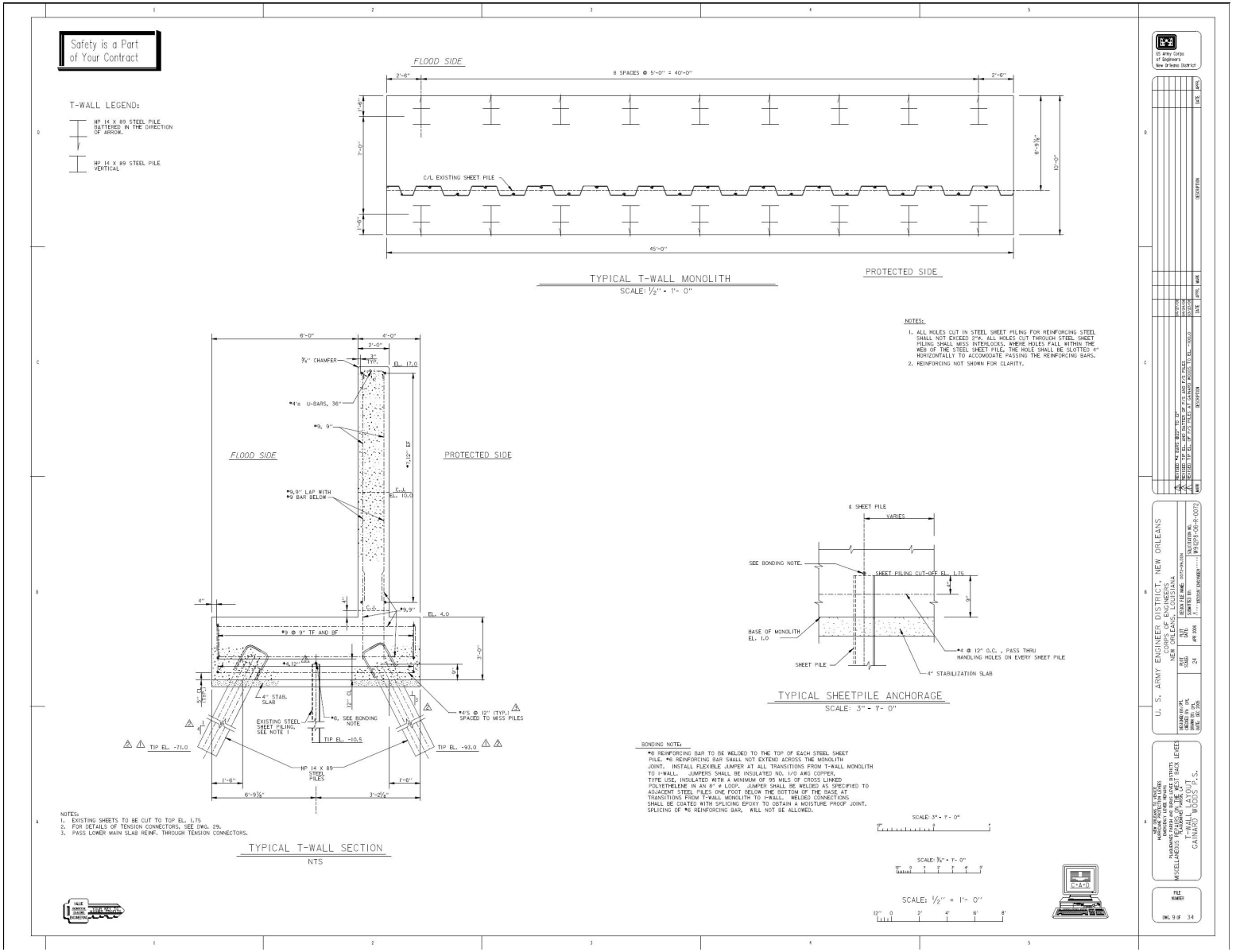

Figure A-10. Gainard Woods Pump Station T-wall Layout

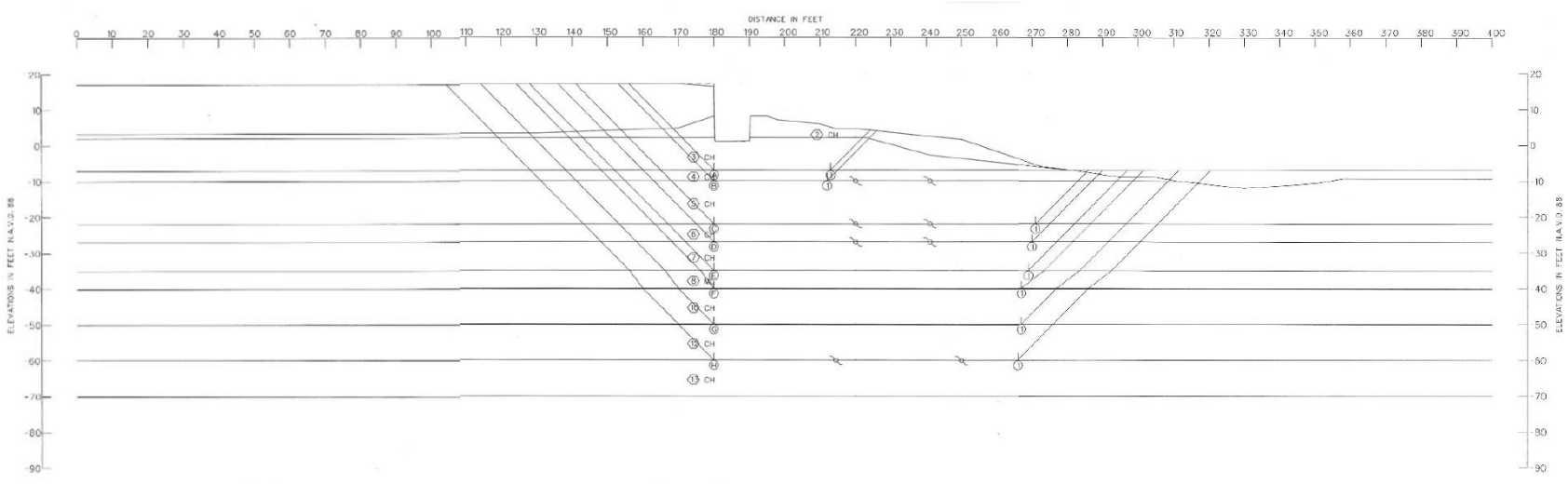

ASSUMED FAILURE SURFACE NO.	ASSUMED FAILURE SURFACE ELEV.	RESISTING FORCES Ka	RESISTING FORCES Kp	RESISTING FORCES Kr	DRIVING FORCES Da	DRIVING FORCES −Dr	SUMMATION OF FORCES RESISTING	SUMMATION OF FORCES DRIVING	FACTOR OF SAFETY
(A) (1)	-7.0	7516	8945	5648	20776	8336	22109	14540	1.52
(B) (1)	-10.0	9235	8712	6880	26717	9735	24827	16982	1.46
(C) (1)	-22.0	17550	50700	5752	59301	11866	74002	47636	1.55
(D) (1)	-27.0	21864	53452	8552	77247	20419	83868	56828	1.48
(E) (1)	-35.0	29807	57862	14050	111856	39373	101739	72483	1.40
(F) (1)	-40.0	34934	59949	20959	137358	54715	115842	82643	1.40
(G) (1)	-50.0	47532	65767	30559	198514	92978	143858	105536	1.36
(H) (1)	-60.0	62488	65392	42050	266701	141364	164930	125337	1.32

STRATUM NO.	SOIL TYPE	TOTAL UNIT WEIGHT P.C.F. VERT.1	VERT.2	VERT.3	VERT.4	VERT.5	C - UNIT COHESION - P.S.F. CENTER OF STRATUM VERT.1	VERT.2	VERT.3	VERT.4	VERT.5	BOTTOM OF STRATUM VERT.1	VERT.2	VERT.3	VERT.4	VERT.5	FRICTION ANGLE DEGREES
(1)	WATER	62	62	62	62	62	0	0	0	0	0	0	0	0	0	0	0
(2)	CH	110	110	110	110	110	400	400	400	400	400	400	400	400	400	400	0
(3)	CH	86	86	86	86	86	300	215	1000	1000	150	300	215	1000	1000	150	0
(4)	CH	98	86	86	86	98	300	215	1000	1000	150	300	215	1000	1000	150	0
(5)	CH	100	92	86	86	100	360	270	1000	1000	210	420	330	1000	1000	270	0
(6)	CH	115	100	100	100	100	445	360	1000	1000	295	470	380	1000	1000	320	0
(7)	CH	115	100	100	100	100	510	420	1000	1000	360	550	460	1000	1000	400	0
(8)	ML	117	117	117	117	117	200	200	1000	1000	200	200	200	1000	1000	200	15
(9)	CH	115	100	100	100	100	600	510	1000	1000	450	600	510	1000	1000	450	0
(10)	CH	115	100	100	100	100	650	565	1000	1000	500	700	615	1000	1000	550	0
(11)	CH	105	100	100	100	100	700	615	1000	1000	550	700	615	1000	1000	550	0
(12)	CH	105	105	105	105	105	750	665	600	600	600	800	715	650	650	650	0
(13)	CH	105	105	105	105	105	800	715	715	650	650	800	715	715	650	650	0

"Proposed Temporary levee repair"
Gainard Wood Pump Station - Plaquemines Parish

U.S. ARMY ENGINEER DISTRICT NEW ORLEA
CORPS OF ENGINEERS 14-JUN-06

Figure A-11. Gainard Woods Pump Station T-wall Method of Planes Stability Analyses

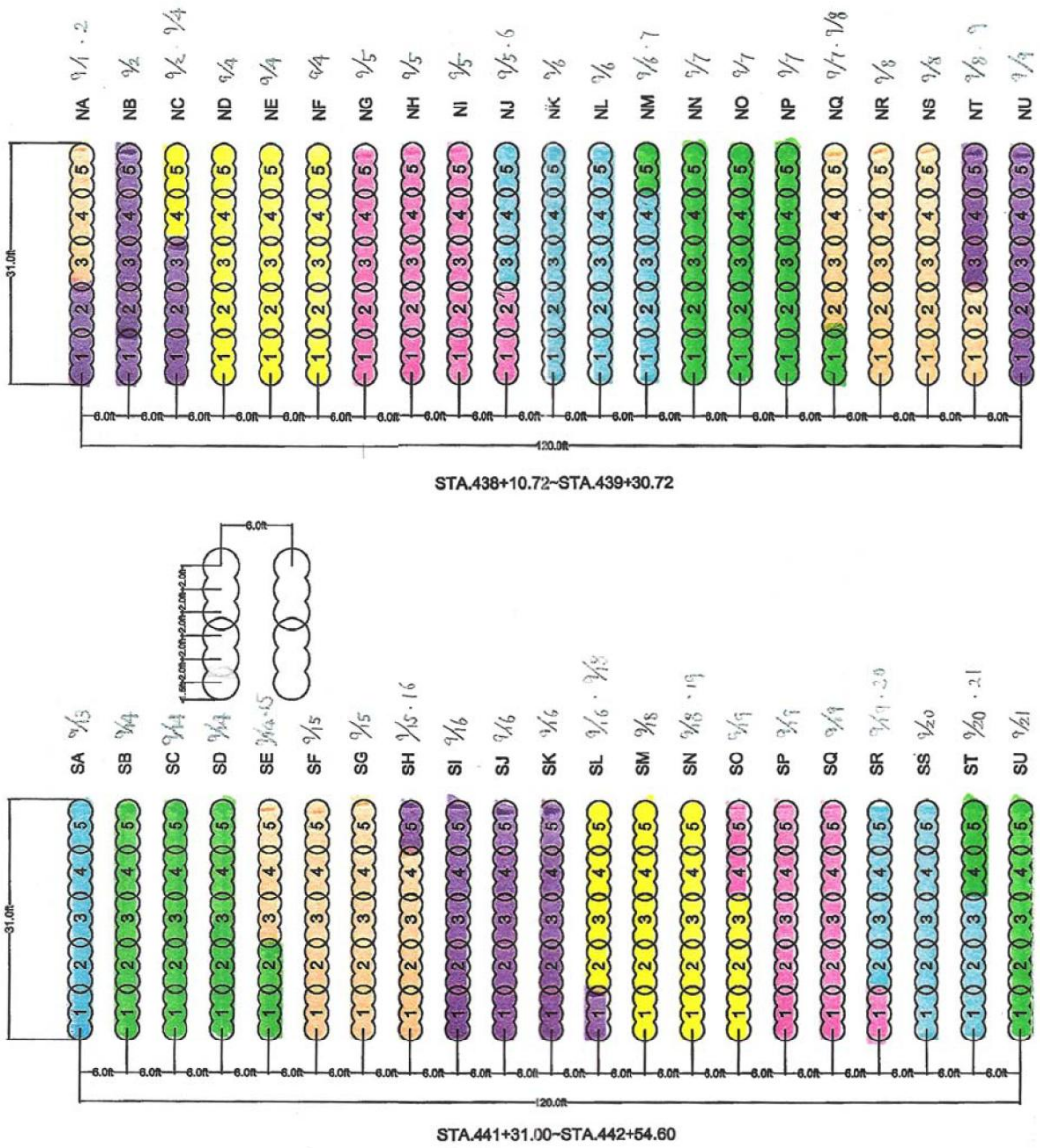

Figure A-12. Gainard Woods Pump Station T-wall Documentation of the DMM Soil-Cement Column Installation

Test Results

		ELEMENT ID																			
Location	Sample	NA-5	ND-3	NG-1	NH-5	NK-3	NL-5	NN-4	NQ-3	NS-2	NU-1	SA-4	SC-2	SF-2	SI-3	SL-2	SN-3	SO-5	SQ-2	SR-4	SU-2
0 - 4	# 1	155	271	200	784	570	163	318	403	143	179	181	130	147	128	273	202	149	257	153	149
4 - 8	# 2	363	228	336	680	265	509	159	194	208	479	320	224	261	475	277	143	336	112	189	397
8 - 12	# 3	302	222	485	297	591	193	181	538	299	458	304	175	155	340	228	175	397	255	163	469
12 - 16	# 4	450	198	357	644	265	244	169	499	249	420	246	242	*238*	283	255	147	391	712	772	523
16 - 20	# 5	273	204	285	591	672	153	309	271	208	187	259	*540*	163	*299*	281	159	328	444	248	336
20 - 24	# 6	238	273	224	529	255	102	242	485	185	289	344	302	320	257	202	187	112	244	299	414
24 - 28	# 7	179	147	414	662	764	255	179	615	216	210	306	128	196	277	220	275	348	723	222	183
28 - 32	# 8	297	220	471	574	744	357	150	530	304	297	204	124	124	326	275	143	165	265	383	208
32 - 36	# 9	209	183	350	346	163	143	173	210	248	432	424	230	*475*	238	177	202	228	244	257	528
36 - 40	# 10	246	94	212	611	244	163	173	407	94	503	312	110	261	*220*	163	183	491	301	255	322
40 - 44	# 11	220	230	198	607	621	183	169	297	234	481	259	*157*	367	275	281	224	151	220	175	191
44 - 48	# 12	196	161	344	601	428	153	287	434	432	226	391	251	187	*234*	191	228	519	151	210	664
48 - 52	# 13	281	320	540	613	163	581	161	617	369	416	306	251	143	198	130	244	269	316	159	403
52 - 56	# 14	196	204	479	744	285	254	194	422	200	473	340	210	322	238	159	167	242	287	397	697
		28 day Breaks	28 day Breaks	28 day Breaks	28 day Breaks	28 day Breaks	28 day Breaks	28 day Breaks	28 day Breaks	28 day Breaks	28 day Breaks	28 day Breaks	28 day Breaks	28 day Breaks	27 day Breaks	28 day Breaks	28 day Breaks	28 day Breaks	28 day Breaks	28 day Breaks	28 day Breaks

Figure A-13. Gainard Woods Pump Station T-wall DMM Strength Test Results

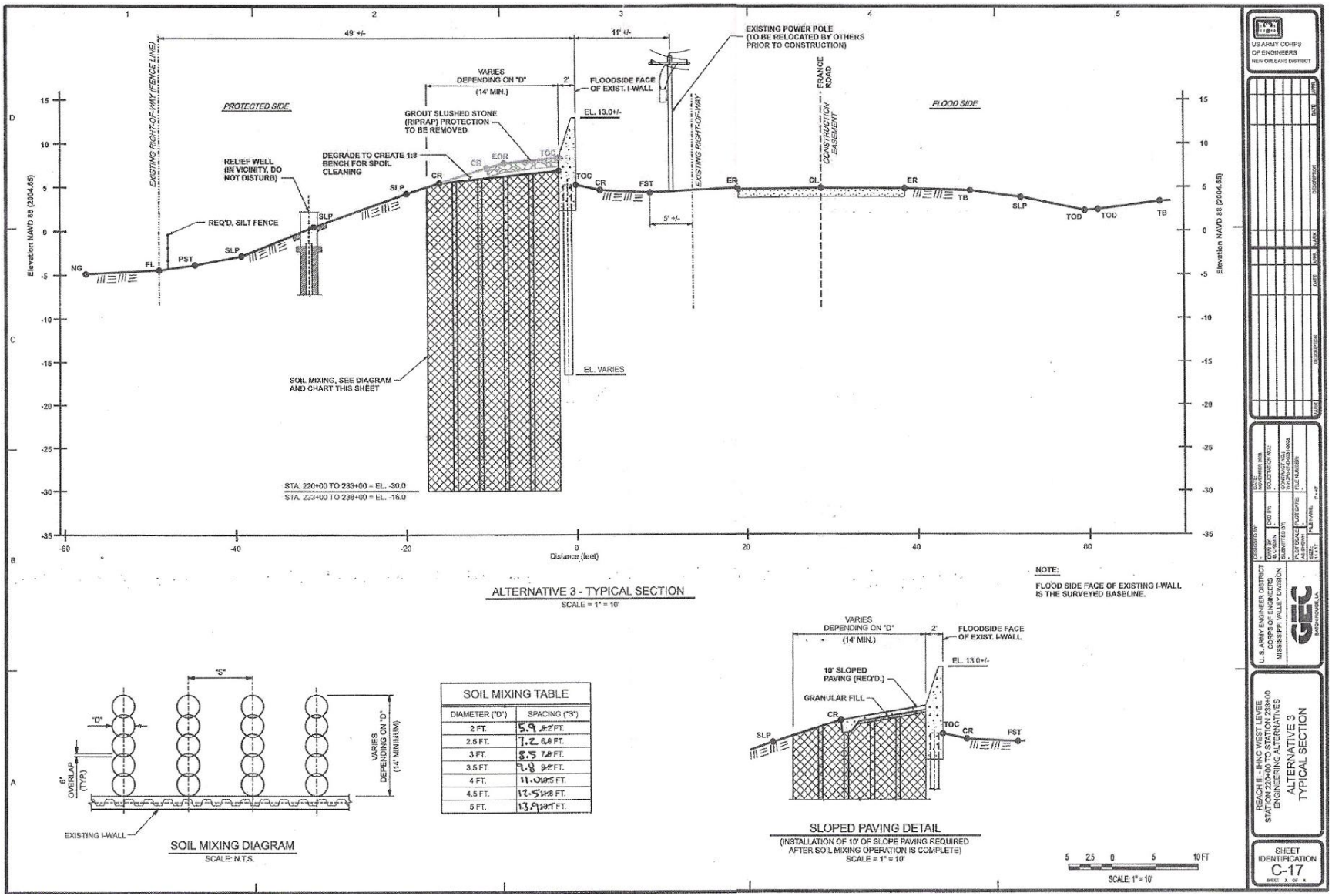

Figure A-14. IHNC Reach III B-1A I-wall DMM Typical Section

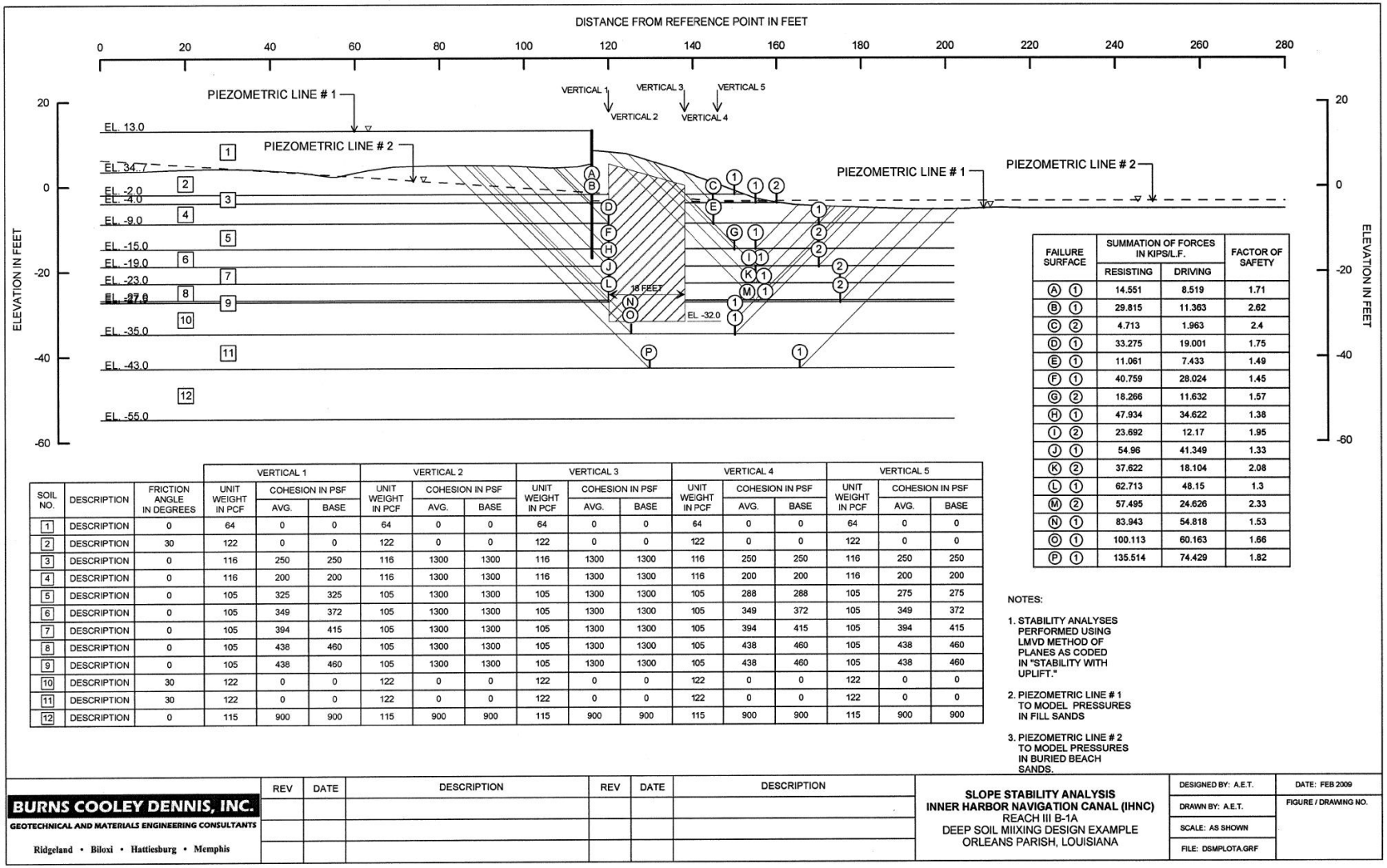

FAILURE SURFACE	SUMMATION OF FORCES IN KIPS/L.F.		FACTOR OF SAFETY
	RESISTING	DRIVING	
A 1	14.551	8.519	1.71
B 1	29.815	11.363	2.62
C 2	4.713	1.963	2.4
D 1	33.275	19.001	1.75
E 1	11.061	7.433	1.49
F 1	40.759	28.024	1.45
G 2	18.266	11.632	1.57
H 1	47.934	34.622	1.38
I 2	23.692	12.17	1.95
J 1	54.96	41.349	1.33
K 2	37.622	18.104	2.08
L 1	62.713	48.15	1.3
M 2	57.495	24.626	2.33
N 1	83.943	54.818	1.53
O 1	100.113	60.163	1.66
P 1	135.514	74.429	1.82

SOIL NO.	DESCRIPTION	FRICTION ANGLE IN DEGREES	VERTICAL 1			VERTICAL 2			VERTICAL 3			VERTICAL 4			VERTICAL 5		
			UNIT WEIGHT IN PCF	COHESION IN PSF		UNIT WEIGHT IN PCF	COHESION IN PSF		UNIT WEIGHT IN PCF	COHESION IN PSF		UNIT WEIGHT IN PCF	COHESION IN PSF		UNIT WEIGHT IN PCF	COHESION IN PSF	
				AVG.	BASE		AVG.	BASE		AVG.	BASE		AVG.	BASE		AVG.	BASE
1	DESCRIPTION	0	64	0	0	64	0	0	64	0	0	64	0	0	64	0	0
2	DESCRIPTION	30	122	0	0	122	0	0	122	0	0	122	0	0	122	0	0
3	DESCRIPTION	0	116	250	250	116	1300	1300	116	1300	1300	116	250	250	116	250	250
4	DESCRIPTION	0	116	200	200	116	1300	1300	116	1300	1300	116	200	200	116	200	200
5	DESCRIPTION	0	105	325	325	105	1300	1300	105	1300	1300	105	288	288	105	275	275
6	DESCRIPTION	0	105	349	372	105	1300	1300	105	1300	1300	105	349	372	105	349	372
7	DESCRIPTION	0	105	394	415	105	1300	1300	105	1300	1300	105	394	415	105	394	415
8	DESCRIPTION	0	105	438	460	105	1300	1300	105	1300	1300	105	438	460	105	438	460
9	DESCRIPTION	0	105	438	460	105	1300	1300	105	1300	1300	105	438	460	105	438	460
10	DESCRIPTION	30	122	0	0	122	0	0	122	0	0	122	0	0	122	0	0
11	DESCRIPTION	30	122	0	0	122	0	0	122	0	0	122	0	0	122	0	0
12	DESCRIPTION	0	115	900	900	115	900	900	115	900	900	115	900	900	115	900	900

NOTES:

1. STABILITY ANALYSES PERFORMED USING LMVD METHOD OF PLANES AS CODED IN "STABILITY WITH UPLIFT."
2. PIEZOMETRIC LINE # 1 TO MODEL PRESSURES IN FILL SANDS
3. PIEZOMETRIC LINE # 2 TO MODEL PRESSURES IN BURIED BEACH SANDS.

BURNS COOLEY DENNIS, INC.
GEOTECHNICAL AND MATERIALS ENGINEERING CONSULTANTS
Ridgeland • Biloxi • Hattiesburg • Memphis

REV	DATE	DESCRIPTION	REV	DATE	DESCRIPTION

SLOPE STABILITY ANALYSIS
INNER HARBOR NAVIGATION CANAL (IHNC)
REACH III B-1A
DEEP SOIL MIIXING DESIGN EXAMPLE
ORLEANS PARISH, LOUISIANA

DESIGNED BY: A.E.T. | DATE: FEB 2009
DRAWN BY: A.E.T. | FIGURE / DRAWING NO.
SCALE: AS SHOWN
FILE: DSMPLOTA.GRF

Figure A-15. IHNC Reach III B-1A I-wall Method of Planes Stability Analyses